National Aeronautics and Space Administration

8.0-10131
NASA CR
160585

Lyndon B. Johnson Space Center
Houston, Texas 77058

SOIL TEXTURAL EFFECTS ON RADAR RESPONSE TO SOIL MOISTURE

Remote Sensing Laboratory
RSL Technical Report 264-30

M. C. Dobson
F. T. Ulaby

Fawwaz T. Ulaby, Principal Investigator
Gerald A. Bradley, Project Manager

OCTOBER 1979

THE UNIVERSITY OF KANSAS CENTER FOR RESEARCH, INC.
2291 Irving Hill Drive—Campus West Lawrence, Kansas 66045

CONTRACT NAS9-14052

TABLE OF CONTENTS

NOMENCLATURE

dB	=	10 $\log_{10}$ (real number)
f	=	frequency, GHz
f_o	=	relaxation frequency
g	=	acceleration due to gravity
h	=	height variations relative to a reference plane
j	=	$\sqrt{-1}$
k	=	Boltzmann's constant
p	=	polarization
pf	=	a measure of suction = $\log_{10}$ (water column height, cm)
r	=	particle radius
r	=	linear correlation coefficient
z	=	viscosity of a liquid
A°	=	angstroms = 10^{-10} meters
A_e	=	external surface area of a soil particle, m^2/g
A_i	=	internal surface area of a soil particle, m^2/g
C_o	=	counterion concentration of the bulk soil solution
C_l	=	counterion concentration near a soil particle surface
CEC	=	cation exchange capacity, meq/100g
D_W	=	diameter of a water molecule ≃ 2.76 A°
ΔE	=	potential energy difference
F	=	dichotomous soil texture variable
FC	=	estimated field capacity equal to water retention at 1/3 bar tension
FM-CW	=	frequency modulated continuous wave
HH	=	like polarized signal, horizontal transmit and receive
HV	=	cross polarized signal, horizontal transmit and vertical receive
K_o	=	free-space permittivity
K_r	=	the complex dielectric constant
K'_r	=	relative permittivity
K''_r	=	effective conductivity

K_s = static relative permittivity

K_∞ = relative permittivity at frequencies much higher than the relaxation frequency

MAS = University of Kansas 1-8 GHz microwave active spectrometer

M_{FC} = percent of field capacity, gravimetric soil moisture normalized by an estimate of moisture at 1/3 bar tension

M_g = gravimetric soil moisture, percent

M_L = volumetric moisture of one monomolecular layer of water surrounding all soil particles, g/cm^3

M_n = normalized soil moisture, ratio of gravimetric or volumetric moisture to the moisture retained at a specific soil tension

M_s = dry mass of soil, g

M_T = gravimetric moisture at a specific soil tension

M_v = volumetric soil moisture, g/cm^3, cm^3/cm^3 or cm/cm

Q = surface charge density of soil, meq/m^2

R = multiple linear correlation coefficient

RMS = root mean square variation in surface height relative to a datum plane, cm

S = specific surface of a soil, m^2/g

S_I = specific surface of illite $\approx$ 100 m^2/g

S_M = specific surface of montmorillonite $\approx$ 700 m^2/g

S_O = specific surface of non-clay, clay-sized minerals $\simeq$ 10 m^2/g

S_t = total porosity of soil, percent

S.D. = standard deviation around the mean

T = absolute temperature

T = tension, bars

T_B = observed brightness temperature, °K

T_g = surface temperature, °K

USDA = United States Department of Agriculture

V = steady falling velocity of a particle

V_b = bulk volume of the soil, cm^3

V_p = total volume of solid soil particles, cm^3

VV = like polarized signal, vertical transmit and receive

W_i = incident energy

W_T = transition moisture, cm^3/cm^3 or g/cm^3

WP = soil moisture at the wilting point of plants $\simeq$ 15 bars of tension

W_α = absorbed energy
W_ρ = reflected energy
W_τ = transmitted energy

α = absorptivity
α = sensitivity
β = ordinate intercept
Γ = voltage reflection coefficient
ϵ = emissivity
η = index of refraction between two media
θ = incidence angle in degrees from nadir
λ = wavelength, cm
μ = micron = 10^{-6} meters
μ_r = relative permeability
ρ = reflectivity
ρ_b = bulk density of soil, g/cm^3
ρ_p = specific particle density of soil, g/cm^3
ρ_s = particle density, g/cm^3
ρ_w = liquid density, g/cm^3
σ^o = radar backscattering coefficient
σ_i = ionic conductivity of a salt solution
T = transmittivity

LIST OF FIGURES

LIST OF TABLES

ABSTRACT

Experimental data on radar response to soil moisture is analyzed with respect to the influence of soil texture. A truck-mounted scatterometer operating between 1 and 8 GHz, at incidence angles of 10° to 20° and at all linear polarizations observed test plots of sandy loam, silty clay loam and silty clay. Surface soil moisture conditions varied from the wilting point to field saturation. All test plots were non-vegetated and smooth with RMS surface variations ≈ 1 cm.

For a single soil texture the linear correlation between observed radar backscatter coefficient (dB) and measured gravimetric or volumetric soil moisture in the upper 5 cm of soil is typically 0.7 to 0.9. However, the sensitivity of radar response to moisture was found to be dependent upon soil texture such that sensitivity is inversely proportional to clay content of the soil. Thus, radar moisture estimation algorithms using either gravimetric or volumetric measures of soil moisture are expected to exhibit poor performance for complex multi-texture terrain if soil texture is unknown. Empirical evaluation of an equally distributed three texture ground scene produced linear correlations of less than 0.7 for the upper 1 cm of soil and correlation was found to degrade dramatically when considering larger depth intervals of soil ($r \simeq 0.0$ for the 0-15 cm soil layer).

In sharp contrast, estimation algorithms incorporating some knowledge of the tension at which soil water is retained by the soil produced strong correlation with sensor response, typically $r = 0.8$, regardless of depth interval considered within the surface 15 cm. The tested tension dependent soil moisture indicators include percent of field capacity, moisture normalized at soil tensions between 0.04 and 31 bars, volumetric moisture in excess of a transition moisture (as defined from dielectric investigations) and estimated soil tension. Importantly, these algorithms were found to be relatively independent of soil texture.

The soil moisture indicators which produce radar estimation algorithms independent of soil texture are evaluated in terms of value to the potential user community of remotely-sensed moisture data. Normalized moisture indices will be difficult to interpret. Moisture in excess of

a transition moisture may prove to be of value if the transition moisture can be uniquely defined. Analysis of the radar data indicates that the transition moisture corresponds to an adsorbed water layer at least 4-6 molecular layers thick surrounding soil particles. Soil tension is found to be the most meaningful moisture indicator since it defines many critical points in the hydrodynamic behavior and agronomic importance of soil water. The current use of soil tension is mainly limited by the difficulty of measuring this parameter over the wide range of values typically assumed under field conditions. The high correlation between radar response and soil tension, a parameter not readily available even as a point measurement, should be carefully considered in any cost-benefit analysis of radar remote sensing of soil moisture.

Key words: radar, scatterometer, soil moisture, soil texture, soil tension, remote sensing

1.0 INTRODUCTION

In recent years, much interest has been expressed in developing capability for the operational remote sensing of soil moisture. Soil moisture information is needed on a local, regional and global scale for input into models in the fields of hydrology, meteorology and agriculture. In situ, point measurements of soil moisture are economically impractical in accounting for the temporal and spatial variability of soil moisture over large areas. Remote sensing research to date has investigated the correlation between soil moisture and surface albedo (Idso, et. al., 1975a), thermal inertia of terrain (Idso, et al., 1975b; Schmugge, et al., 1978; Idso, et al., 1976), radar backscatter coefficient (Cihlar and Ulaby, 1975; Batlivala and Ulaby, 1977) and the microwave emissivity of soils (Ulaby, et al., 1974; Newton, 1977; Schmugge, 1978).

Hydrologists require knowledge of soil moisture in the upper 10 cm for the partitioning of rainfall into runoff, deep percolation and ground storage for assessment of watershed yield, reservoir management models and flood forecasting (Lawson, 1977; Salomonson, et al., 1975; Armstrong, 1978). Regional meteorological models require soil moisture data for approximately the same surface layer to estimate moisture and heat fluxes into the atmosphere from land surfaces (Miller and Thompson, 1970). Agricultural interest in soil moisture ranges from that present in the surface layer which determines: tillage calendars, the germination and early growth of plants, the subsequent incidence of crop diseases, and hatching rates of insect populations (Idso, et al., 1975c; Hammond, 1975) to that present at depths of one or more meters in the soil which effects the growth of maturing crops and their yield (Erickson, 1977). At present, all remote sensing techniques are sensitive to the moisture present only in the surface layer, therefore moisture information at depths of one or more meters must be derived by modeling techniques (Baier and Robertson, 1966 and 1968; Hildreth, 1978; Reed, 1977, Cihlar and Ulaby, 1977; Rango, 1978).

Events of the past decade have emphasized the fact that we live on a planet of finite resources and capability to efficiently regenerate renewable resources. The politics of food have important potential implications due to trends in world population and the vagaries of world

climate and food production (Schneider, 1976; CIA, 1976; Bryson, 1977; Smith, 1976). Rational resource planning and development requires inventories and periodic monitoring of pertinent resource parameters such as soil moisture.

Microwave sensors offer one of the most promising techniques for the remote sensing of soil moisture because of their all weather, day or night capabilities combined with an ability to penetrate a vegetation canopy with minimal attenuation of the emitted or backscattered signal. The great potential of microwave remote sensing systems is due to the large difference in the dielectric properties of water and those of dry soils at microwave frequencies.

Recent research efforts have focussed primarily upon the selection of sensor parameters: frequency, incidence angle and polarization in a configuration that will minimize the impact of target parameters other than soil moisture. Pertinent target parameters include: vegetation type, density and moisture; surface aspect or slope; surface roughness; and soil type. Numerous experimental investigations using spaceborne, airborne and truck-mounted passive and active microwave sensors have demonstrated the feasibility of sensing surface soil moisture at microwave frequencies (Cihlar and Ulaby, 1975; Batlivala and Ulaby, 1977; Newton, 1977; Eagleman, 1975; and others) and will not be discussed herein. Site specific experiments have verified the following as regards radar response to soil moisture (Batlivala and Ulaby, 1977; Ulaby, et al., 1977; Ulaby, et al., 1978; Ulaby et al., 1979; Bush and Ulaby, 1977):

a) the radar backscattering coefficient is sensitive to soil moisture content at all microwave frequencies,

b) signal attenuation by crop canopies is minimized at frequencies below 8 GHz,

c) effects of surface roughness typical of dryland farming practices are minimized by the selection of a 4.5 GHz like polarized system operating between 7° - 17° incidence angle,

d) sensitivity of radar response to surface slope is reduced at frequencies greater than 3 GHz, and

e) radar sensitivity to soil moisture is dependent upon some aspect of soil type.

Soils are derived from a host of parent materials and subsequently modified by the interaction of complex geographic distributions of climatic regimes and associated plant communities. Soil associations vary regionally as a function of the above parameters, and soil texture as defined by the particle size distribution of soil solids is observed to vary considerably over tens of meters. Thus, assuming that other target "noise" such as water bodies and man-made structures can be filtered from the radar data and that vegetation and roughness effects are minimized by optimizing sensor selection, effective soil moisture estimation algorithms must account for the observed dependence of radar response to soil type.

1.1 Statement of Problem and Purpose

The complex dielectric constant and thus passive and active sensors operating at microwave frequencies have all been observed to exhibit some dependence upon soil texture in their response to soil moisture. Since most prior experimentation was site specific and examined only one soil texture, the influence of soil texture upon the sensor response to soil moisture was found to be significant only through comparison of results from several experiments.

The purpose of this study is to: a) experimentally verify prior observations that 1-8 GHz radar response to soil moisture is influenced by soil texture, b) investigate the behavior of soil water as a function of soil texture and the electromagnetic characteristics of the soil solution at microwave frequencies, c) examine available quantifiers of soil moisture such as gravimetric and volumetric moisture, percent of field capacity and soil tension with respect to radar response and soil texture, and d) evaluate those moisture indicators found to produce texturally independent soil moisture algorithms in terms of their value to a user community of soil moisture information.

In order to accomplish the above objectives, the 1977 Bare Soil Experiment (Dobson, 1979) was conducted using the University of Kansas truck-mounted Microwave Active Spectrometer 1-8 GHz system to observe carefully selected and prepared bare soil fields of sandy loam, silty clay loam and silty clay at incidence angles between 10° and 20° relative to nadir.

Radar backscattering measurements were made at each field for surface soil moisture conditions ranging from the wilting point of plants to saturation and partial flooding of the test fields. In conjunction with the radar measurements, many target parameters were monitored during the course of the experiment including: gravimetric moisture profile, soil bulk density, soil texture, organic matter content, surface slope, surface roughness, soil water desorption characteristics and precipitation.

The radar data acquired from this experiment was used to develop algorithms using various soil moisture indicators for each soil texture independently and for all soil textures considered simultaneously. These algorithms were then compared to evaluate their respective independence to soil texture.

1.2 Chapter Outline

This study is divided into five chapters. Chapter 2 treats soil textural effects upon soil water retention and upon the electromagnetic behavior of soil water at microwave frequencies. Soil water retention is examined with respect to soil composition, structure and mineralogy which collectively determine the pore size distribution, the specific surface area and the affinity of the soil solution to the soil solid surfaces. The behavior, composition and structure of the soil solution is examined as a function of distance from soil particle surfaces. Dielectric measurements of moist soils at microwave frequencies are reviewed and linked to results of soil moisture experiments utilizing radiometers and radar for observation of a variety of soil textures. Soil moisture quantifiers are reviewed with respect to their dependence on soil texture.

Chapter 3 describes, in brief, the 1977 Bare Soil Experiment. Target characteristics and the homogeneity of each test field are summarized. The angular and frequency response of the radar with respect to gravimetric soil moisture is examined and found to be consistent with results derived from other experiments with the MAS 1-8 GHz system (Batlivala and Ulaby, 1977).

The results of the 1977 Bare Soil Experiment are analyzed in Chapter 4 to evaluate the textural independence of the following soil moisture indicators with respect to radar backscatter: gravimetric moisture,

volumetric moisture, normalized moisture (such as percent of field capacity), volumetric moisture above some transition moisture and soil tension.

Chapter 5 presents an evaluation of those soil moisture indicators found to show minimal dependence upon soil texture in the preceding analysis which can be readily interpreted by the potential user community of agronomists, hydrologists and meteorologists. Specific recommendations are made for future experiments in light of these findings.

2.0 BASIC CONSIDERATIONS OF SOIL WATER AND THE ELECTRICAL BEHAVIOR OF SOIL WATER

As a prelude to an understanding of the interaction of an impressed microwave field on the soil-water system, it is necessary to address the physics of the soil and its components. Soil consists of unconsolidated mineral material derived as the weathering product of parent rock either in situ or as a sediment of some transporting agent (water, wind or ice). Soil can be considered as a three component system: soil solids, soil water and air; the interaction of these components imparts characteristic structure, soil water and density relationships within a given soil.

In the surface horizon of agricultural soils, soil solids consist of organic and inorganic mineral fractions. The organic fraction is concentrated near the surface and consists of live plant material, such as roots, decaying organic debris and carbonaceous decay resistant humus. The organic fraction is usually less than 10% of the dry soil by weight (and typically less than 5%); it is extremely active in terms of soil chemistry and soil moisture dynamics, especially the colloidal humus. Soil organic matter is a prime determinant of surface soil structure, the water-holding capacity of soils and the soil's cation exchange capacity. The inorganic fraction consists of the weathered mineral grains of the parent rock. The grains can be described in terms of their mineralogy and particle size distribution.

2.1 Soil Moisture Concepts

Soil chemistry and water-capacity are governed primarily by the interaction of soil structure and soil composition. Soil structure establishes the volume and size distribution of pore spaces which can

be occupied by soil water. Soil composition, defined herein as the soil particle size distribution and particle mineralogy, determines the net effective soil surface area to which water molecules may adhere and the electro-chemical properties of the particle surfaces.

2.1.1 Soil particle size

The arrangement of solid particles determines the structure, porosity and bulk density of the soil. Soil solids range in size from colloids on the order of 50 A^0 in diameter to gravel. Soil particle sizes are classified into categories of soil textural separates. Many classification schemes are available (Figure 2.1), but use of the 1951 United States Department of Agriculture (USDA) size categories will be adhered to in the present discussion. Soil particles are classified into textural separates by mechanically passing the inorganic fraction (either wet or dry) through sieves and subsequent sedimentation of the fine material. Sieving and sedimentation techniques both assume spherical soil particles; however, soil particles are not generally spherical and this assumption is particularly weak for the clay size fraction. In mechanical sieving, the mesh size of the screen refers to the equivalent diameter of a sphere that will pass through that screen. Textural separates smaller than sand must be isolated using sedimentation techniques based upon Stoke's law which predicts the settling velocity of spherical particles for a given set of environmental conditions.

$$V = 2/9 \quad gr^2 \left(\frac{\rho_s - \rho_w}{z}\right) \qquad (2.1)$$

where: V = the steady falling velocity of a particle
g = acceleration due to gravity
r = particle radius
ρ_s = particle denisty
ρ_w = liquid density
z = viscosity of liquid

Soil particles are classified as having diameters equivalent to those of spheres of the same denisty and settling velocity. The sedimentation technique commonly employs either a hydrometer to monitor the density of the soil suspension as a function of time or pipetting of the suspension

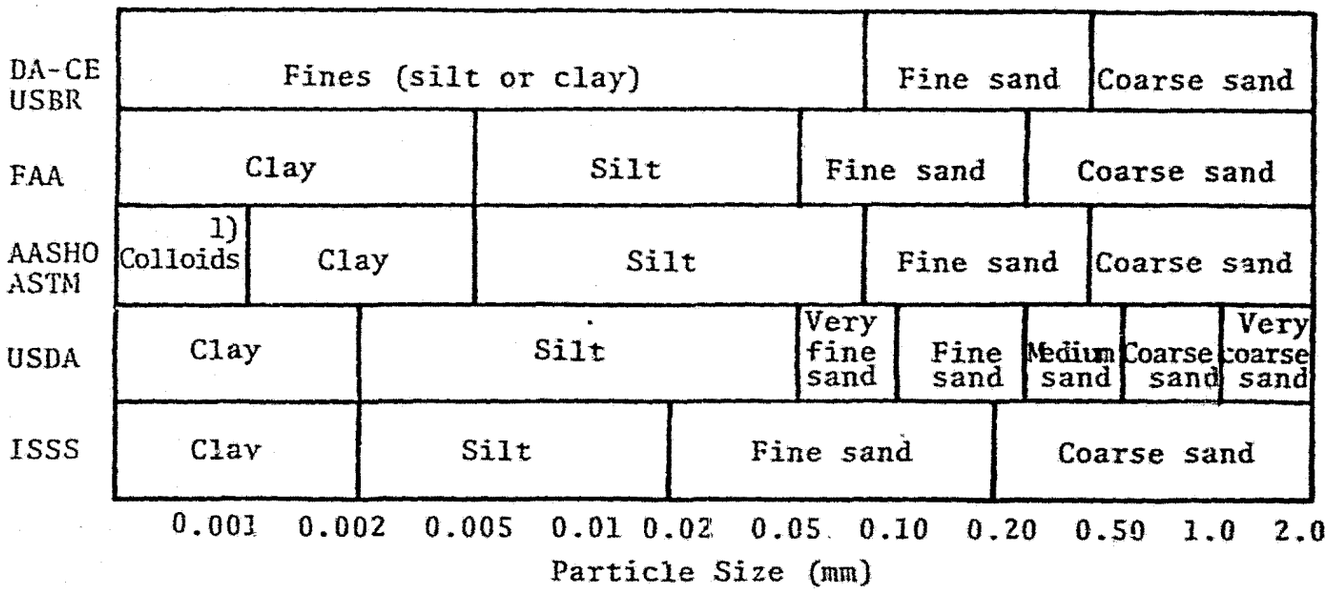

DA-CE = Department of Army, Corps of Engineers
USBR = U.S. Bureau of Reclamation
FAA = Federal Aviation Authority
AASHO = American Association of State Highway Officials
ASTM = American Society of Testing and Materials
USDA = U.S. Department of Agriculture
ISSS = International Society of Soil Science
Note (1) = Reported with clay

Figure 2.1 Classification of soil separates ≤ 2.0 mm on the basis of particle size (from Baver, Gardner and Gardner, 1972).

to gravimetrically determine the mass of soil solids remaining in suspension as a function of time. It should be remembered that all determinations of soil textural separates are biased by the relative validity of assumed spherical particles. The sphericity of a particle is governed by its mineralogy and weathering history and will be more fully discussed in the following section.

Since all soils contain a distribution of particle sizes, it is convenient to classify a soil by the weight percent of the soil within specific size categories (sand, silt, clay). For a soil having the particle size distribution shown in Figure 2.2, the soil textural separates of sand, silt and clay represent the integrals of the distribution between the limits shown ratioed to the integral of the entire distribution. The percent by weight of each size interval then determines the soil textural class using the USDA triaxial classification based on sand, silt and clay fractions shown in Figure 2.3.

2.1.2 Soil Particle Surface Area

The net soil surface area available to interaction with the soil solution consists of the sum of component particle external surface areas and clay particle internal (interlayer) areas as limited by soil particle contacts.

$$S = \Sigma A_e + \Sigma A_i \qquad (2.2)$$

where: S = the specific surface of a soil in m^2/g

A_e = external surface area of a soil particle in m^2/g

A_i = internal surface area of a soil particle in m^2/g

The external surface area of soil particles is a function of particle size and shape. Figure 2.4 shows the relationship between particle size, the number of particles per gram and external surface area assuming spherical particles. It is apparent that .002mm diameter (2μ) clay has approximately 50 times the external surface area of an equal weight of .1 mm diameter fine sand. Table 2.1 assumes closest hexagonal packing of spherical particles to compare external surface area on a volume basis. It is obvious that, for a given soil, A_e is dominated by the percent clay fraction.

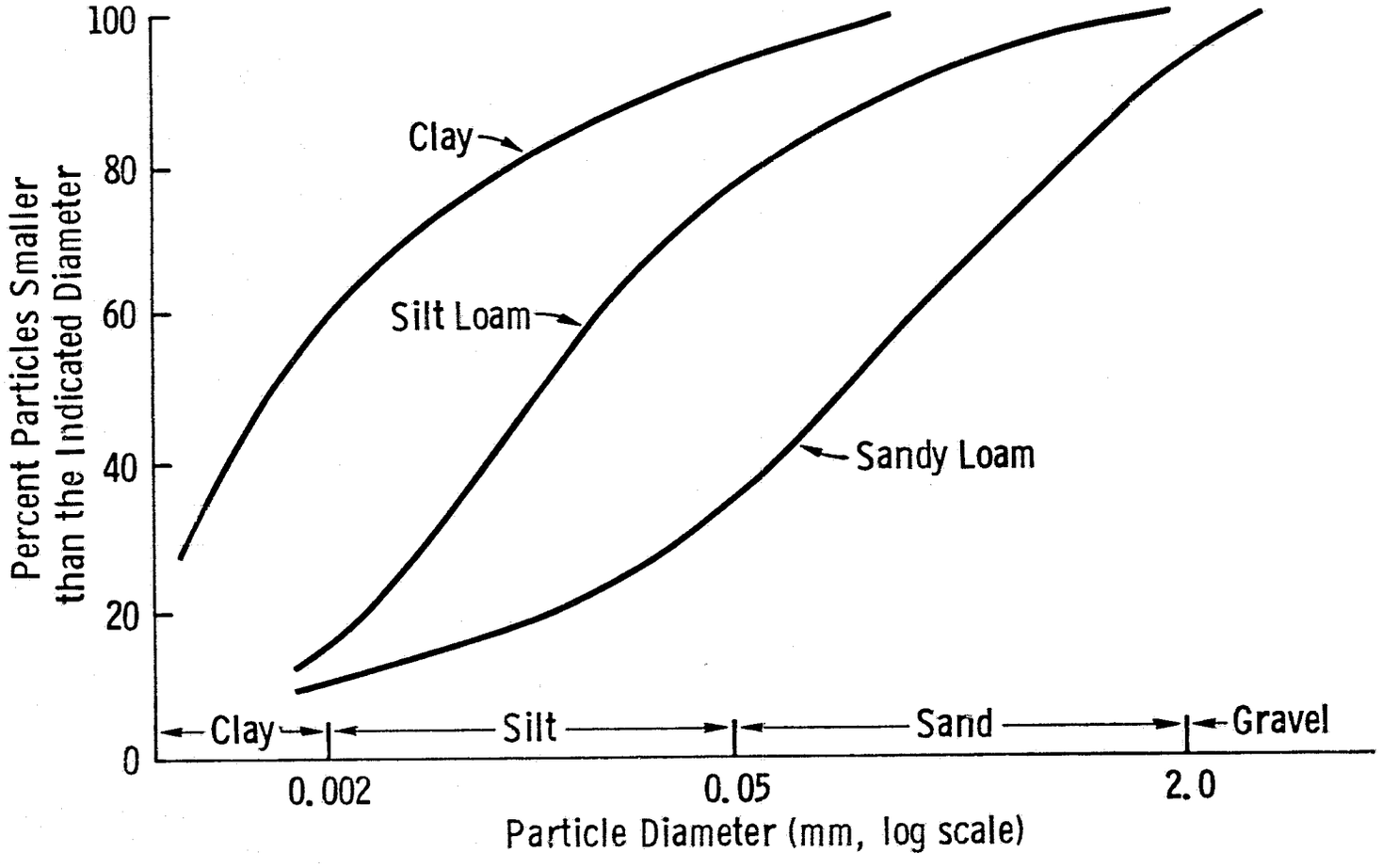

Figure 2.2. Particle size distribution in three soils varying widely in their textures. Note that there is a gradual transition in the particle size distribution (from Brady, 1974).

Figure 2.3 USDA soil textural classification triangle.

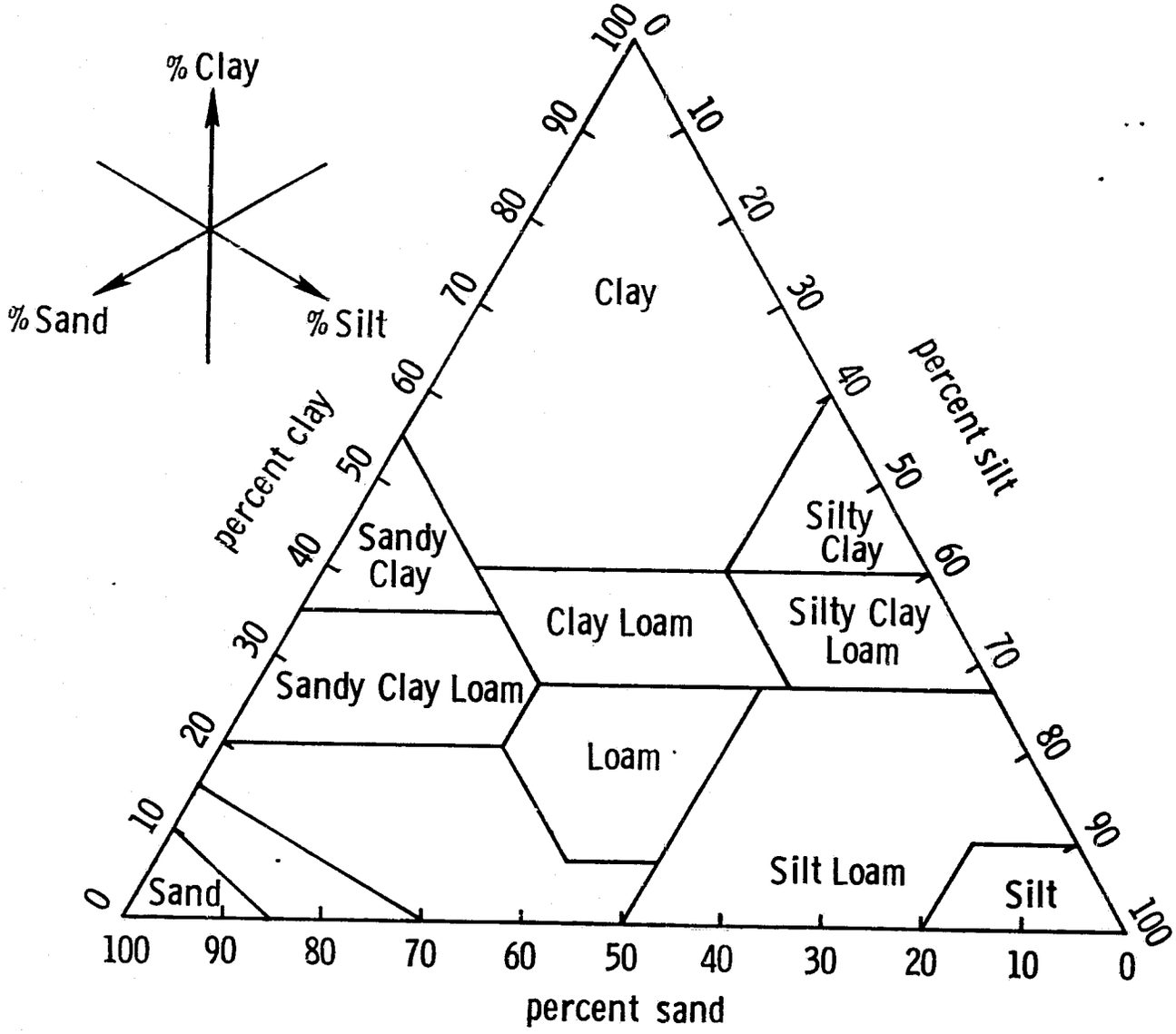

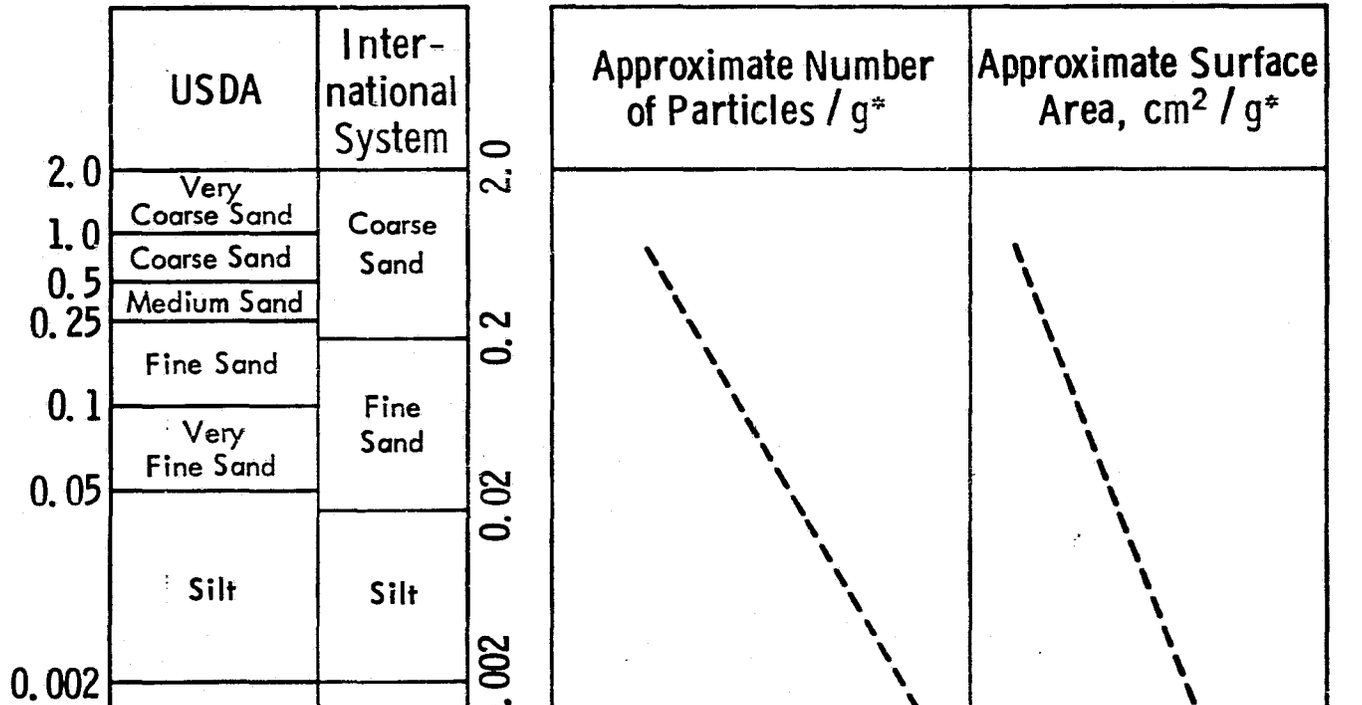

Figure 2.4. Particle size classes, number of particles and external surface area based on spherical particles of density 2.65 g/cm^3 (modified from Birkeland, 1974).

TABLE 2.1

The relation of particle size to external surface (from Baver, Gardner and Gardner, 1972).

Diameter of sphere	Textural name	Volume per particle $(\pi/6)\ D^3$	Number of particles in $\frac{\pi}{6}$ cc	Total surface πD^2 x number of particles
1 cm	Gravel	$(\pi/6)\ (1)^3$	1	3.14 cm^2 (0.49 $in.^2$)
0.1 cm (1 mm)	Coarse sand	$(\pi/6)\ (0.1)^3$	1×10^3	31.42 cm^2 (4.87 $in.^2$)
0.05 cm (500 μ)	Medium sand	$(\pi/6)\ (0.05)^3$	8×10^3	62.83 cm^2 (9.74 $in.^2$)
0.01 cm (100 μ)	Very fine sand	$(\pi/6)\ (0.01)^3$	1×10^6	314.16 cm^2 (48.67 $in.^2$)
0.005 cm (50 μ)	Coarse silt	$(\pi/6)\ (0.005)^3$	8×10^6	628.32 cm^2 (97.34 $in.^2$)
0.002 cm (20 μ)	Silt	$(\pi/6)\ (0.002)^3$	125×10^6	1,570.8 cm^2 (1.69 ft^2)
0.0005 cm (5 μ)	Fine silt	$(\pi/6)\ (0.0005)^3$	8×10^9	6,283.2 cm^2 (6.76 ft^2)
0.0002 cm (2 μ)	Clay	$(\pi/6)\ (0.0002)^3$	125×10^9	15,708 cm^2 (16.9 ft^2)
0.0001 cm (1 μ)	Clay	$(\pi/6)\ (0.0001)^3$	1×10^{12}	31,416 cm^2 (33.8 ft^2)
0.00005 cm (500 mμ)	Clay	$(\pi/6)\ (0.00005)^3$	8×10^{12}	62,832 cm^2 (67.6 ft^2)
0.00002 cm (200 mμ)	Colloidal Clay	$(\pi/6)\ (0.00002)^3$	125×10^{12}	157,080 cm^2 (169 ft^2)
0.00001 cm (100 mμ)	Colloidal Clay	$(\pi/6)\ (0.00001)^3$	1×10^{15}	314,160 cm^2 (338 ft^2)
0.000005 cm (50 mμ)	Colloidal Clay	$(\pi/6)\ (0.000005)^3$	8×10^{15}	628,320 cm^2 (676 ft^2)

Many soil characteristics are surface phenomena: particle attraction, water, gas and nutrient adsorption among others. Figure 2.5 emphasizes the significance of the high specific surface area of clay sized particles.

The rate of increase in specific surface area with decreasing particle diameter is amplified by considerations of particle shape. The spherical particles assumed above have the smallest possible area to volume ratio; as particles become less spherical, the area to volume ratio increases. Soil particles are rarely spherical and, in general, become more plate-like as effective diameter decreases. The loss of sphericity with decreasing particle size is the result of mineralogic control as influenced by weathering processes. Sand and most silt sized particles are composed of primary weathering minerals, usually quartz, feldspars and ferro-magnesium minerals which may have been mechanically reduced in size; these particles are subangular to rounded in shape depending, in part, upon abrasion. Silt size particles are diverse, irregularly shaped fragments which are rarely smooth or flat; similar to sand, quartz is the dominant mineral. Clay sized particles include primarily clay minerals mixed with relatively coarse grained amorphous crystalline minerals (Table 2.2). The clay minerals are complex layer-lattice alumino-silicate sheet structures which have a characteristic plate-like shape and are often colloidal. Soil clay platelets may be only 50 A^{o} in diameter and 10 A^{o} thick where $1\mu = 10^{4}$ A^{o} (Taylor and Ashcroft, 1972).

Table 2.3 demonstrates the effect of particle shape on external surface area. The introduction of plate-like particle shape produces a dramatic increase in external surface area when compared to a reference sphere. A disk .2μ thick has a surface area 257 times greater than the 2μ reference sphere where 2μ is the maximum equivalent diameter of clay size particles.

Internal surface area, A_i, is primarily a phenomenon of the clay minerals. The clay minerals can have very high internal surface areas in the interlayers of the particle crystal lattice. It is necessary to introduce some basic concepts of clay mineral structure in order to understand the nature of clay internal surface area.

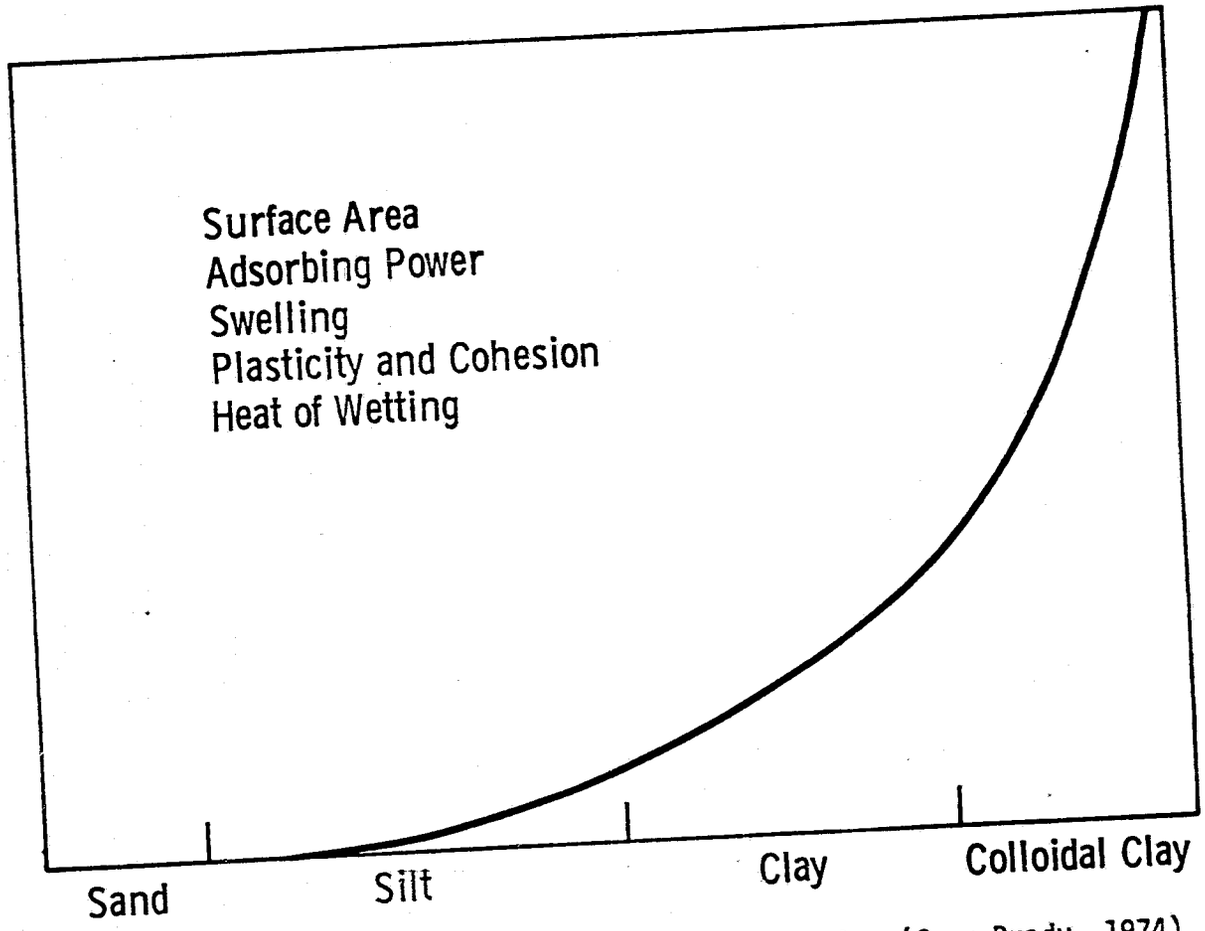

Figure 2.5. Soil physical properties as a function of particle size (from Brady, 1974).

TABLE 2.2

Principal Secondary Minerals of the Clay Size Fraction (from Townsend, 1973).

Amorphous	oxides	silica $SiO_2.nH_2O$ hydrated iron oxides $Fe(OH)_3.nH_2O$ alumina $Al_2O_3.nH_2O$
	silicates	allophane $Al_2O_3.2SiO_2.nH_2O$ hisengerite $Fe_2O_3.2SiO_2.nH_2O$
	phosphates	evansite $Al_3PO_4(OH)_6.nH_2O$ azovskite $Fe_3PO_4(OH)_6.nH_2O$
	carbonates	calcite $CaCO_3$ magnesite $MgCO_3$ dolomite $CaCO_3.MgCO_3$ siderite $Fe\ CO_3$
Crystalline	oxides	goethite $\alpha FeO.OH$ lepidocrocite $\gamma FeO.OH$ maghemite γFe_2O_3 gibbsite Al_2O_3
	silicates	complex alumino-silicates, grouped according to their structural characteristics.

TABLE 2.3

Surface Area in Relation to Shape of Particle (from Baver, Gardner and Gardner, 1972).

Shape	Radius (cm)	Volume (cm^3)	Surface (cm^2)	Increase in surface (percent)
Sphere	1×10^{-4}	4.2×10^{-12}	1.26×10^{-7}	
Disk				
$h = 1 \times 10^{-4}$ cm	1.155×10^{-4}	4.2×10^{-12}	1.56×10^{-7}	23.8
$h = 5 \times 10^{-5}$ cm	1.67×10^{-4}	4.2×10^{-12}	1.84×10^{-7}	45.8
$h = 2 \times 10^{-5}$ cm	2.58×10^{-4}	4.2×10^{-12}	4.51×10^{-7}	257.8
$h = 1 \times 10^{-5}$ cm	3.65×10^{-4}	4.2×10^{-12}	8.59×10^{-7}	538.9

2.1.3 Some Properties of Clay Minerals

Since quartz particles are very inactive chemically, the sand and silt sized soil fractions contribute little to soil chemistry. On the other hand, the clay minerals are quite surface active due to their aluminosilicate sheet structure and dominate the chemical behavior of the soil inorganic fraction.

Based upon mineral structure, three main types of aluminosilicate layer clays can be identified: montmorillonite, illite and kaolinite. Table 2.4 lists other principal crystalline silicate clay minerals as well. The distinguishing features between various clays are the numbers and kinds of layers in a crystal unit layer and the isomorphous substitutions of ions within these structures.

The basic molecular components of clay aluminosilicates are the silica tetrahedron and the alumina octahedron, a silicon atom surrounded by four oxygen atoms and an aluminum atom surrounded by six hydroxyls or oxygen atoms respectively. Each basic building block or crystal unit cell is arranged in planar sheet structures bound by common oxygen atoms. The tetrahedral and octahedral sheets are variously arranged and stacked, and are bound by common oxygen atoms to produce the crystal unit layers distinctive of each aluminosilicate layer clay. Thus, crystal unit layers of the 1:1 family consists of one silica tetrahedral sheet bound to one alumina octahedral sheet and the 2:1 family has an alumina octahedral layer in between two silica tetrahedral layers. The crystal unit layers are then stacked with various bonding energies in either single mineral form or as mixed layer clays to form the clay particles of an equivalent diameter as identified by mechanical size fractionation.

The aluminosilicate layer clays are further classified by the isomorphous substitution of ions within the lattice of a given crystal unit cell and the bonding characteristics between unit layers. The idealized clay structures presented above are electrostatically neutral, this rarely occurs in nature. The idealized crystal unit layers are disrupted by the isomorphous substitution of other cations of similar size and lower valence in the crystal lattice which causes the crystal to become negatively charged. Table 2.5 gives the ionic radii of elements commonly substituted and adsorbed to silicate clays. These negative charges are commonly balanced by the presence of an additional cation

TABLE 2.4

Principal Crystalline Silicate Clay Minerals
(from Townsend, 1973).

Chain structures		palygorskite
Layer structures	1 : 1 family	kaolinite nacrite dickite halloysite
	2 : 1 family	montmorillonite beidellite vermiculite mica illite nontronite

TABLE 2-5

Ionic Radii of Elements Common in Silicate Clays and an Indication of Which are Found in the Tetrahedral and Octahedral Layers (from Brady, 1974).

Note that aluminum can fit in either layer.

Ion	Radius (Å)*	Found in
Si^{4+}	0.41	Silica tetrahedra
Al^{3+}	0.50	Silica tetrahedra
Fe^{3+}	0.64	Alumina octahedra
Mg^{++}	0.65	Alumina octahedra
Zn^{++}	0.70	Alumina octahedra
Fe^{++}	0.75	Alumina octahedra
Ca^{++}	0.94	Exchange sites
Na^{+}	0.98	Exchange sites
K^{+}	1.33	Exchange sites
$O^{=}$	1.45	Both layers

* An Ångström unit (Å) is 10^{-8} centimeter.

adsorbed to the surface of the crystal layer in the vicinity of the crystal lattice substitution. The adsorbed cations are termed exchangeable cations since they can be replaced at the surface of the clay layers by other cations and water molecules. The extent and nature of isomorphous substitution determines the net surface charge of the layer silicate clays.

Kaolinite is the most prominent member of the 1:1 lattice clays. The alumina octahedral and silica tetrahedral layers are tightly held together by hydrogen bonding of pairs of adjacent oxygen and hydroxyl groups. The hydrogen bonding gives the crystal structure great strength and permits little substitution within the lattice; therefore cations and water are not absorbed between crystal units and no swelling of this clay ordinarily occurs. The specific surface of kaolinite is thus defined by its external surface area only, which is relatively small since the hydrogen bonding results in large particle sizes, typically .2 to 2 μm across (Brady, 1974). Hence, the surface activity of kaolinite as defined by the area density of exchangeable cations is low since substitution is rare and surface activity is primarily determined by broken bonds at the edges of crystal sheets in the lateral dimension along the particle edges.

Hydrous micas are 2:1 lattice clays which, like kaolinite, are also non-expanding clays. Illite is the most common member of this group and is often found associated with montmorillonite. The clay mineral fractions of the soils examined during the 1977 Bare Soil Experiment are approximately 30% illite and 60% montmorillonite. Isomorphous substitution occurs mainly in the silica tetrahedral layer where approximately 15 to 25% of the tetravalent silicon atoms are replaced by larger trivalent aluminum atoms (Townsend, 1973). Non-exchangeable potassium ions on the surfaces of the crystal unit cell are tightly bound between adjacent tetrahedral layers, thus bonding adjacent unit cells. The potassium acts to restrict the expansion potential of the illite particle structure thereby limiting cation exchange sites to the particle external surface area. Cation exchange can occur at the planar surfaces of the particle and along the frayed lateral edges of the structure. Illite particles tend to be intermediate in size between those of kaolinite and montmorillonite.

Montmorillonite is a 2:1 lattice clay with considerable potential to expand. Isomorphous substitution occurs in both the tetrahedral and octahedral layers. Commonly, aluminum substitutes for silicon in the tetrahedral layers and magnesium and iron substitute for aluminum in the octahedral layers. The high degree of substitution imparts a large negative net surface charge on montmorillonite crystals which is satisfied by a swarm of exchangeable cations adsorbed to both the internal and external surfaces of a particle. Within a particle, the clay crystal unit cells are very loosely held by only van de Waal's forces and weak oxygen to oxygen affinities. This weak bonding of the clay unit cells allows the tremendous expansion of the particle structure when cations and water are introduced into the interlayers of the clay lattice. The very large internal surface of montmorillonite combined with a large relative external surface area (typically .01 to 1 μm equivalent particle diameter) and the high degree of isomorphous substitution causes the cation exchange capacity (CEC) of montmorillonite to be an order of magnitude greater than that for either kaolinite or illite (Table 2.6).

In summary, the total CEC of a given clay mineral is determined by the degree and type of isomorphous substitution within the crystal lattice and the number of broken bonds at the frayed crystal edges. The part of the CEC determined by isomorphous substitution is relatively constant in magnitude for a given soil, while the CEC determined by broken edge bonds is dependent upon the pH of the soil solution. At the crystal edges, the contribution to total CEC is proportional to soil pH; as pH increases more hydroxyl groups are dissociated with the hydrogen being readily exchangeable. The net effect of this pH dependent charge is small compared to the particle surface charge determined by isomorphous substitution (Figure 2.6).

The CEC and the relative specific surface of clay minerals is important to the present discussion because of the manner in which electrostatically charged solid surfaces modify the distribution and electromagnetic behavior of water molecules in the soil solution. Also, it is obvious from Figure 2.5 that the cation exchange capacity of even small quantities of the colloidal fraction of organic humus will have a profound effect. These issues will be discussed after consideration of soil water.

TABLE 2.6

Comparative Properties of Three Major Types of Clay (from Brady, 1974).

Property	Type of Clay		
	Montmorillonite	Illite	Kaolinite
Size (μm)	0.01–1.0	0.1–2.0	0.1–5.0
Shape	Irregular flakes	Irregular flakes	Hexagonal crystals
Specific surface (m^2/g)	700–800	100–120	5–20
External surface	High	Medium	Low
Internal surface	Very high	Medium	None
Cohesion, plasticity	High	Medium	Low
Swelling capacity	High	Medium	Low
Cation exchange capacity (meq/100 g)	80–100	15–40	3–15

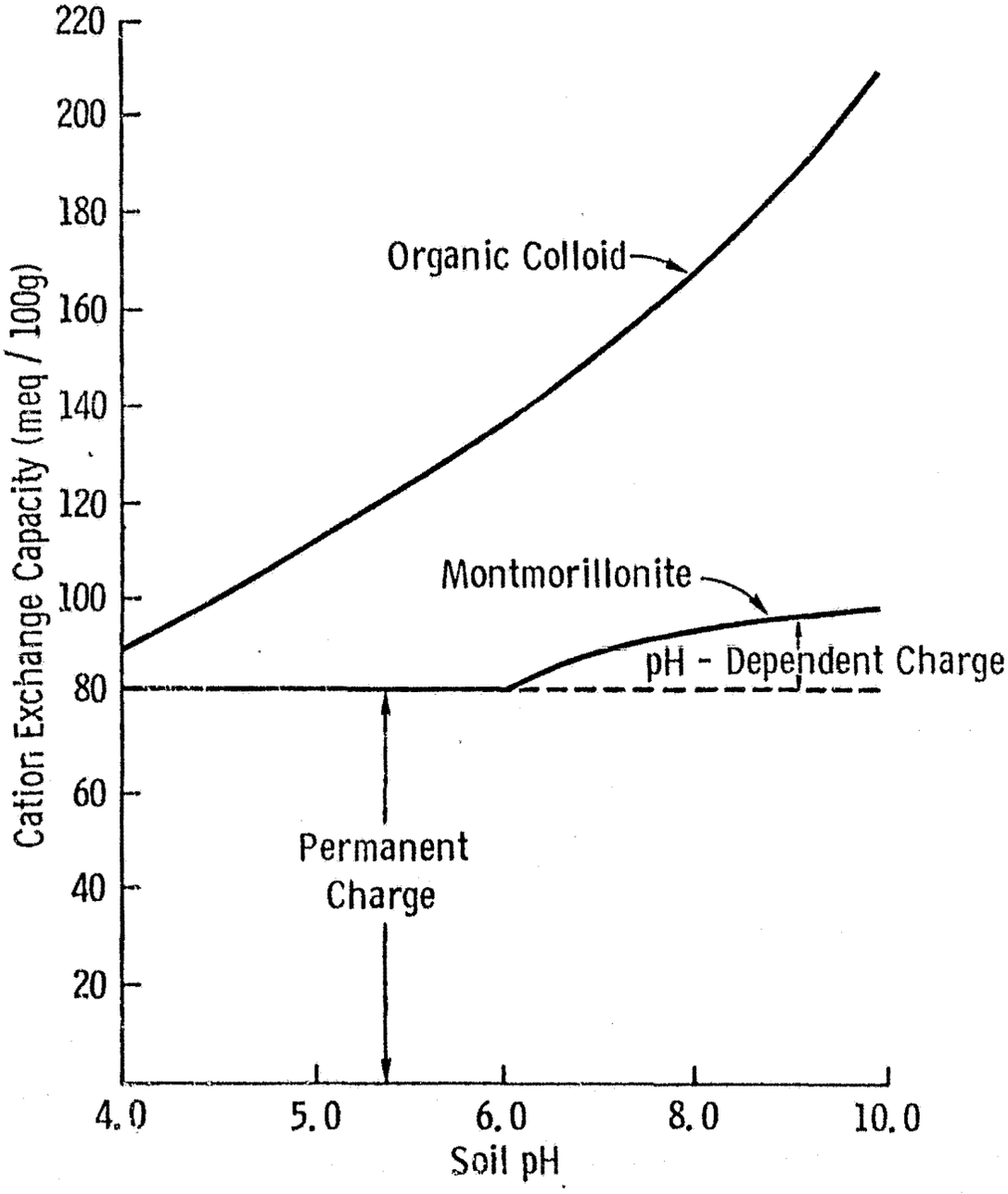

Figure 2.6. Influence of pH on the cation exchange capacity (a measure of the negative charge) of montmorillonite and humus. Note that below pH 6.0 the charge for the clay mineral is relatively constant. This charge is considered permanent and is due to ionic substitution in the crystal unit. Above pH 6.0 the charge on the mineral colloid increases because of ionization of hydrogen from exposed O-H groups at crystal edges. In constrast to the clay, essentially all of the charges on the organic colloid are considered pH dependent (from Brady, 1974).

2.1.4 Measurement of Soil Water

Water content of soils may be determined by direct or indirect methods. Direct methods use a variety of processes to separate water from the soil solids, such as the oven drying of soil, for comparison of the mass of water to the mass of soil. Indirect methods measure a property of the soil which is related to water content such as: gamma ray and neutron attenuation, electrical conductivity and resistivity or the tension at which soil water is held. The last three methods are related to moisture content by its relationship to soil moisture tension, which is a pressure or work per unit volume usually referenced to atmospheric pressure in bars.

All determinations of soil water are made with respect to some arbitrary reference zero. In the gravimetric determination of soil moisture, the reference zero is commonly the mass of soil after drying at 100 to 110°C to a constant weight, usually requiring about 24 hours. Other reference zero points are possible since there is nothing unique about dehydration at 110°C (Figure 2.7). It is necessary to understand the structural nature of water retained by soils to explain the observed differences in dehydration as a function of temperature.

The inclusion of organic matter in the soil matrix further confounds the selection of a reference zero. The organic fraction of soil contains many volatiles which oxidize at temperatures of 110°C although the net effect is usually quite small for agricultural soils where organic matter content is often less than 5% of the total dry weight of soil. After a 10 day drying period, a silt loam with 3% organic matter was found to have a weight loss of only 0.3% moisture by weight (Black, 1964).

The volumetric moisture content of the soil, M_v, is the volume fraction of the soil occupied by water. M_v is a function of the weight percent of water and the bulk density of the soil,

$$M_v = .01\ M_g \times \rho_b/\rho_w \qquad (2.3)$$

where: M_g = percent of water per gram of dry soil
ρ_b = bulk density of the soil, g/cm^3
ρ_w = density of water $\approx$ 1.0 g/cm^3

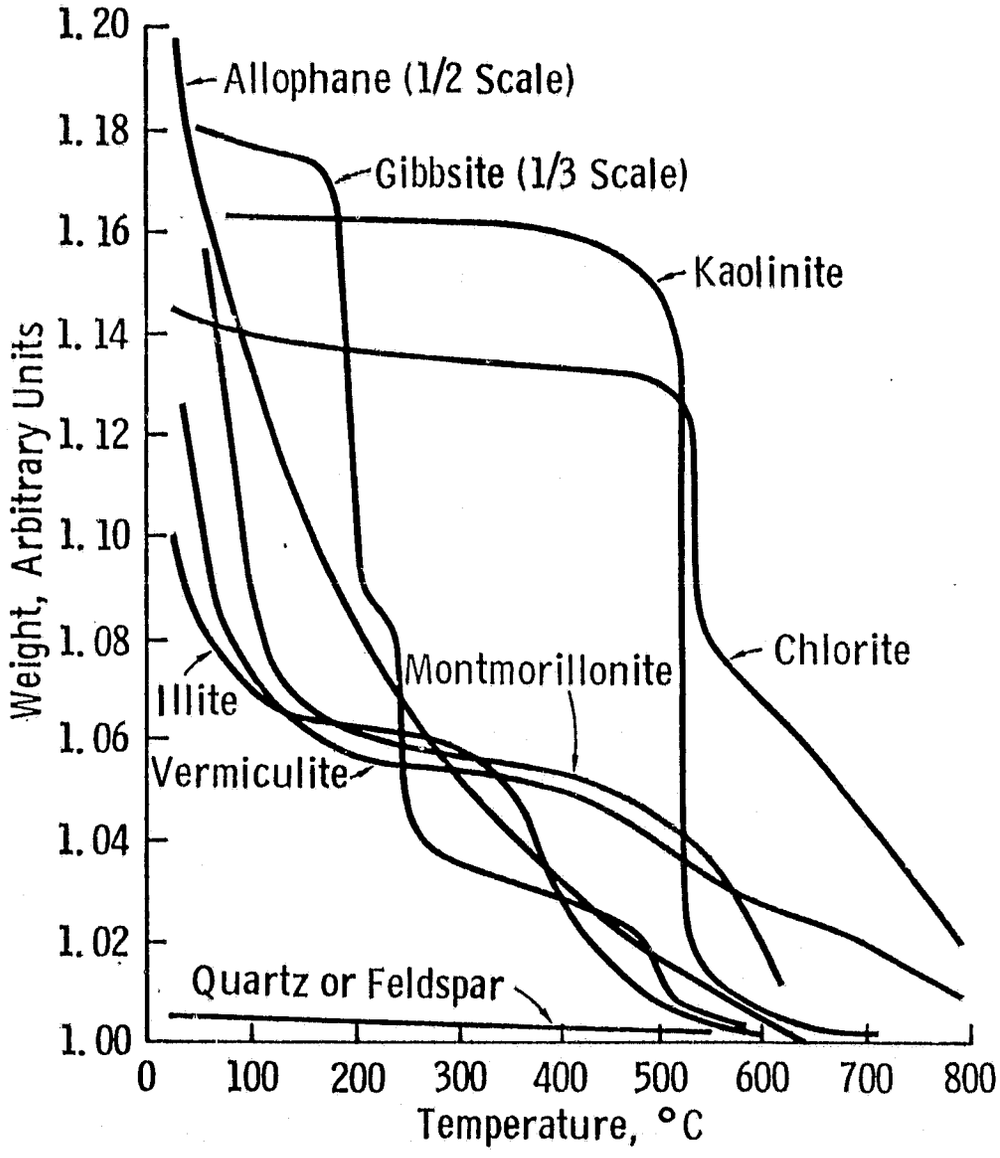

Figure 2.7. Weight loss of clay minerals as a function of temperature. The weight of the sample at a temperature of 800°C or greater is taken to be unity. Water content percentages on a mass basis may be obtained by subtracting 1 from the ordinate figure and multiplying by 100. (The numbers to the right of the decimal thus may be regarded as percentages.) (From Black, 1964).

In clay soils, gravimetric moisture M_g and bulk density are not independent due to the expansion of clay particles by adsorption of interlayer water. Thus, M_g is inversely proportional to ρ_b in clay soils. The effects of this dependence can produce a considerable error in the calculation of volumetric moisture content from M_g, up to approximately 20%, if bulk density is treated as a constant as a function of M_g. As a consequence, accurate volumetric moisture determination necessitates the concurrent measurement of soil bulk density of clay soils. Since the field measurement of bulk density is difficult and the accuracy of a particular method is often restricted to a small range of M_g, it is often impractical to make concurrent determinations of M_g and ρ_b. Appendix A further treats the problem of bulk density sampling and presents a simple physical model for estimating ρ_b as a function of M_g for clay soils.

Soil is composed of solid, liquid and gas phases. At most, the liquid phase can only occupy that volume fraction of the soil not occupied by solids, or the pore space. The pore space of a soil is defined by soil bulk density and the specific density of the soil solids. The bulk volume of soil is given as:

$$V_b = M_s/\rho_b \tag{2.4}$$

where: V_b = bulk volume of the soil, cm^3

M_s = dry mass of soil, g

ρ_b = bulk density of soil, g/cm^3

Similarly, the particle volume is determined by:

$$V_p = M_s/\rho_p \tag{2.5}$$

where: V_p = the total volume of solid particles, cm^3

M_s = dry mass of solid particles, g

ρ_p = the specific particle density of soil $\approx$ 2.65 g/cm^3

From these definitions, it follows that the volume of soil occupied by solids is given by the ratio V_p/V_b; and the porosity of the soil is $1-V_p/V_b$. The total percent porosity S_t can then be defined as:

$$S_t = 100\ (1 - \rho_b/\rho_p) \qquad (2.6)$$

By definition, percent volumetric moisture must be less than or equal to porosity,

$$100\ M_v \leq S_t$$

It should be noted that for expanding lattice clays, ρ_b is known to be dependent upon soil water content (Figure 2.8). Thus it is to be expected that the total porosity of clay soils will be proportional to moisture content.

While maximal water content of a soil is determined by its porosity, the water content of a soil, at any given point in time, is determined by the interaction of soil structure and soil-water energy relationships.

Structurally, soil water consists of pore water, solvate water, adsorbed water and structural water (Kezdi, 1974). Pore water occupies the macropores of the soil matrix; its volume is established by the effect of hydrodynamic forces acting upon the capillarity of the pore size distribution within the soil. The behavior of pore water is physically and chemically equivalent to that of bulk water having the same salt concentration. Solvate water forms a hydration layer around soil particles. The thickness of the solvate water layer around an individual particle is dependent upon the electrostatic charge of the particle surface, ionic bonding forces within the soil solution and the polar nature of water; the solvate layer is typically 20 to 400 A° thick which corresponds to a water layer 8 to 160 molecules thick depending upon the specific particle and solution considered (Bolt and Bruggenwert, 1976). Solvate water may have a greater density and viscosity than bulk water, although much of it can still flow under the hydrodynamic forces governing the flow of pore water. Adsorbed water is a tightly held hydration shell of 1 to 10 monomolecular layers of water adjacent to the solid surface depending upon the mineralogy of the particle and the ion concentration of the

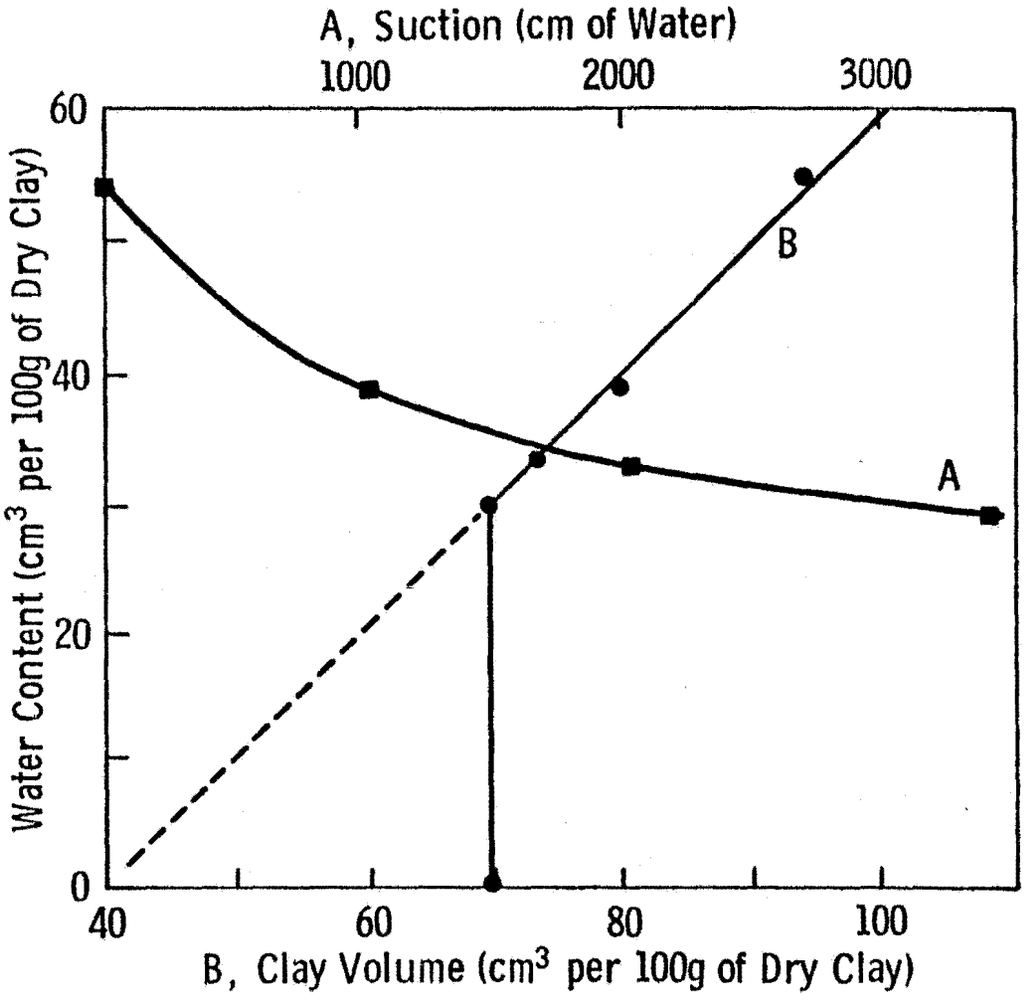

Figure 2.8. The moisture characteristic and swelling curve of a sample of kaolin clay (from Childs, 1969).

solution (van Olphen, 1963). The adsorbed water cannot be moved by the influence of normal hydrodynamic forces and cannot be completely removed by traditional oven drying procedures at 110°C. Structural water is not true water in the formal sense of the term, and is composed of the hydroxyl groups within the crystal lattice structure of primarily the layer aluminosilicates. Structural water cannot be removed from the crystal lattice without severe modification of the crystal.

The dehydration curves of common soil minerals in Figure 2.7 illustrate the relative differences in the volume of water held in given structural states. The pore water and most solvate water is evaporated from all the minerals at 100°C. The remaining solvate water and the adsorbed water are typically evaporated at temperatures less than 200°C. The amount of structural water is shown by the relatively horizontal portions of the curves at 16%, 6% and 1% for kaolinite, montmorillonite and quartz respectively. Evaporation of hydroxyl groups is responsible for the weight loss of the clay minerals at about 600°C. Differential thermal analysis of a calcium montmorillonite (Figure 2.9) illustrates the amount of heat required to liberate the various forms of water held by the clay. All pore and solvate water is evaporated by the adsorbed heat between 0° and the endothermic peak at ≈ 120°C. The shoulder on this endothermic peak is due to the vaporization of adsorbed water at temperatures between ≈ 150 to 200°C. The loss of hydroxyl water at 600°C causes a second endothermic peak. The exothermic peak at 900°C is attributed to phase changes in the crystal lattice structure and is preceded by the endothermic evaporation of the final traces of structural hydroxyl water (van Olphen, 1963).

2.1.5 Energy of Soil Water

The free energy of soil water characterizes the summation of potential, kinetic and electrical energy acting upon the soil water system. The dominant forces affecting the free energy of soil water are gravitational, matric and osmotic. The status of free energy of soil water is measured as a potential, where soil water potential is defined as the difference between the energy of soil water and that of pure water (Brady, 1974). The soil water potential is commonly referenced to the energy of pure water at an arbitrary water table. The soil

Figure 2.9. Differential thermal analysis (DTA) of a montmorillonite (schematic) (from van Olphen, 1963).

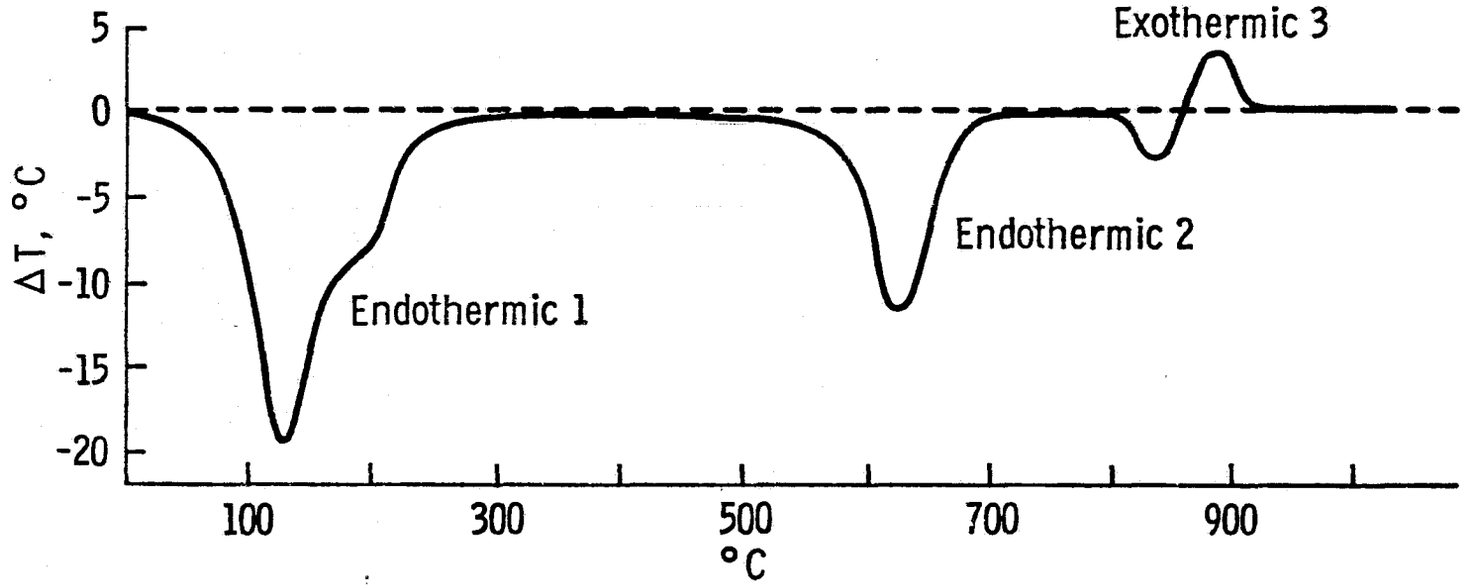

Endothermic Reaction 1 = Loss of Surface Hydration Water
Endothermic Reaction 2 = Loss of Lattice Hydroxyl Water
Exothermic Reaction 3 = Crystal Phase Change

solution may occur as thin films covering the soil particles or as pore water at higher moisture contents. Only at moistures near saturation does the soil solution exhibit the properties of flow, vaporization and internal energy that characterize bulk water. As a result, the energy relations of film and pore water have proven themselves more useful in the study of plant-soil-water relations than the properties of bulk water (Taylor and Ashcroft, 1972).

Total soil water potential is the sum of the potentials arising from each of the forces acting upon the soil water system (Figure 2.10). The gravitational force produces a positive potential and functions to transport water to lower elevation in the soil profile. The gravitational force acts primarily on the pore and some solvate water in the capillary maze of the soil matrix. The matric potential measures the attraction of the soil water molecules to each other and to soil solid surfaces due to cohesive and adhesive forces respectively. The cohesive force produces the surface tension of water. The phenomenon of capillarity is due to the combined effects of surface tension and adhesion of water to the soil solid surfaces. Thus, the matric potential is negative since it functions to reduce the free energy of soil water.

The osmotic potential of soil water is also negative; it is the result of attractive forces of ions and other solutes which tend to hydrate by orienting polar water molecules. The electrostatic fields of ions cause a polarization and binding of surrounding water molecules in a manner described by a model of three concentric water regions enveloping the ion (Kavanau, 1964). An innermost region of structured, polarized and electrostructured water molecules grades into an intermediate region where the water is less structured than ordinary water and an outermost region of bulk water. Polarization is found to be proportional to the charge of the ion and inversely proportional to ionic radius squared (Nielson, et al., 1972). Thus, the polarizing effects are observed to be most pronounced for small highly charged ions such as sodium (Shainberg and Kemper, 1966).

Since osmotic and matric potentials are negative, it is convenient to describe them in terms of positive tensions or suctions by which the water is held within the soil. The tension of soil water describes the

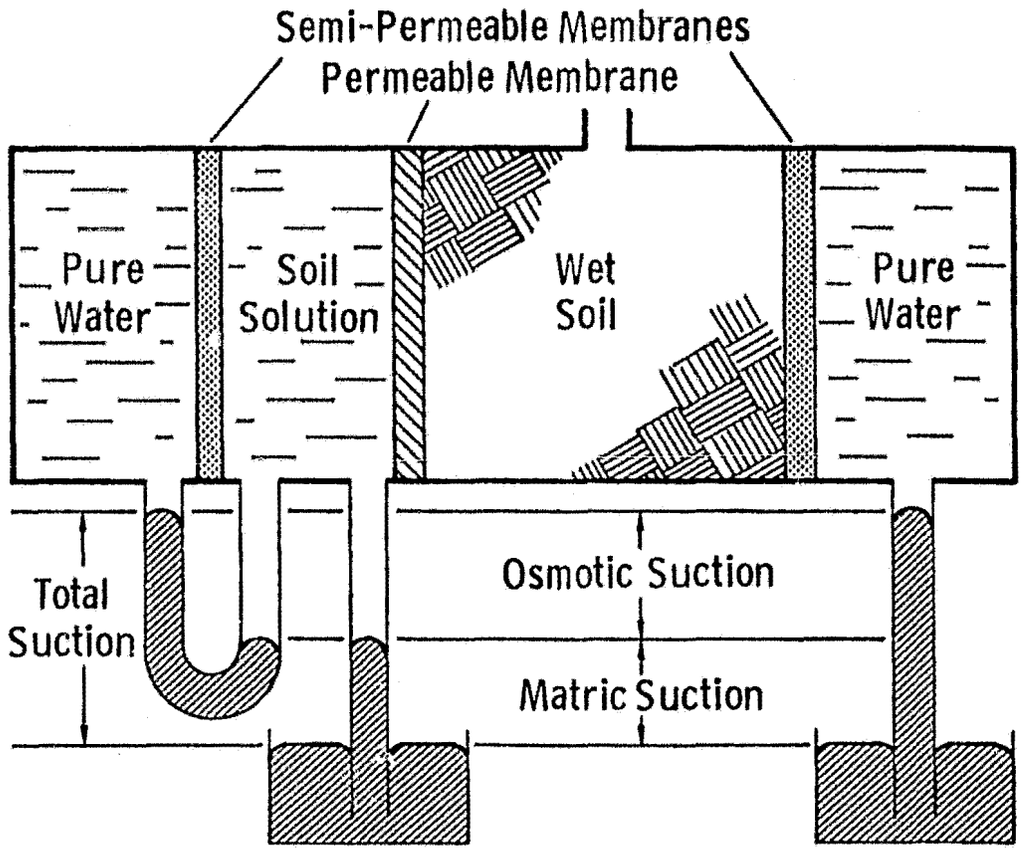

Figure 2.10. Soil water potential. In an isothermal equilibrium system, matric suction is the pressure difference across a membrane separating soil solution (equilibrium dialyzate) in bulk from soil containing the solution, the membrane being permeable to solution, but not to matrix or to mass flow of gas; osmotic suction is the pressure difference across a semipermeable membrane separating bulk phases of pure water and the soil solution; total suction is the sum of the matric suction and the osmotic suction and is the pressure difference across a semipermeable membrane separating pure water and soil that contains solution. An ideal semipermeable membrane is permeable to water only (modified from Black, 1964).

free energy of the soil water and its availability to plants or for mass movement under the influence of hydrodynamic forces. Suction is commonly expressed in terms of the height of a water column whose weight equals the suction or as pF which is the logarithm to the base 10 of this column height in cm. Approximate equivalents between suction expressed as cm of water, pF and atmospheres are given in Table 2.7. In the American literature, suction or tension is more commonly expressed in terms of atmospheres or bars of pressure. The relevant conversion factors are:

$$1 \text{ bar} = 1 \times 10^6 \text{ dynes/cm}^2$$

$$1 \text{ millibar} = 1 \times 10^3 \text{ dynes/cm}^2$$

$$1 \text{ bar} = 0.98692 \text{ atmosphere}$$

$$1.0133 \text{ bar} = 1.0 \text{ atmosphere}$$

$$1 \text{ bar} = 1033.26 \text{ g/cm}^2$$

$$1 \text{ bar} = 1022.7 \text{ cm of pure water at } 25^{\circ}\text{C}$$

Soil water energy potential, as measured by soil suction, is related to soil water content for a given soil and moisture history. However, soil tension is not a direct expression of the thickness of water films around soil particles but also depends upon soil structure, specific surface and the solute content of the soil water.

The differences in soil water retention at various tensions between soil textural classes observed in Figure 2.11 correspond to differences in pore size and shape distributions combined with differences in the nature and strength of adsorptive forces for soil particles with differing mineralogy. Coarse textured soils, such as sand, are characterized by comparatively large pores which can hold water only at low suctions. On the other hand, clay soils have a much finer network of pores and soil water retention is dominated by the interaction of soil water with a large relative surface area. Thus, a considerable range of the water content of clays is highly controlled by higher tension matric and osmotic forces.

An explanation of the dramatic differences in soil water retention between soil textural classes at suctions greater than ≈ 1 bar lies

TABLE 2.7

Approximate Equivalents of Common Means of Expressing Differences in Energy Levels of Soil Water (from Brady, 1974).

Height of Unit Column of Water (cm)	Logarithm of Water Height (pF)	Atmosphere (bars)
10	1	0.01
100	2	0.10
346	2.53	$\frac{1}{3}$
1,000	3	1
10,000	4	10
15,849	4.18	15
31,623	4.5	31
100,000	5	100
1,000,000	6	1,000
10,000,000	7	10,000

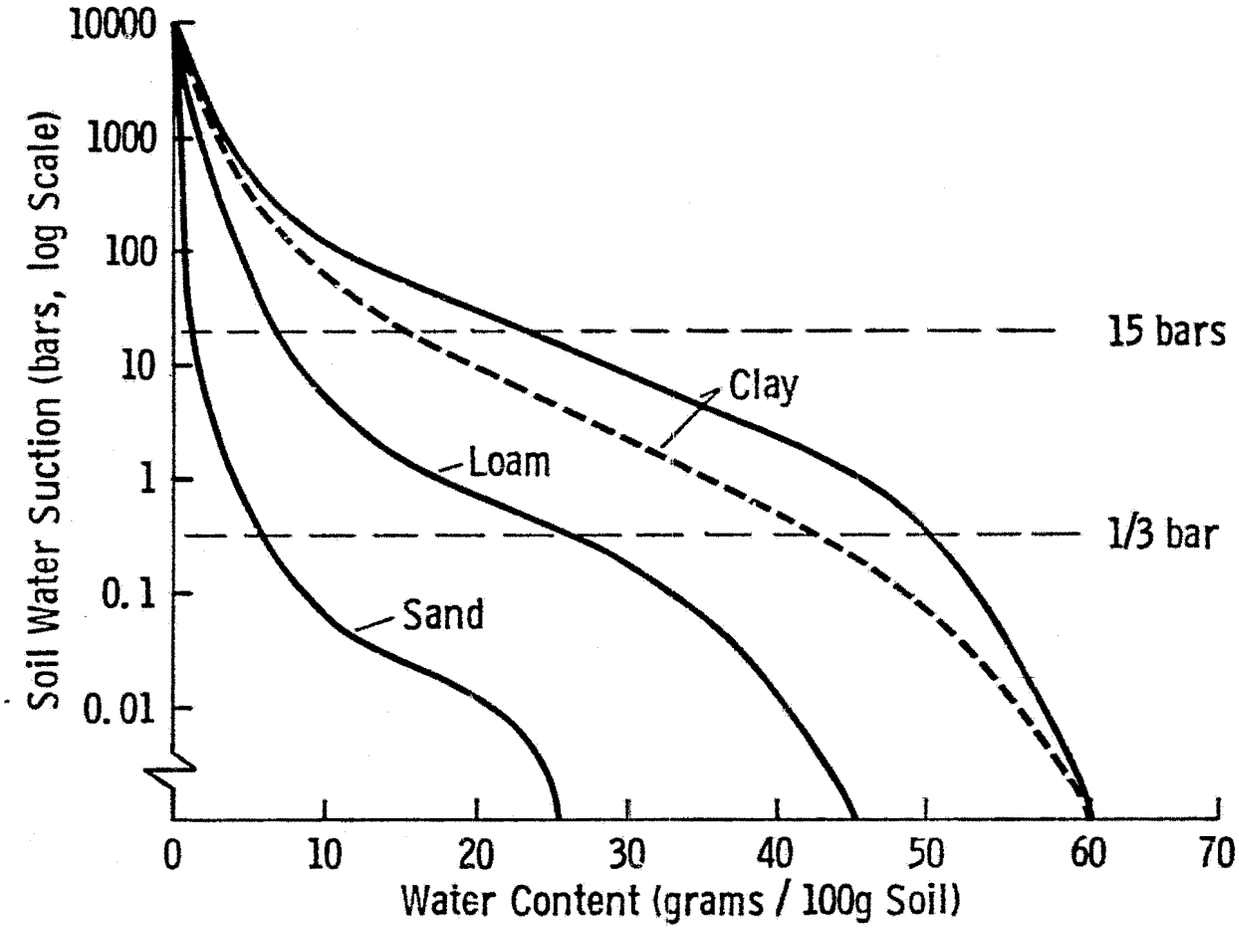

Figure 2.11. Soil moisture suction curves for three representative mineral soils. The solid lines show the relationship obtained by slowly drying completely saturated soils. The dotted line for the clay soil is the relationship expected when a dry soil is wetted. The difference between the two clay lines is due to hysteresis (modified from Brady, 1974).

in the differences in net surface area per unit volume and the behavior of water at the soil solid surfaces. It was previously stressed that the specific surface area of soil increases as particle size decreases, as particle shape becomes less spherical and as clay content increases (thus increasing internal interlayer surface area). The remainder of this section will deal with the surface interaction between the soil solution and the soil solids.

As was mentioned earlier, the internal structure of the clay crystal lattice has a charge imbalance due to the isomorphous substitution of lower valence cations for silicon and aluminum ions. As a result, the clay mineral particles have a constant negative surface charge distributed on the layer surfaces whose magnitude is dependent upon the mineralogy of the lattice structure. The electroneutrality of the clay particle is maintained by the adsorption of cations (Na^+, Ca^{++}, K^+, M_g^{++}) on the crystal unit layer surfaces. These exchangeable surface cations can become completely disassociated from the particle when hydrated.

In contrast, the surface charge of oxides (such as SiO^2 or quartz) is determined by the incomplete terminal molecular layer at the crystal edge. The loss of coordinating cations at the frayed particle edge leads to the partial hydroxylization of the surface which, when hydrated, produces a surface charge highly dependent upon pH. This means that for soil solutions very high in H-ion concentration, the surface may adsorb more protons than needed for neutralization and result in a positive surface charge (Bolt and Bruggenwert, 1976). This situation also exists at the broken edges of silicon tetrahedral layers in the clay minerals such that there exists a pH dependent potential surface charge at the frayed edges and a constant negative surface charge on the layer faces.

Within the liquid layer adjacent to the charged particle surfaces, the dissociated exchangeable cations tend to remain in the neighborhood of the spatially fixed lattice surface charge imbalances. The surface charge density Q of a given soil is the ratio of the cation exchange capacity to the specific surface,

$$Q = CEC/S, \ meq/m^2. \qquad (2.7)$$

The density of the surface charges determines the magnitude of an electrostatic field extending into the adjacent liquid layer. The electric field attracts compensating dissociated counter-ions and repels ions of like charge thus producing what is termed the electric double layer (Gouy, 1910; Stern, 1924). The accumulation of counter-ions within the hydration shell adjacent to the solid surface is not complete, however, since the adsorptive force of the electric field is opposed by the diffusion of counterions from the surface toward the lower ionic concentration in the bulk solution. The opposing tendencies of entropy and electrostatic attraction produce an exponential decrease in counterion concentration as a function of distance from the soil solid surface (Figure 2.12). The resultant counterion atmosphere is known as the Gouy layer which represents a condition of minimum free energy in the system. The Gouy layer also consists of a distribution of co-ions (charge similar to that of the surface charge) whose concentration increases exponentially with distance from the solid surface due to electrostatic repulsion (van Olphen, 1963). By use of the Poisson-Boltzmann equation from electrostatic and diffusion theory, the distribution of positive and negative ion concentrations can be calculated as a function of distance from a solid surface of known charge density.

$$C_1/C_0 = e^{(-\Delta E/kT)} \qquad (2.3)$$

where: C_1/C_0 = ratio of counterion concentration near the surface to that of the bulk solution

ΔE = the potential energy difference of ions in the attractive field

kT = the kinetic energy of the ion where k is Boltzmann's constant and T is the absolute temperature.

The ion concentration of the Gouy layer is shown in Figure 2.13 for a negatively charged particle surface. The effects of a change in the solute concentration of the bulk solution are shown for a frayed particle edge which is typified by a constant surface potential and for a clay unit layer face which is typified by a constant surface charge in Figures 2.13a and b, respectively. The lines AD and CD represent the

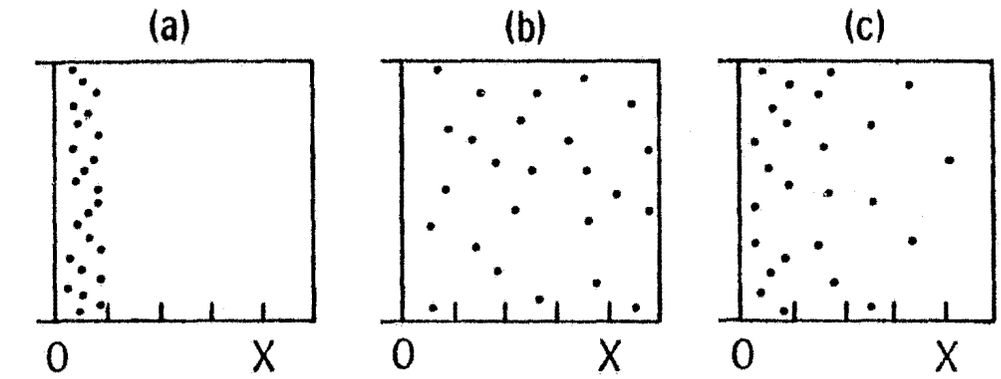

Distribution of counterions

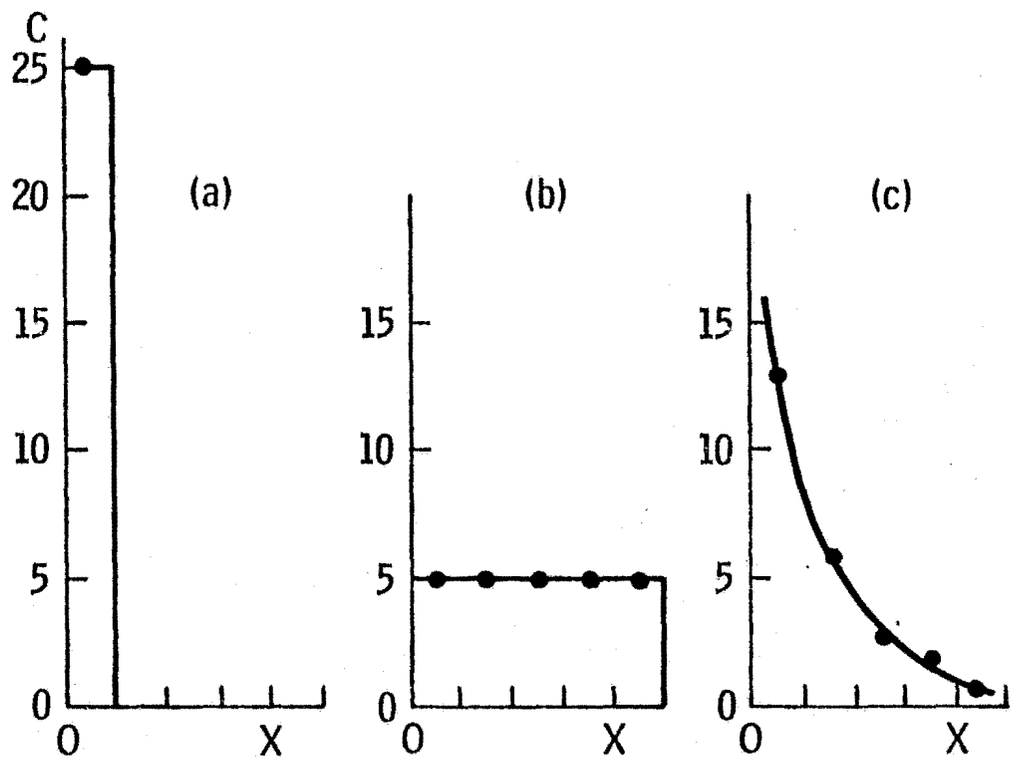

Concentration of counterions in the double layer

Figure 2.12. Distribution and concentration of counterions in the electric double layer for a) condition of minimum Energy, b) condition of maximum Entropy, and c) condition of minimum Free Energy, actual distribution (modified from Bolt and Bruggenwert, 1976).

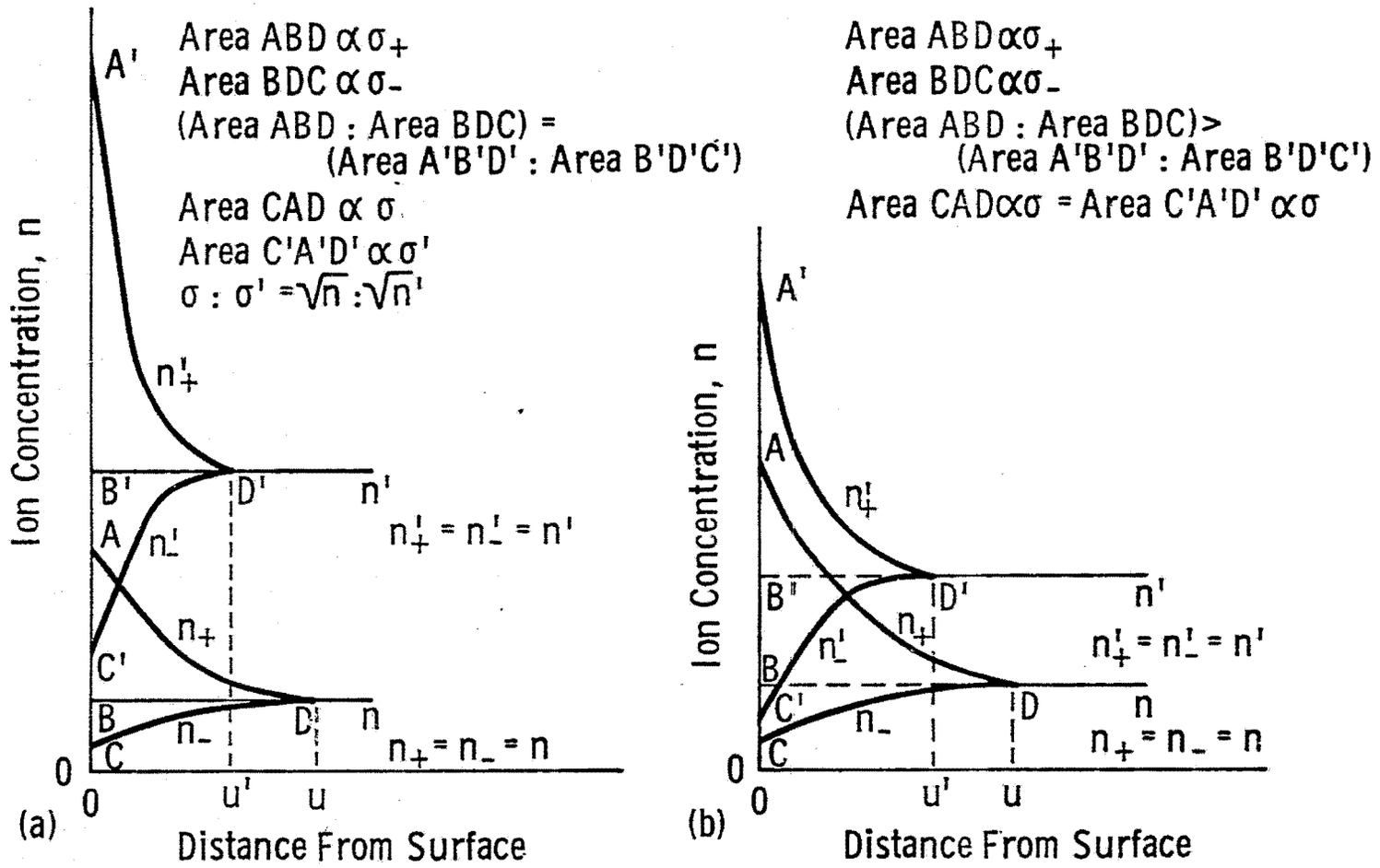

Figure 2.13. Charge distribution in the diffuse double layer of a negative particle at two electrolyte concentrations. a) constant surface potential at crystal edges and b) constant surface charge at clay layer faces (modified from van Olphen, 1963).

respective counterion and co-ion concentrations in the soil solution as a function of distance from the particle surface. The extent of the diffuse double layer into the bulk soil solution is given as the distance from the solid surface at which the co-ion and counterion concentrations are equivalent to those of the bulk solution; this is shown graphically as the relative length of line BD. The net surface charge of the particle surface is equal to the area defined by CAD. In Figure 2.13a the Gouy layer of the frayed crystal edges is shown to be pH dependent; an increase in the bulk electrolyte concentration from level BD to B'D' results in the compression of the double layer towards the particle surface from distance μ to μ' and results in a net increase of the surface charge. In contrast, an increase of the bulk electrolyte concentration adjacent to a clay layer face (Figure 2.13b) causes no change in the net surface charge although the Gouy layer is also shown to be compressed towards the particle surface. It should be remembered that the effects shown in Figure 2.13b dominate the net behavior of the soil when clay is present because of the large specific surface of clay crystal layer faces having a constant surface charge relative to the area of crystal edges or the external surfaces of coarser silt and sand sized particles which have a constant surface potential.

The theoretical thickness of the diffuse double layer, as defined above, is shown in Table 2.8 for various electrolyte concentrations of monovalent and divalent counterions. For normal soils, the total electrolyte concentration varies from about .01 normal at field capacity to roughly .1 normal at wilting point with approximately equal amounts of monovalent and divalent cations in solution, while saline soils are about .1 normal electrolyte concentration at field capacity (Bolt and Bruggenwert, 1976). If the diameter of a water molecule is taken as approximately 2.76A^{o}, the thicknesses shown in Table 2.8 correspond to from 2 to 362 monomolecular layers of water.

The theoretical thicknesses of the double layer given in Table 2.8 assume that a particle surface is adjacent to an infinite volume of bulk solution; this condition is not usually true within the soil matrix. Within the soil, interparticle distances are often less than twice the electric double layer; Figure 2.14 compares the counterion concentration for such a situation with that of unimpeded Gouy layers.

TABLE 2.8

Approximate "Thickness" of the Electric Double Layer As a Function of Electrolyte Concentration at a Constant Surface Potential (from van Olphen, 1963).

Concentration of ions of opposite charge to that of the particle, mole/liter	"Thickness" of the double layer, Å	
	Monovalent ions	Divalent ions
0.01	1000	500
1.0	100	50
100.	10	5

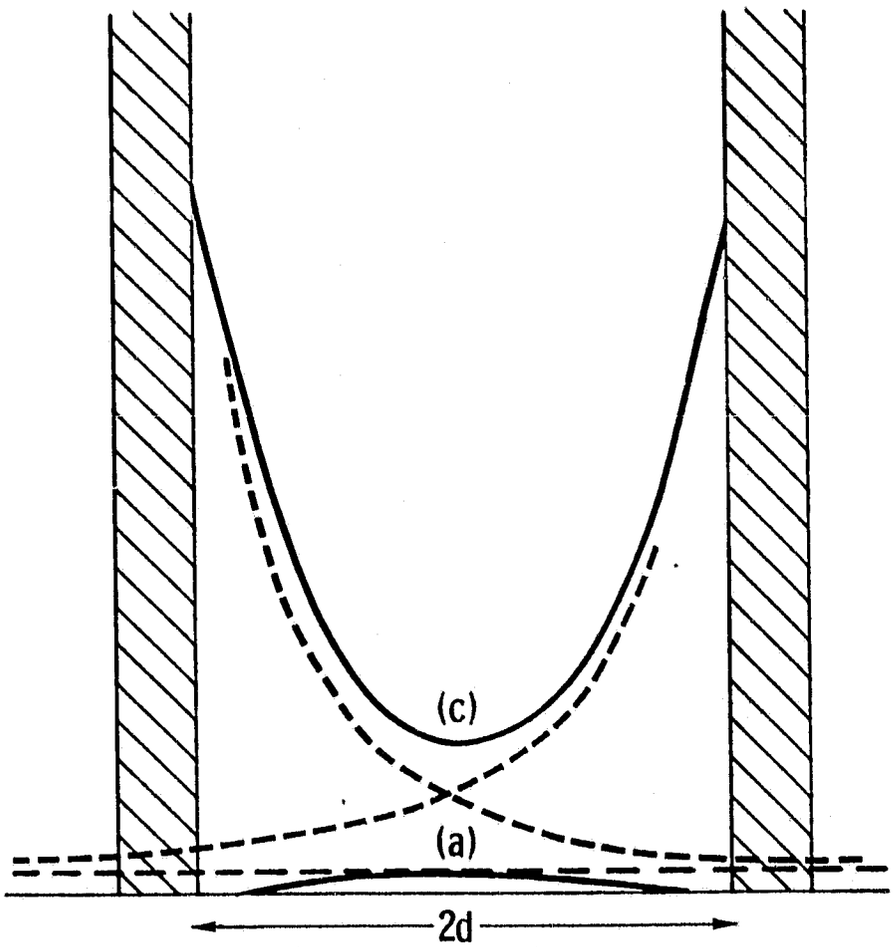

Figure 2.14. The distribution of ions in the Gouy layer between two parallel plane micelles. Broken lines indicate unimpeded Gouy layers (from Childs, 1969).

As a soil is dried by evaporation, water is removed in the vapor phase and ions are forced to remain in the liquid phase. Thus, as drying proceeds due to evapotranspirative demands, the electrolyte concentration of soil water tends to increase. Below a certain moisture, the voids between adjacent soil solid surfaces will no longer be completely filled with soil solution and water will consist of film layers around the soil particle surfaces (both external and internal). Continuing dehydration will cause the thickness of the water film layer to become smaller than the double layer thickness. Truncation of the diffuse electric double layer causes continued adjustment of the ionic concentrations in solution (Figure 2.15). A truncated double layer develops a powerful swelling pressure when brought into contact with additional water. This swelling pressure can be of sufficient magnitude in expanding lattice clays, such as montmorillonite, to close inter-aggregate pores and reduce the hydraulic conductivity of the soil.

The spacing between the centers of adjacent crystal unit layers of dry 1:1 and 2:1 alumina silicates is approximately 7.2A^{o} and 9.6A^{o}, respectively (van Olpehn, 1963). In the case of montmorillonite, the initial contact with water produces an increased spacing on the order of 12.5-20A^{o}, depending upon the specific clay and counterions present. This initial interlayer swelling, at most, doubles the volume of the dry soil by adding 1 to 4 monomolecular water layers in a very stable configuration; the initial swelling is attributed to surface hydration and counterion hydration within the electric double layer. The forces holding water to the soil surface in this region are very strong; van Olphen (1963) estimates that the energy required to remove the last few layers of water is on the order of 50-100 ergs/cm^{2} which corresponds to a pressure of approximately 60,000 psi or 4,000 atmospheres.

At crystal unit layer separations in excess of 10A° the surface hydration energy is no longer important and subsequent swelling of clays is due to osmotic swelling. Osmotic swelling is caused by the double layer repulsion between adjacent solid surfaces and the extent of such swelling is limited by van der Waals attraction between the solids and the presence of positively charged particle edge to negatively charged layer face linkages (Mitchell, 1976). Osmotic swelling reduces the truncation of

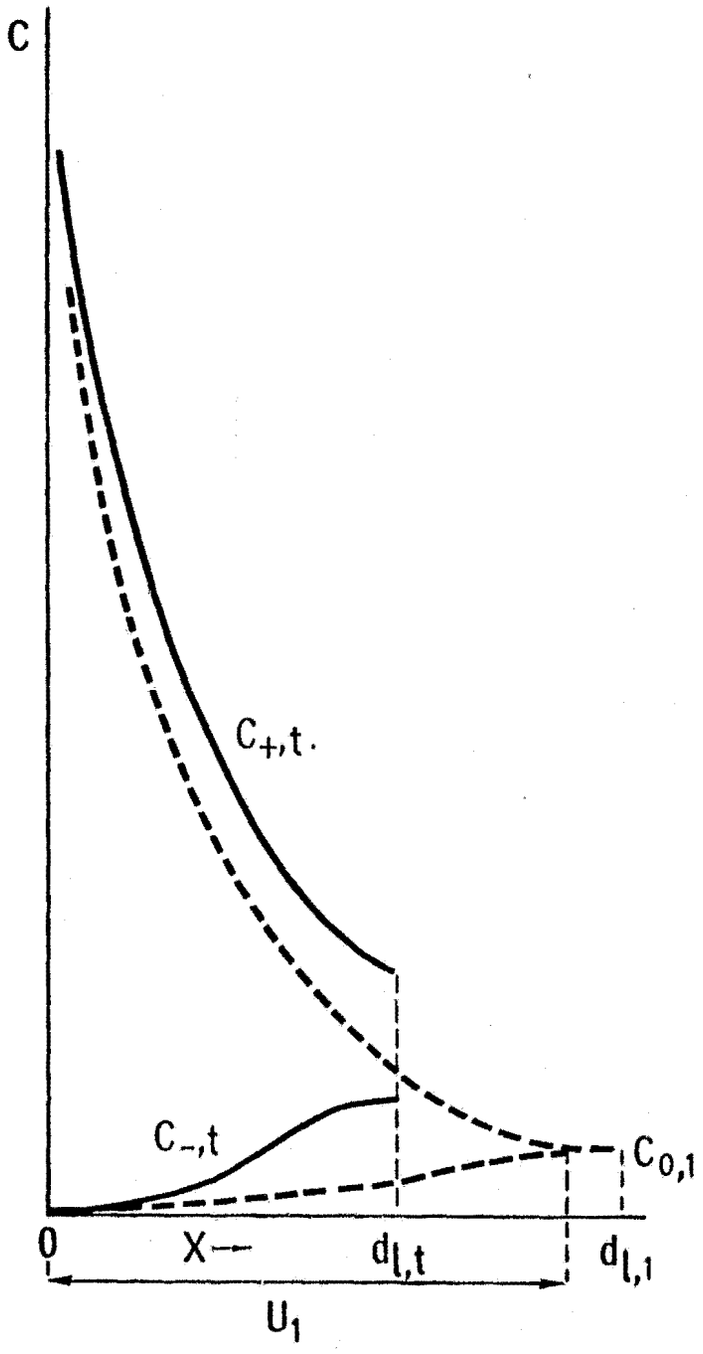

Figure 2.15. Concentration distribution in a truncated double layer formed by removing part of the water from a system with an initial thickness of the water layer $d_{1,i} > u_i$ while in equilibrium with $c_{0,1}$. Note that $\int_0^{d_i} c\,dx$ remains constant as no salt is removed (from Bolt and Bruggenwert, 1976).

adjacent Gouy double layers to the extent permitted by the above mentioned inter-particle attractive forces. Osmotic swelling pressures decrease with increasing water content of the soil from a soil suction of about 30 atmospheres to less than 0.1 atmosphere (van Olphen, 1963). Osmotic swelling can be responsible for the addition of up to 20 monomolecular layers of interlayer water depending upon the clay mineralogy and the electrolyte concentration.

For a given particle surface of known charge density and a solution of known electrolyte concentration, the average electric potential can be computed at any point with respect to the surface from the Gouy layer model. The potential will have a maximum value at the surface and decrease exponentially with distance from the surface (Figure 2.16). An increase in electrolyte concentration around oxides such as quartz or clay crystal edges will result in a more rapid decay of electric potential with distance from a constant surface potential (Figure 2.16a), while the effect upon the constant surface charged clay layer faces is to uniformly reduce the electrical potential at all distances (Figure 2.16b).

The magnitude of the electric potential at any given point in the soil solution determines the degree of orientation of dipolar water molecules within the electrostatic field maintained by the soil solid surfaces. Since the field strength and electric potential decrease with distance from the particle surface, the rigidity of water molecule orientation also decreases exponentially with distance (Nielson, et al., 1972). In addition, the freedom of water molecules to oscillate within an impressed field of microwave energy is inversely proportional to the force by which water is rigidly oriented relative to the soil solid surface. Thus, the dielectric constant of water at microwave frequencies can be expected to increase exponentially with distance from the soil solid surface as electrostatic attractive forces diminish.

The compression of the electric double layer with increasing electrolyte concentration (Figures 2.13 and 2.14) is important to the present discussion because of its effect upon the dielectric constant of soils with low moisture contents and of saline soils at any moisture content. In general, the effect of increased electrolyte concentration will be to decrease the

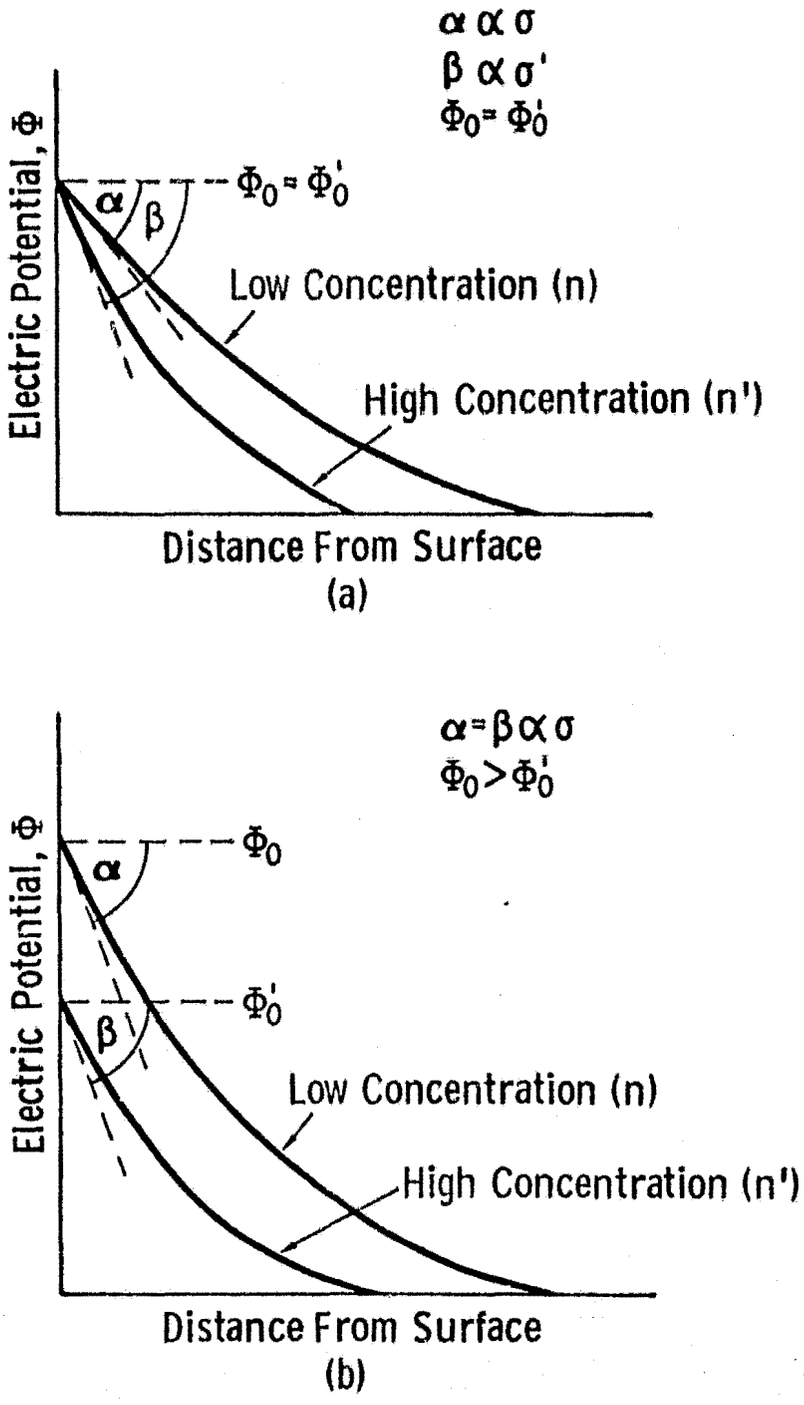

Figure 2.16. Electric-potential distribution in the diffuse double layer at two electrolyte concentrations. (a) Constant surface potential. (b) Constant surface charge (from van Olphen, 1963).

electric potential of water molecules relative to the solid surface and thereby increase dielectric constant. As a result, the dielectric constant of saline soils will be higher than that of more neutral soils (all other parameters being equal). At high moisture contents of the soil where the volume of soil water is in excess of that needed to hydrate all of the diffuse electrical double layer, the excess water will have the dielectric characteristics of bulk water at that particular electrolyte concentration.

In summation, the dielectric behavior of soil is governed by the dielectric constant of soil solids and the dielectric constant of soil water which is dependent upon the surface charge density of the solids at a given electrolyte concentration, the specific surface and the total water content of the soil. Since the surface charge densities of commonly occurring soil minerals are very similar in spite of large differences in CEC (Table 2.9), the net dielectric behavior of soils are dominated by the specific surface area of soils due to particle size distribution and internal surface area acting in conjunction with the volume of water at given electrolyte concentrations. Hence, it is to be expected that the dielectric constant of moist soils should exhibit a pronounced dependence upon soil texture.

2.2 Electrical Behavior of Soil Water

Variance in the electrical behavior of soil water has been observed at microwave frequencies in measurements of the dielectric constant and in measurements with passive and active microwave sensor systems. These differences have been variously attributed to the effects of salinity, bulk density, and "bound" water among others.

2.2.1 Dielectric measurements of soils

The effects of soil texture on microwave sensor response to soil moisture are predicated upon the complex dielectric constant of moist soils. In general, the real part of the dielectric constant is about 3.5 for the dry mineral constituents of soil and about 79.0 for pure water, more than an order of magnitude in difference. Dielectric measurements of soils have been made by numerous investigators for a

TABLE 2.9

Properties of Various Clay Minerals
(from Baver, Gardner and Gardner, 1972).

a. The Specific Surface, Cation-Exchange Capacity, and Density of Charge :

Clay mineral	Specific surface (m^2/g)			Cation-exchange capacity (me/g)	Density of charge ($me/m^2 \times 10^3$)	
Kaolinites	5- 20*			0.03-0.15†	6-7.5‡	
Illites	100-200*			0.10-0.40†	1.0-2.0‡	
Vermiculites	300-500*			1.00-1.50†	3.0-3.3‡	
Montmorillonites	700-800*			0.80-1.50†	1.1-1.9‡	
	N_2	CPB	E.G.		N_2	CPB
Illite-1§	93	96	91	0.26	2.8	2.7
Illite-2§	132	138	144	0.41	3.1	2.9
Kaolinite-1§	17	21	21	0.043	2.5	2.0
Kaolinite-2§	36	36	—	0.050	1.4	1.4
Kaolinite-3§	40	9	13	0.030	0.75	3.3
Montmorillonite-1§	47	800	—	0.98	21.0	1.22
Montmorillonite-2§	49	600	—	0.98	21.0	1.6
Montmorillonite-3§	101	800	—	0.99	9.8	1.22

* Fripiat (1964).
† Grim (1962). (Used with permission of McGraw-Hill Book Co.)
‡ Calculated from the data in second and third columns.
§ Greenland and Quirk (1964).
CPB = cetyl pyridinium bromide.
E.G. = ethylene glycol.

b. Heat of Wetting, Specific Surface, Cation-Exchange Capacity, and Density of Charge (from Greene-Kelly, 1962).

Clay mineral	Heat of wetting (cal/g)	Specific surface (m^2/g)	CEC (me/g)	Density of charge ($me/m^2 \times 10^3$)
Kaolinite-1	1.6	14.8	0.035	2.4
2	1.4	12.0	0.023	1.9
3	1.4	11.0	0.019	1.9
4	2.1	25.0	0.043	1.7
Hydrous mica-1	7.6	150	0.25	1.7
2	4.8	110	0.17	1.5
3	7.9	160	0.30	1.9
4	16.5	250	0.43	1.7
Montmorillonite-1	16.5	690	0.92	1.3
2	17.4	640	0.83	1.3
3	22.2	700	1.13	1.6

variety of soil textures. Results pertinent to the present discussion are presented below.

The complex dielectric constant consists of a real and an imaginary part:

$$K_r = K'_r - jK''_r \qquad (2.9)$$

where: $j = \sqrt{-1}$

K'_r = the relative permittivity

K''_r = the effective conductivity

The real and imaginary parts of the complex dielectric constant for water can be computed from the Debye equations as modified by Lane and Saxton (1952) to include ionic conductivity effects of salt solutions:

$$K'_{rw} = K_\infty + \frac{(K_s - K_\infty)}{1 + (f/fo)2} \qquad (2.10)$$

and

$$K''_{rw} = (f/fo)\frac{(K_s - K_\infty)}{1 + (f/fo)2} + \frac{\sigma_i}{2\pi f K_o} \qquad (2.11)$$

where: $K'_{rw} = K'_r$ for water

$K''_{rw} = K''_r$ for water

K_∞ = relative permittivity at frequencies much higher than the relaxation frequency

f_o = the relaxation frequency

K_s = static relative permittivity ($f = 0$)

σ_i = ionic conductivity of the salt solution

K_o = free-space permittivity.

Cihlar and Ulaby (1974) summarized many of the dielectric measurements of soil and noted the following as regards the general behavior of dielectric constant as a function of soil moisture:

a) Moisture Effects. At low soil moistures the real part of the dielectric constant increases slowly with increasing moisture to a transition point proportional to the clay fraction of the soil (Figure 2.17). This region of low sensitivity to soil moisture is attributed to the effect of adsorbed water on the soil particle surfaces. At moistures above the transition point, the real part of the dielectric constant increases at a much faster rate with increasing moisture. The imaginary part of the dielectric constant is smaller than the real part at most frequencies and usually increases monotonically with increasing moisture content although some investigators (Geiger and Williams, 1972; Newton, 1977; Wang and Schmugge, 1978) have noted an inflection point similar to the transition point defined for the real part.

b) Bulk Density Effects. Bulk density has been shown to have a considerable effect on K_r' for given soils and minerals at constant gravimetric moisture. Cihlar and Ulaby (1974) report that studies of pumice at 10 GHz (Peake, et al., 1966) and of soil (Edgerton, et al., 1971) supports the following relationship as shown in Figure 2.18:

$$K_r' = (1 + \frac{\rho_b}{2})^2 \qquad (2.12)$$

As a result, it is necessary to express soil moisture as a volume percent to account for the dependence of K_r' on bulk density. Figure 2.19 illustrates the effect of using volumetric moisture as the soil water descriptor in place of gravimetric moisture. It can be seen that volumetric moisture units adequately account for variance in K_r' values at all measured moistures regardless of soil compaction.

c) Soil Textural Effects. As previously mentioned, the primary effect of soil texture on the measured dielectric constant appears to be the value of the transition moisture. The existance of a transition moisture or moisture range is supported by the electric double layer model which contends that the first few layers of absorbed water should have a limited mobility and thus inhibit vibration at microwave frequencies. There exists some uncertainty as to the structure of the first few layers of water forming a hydration shell around hydrophilic particles. If this water has a hexagonal grouping structure similar, but not identical, to that of ice (Hendricks and Jefferson, 1938; Ravina and Low, 1972), it could

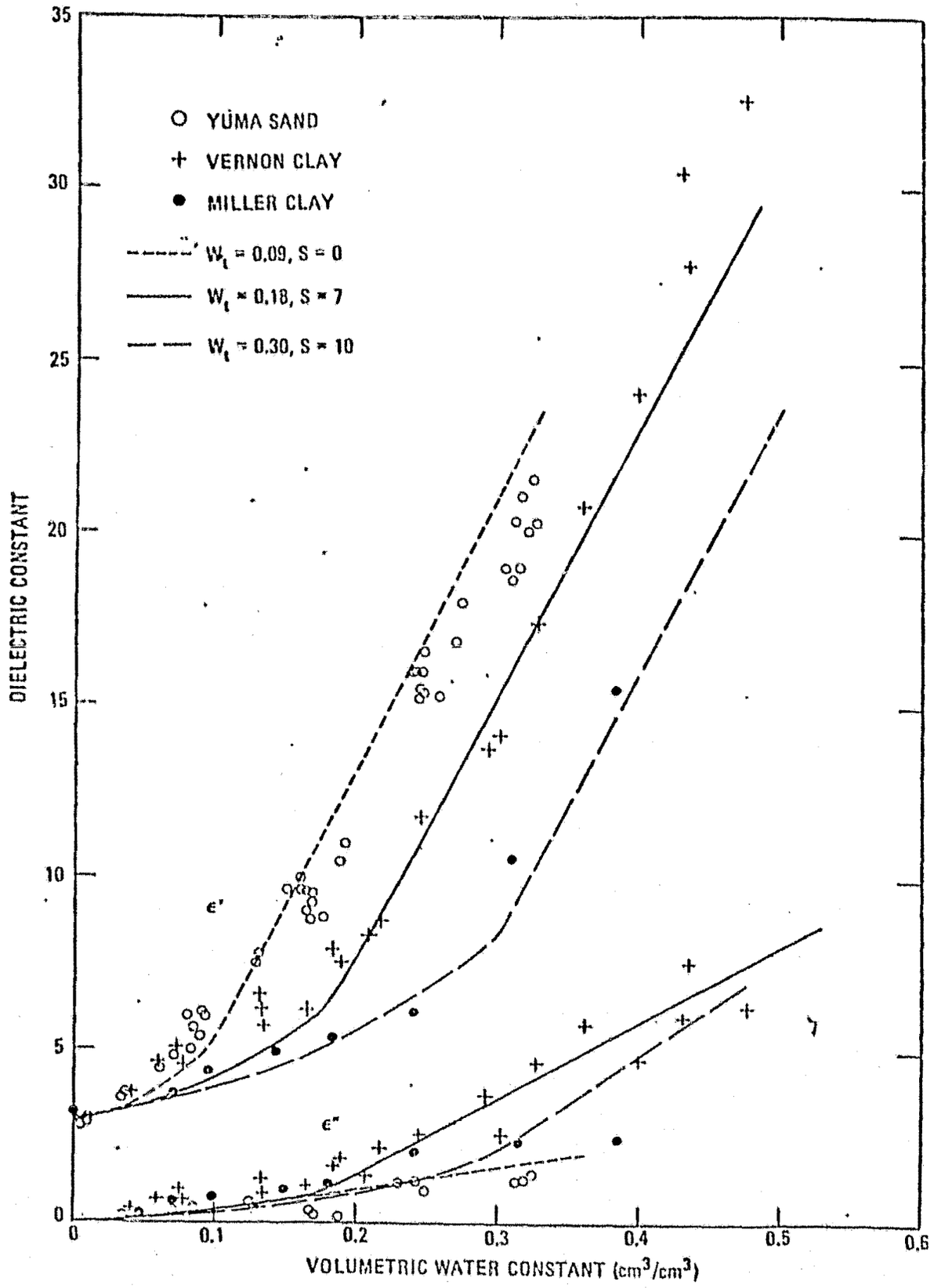

Figure 2.17 A comparison between the calculated dielectric constants from the empirical model and the measured values at 1.4 GHz. (From Wang and Schmugge, 1978).

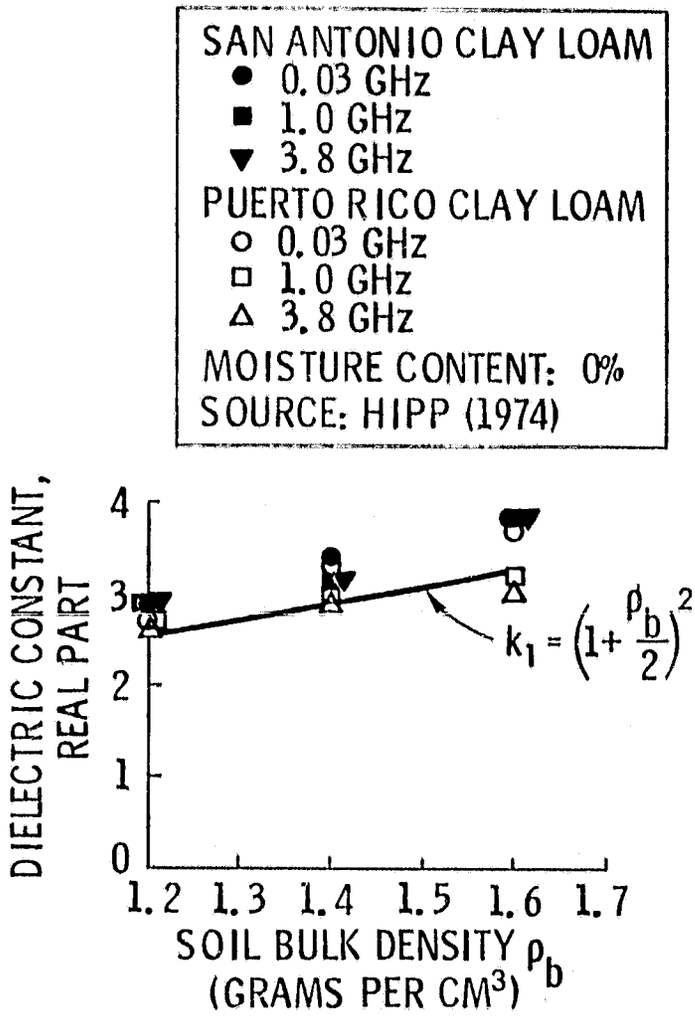

Figure 2.18 Effect of bulk density on the relative dielectric constant. (from Cihlar and Ulaby, 1974).

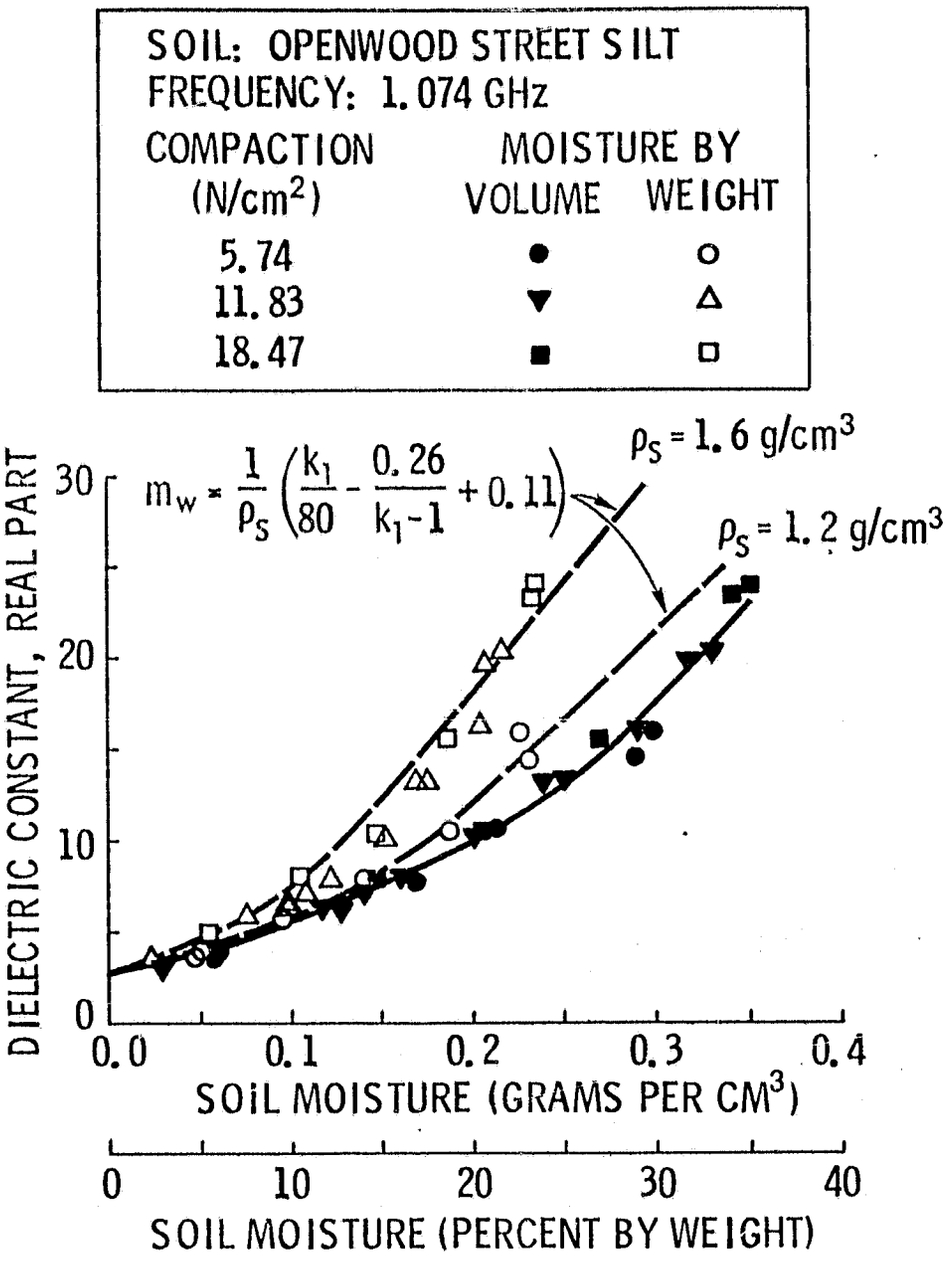

Figure 2.19 Change in relative dielectric constant due to soil moisture units used (from Cihlar and Ulaby, 1974).

have a dielectric constant about 0.1 that of free water (Grim, 1968). However, there exists evidence suggesting that water within the hydration shell is more dense than free water and more highly ordered than ice (Mitchell, 1976). The double layer model also predicts that conductivity should increase at low moisture contents due to the presence of ion concentrations inversely proportional to distance from particle surfaces. Since the imaginary part of the dielectric constant K_r'' is proportional to conductivity, the magnitude of K_r'' is proportional to the specific surface area of soils at a given moisture. Measurements of K_r'' for sand and loam at .13 to 3 GHz (Leschanskii, et al., 1971; Lundien, 1971) demonstrate that K_r'' of loam (Figure 2.20) is much higher than that of sand (Figure 2.21). These figures also demonstrate that the difference between K_r'' of loam and sand decreases with increasing frequency.

There have been many theoretical mixing formulas applied to describe the dielectric behavior of the soil-water-air system (Table 2.10). A comparison between the mixing formulas reported in the literature and actual values measured for sand, clay loam and clay (Figure 2.22) demonstrates that these theoretical models are poor descriptors of the observed dielectric behavior and fail to account for the pronounced differences between soil textural classes (Wang and Schmugge, 1978). More complex empirically derived mixing formulas have been developed which more accurately predict the observed dielectric constant as a function of volumetric moisture M_v and can account for the effects of soil texture (Wobschall, 1977; Wang and Schmugge, 1978). Wobschall (1977) treats the soil-water-air system as a complex multiple mixture of various portions of the soil solution and soil solids which appear to be qualitatively related to the double layer model and soil tension. In a more explicit approach relative to soil physics, Wang and Schmugge (1978) separate volumetric moisture into a portion above the transition moisture which is treated as bulk water and a portion less than the transition moisture which is treated as adsorbed water having the dielectric constant of ice. In Figure 2.17 the transition moisture is indicated graphically as the intersection of the two line segments for each soil. Transition moisture was observed to be independent of frequency for a given soil and was found to be highly correlated with an estimate of the water content at 15 bars of

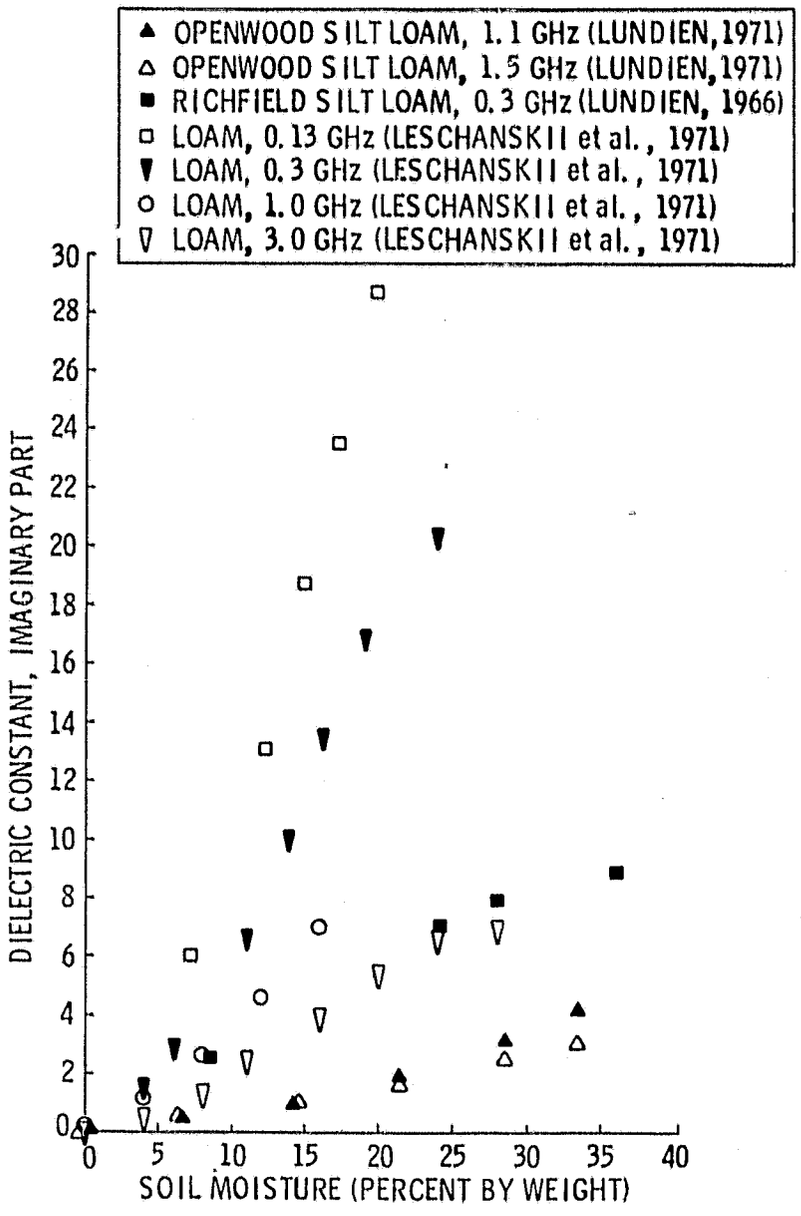

Figure 2.20

Relative dielectric constant values of soil as a function of gravimetric water content: Loam; frequency 0.13 GHz - 3.0 GHz; imaginary part (from Cihlar and Ulaby, 1974).

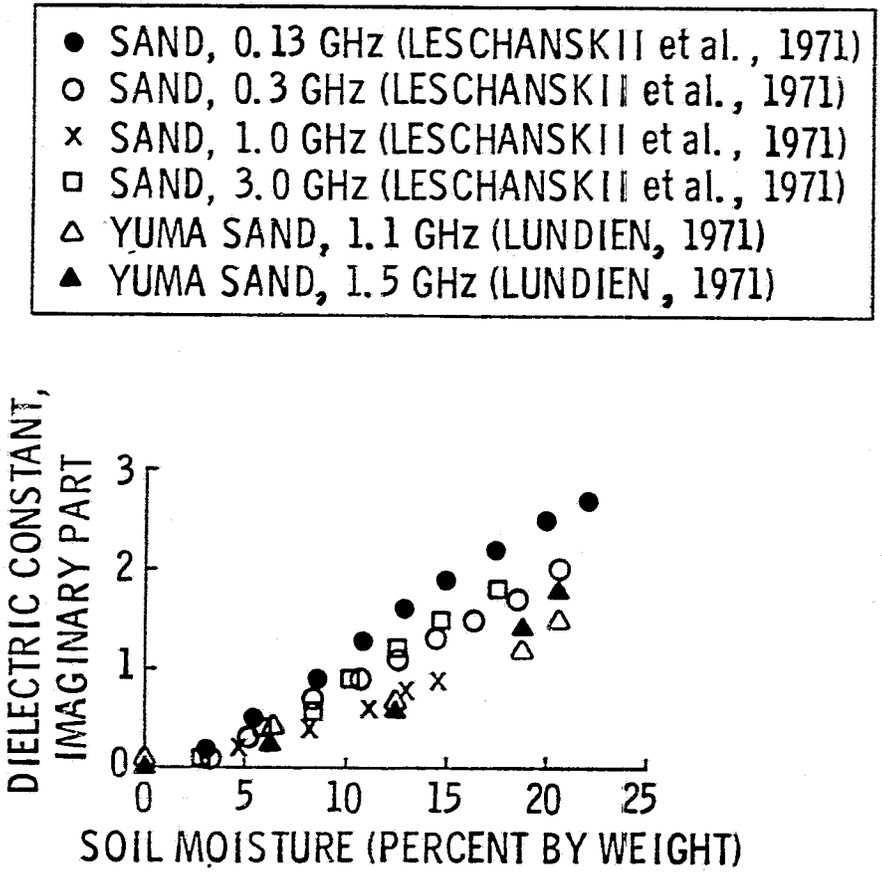

Figure 2.21 Relative dielectric constant values of soil as a function of gravimetric water content: Sand; freqeuncy 0.13 GHz - 3.0 GHz; imaginary part (from Cihlar and Ulaby, 1974).

TABLE 2.10

The Mixing Formulas Used for Comparison with the Measured Dielectric Constants of Soil-Water Mixtures (from Wang and Schmugge, 1978).

Source	Formula	Remarks
1. Rayleigh (1892)	$\frac{\epsilon - 1}{\epsilon + 2} = f_0 \frac{\epsilon_0 - 1}{\epsilon_0 + 2} + f_1 \frac{\epsilon_1 - 1}{\epsilon_1 + 2}$	$f_0 + f_1 = 1$
2. Bötteher (1952)	$\frac{\epsilon - \epsilon_1}{3\epsilon} = f_0 \frac{\epsilon_0 - \epsilon_1}{\epsilon_0 + 2\epsilon}$	
3. Brown (1956)	$\epsilon = f_0 \epsilon_0 + f_1 \epsilon_1$	$f_0 + f_1 = 1$
4. Birchak et. al. (1974)	$\sqrt{\epsilon} = f_0 \sqrt{\epsilon_0} + f_1 \sqrt{\epsilon_1}$	$f_0 + f_1 = 1$
5. Bruggeman (1935)	$\frac{\epsilon}{\epsilon_1}(1 - f_0)^3 = \left(\frac{\epsilon_0 - \epsilon}{\epsilon_0 - \epsilon_1}\right)^3$	
6. Wagner (1914)	$\frac{\epsilon - \epsilon_1}{3\epsilon_1} = f_0 \frac{\epsilon_0 - \epsilon_1}{\epsilon_0 + 2\epsilon_1}$	
7. Kharadly and Jackson (1953)	$\frac{\epsilon - \epsilon_1}{\epsilon + 2\epsilon_1} = f_0 \frac{\epsilon_0 - \epsilon_1}{\epsilon_0 + 2\epsilon_1}$	
8. Nerpin and Chudnovskii (1970)	$\epsilon = 1 \frac{3\sum_i \frac{\epsilon_i - 1}{\epsilon_i + 2} f_i}{1\sum_i \frac{\epsilon_i - 1}{\epsilon_i + 2} f_i}$	f_i = fractional volume of each constituent
9. Wiener (1910)	$\epsilon = \frac{f_0 \epsilon_0 U + \epsilon_1 f_1}{f_0 U + f_1}$; $U = \frac{\epsilon_1 + F}{\epsilon_0 + F}$	$f_0 + f_1 = 1$. F is an adjustable parameter
10. Pearce (1955)	$\epsilon = \epsilon_0 = \frac{f_1(1 - F)}{1 - f_1 F}(\epsilon_1 - \epsilon_0)$	$-1 \leq F \leq 1$

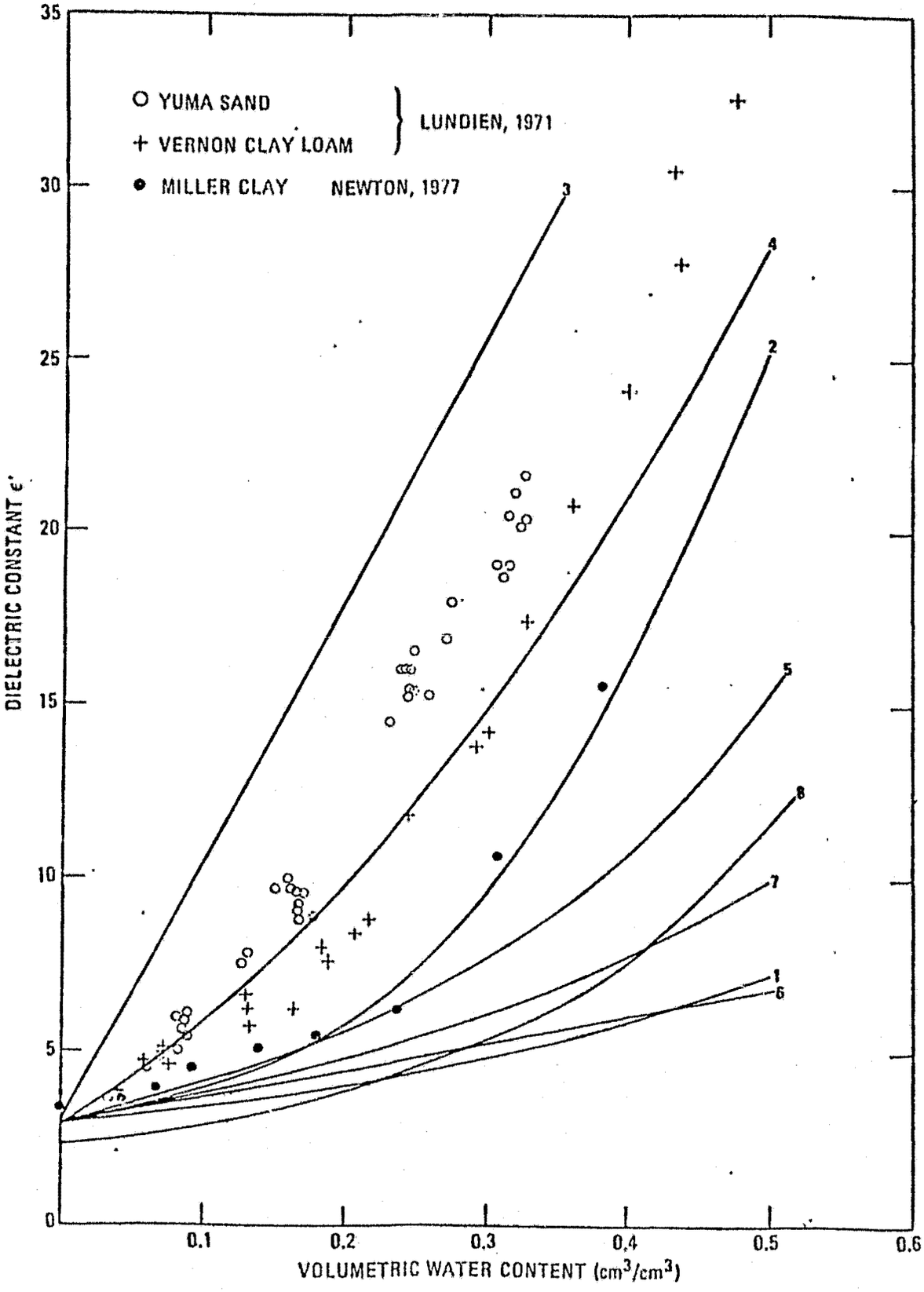

Figure 2.22. A comparison between some mixing formulas reported in the literature and the measured dielectric constants of 3 soils as a function of water content. Curves are labeled according to Table 2.10 (From Wang and Schmugge, 1978).

tension:

$$W_T = 0.09 + 0.59 \times WP \qquad (2.13)$$

where: W_T = transition moisture, cm^3/cm^3

WP = an estimate of moisture at the wilting point at 15 bars of tension, cm^3/cm^3

WP = 0.06774 - 0.00064 x % sand + 0.00478 x % clay

From observations of the behavior of the transition moisture as a function of particle size distribution, Newton (1977) postulates a direct dependence of the complex dielectric constant on the tension of soil water. In lieu of experimental measurements of K_r' and K_r'' as a function of tension, Newton (1977) assumes the moisture-tension characteristic of the clay loam (Figure 2.23) to be equivalent to that measured for the compositionally similar Avondale clay loam. Furthermore, assuming relative permittivity to be solely dependent upon soil tension in the manner given by the clay loam (Figure 2.23), the relationship between relative permittivity and tension is obtained (Figure 2.24), which is texture independent by definition. Combining Figures 2.23 and 2.24 yields estimated volumetric moisture-tension characteristic curves for sand and clay as seen in Figure 2.25. The strong similarity between the families of estimated and measured moisture-tension characteristics, Figures 2.25 and 2.26 respectively, supports the validity of the postulated dependence of the dielectric constant on soil water tension.

2.2.2 Observed soil textural effects on microwave sensor response to soil moisture

Microwave sensor response to a target is determined by the relationship between the frequency, incidence angle and polarization of the sensor and the dielectric and geometric properties of the target. Conservation of energy dictates that all energy incident upon a surface must be absorbed, reflected or transmitted.

$$W_i = W_\alpha + W_\rho + W_\tau \qquad (2.14)$$

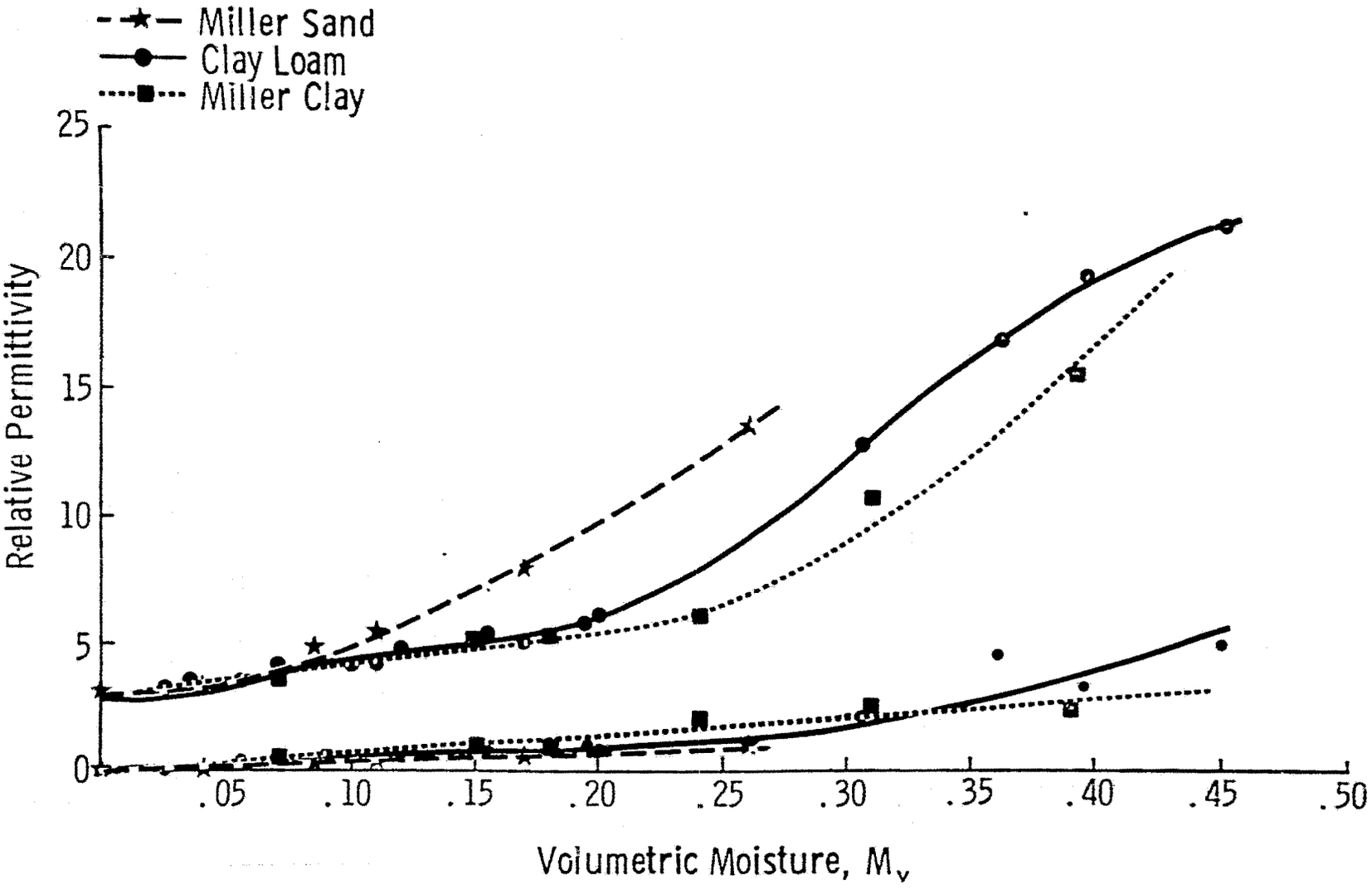

Figure 2.23 Relative Permittivity of Sand, Clay Loam and Clay as a Function of Volumetric Soil Moisture at 1.4 GHz (Data from Newton, 1977)

Figure 2.24 RELATIVE PERMITTIVITY OF A SAND, CLAY LOAM AND CLAY AS A FUNCTION OF SOIL TENSION AT 1.4 GHZ. (Data from Newton, 1977).

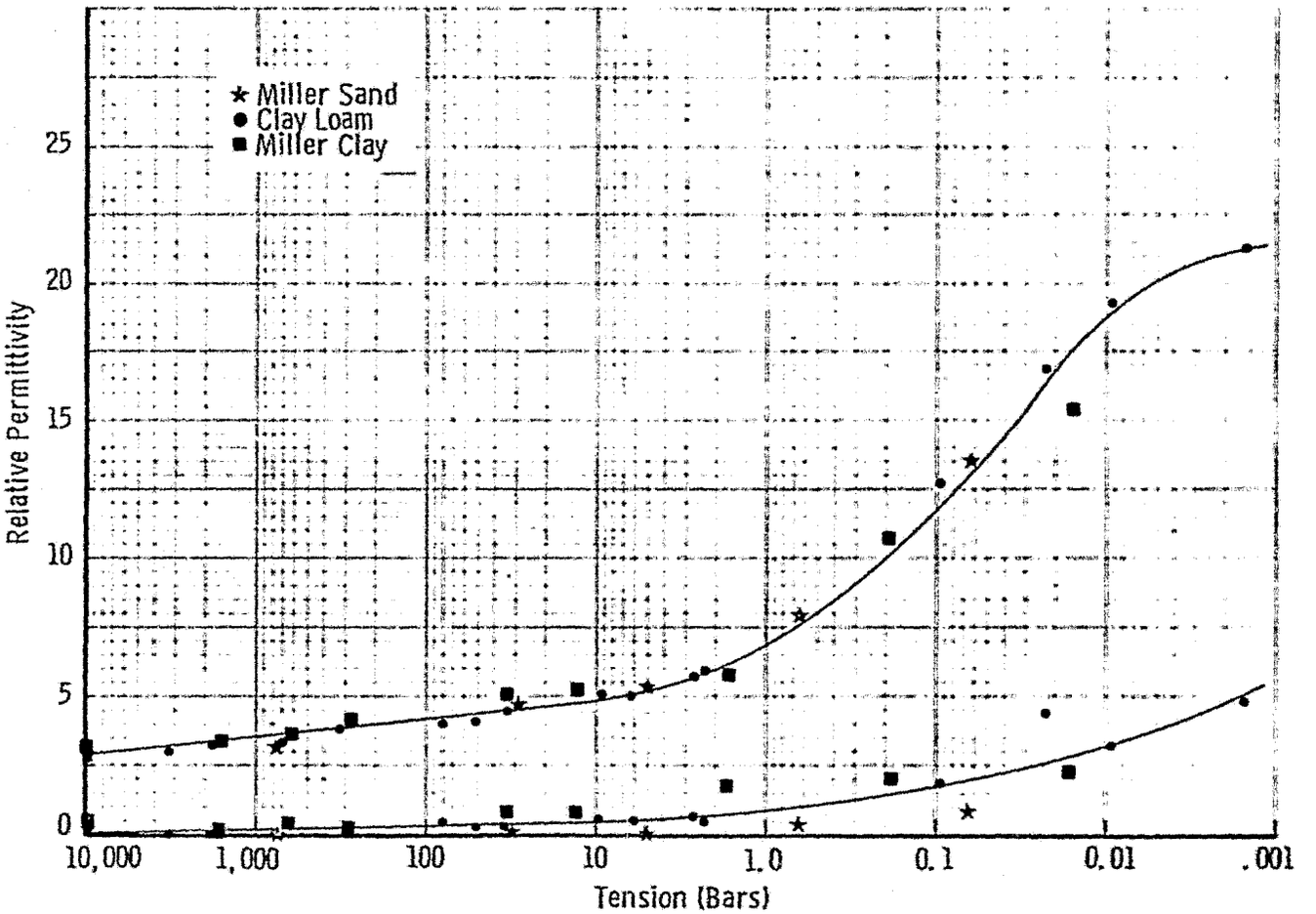

Figure 2.25 Estimated soil tension as a function of volumetric moisture content for sand, clay loam and clay. (Data from Newton, 1977).

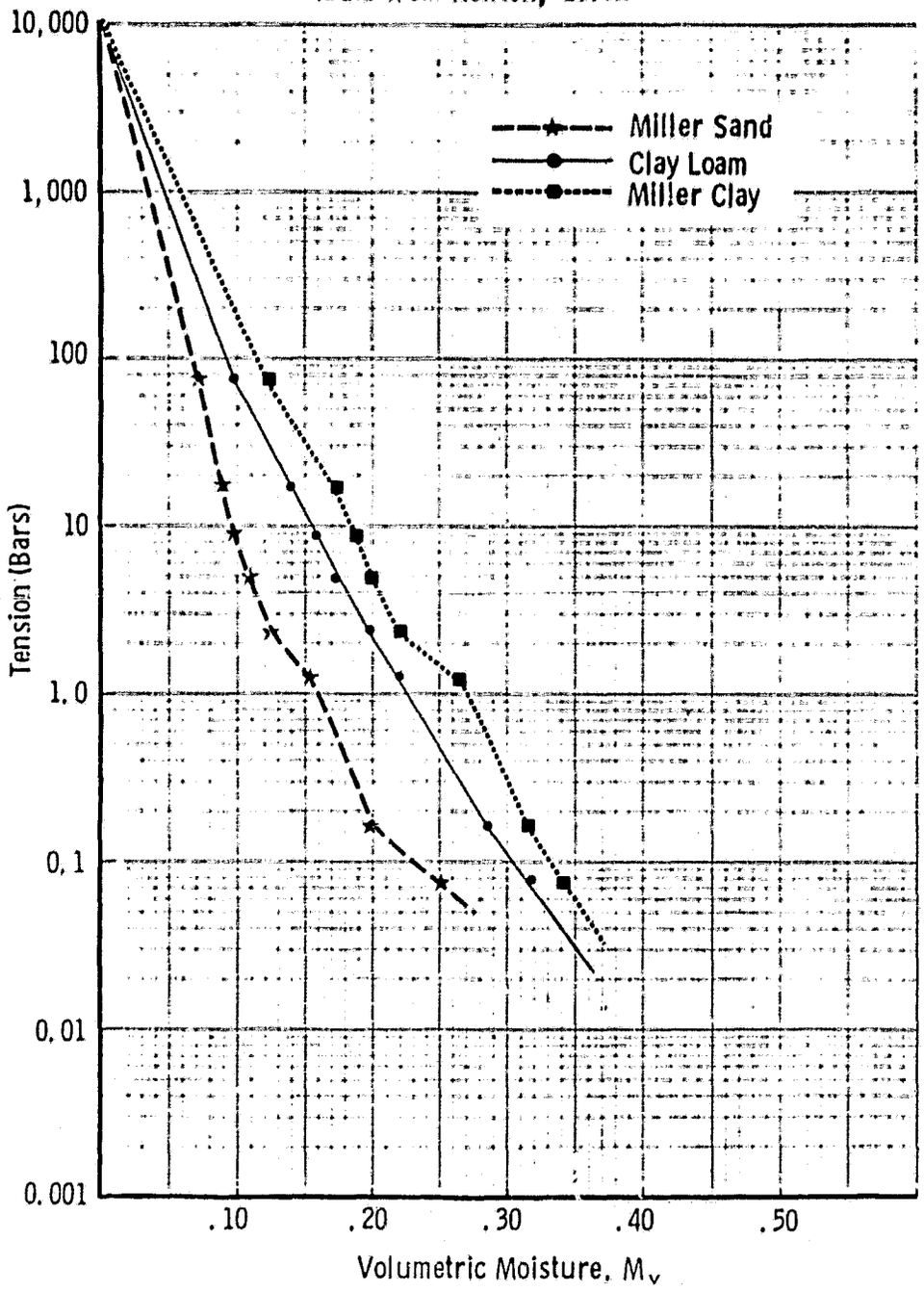

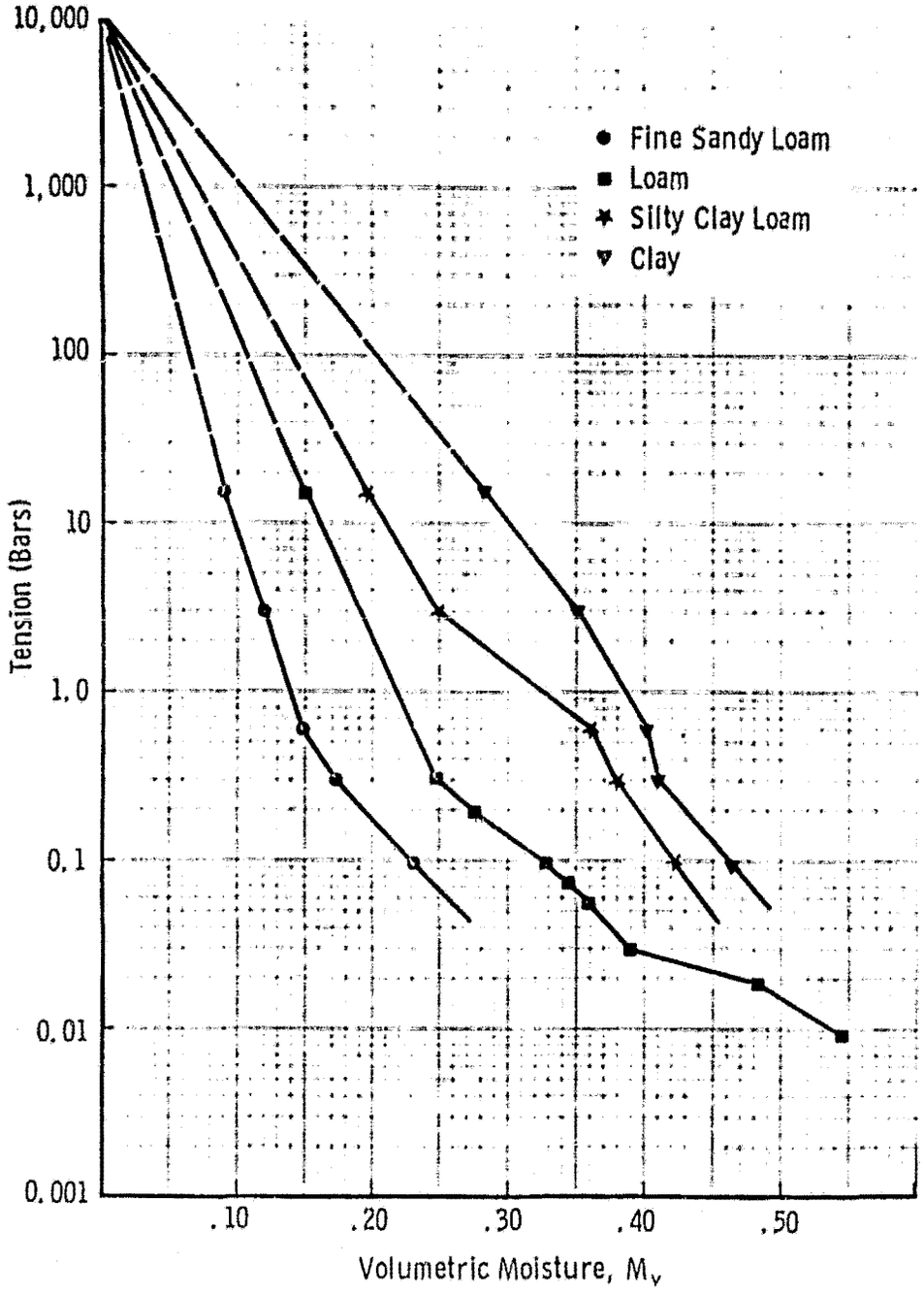

Figure 2.26 Soil Tension as a Function of Volumetric Moisture Content for Various Soil Textures. Data from Holtan, et al. (1968) and Carlisle, et al. (1978)

where: W_i = incident energy

W_α = absorbed energy

W_ρ = reflected energy

W_τ = transmitted energy

Normalizing equation 2.14by W_i at a given wavelength λ yields:

$$1 = \alpha(\lambda) + \rho(\lambda) + \tau(\lambda) \qquad (2.15)$$

where: α = absorptivity

ρ = reflectivity

τ = transmittivity

λ = wavelength

For an opaque surface, transmittance = 0 and equation (2.15) can be simplified to:

$$1 = \alpha(\lambda) + \rho(\lambda) \qquad (2.16)$$

Kirchhoff's Law states that absorptivity equals emissivity ε.

$$\alpha(\lambda) = \varepsilon(\lambda) \qquad (2.17)$$

By substituting equation 2.17 into 2.16:

$$\varepsilon(\lambda) = 1 - \rho(\lambda) \qquad (2.18)$$

Passive microwave radiometers measure the brightness temperature of the surface which is a function of the emissivity and the surface temperature,

$$T_B = \varepsilon T_g \qquad (2.19)$$

where: T_B = observed brightness temperature °K

T_g = surface temperature °K

Active microwave sensors measure the backscattering coefficient σ^o of the surface which is related to the power reflection coefficient R at a given incidence angle θ and the surface geometry.

$$\sigma^o_\theta = f(R_\theta, \text{roughness}) \tag{2.20}$$

The reflectivity of a surface is governed by the geometric roughness relative to the sensor wavelength and the dielectric properties of the surface. According to the Rayleigh criterion, a surface may be considered electromagnetically smooth if

$$h \lesssim \lambda/(8 \cos\theta) \tag{2.21}$$

where: h = height variations above a reference plane
θ = incidence angle (relative to nadir)

For a smooth surface, reflectivity is equal to the power reflection coefficient and the square of the voltage reflection coefficient

$$\rho = R = r^2 \tag{2.22}$$

which is a function of the complex dielectric constant. The Fresnel voltage reflection coefficient r is defined separately for each polarization of the incident electric field by:

$$r_V \exp(j\phi_r) = \frac{-\eta^2 \cos\theta_i + (\eta^2 - \sin^2\theta_i)^{\frac{1}{2}}}{\eta^2 \cos\theta_i + (\eta^2 - \sin^2\theta_i)^{\frac{1}{2}}} \tag{2.23}$$

and,

$$r_H \exp(j\phi_h) = \frac{\cos\theta_i - (\eta^2 - \sin^2\theta_i)^{\frac{1}{2}}}{\cos\theta_i + (\eta^2 - \sin^2\theta_i)^{\frac{1}{2}}} \tag{2.24}$$

where: r = voltage reflection coefficient for the vertical or horizontal polarization, r_V and r_H respectively.

$\exp(j\phi)$ = the phase relation between the incident and reflected electric field.

η = the index of refraction between two media.

Since at microwave frequencies

$$n = (\mu_r k_r)^{\frac{1}{2}}, \qquad (2.25)$$

where: μ_r = relative permeability = 1.0 for soils. Equations (2.23) and (2.24) can be expressed in terms of the dielectric constant K_r as:

$$r_V = \frac{k_r \cos\theta - (k_r - \sin^2\theta)^{\frac{1}{2}}}{k_r \cos\theta + (k_r - \sin^2\theta)^{\frac{1}{2}}} \qquad (2.26)$$

and,

$$r_H = \frac{\cos\theta - (k_r - \sin^2\theta)^{\frac{1}{2}}}{\cos\theta + (k_r - \sin^2\theta)^{\frac{1}{2}}} \qquad (2.27)$$

At normal incidence angle and for a smooth surface, the above equations reduce to a single expression independent of polarization,

$$r = \left| \frac{\sqrt{k_r - 1}}{\sqrt{k_r + 1}} \right| \qquad (2.28)$$

Using the data from Figure 2.23, the relationship shown in Figure 2.27 is obtained for R (in dB) at an incidence angle of 0^o. The sensitivity of R as a function of volumetric moisture M_v is observed to be inversely proportional to clay content. Since the radar backscatter coefficient σ^o and the normalized antenna temperature are proportional to R and (1 - R) respectively, it is apparent that the sensitivity of active and passive microwave sensor response to M_v should also be inversely related to percent clay content of soil. Furthermore, if it is assumed that the dielectric constant is a function of tension and independent of soil texture as shown in Figure 2.24, then it follows that R will also be texture independent as a function of tension (Figure 2.28). Moreover, expressed in dB, R appears to be linearly related to the logarithm of tension (Figure 2.29).

Experimental verification of the relationship postulated by Figure 2.29 cannot be derived directly from prior passive or active microwave soil moisture experiments because soil tension was not measured as a part of the

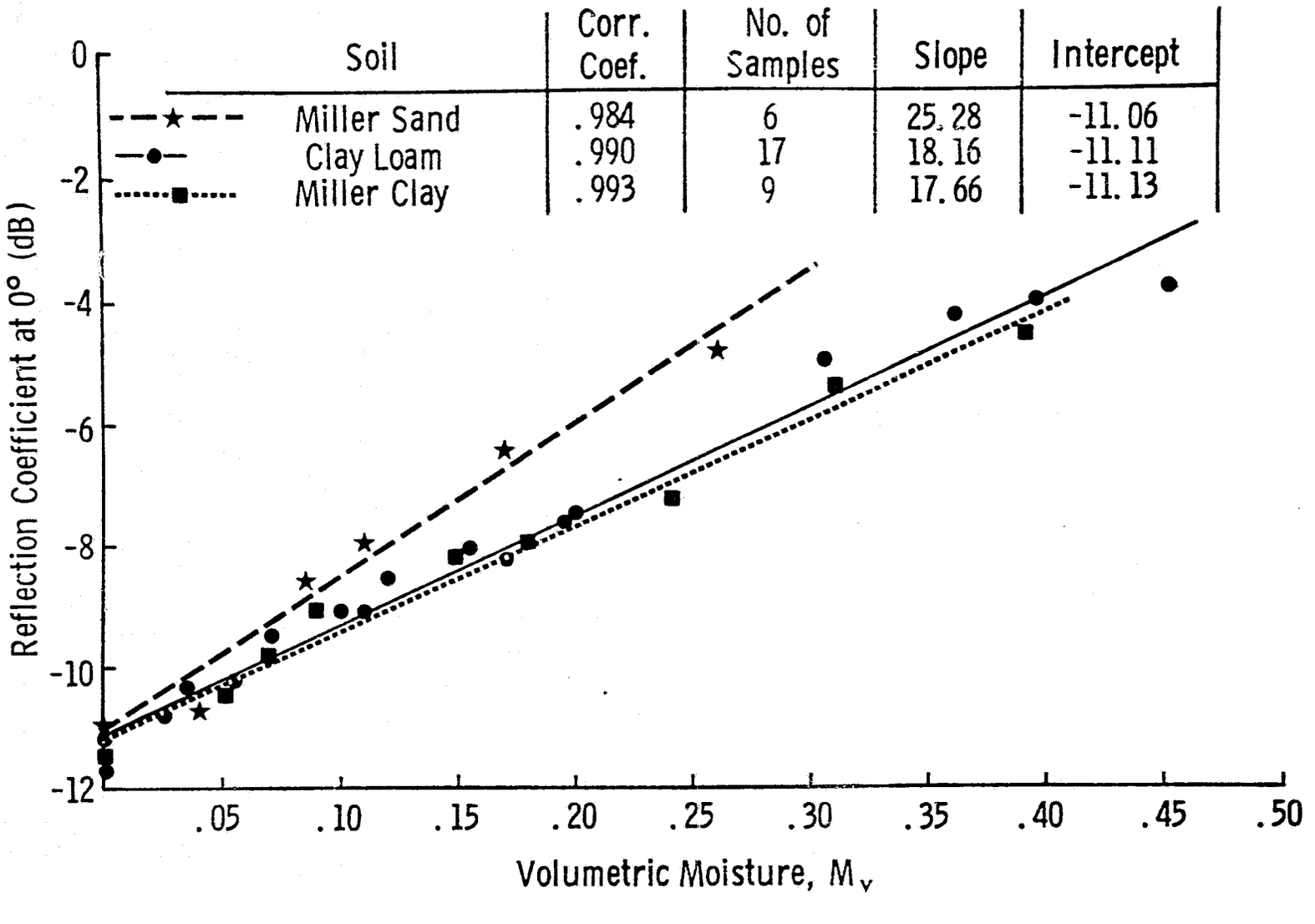

Figure 2.27 Reflection Coefficient (dB) at 1.4 GHz, 0° as a Function of Volumetric Soil Moisture for Sand, Clay Loam and Clay. (Data from Newton, 1977)

Figure 2.28 REFLECTION COEFFICIENT OF SAND, CLAY LOAM AND CLAY AS A FUNCTION OF SOIL TENSION AT 1.4 GHZ, 0° (Data from Newton, 1977).

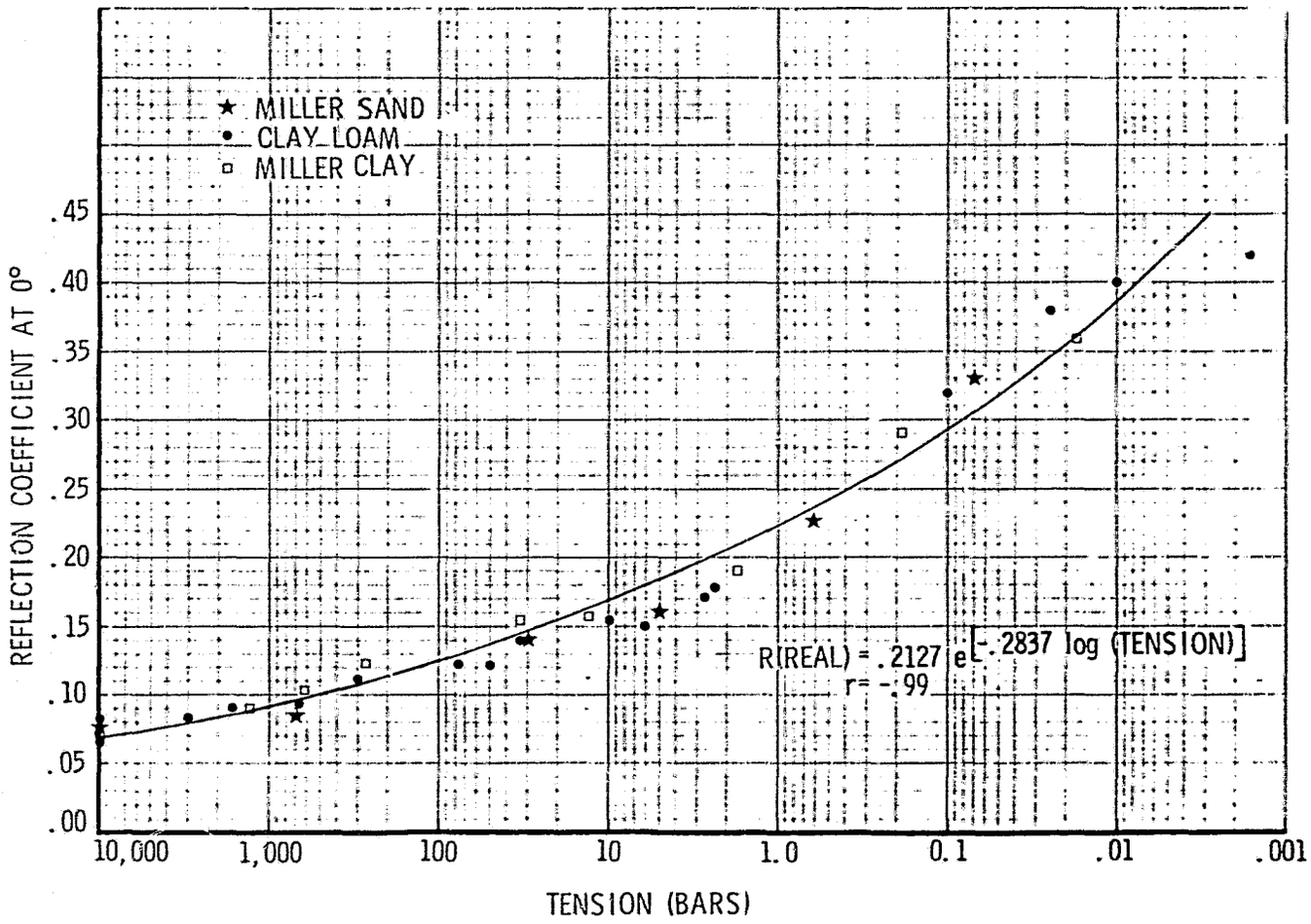

FIGURE 2.29 REFLECTION COEFFICIENT (dB) OF SAND, CLAY LOAM AND CLAY AS A FUNCTION OF SOIL TENSION AT 1.4 GHZ, 0°. (Data from Newton, 1977).

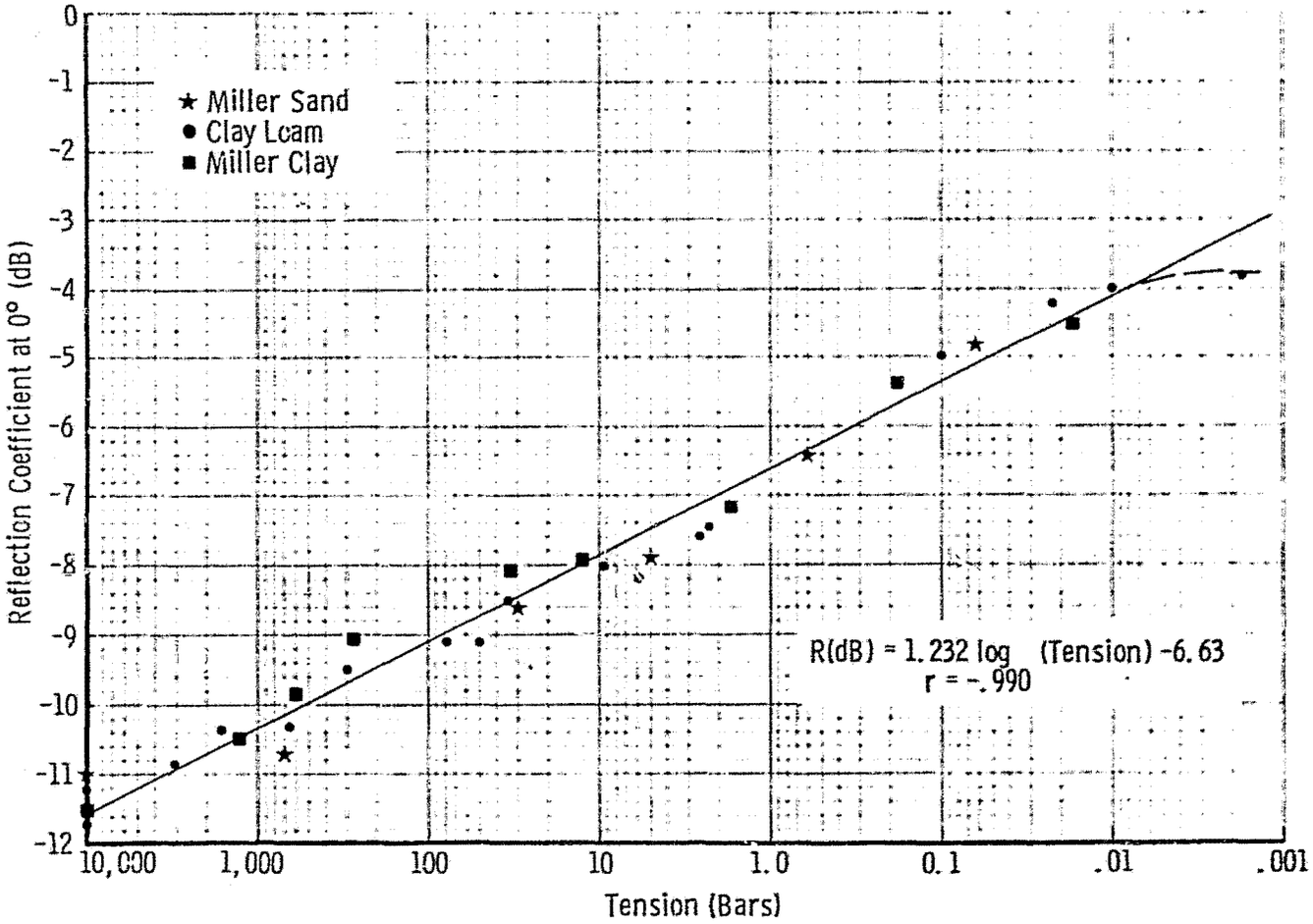

"ground truth". However, support for the above does come from the use of a normalized moisture M_n defined as:

$$M_n = 100M_v/M_v(1/3 \text{ bar tension}) \qquad (2.29)$$

where: M_v = volumetric moisture, g/cm^3

$M_v(1/3 \text{ bar tension}) = M_v$ at 1/3 bar tension

Passive microwave experiments near Phoenix, Arizona using a 21 and 1.55 cm airborne radiometer showed that the sensitivity of brightness temperature to M_v was inversely proportional to clay content as demonstrated in Figure 2.30 (Schmugge, 1976a, b). It was found that conversion of gravimetric moisture Mg to normalized moisture M_n produced a relatively texture independent relationship. Percent of field capacity was estimated by Schmugge (1976a) from gravimetric moisture Mg by:

$$M_{FC} = 100 \times Mg/FC \qquad (2.30)$$

where: FC = estimated field capacity or Mg at 1/3 bar tension

and,

$$FC = 25.1 - 0.21 \text{ (\% sand)} + 0.22 \text{ (\% clay)} \qquad (2.31)$$

While equation 2.31 is only one of many different empirical relationships (Table 2.11) derived to relate moisture at a given tension to soil texture, they all produce similar values of FC and the semantic ambiguity of "field capacity" as defined by an estimate of any laboratory determined water retention is overshadowed by the significance of the texture independent relationship displayed in Figure 2.31. The findings of Schmugge (1976a, b) offer additional support to the previously postulated dependence of K_r on soil tension since the data from Figures 2.27 to 2.29 also exhibit a linear dependence of R(dB) on M_n (Figure 2.32).

The above relationship is further supported by results derived from a series of truck-mounted radar investigations of soil moisture for both bare and vegetation covered test fields. In a comparison of non-vegetated

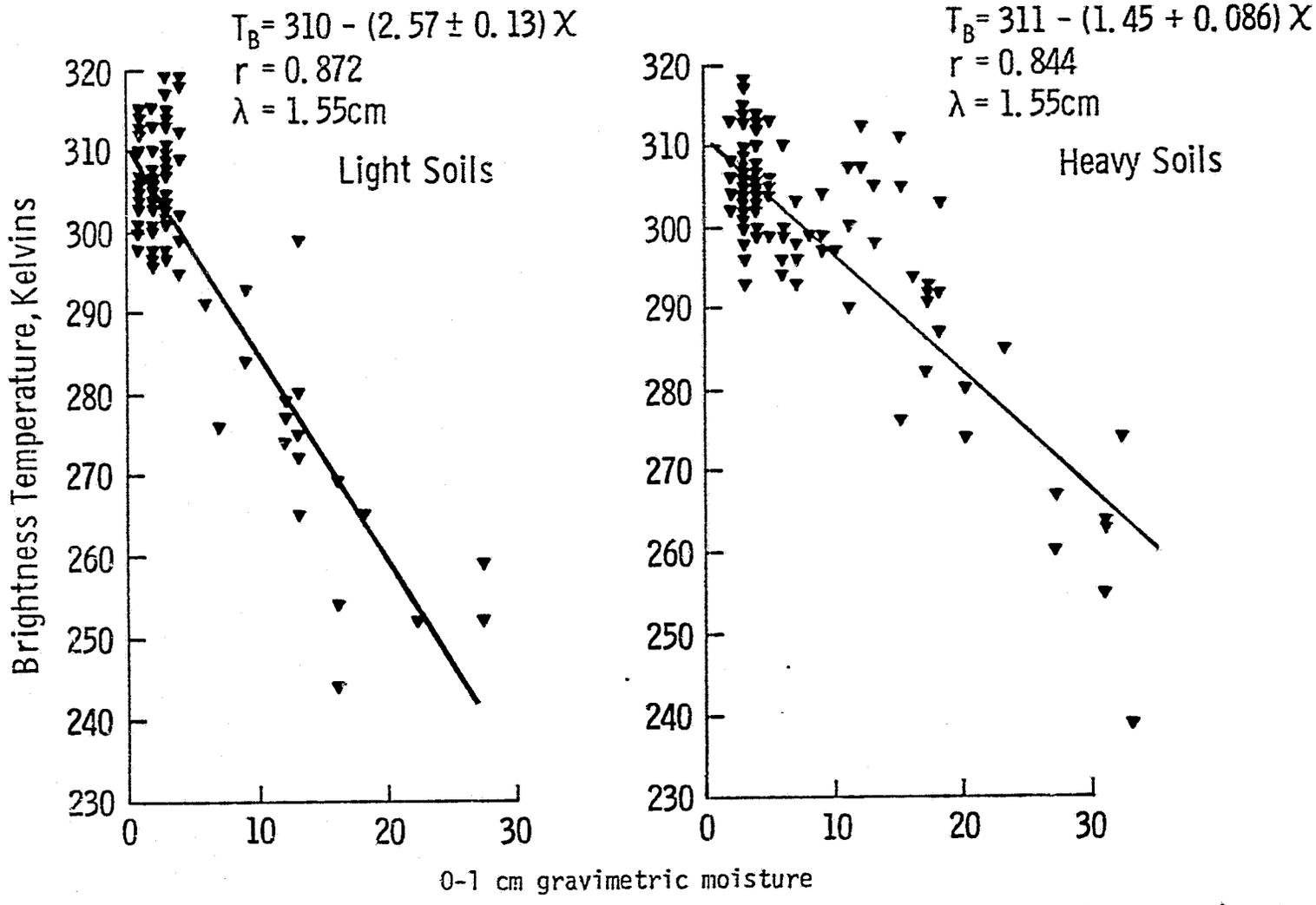

Figure 2.30. Plots of 1.55 cm brightness temperature versus soil moisture for light soil (sandy loam and loam) and heavy soil (clay loam) for bare fields (from Schmugge, 1976).

TABLE 2.11

Estimation of Field Capacity and Wilting Point from Soil Texture and Other Commonly Measured Soil Variables

Definitions: Field Capacity = FC = moisture at 1/3 bar tension
Wilting Point = WP = moisture at 15 bars tension
Available Water Capacity = FC-WP = water available to plants
Textural classes are based on USDA 1951 classification.

I. Salter & Williams (National Vegetable Research Station, Britain)
AWC (cm/cm) = 22.32 - 0.132 (% coarse sand) + 0.216 (% silt)
Mean Error of Estimate = ±10.0%
Regression is based on 27 different soil textures from soils analyzed by the authors.

II. Schmugge, et al. (NASA TN D-8321)
WP (%) = 7.2 - 0.07 (% sand) + 0.24 (% clay) Multiple R = 0.945
FC (%) = 25.1 - 0.21 (% sand) + 0.22 (% clay) Multiple R = 0.904

Regressions are based on 111 cases of 37 independent soil textures from soils near Phoenix, Arizona and the Rio Grande Valley in Texas. The soil data is derived from local Soil Conservation Service reports.

III. Dobson & Ulaby
WP (%) = 4.80 + 2.47 (% organic carbon) + 0.24 (% clay) Multiple R = 0.8
Standard Error of Estimate = 3.66
FC (%) = 35.29 + 3.74 (% organic carbon) - 0.30 (% sand) - 0.15 (% silt)
Multiple R = 0.80
Standard Error of Estimate = 6.31

Regressions are based on the surface horizon of 190 independent soil types from the Soil Conservation Service Laboratory Reports

IV. Brasher, Flach and Nettleton
FC (%) = 0.467 (% clay) + 0.356 (% fine silt) - 17.36 (bulk density at oven drying) + 0.039 (soil depth in cm)
Multiple R = .842
Standard Error of Estimate = 5.7

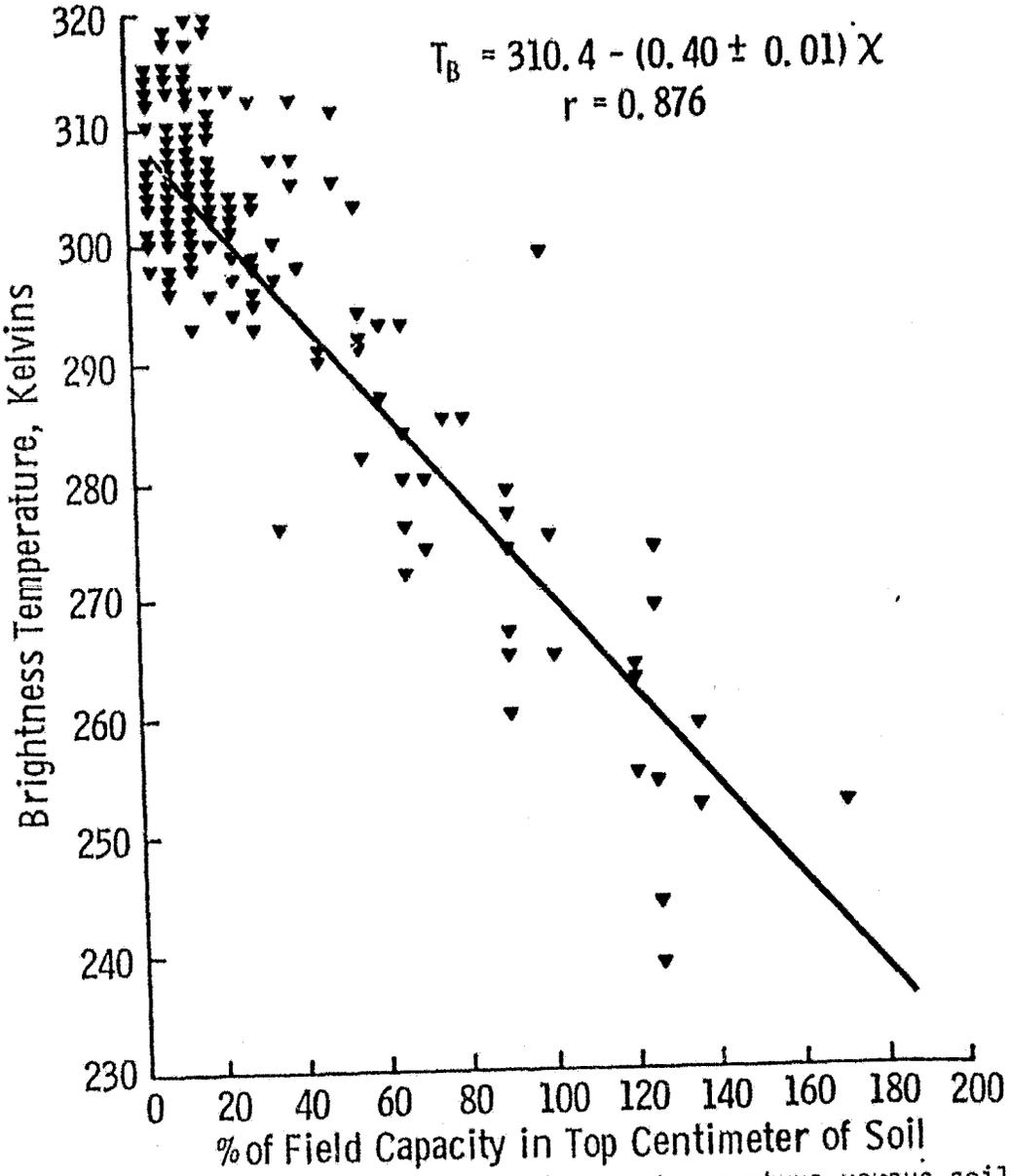

Figure 2.31. Plot of 1.55 cm brightness temperature versus soil moisture expressed as a percent of field capacity for bare fields (from Schmugge, 1976).

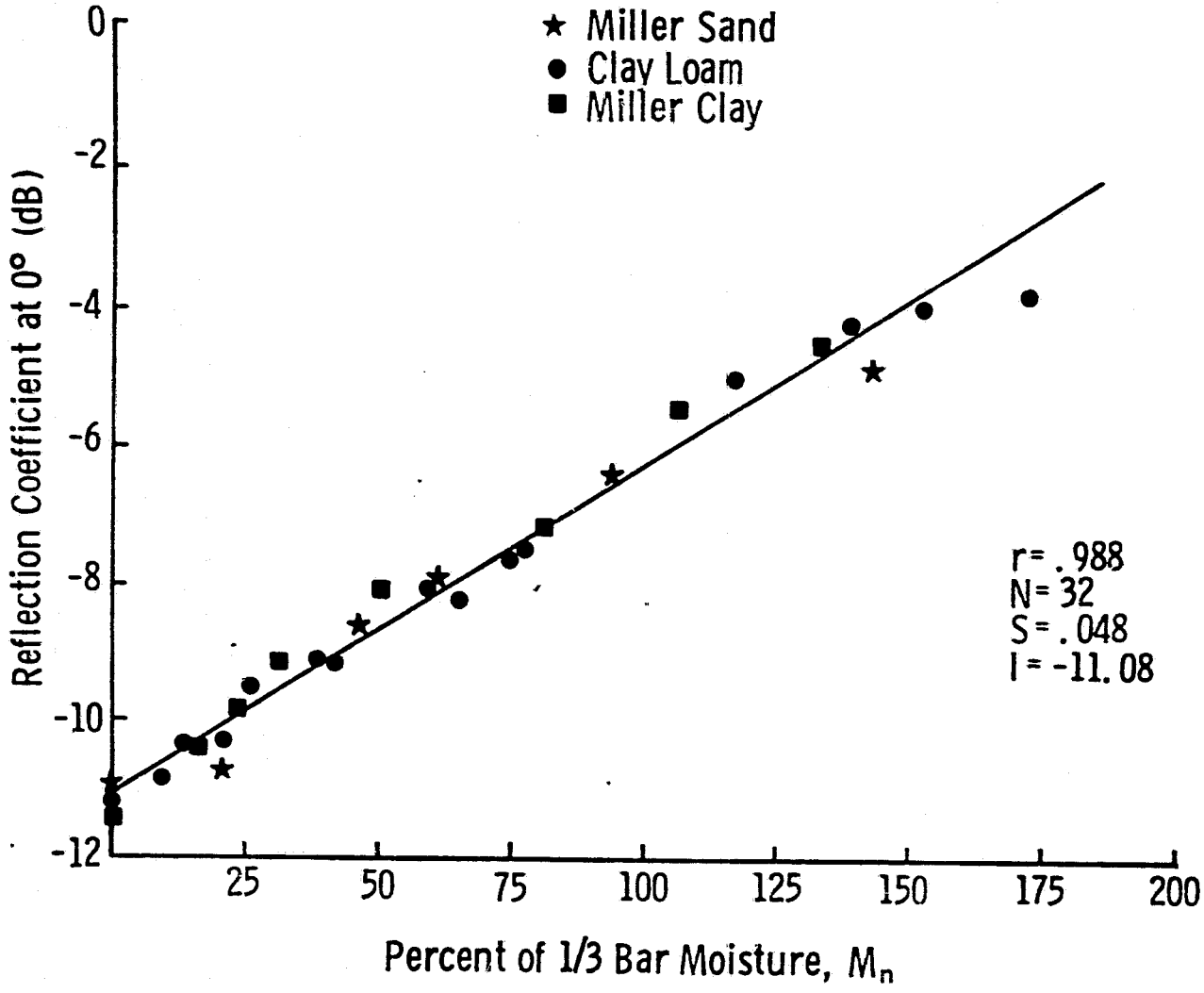

Figure 2.32 Reflection Coefficient (dB) at 1.4 GHz, 0° as a Function of Normalized Volumetric Soil Moisture, Percent of 1/3 Bar Water Content, for Sand, Clay Loam and Clay. (Data from Newton, 1977)

soil results from 44 observations of Miller clay and 80 observations of Eudora silt loam, it is evident that the sensitivity of σ^o at C-band to M_v is dependent upon soil texture (Figure 2.33a) while conversion of M_v to M_{FC} by use of Equation (2.29) produces the texture independent relationship (Figure 2.33b) found by Batlivala and Ulaby (1977). Furthermore, the value of M_{FC} is substantiated for σ^o response to soil moisture under a variety of vegetation canopies including corn, soybeans, grain sorghum and wheat over an entire growing season from a flood plain test site encompassing soils ranging from sandy loam to silty clay (Ulaby, et al., 1979). Figure 2.34 is a scatter plot of σ^o at 4.25 GHz, HH polarization and 10^o incidence angle as a function of M_{FC} in the 0-5 cm soil layer; correlation coefficient is found to be 0.917. A comparison of the linear regression fits of σ^o to individual crops for moisture expressed gravimetrically (Figure 2.35a) and as a percent of field capacity M_{FC} (Figure 2.35b) shows a significant improvement in the combined correlation coefficient from 0.82 to 0.92 when M_{FC} is employed as the soil moisture descriptor. Furthermore, the above result is not unique to a specific depth interval over which soil moisture is averaged; M_{FC} is demonstrably superior to either gravimetric or volumetric moisture over any depth interval considered (Figure 2.36).

3.0 1977 BARE SOIL EXPERIMENT

An experiment was conducted from August 4 to October 21, 1977 using the truck-mounted University of Kansas Microwave Active Spectrometer (MAS) 1-8 GHz system on test fields located in the Kansas and Wakarusa River floodplains east of Lawrence, Kansas. Measurements acquired during the experiment are summarized in Table 3.1. The MAS 1-8 system is a calibrated FM-CW Radar which operated during the experiment at 8 frequencies between 1.2 and 7.6 GHz at all three linear polarization configurations and at incidence angles of 10, 15 and 20° (Table 3.2). The system is fully described in Brunfeldt, et al (1979) and Ulaby, et al (1979); its calibration and accuracy are described in Stiles, et al., (1979). The selection of the incidence angle θ to be in the $10\text{-}20^o$ range was based upon the optimum radar soil moisture sensor parameters recommended by

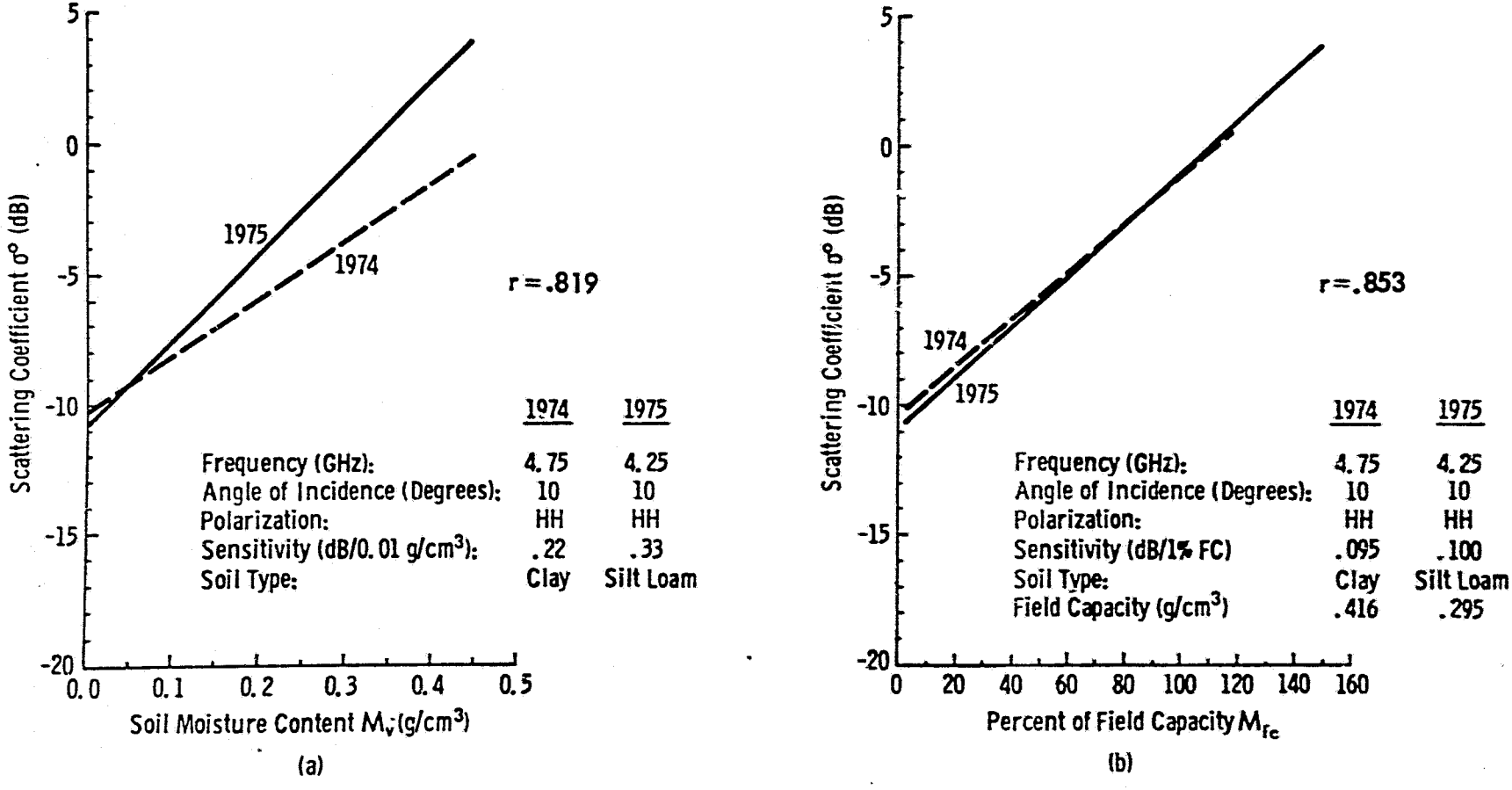

Figure 2.33. Comparison of regression results of 1974 and 1975 bare soil experiments with moisture expressed (a) volumetrically and (b) as percent of field capacity (modified from Batlivala and Ulaby, 1977).

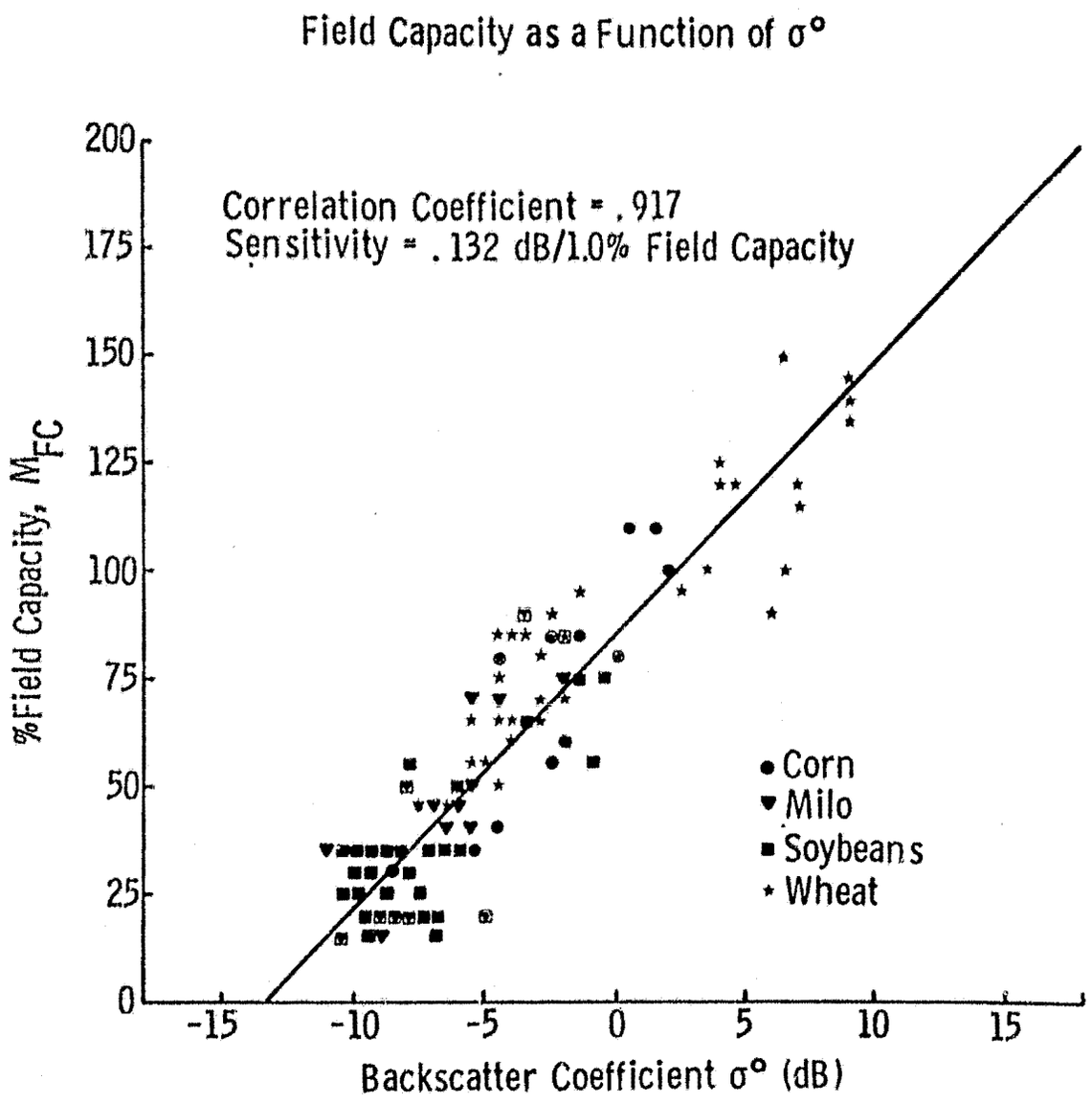

Figure 2.34 Percent Field Capacity in the 0-5 cm Soil Layer as a Function of Backscatter Coefficient at 4.25 GHz, HH, 10° for Corn, Milo, Soybean and Wheat Data Sets Combined. (Adopted from Ulaby, et al., 1979b)

Figure 2.35 σ° RESPONSE TO SOIL MOISTURE FOR THE 1975 VEGETATION EXPERIMENTS
0-5cm soil moisture is expressed a) gravimetrically b) as a percent of the estimated field capacity. σ° at 4.25 GHz, 10°, HH.

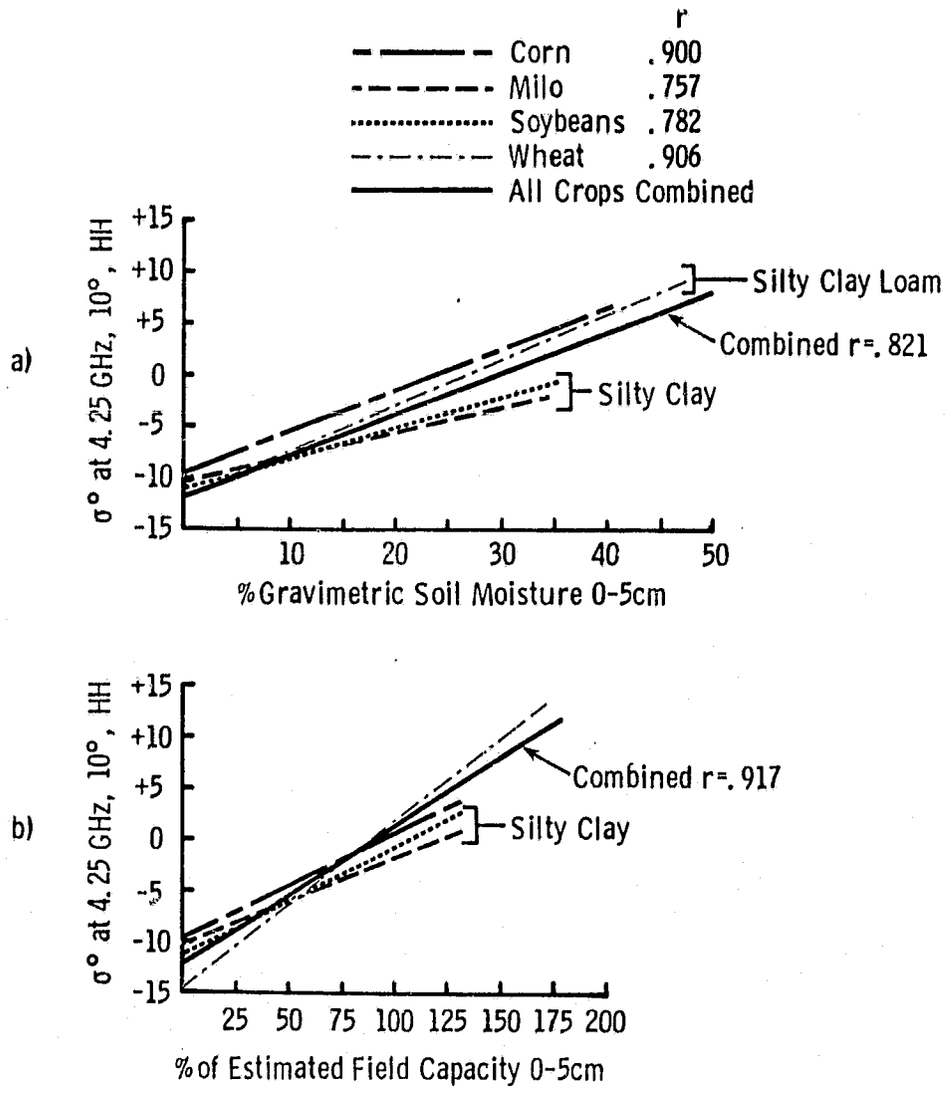

C-2

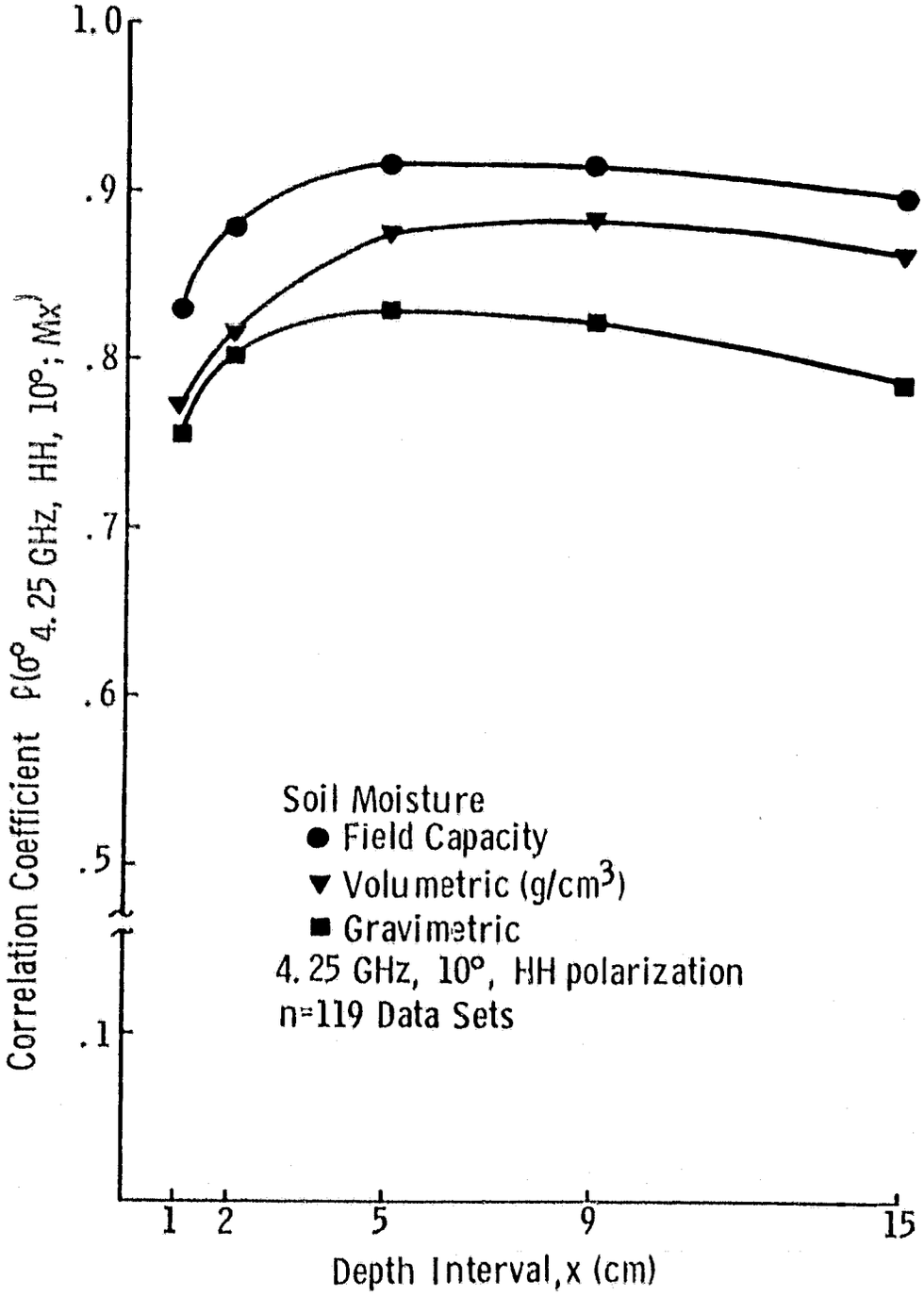

Figure 2.36 | Correlation coefficient as a function of depth for soil moisture expressed as % field capacity. % gravimetric soil moisture, and volumetric soil moisture. Data includes corn, milo, soybeans and wheat.

TABLE 3.1

1977 Bare Soil Experiment Data Acquisition Summary

August 4 - October 21

88 data sets
4 soil types (Field capacity range 12% - 35%)
All four test fields had approximately the same surface roughness

Sensor:

Measured characteristic	frequency range	angular range	polarizattion
Backscatter coefficient (σ^o)	1-8 GHz	10°, 15°, 20°	HH, VV, HV

Target:

Measured characteristic	soil intervals measured	number of sampling location	frequency of measurement
1. Precipitation		4	continuous
2. Temperature		1	continuous
3. Relative humidity		1	continuous
4. Soil moisture	0-1 & 1-2 cm 2-5, 5-9 & 9-15 cm	8 per field 4 per field	once per data set once per data set
5. Soil conductivity	0-1, 1-2 & 2-5 cm	1	continuously during a radar data set
6. Soil bulk density	full profile	8	at least 3 times per field
7. Soil texture	full profile	8	once per field
8. Organic matter	full profile	8	once per field
9. Soil water retention characteristics	full profile	1	once per field
10. Surface slope			once per field
11. Surface roughness		1	once per measure-ment day

TABLE 3.2

1977 MAS 1-8 System Specifications

Platform Height: 26 meters

Antennas:

- Dishes: 1.22 meter parabolic
- Feeds: Dual Polarized log periodic
- Polarizations: HH HV VV (transmit, receive)

Incidence Angle: 10, 15, 20

Samples at each Angle: 20

Radar:

- Type: FM-CW
- Modulation: Triangular
- Center Frequencies (GHz): 1.225, 1.625, 2.385, 3.291, 4.625, 5.625, 6.625, 7.625
- Frequency Sweep: 250 MHz
- Intermediate Frequency: 50 kHz
- IF Bandwidth: 20 kHz
- Transmitter power: +15 dbm

Calibration:

- Internal: Delay line
- External: Luneberg lens

For details see Brunfeldt, et al. (1979)

Batlivala and Ulaby (1977) and Ulaby and Batlivala (1977). The scope, duration, test site, data acquisition procedures and data products of the 1977 Bare Soil Experiment are fully documented in Dobson (1979).

3.1 Experiment Description

The purpose of the 1977 Bare Soil Experiment was to verify that the 1-8 GHz radar response to gravimetric and volumetric soil moisture is dependent upon soil texture and provide a comprehensive data base capable of producing more versatile soil moisture estimation algorithms that minimize the error component related to soil texture.

Prior research has established the following list of target parameters as having probable significance in determining the 1-8 GHz radar backscattering characteristics of the soil surface:

a) soil moisture
b) soil surface roughness
    1. surface gradient relative to incidence angle of sensor
    2. macroroughness as defined by the periodic ridge-furrow patterns induced by agricultural implements
    3. microroughness as defined by the size distribution of surface aggregates such as clods and soil peds
c) soil bulk density
d) soil composition
    1. texture as defined by the particle size distribution of the soil mineral fraction
    2. organic matter content
    3. soil salinity
e) vegetation canopy
    1. type
    2. height
    3. density of biomass
    4. moisture content
    5. plant geometry

The success of the experiment in regard to stated purpose was predicated upon the selection of test fields which were internally homogeneous and similar with respect to all target parameters, except soil texture and soil moisture, for the duration of the experiment. Test fields were selected and groomed such that they:

1) were devoid of a vegetation canopy,
2) had surface gradients of less than .5%,
3) were smooth with respect to macroroughness, and
4) had similar microroughness.

These field conditions were attained by repeated disking of each field followed by a one to three week stabilization period prior to radar observation during which time events of saturating rain and strong wind further smoothed the soil surface and acted to stabilize the soil structure of the disturbed surface layer. Table 3.3 summarizes the initial field preparations and final microroughness (quantified as root mean square height).

TABLE 3.3
Field Preparations for 1977 Bare Soil Experiment

Field	Preparation Date	Number of Times Disked	Date of 1st observation	Final RMS Height (cm)
#1	7/23/77	4	8/4/77	1.3
#2	7/23/77	8	8/15/77	0.8
#3	8/20/77	9	9/3/77	1.0
#4	7/23/77	11	8/15/77	0.7

The microroughness of fields observed during the 1977 Bare Soil Experiment compare with only the smoothest of bare soil fields previously examined by the MAS 1-8 system in 1974 and 1975 (Table 3.4).

Fields of sandy loam, silty clay loam and silty clay were examined over a broad range of moisture conditions. Importantly, test fields for each soil texture were found to be internally homogeneous with respect to soil texture and bulk density and will be discussed in more detail in the following section.

TABLE 3.4

Comparison of Mean RMS Heights for Test Fields for 1974, 1975 and 1977 Bare Soil Experiments

Year	Field Designation	Mean RMS Height (cm)
1974	R	4.3
	M	2.6
	S	0.88
1975	1	4.1
	2	2.2
	3	3.0
	4	1.8
	5	1.1
1977	1	1.32
	2	0.79
	3	1.03
	4	0.70

The experiment was conducted during an abnormally wet fall and resulted in surface soil moisture conditions skewed toward conditions wetter than those found during either the 1974 or the 1975 experiments (Batlivala and Cihlar, 1975; Batlivala and Dobson, 1976). Table 3.5 shows the mean gravimetric soil moistures from each of the three experiments and their associated standard deviations. The prevalence of wet conditions during the MAS 1-8 1977 experiment signifies that it will augment the moisture range of the combined 1974 and 1975 bare soil data base in the derivation of soil moisture algorithms. The larger standard deviation about the mean 1977 moistures reflects the variety of textures included in the experiment in contrast to the single textures examined in both the 1974 and 1975 experiments.

TABLE 3.5

Mean Gravimetric Moisture Conditions for the 1974, 1975 and 1977 Bare Soil Experiments

Depth(cm)	YEAR 1974 Mean	1974 S.D.	1975 Mean	1975 S.D.	1977 Mean	1977 S.D.
0-1	13.53	7.63	16.18	8.37	21.85	13.25
0-2	15.74	6.86	18.19	5.63	24.98	11.91
0-5	19.38	5.70	19.97	3.88	29.23	10.67
0-9	20.20	5.23	20.44	2.78	31.02	9.88
0-15	21.10	4.65	20.41	2.27	30.88	9.06
Number of Textures	1		1		3	
Number of Data Sets	44		80		88	

3.2 Target Characteristics and Homogeneity

Extensive measurements of soil texture, bulk density and surface roughness were made during the experiment to establish the homogeneity of these parameters within each test field. The data acquisition procedures and results are fully treated in Dobson (1979) and will only be summarized in the following sections.

3.2.1 Soil texture

A total of 28 samples were collected from each test field at the soil moisture sampling locations and depths indicated on Figure 3.1. Soil textural separates were defined by the hydrometer method and organic matter determinations were made using a variant of the Walkley-Black method of oxidation with chromic acid.(Allison, 1965). The values of organic matter content are estimated as 1.724 times the organic carbon content. A summary of the mean 0-15 cm soil texture and organic matter content from each field is given in Table 3.6

Figure 3.1 1977 Bare Soil Moisture Experiment: Field Layout and Sampling Grid

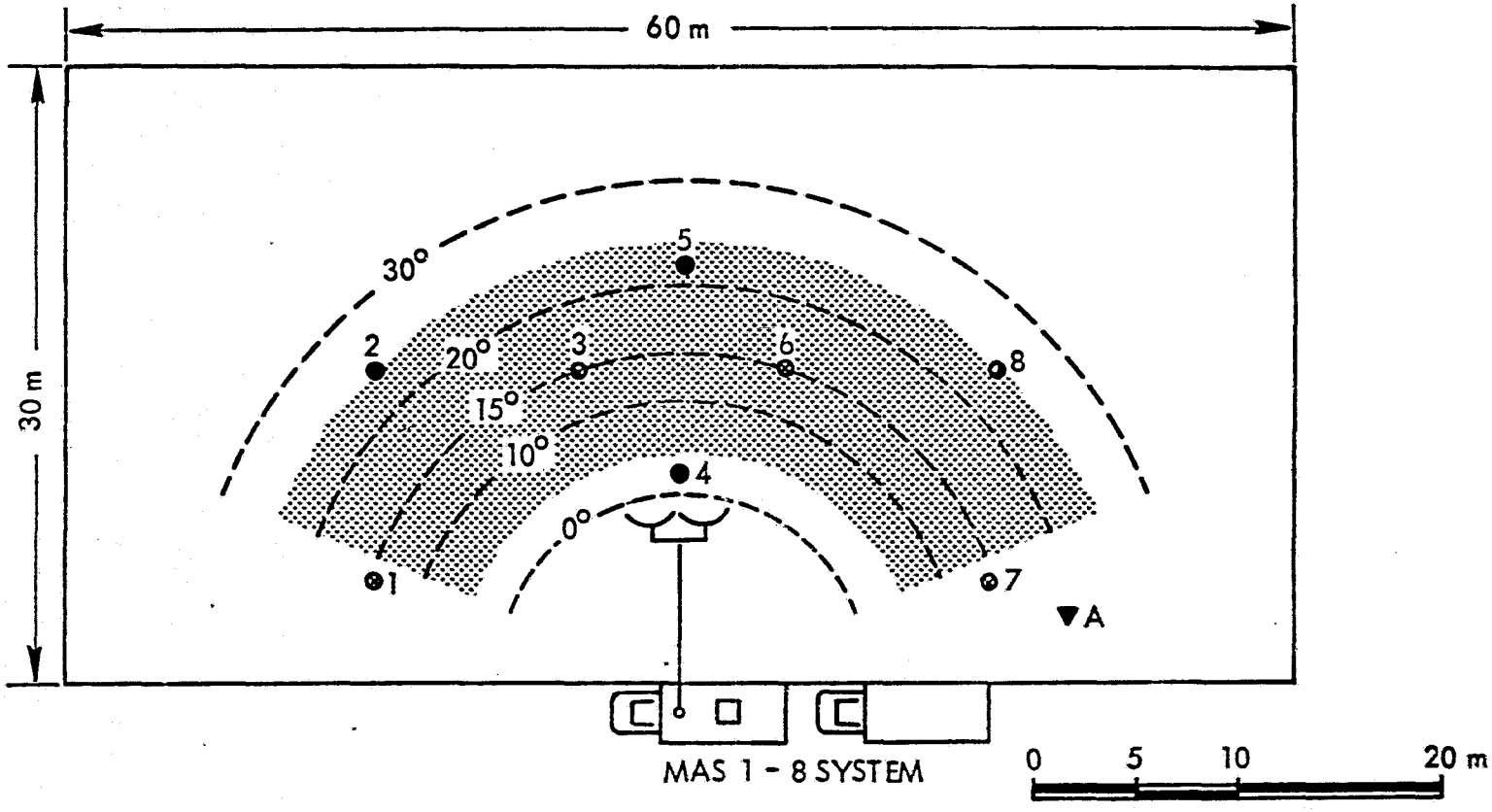

Soil Sampling Locations:

- ● 0 - 1 cm and 1 - 2 cm samples only (locations 2, 4, 5, and 8)
- ⊗ 0 - 1, 1 - 2, 2 - 5, 5 - 9, and 9 - 15 cm samples (locations 1, 3, 6, and 7)
- A Location of soil conductivity sensors for 0 - 1, 1 - 2, and 2 - 5 cm depth intervals
- ▒ Indicates maximum area illuminated at 1.1 GHz

Dashed lines indicate the center of illumination by the MAS 1 - 8 at various angles of incidence. Elevation beamwidths vary with frequency from 12° at 1.1 GHz to 2° at 7.25 GHz.

TABLE 3.6

Summary of Organic Matter Content and Soil Texture of Test Fields

Field	0-15 cm Mean Organic Matter Content (% by weight of dry soil)	0-15 cm Mean Soil Texture			Soil Textural Class
		% Sand	% Silt	% Clay	
#1	0.7	55.0	42.2	2.8	Sandy loam
#2	3.1	9.1	53.9	37.0	Silty clay loam
#3	3.9	11.5	52.2	36.2	Silty clay loam
#4	3.8	9.0	45.1	45.8	Silty clay

Within each field, the textural separates within each of the sampled layers (0-1, 1-2, 2-5, 5-9 and 9-15 cm) were treated as a sample population. The sample means and standard deviations are presented in Table 3.7. An indication of textural homogeneity within a field is given by the low standard deviation about the sample means which is typically less than 3% with the notable exception of the top one cm layer of field 2 where the standard deviations exceed 6%.

Skewness shows the degree to which a distribution approximates a normal curve since it measures deviations from symmetry. The skewness of a normal distribution is zero, while a positive or negative skewness indicates that cases are clustered below or above the mean respectively. Kurtosis measures the relative peakedness of the curve defined by the distribution of cases. The kurtosis of a normal distribution is zero, while a positive or negative kurtosis indicates that the distribution is more peaked or flatter than a normal distribution. Calculation of the skewness and kurtosis of all textural sample distributions indicates approximately normal but flatter distributions. In only one case, field 1, 1-2 cm clay, is kurtosis found to exceed 0. Values fall within the following ranges:

$$-0.737 \leq \text{skewness} \leq 1.268 \text{ and}$$

$$-2.428 \leq \text{kurtosis} \leq .301$$

The above findings are consistent with an assumption of field homogeneity with respect to soil texture with the exception of the surface layer of field 2 where considerable variance was observed over short distances especially for sand and clay fractions (up to 14% change between adjacent sample locations in Figure 3.1).

Fields 2 and 3 have very similar mean textures; both are silty clay loams by the USDA classification. This conclusion is supported by t-tests run between the field sample distributions for each depth interval. The validity of the t-tests is based upon assumptions that the sample distributions are both normally distributed and have equal variances. The first assumption is validated by the skewness and kurtosis measurements of each sample distribution, and the validity of the second

TABLE 3.7

Mean Soil Texture at Each Depth

a. Field 1

DEPTH (CM)	% SAND		% SILT		% CLAY	
	MEAN	S.D.	MEAN	S.D.	MEAN	S.D.
0-1	55.00	2.56	43.00	2.20	2.00	1.20
1-2	55.38	3.31	41.88	3.23	2.75	1.67
2-5	56.00	1.73	41.75	1.89	2.25	0.50
5-9	53.50	2.58	43.00	3.37	3.50	2.16
9-15	55.50	1.15	41.75	1.26	2.75	0.96
0-15 Weighted Mean	55.03		42.18		2.80	

b. Field 2

DEPTH (CM)	% SAND		% SILT		% CLAY	
	MEAN	S.D.	MEAN	S.D.	MEAN	S.D.
0-1	11.26	6.14	55.53	6.84	33.25	6.14
1-2	10.48	2.45	56.28	3.23	33.25	2.78
2-5	9.68	2.71	54.43	4.38	35.90	1.73
5-9	9.78	0.51	55.25	1.26	34.98	1.67
9-15	7.71	3.25	52.11	5.16	40.21	4.35
0-15 Weighted Mean	9.08		53.92		37.02	

c. Field 3

DEPTH (CM)	% SAND		% SILT		% CLAY	
	MEAN	S.D.	MEAN	S.D.	MEAN	S.D.
0-1	10.87	1.93	53.33	2.03	35.75	1.68
1-2	11.92	1.31	51.16	0.65	36.90	1.75
2-5	12.95	1.00	52.53	3.88	34.50	3.34
5-9	11.15	1.92	52.70	3.85	36.15	2.35
9-15	11.11	1.93	51.79	2.72	37.11	3.80
0-15 Weighted Mean	11.53		52.24		36.23	

d. Field 4

DEPTH (CM)	% SAND		% SILT		% CLAY	
	MEAN	S.D.	MEAN	S.D.	MEAN	S.D.
0-1	8.87	2.71	46.90	4.67	44.21	4.50
1-2	8.31	2.11	46.31	2.33	45.36	1.99
2-5	10.42	2.05	46.31	5.66	43.27	5.14
5-9	9.70	2.57	42.35	2.79	47.93	5.14
9-15	8.06	2.22	45.88	3.74	46.05	4.50
0-15 Weighted Mean	9.04		45.12		45.83	

assumption was checked using variance ratio or F-tests. F-tests rejected the hypothesis of equal variance in 40% of the between field comparisons at a 0.10 significance level where in excess of 60% of the rejections involved field 2 which tended to have a higher variance. The results of the t-tests are summarized in Table 3.8 for the top cm and the 0-15 cm layer; other depth intervals do not deviate significantly from these results.

In summary, all fields except field 2 were found to be internally homogeneous with respect to soil texture and fields 2 and 3 were found to represent the same textural population. Cumulative plots of the particle size distribution from a representative sample of each field are shown in Figure 3.2 and are summarized as a histogram in Figure 3.3. In addition, all fields were found to have comparable organic matter contents of less than 4.0% by weight.

3.2.2 Surface Roughness

A total of 116 roughness profiles were obtained from the four test fields using a five foot aluminum panel. A subset of 24 profiles were digitized along the transects at a maximal spacing of 0.15 cm. The profiles were chosen to represent the initial, median and final roughness conditions of each field both parallel and perpendicular to the radar look direction. Plots of the initial roughness conditions are shown in Figure 3.4. The root mean square variations in surface height of all digitized profiles are given in Table 3.9. These measurements confirm the field observation that all fields became increasingly smooth as a function of time, especially fields 2 and 3. The comparatively large RMS roughness of field 1 is primarily the result of residual small scale macroroughness produced by disking while the persistent comparatively small RMS roughness of field 4 was due to the presence of surface crumbs and small aggregates which proved to be very cohesive and resistant to crumbling. The marked change in the roughness of fields 2 and 3 as a function of time is largely due to their intermediate textural composition (compared to fields 1 and 4); initial clods and aggregates possessed only weak structure and thus disintegrated with time.

Analysis of the radar data assumes that the mean surface roughness of all fields are equivalent. This assumption was tested with t-tests and

TABLE 3.8

Results of t-tests of Soil Textural Distributions
Between Fields. Two-tailed Test, Level of Significance = 0.01

Depth Interval	Textural Separate	Fields which cannot be rejected as having unequal mean textures.
0-1 cm	sand	2, 3, 4
	silt	2, 3
	clay	2, 3
0-15 cm	sand	2, 3, 4
	silt	2, 3
	clay	2, 3

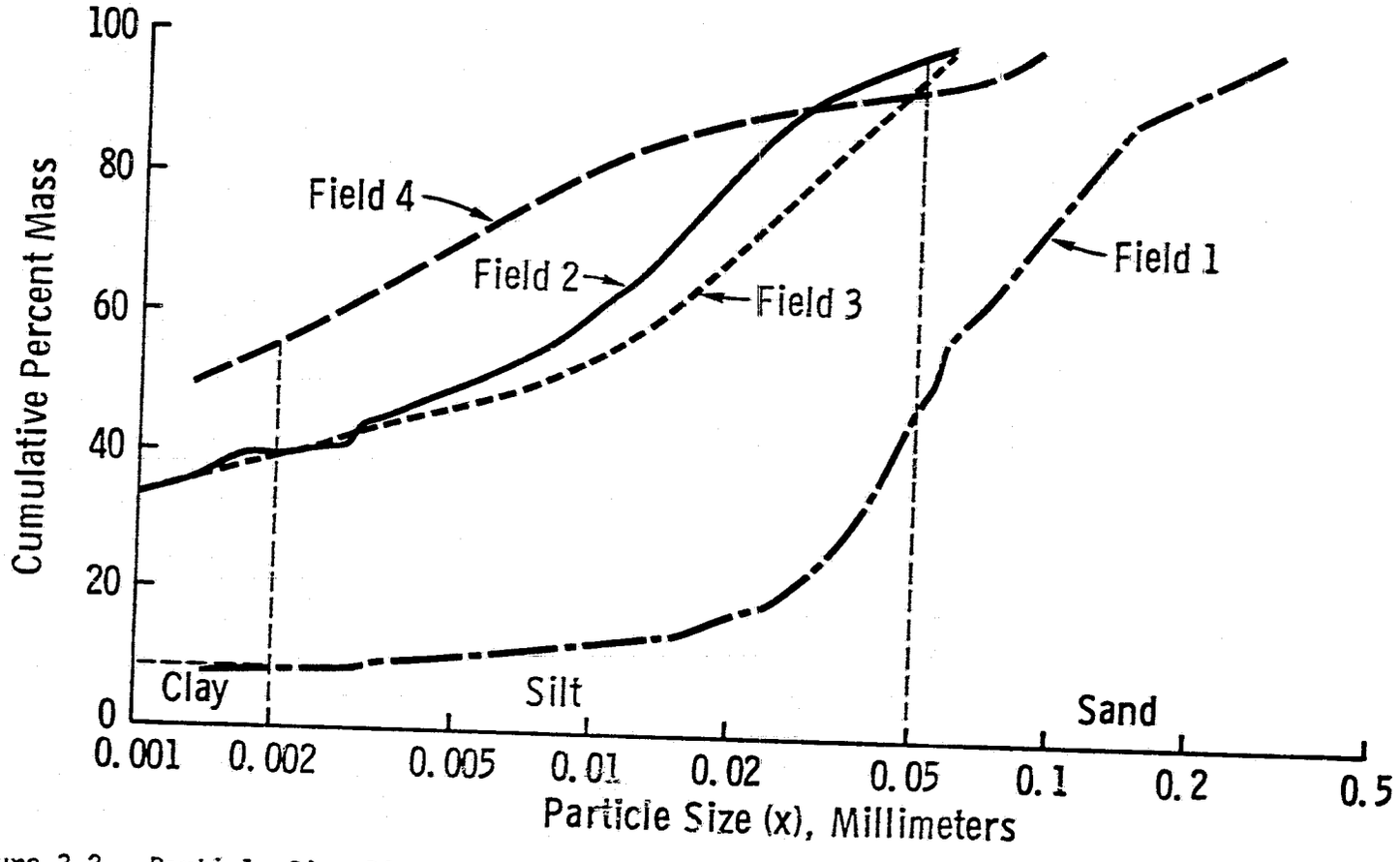

Figure 3.2. Particle Size Distribution: 0-5 cm layer of sandy loam, silty clay loam and silty clay fields from the 1977 Bare Soil Experiment.

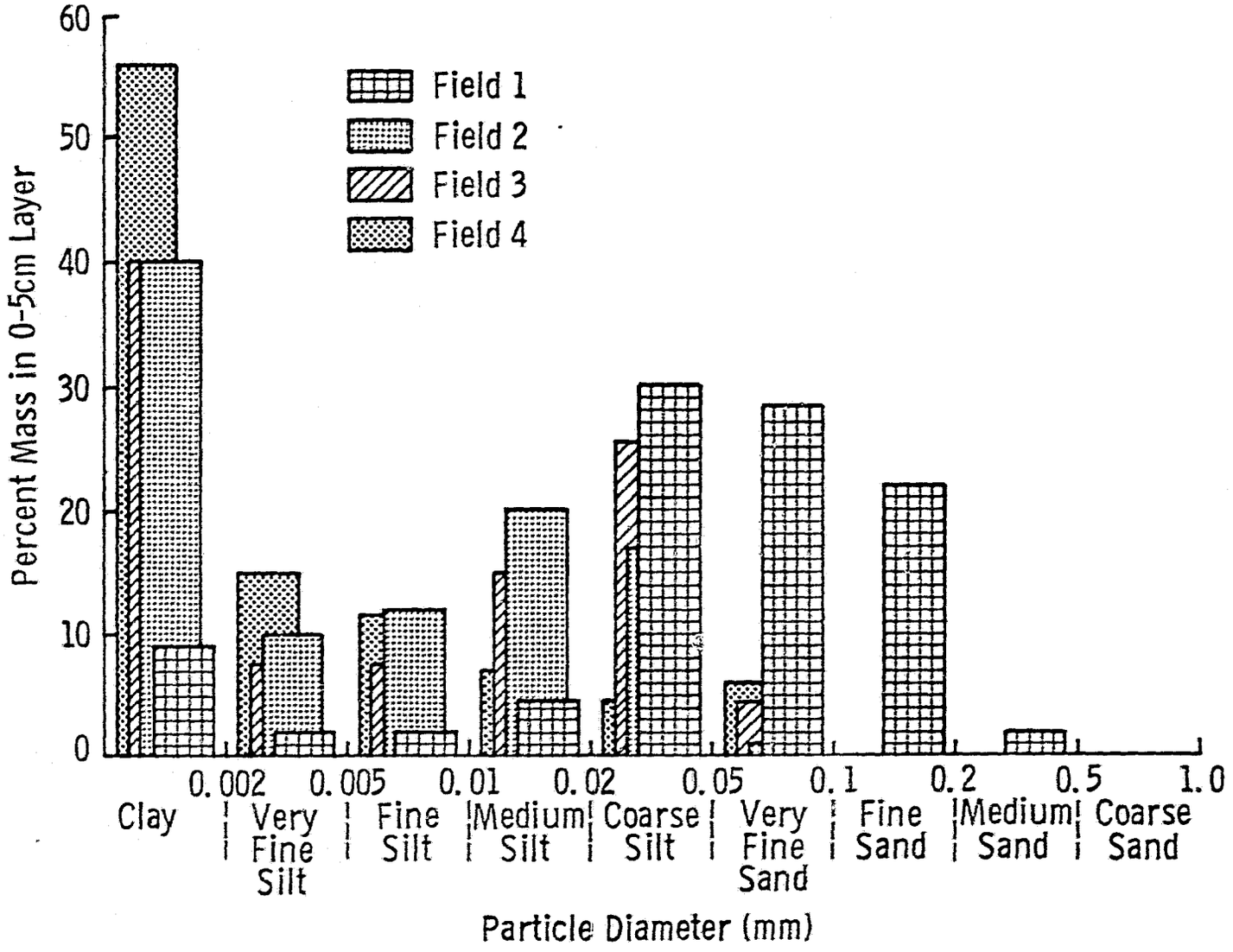

Figure 3.3. Histogram of soil particle size distribution for soils examined during the 1977 Bare Soil Experiment.

Figure 3.4

Initial Soil Roughness Conditions on Bare Soil 1977 Fields 1 to 4. Plots of Detrended Soil Surface vs. Surface Height. Transects are Parallel to Radar Look Direction.

a) Field 1 Date: 8/15/77 RMS Height: 1.66cm

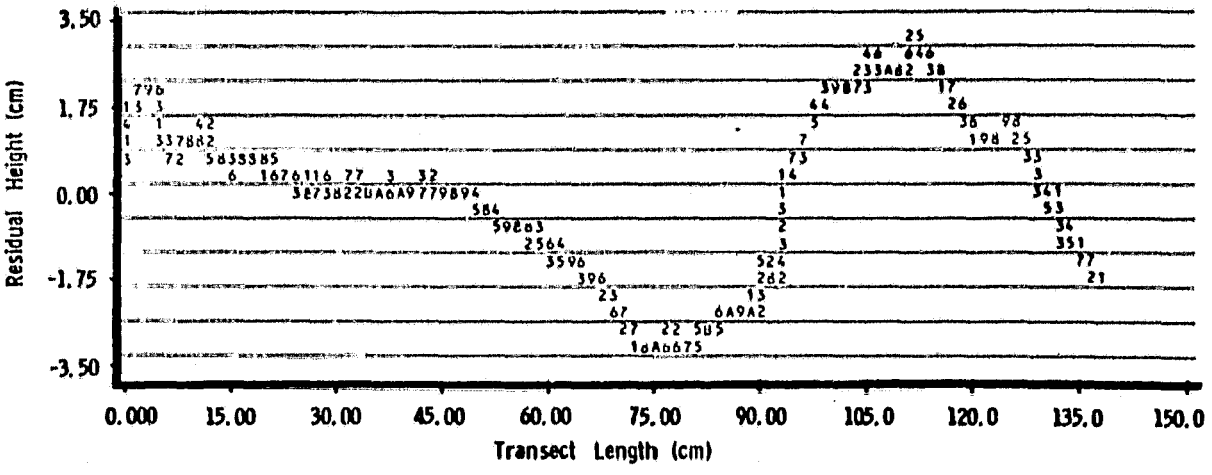

b) Field 2 Date: 8/15/77 RMS Height: 1.49cm

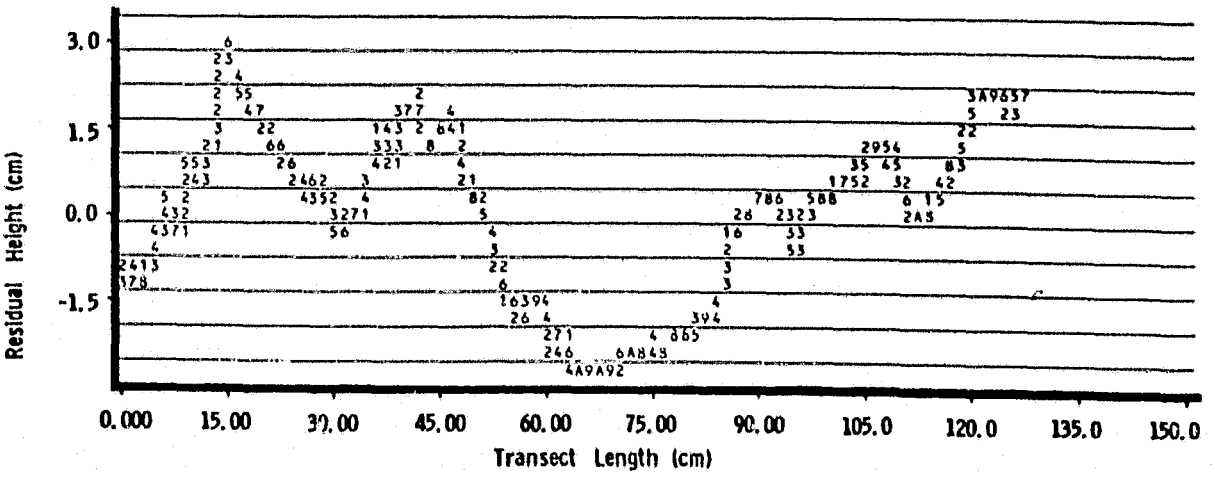

c) Field 3 Date: 9/3/77 RMS Height: 1.75cm

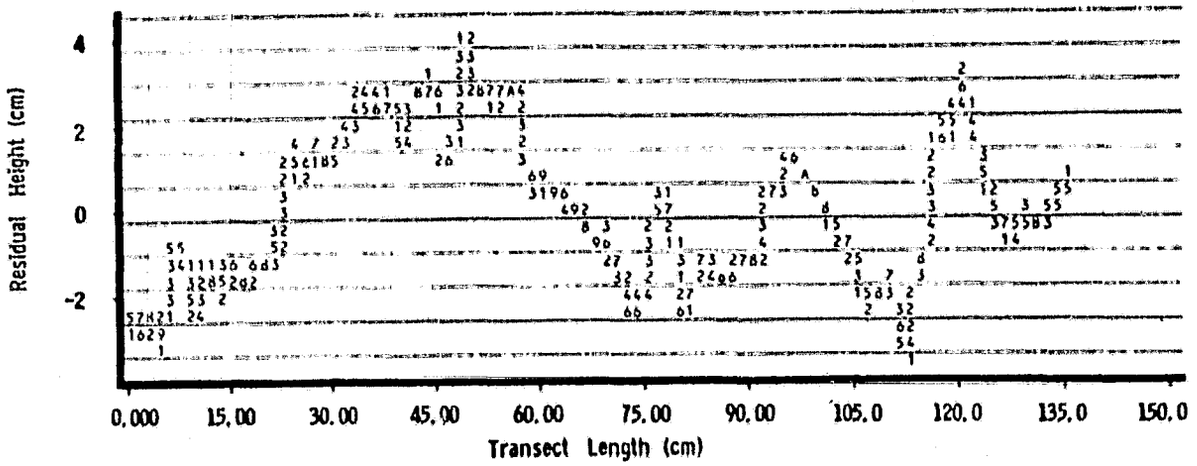

d) Field 4 Date: 8/15/77 RMS Height: 0.72cm

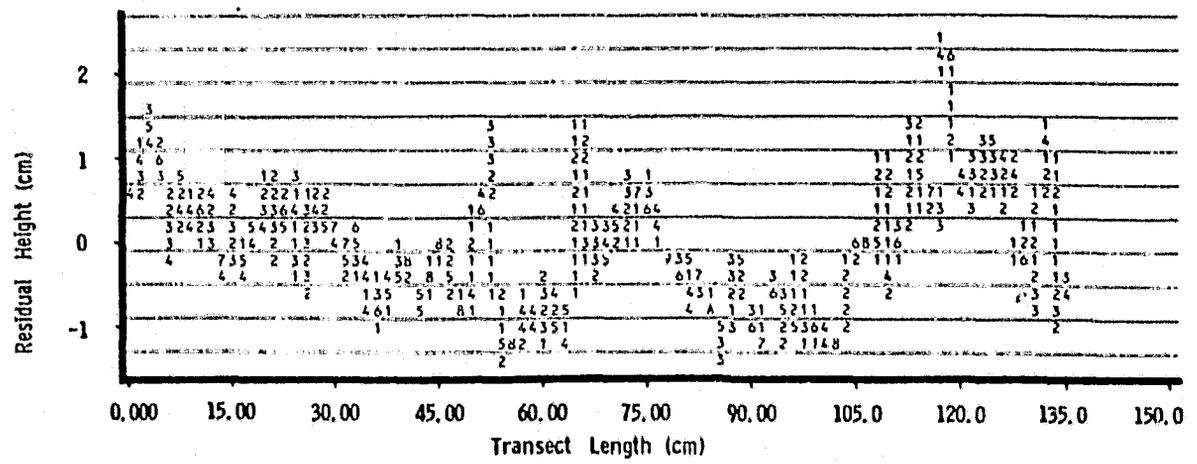

TABLE 3.9

1977 Bare Soil RMS Surface Roughness (cm)

Field Number	1		2		3		4	
Direction of Transect (Relative to radar look direction)	Parallel	Perpendicular	Parallel	Perpendicular	Parallel	Perpendicular	Parallel	Perpendicular
DATE: 8/15	1.66	1.33	1.49	0.94			0.72	0.60
8/22			0.42	0.61				
9/2	1.15	0.85						
9/3					1.75	2.06		
9/6							0.68	0.97
9/20	1.17	1.04						
9/24					0.52	0.79		
9/28			0.47	0.55				
9/30					0.83	1.10	0.69	0.33
MEAN	1.32	1.07	0.79	0.70	1.03	1.32	0.70	0.63

variance ratio tests. The variance ratio test results indicated that the variances about the four field means could not be considered unequal at the 0.1 level of significance. Two-tailed t-tests of the sample means at the 0.01 significance level indicated a high probability that only fields 1 and 4 are different with respect to RMS height, all other field pairs were found to be similar at the stated significance level.

Inspection of the mean values shown in Table 3.9 indicates that, on the basis of RMS surface roughness, the four test fields cluster into two groups:

a) fields 1 and 3 with a net mean RMS height in all look directions of 1.19 cm, and

b) fields 2 and 4 with a net mean RMS height in all look directions of 0.71 cm.

3.2.3 Soil Bulk Density

Soil bulk density is not easily measured for the thin soil layers sampled during the bare soil experiment. Because of the time involved in the careful extraction and delicate handling of an accurate bulk density sample, adequate bulk density sampling was adjudged to consist of a minimum of three samples at each grid location and depth shown on Figure 3.1. Bulk density samples were taken when field moisture profiles permitted minimal soil compaction during sampling. The drainage characteristics of field 1 were such that bulk density profiles could be taken in conjunction with soil moisture samples during 60% of the data sets, while the other three fields could only be sampled for bulk density three to six times during the course of the experiment. Table 3.10 shows the number of bulk density samples acquired at each location and depth during the course of the experiment. The high percentage of clay present in Field 4 and the saturated soil profiles common to this field made accurate bulk density sampling of the surface layers nearly impossible during the experiment and is responsible for the low sample size presented in Table 3.10.

Two methods were employed to collect bulk density samples. The standard method was to extract core samples of known volume and then dry the soil to compute bulk density. When the above method proved to be unacceptable due to soil compaction by the coring tool, bulk density was

TABLE 3.10

Number of Bulk Density Samples
Collected at Each Sample Grid Location

Field	Depth (cm)	Locations 1	2	3	4	5	6	7	8	Total
1	0-1	14	14	14	13	12	15	14	13	109
	1-2	15	14	14	13	13	15	14	13	111
	2-5	15		14			14	14		57
	5-9	12		10			9	11		42
	9-15	11		10			9	11		41
2	0-1	5	5	5	5	4	5	4	3	36
	1-2	5	5	6	6	5	6	3	2	38
	2-5	9		8			8	7		32
	5-9	6		6			5	4		21
	9-15	7		6			5	5		23
3	0-1	3	4	5	4	3	3	3	3	28
	1-2	3	4	5	4	3	3	3	3	28
	2-5	5		5			6	6		22
	5-9	4		6			5	5		20
	9-15	4		6			5	5		20
4	0-1	1	1	2	1	1	1	2	1	10
	1-2	1	2	1	1	1	1	2	1	10
	2-5	3		1			---	3		7
	5-9	7		4			5	8		24
	9-15	7		5			5	8		25

determined from the liquid volume displacement of saran coated soil clods extracted from the locations and depths given in Figure 3.1.

A summary of the depth weighted mean bulk densities of each field is presented in Table 3.11a. The standard deviation associated with each of these field means is given in Table 3.11b. These statistics are derived from the distribution of the mean bulk densities at each location within a field.

Initial analysis of the above bulk density data indicates that the four test fields are relatively homogeneous. These results validate the assumption that the soil fabric of the individual test fields had stabilized prior to the beginning of the experiment. The actual density values of each field are highly deperdent upon soil texture, and hence, a low intrafield variance in bulk density supports the contention of low intrafield variance in soil texture.

However, a more complex picture emerges when consideration is given to the distribution of all samples given in Table 3.10 for a particular field and depth. Table 3.12 presents the sample distributions of bulk density in the 1-2 cm layer of fields 1 and 2. The tendency toward a bimodal distribution of density as seen in Table 3.12b for field 2 is typical of fields 2, 3 and 4. The characteristics of all such sample distributions are summarized by statistics for the mean density, 90% confidence interval, skewness and kurtosis given in Table 3.13. The large 90% confidence interval around the mean, commonly .2 to .3 g/cm^3, is due to the combined effects of sampling error, locational variance, density changes in the surface layer associated with the development of soil structure through time and the functional dependence of density on moisture in fields with a high clay content such as fields 2, 3 or 4. The values of skewness and kurtosis indicate that densities are normally distributed about the means and the distributions are generally less peaked than a normal distribution; this is due primarily to the fact that, with the exception of field 1, density was sampled over a very small range of gravimetric moisture especially in the surface layers. The negative values of skewness obtained primarily for the deeper depth intervals of the high clay fields is indicative of the correlation between density and moisture which was found to be as high as -0.7 for these layers.

TABLE 3.11

Comparison of Mean Bulk Densities from
Fields 1 to 4 of the 1977 Bare Soil Experiment

A. Weighted Mean Bulk Density 0-1, 0-2, 0-5, 0-9 and 0-15 cm as computed from measurements at each location.

Depth Interval (cm)	Field Designation			
	1	2	3	4
0-1	1.43	1.22	1.20	1.30
0-2	1.42	1.22	1.24	1.34
0-5	1.27	1.00	1.11	1.17
0-9	1.32	1.12	1.21	1.27
0-15	1.43	1.26	1.30	1.33

B. Standard Deviation of Location Means around the field mean bulk density at each depth.

Depth Interval (cm)	Field Designation			
	1	2	3	4
0-1	0.04	0.05	0.04	0.02
0-2	0.03	0.06	0.05	0.11
0-5	0.01	0.03	0.04	0.04
0-9	0.03	0.02	0.02	0.01
0-15	0.02	0.02	0.01	0.03

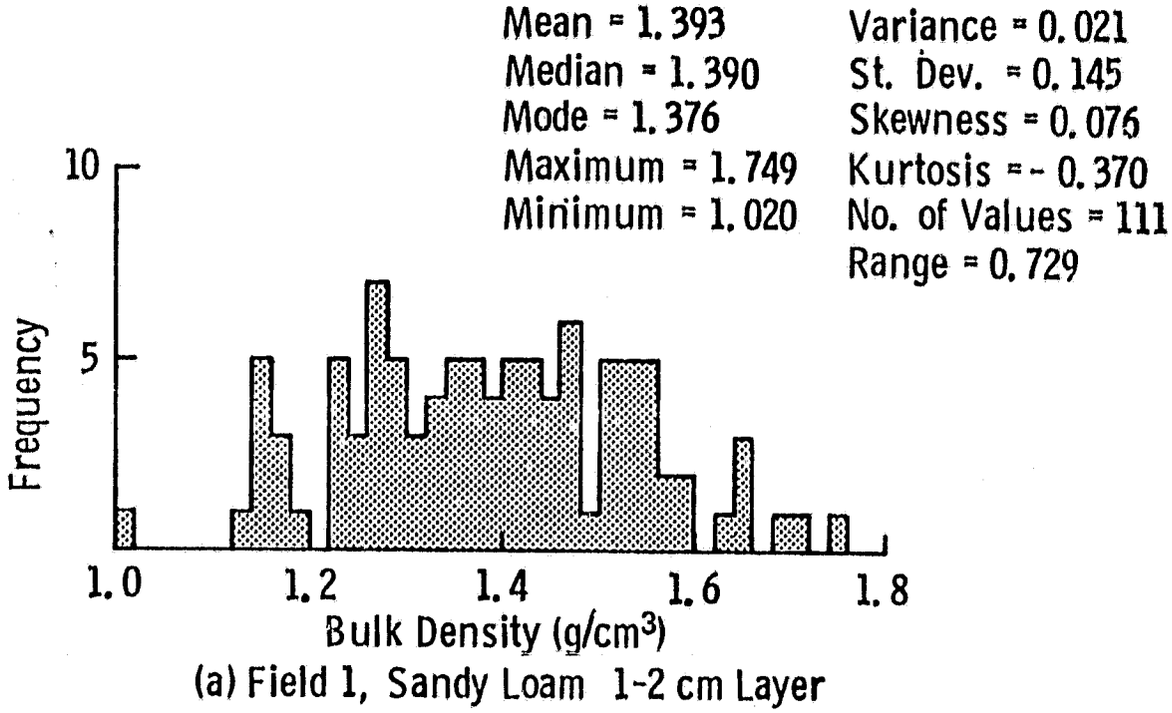

(a) Field 1, Sandy Loam 1-2 cm Layer

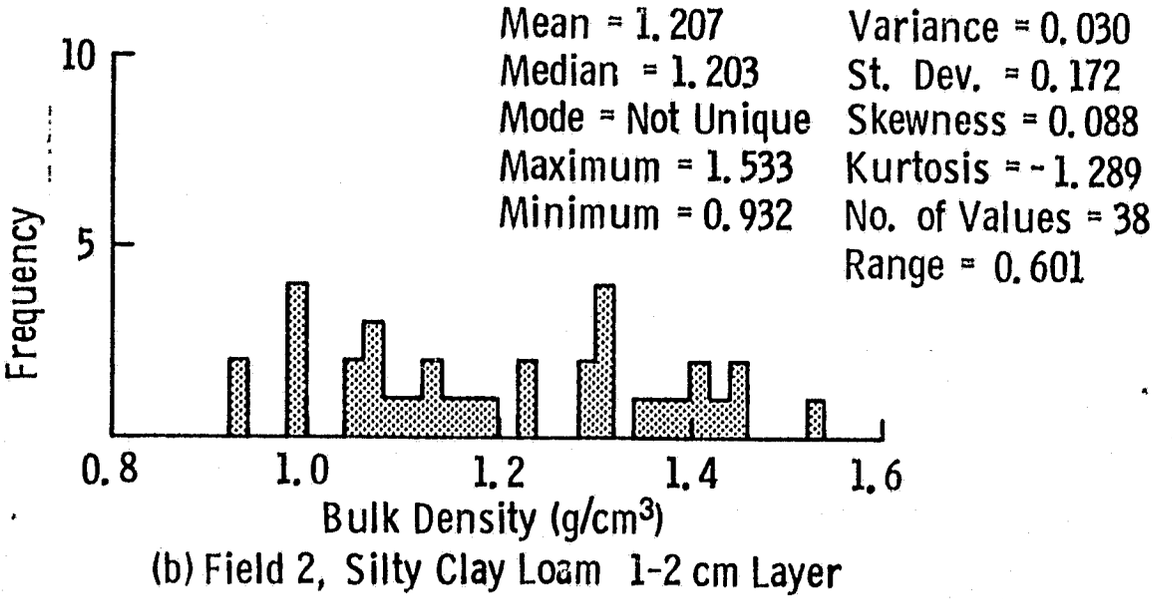

(b) Field 2, Silty Clay Loam 1-2 cm Layer

TABLE 3.12

Sampling Distribution of Bulk Density in the 1-2 cm Layer for a) Field 1, sandy loam and b) Field 2, silty clay loam.

TABLE 3.13

Skewness, Kurtosis and 90% Confidence Limits
Around Mean Bulk Density at Each Depth Interval

Field	Depth Interval (cm)	Mean Density (g/cm^3)	90% Confidence Interval (+/-g/cm^3)	Skewness	Kurtosis
1	0-1	1.435	.29	.636	.574
	1-2	1.393	.24	.076	-.370
	2-5	1.187	.25	.446	.640
	5-9	1.257	.15	.042	-.626
	9-15	1.433	.17	.350	-.231
2	0-1	1.219	.26	.172	-.260
	1-2	1.207	.28	.087	-1.289
	2-5	.846	.18	.155	-.636
	5-9	1.267	.16	.376	-.421
	9-15	1.462	.11	-.049	-.905
3	0-1	1.209	.30	-.068	-.878
	1-2	1.260	.24	.877	.478
	2-5	1.008	.21	.087	-.778
	5-9	1.343	.20	-.318	-1.343
	9-15	1.439	.14	.157	-.723
4	0-1	1.291	.19	.154	-.945
	1-2	1.348	.27	.220	-1.806
	2-5	1.053	.23	.138	-1.403
	5-9	1.370	.18	-.958	.446
	9-15	1.423	.14	-.570	.944

Since most of the bulk density samples for fields 2, 3 and 4 were obtained over a relatively small range of gravimetric soil moisture, possible shrink-swell effects upon bulk density as a function of moisture are not accounted for by use of a mean field bulk density. Thus, the use of a mean bulk density as an assumed constant for each field and depth interval may introduce a bias into the volumetric moisture values. A simple physical model to account for shrink-swell effects on bulk density is presented in Appendix A.

3.2.4 Soil Moisture

Soil samples were extracted from the sampling grid locations shown in Figure 3.1 for the determination of gravimetric moisture M_g in conjunction with each radar data set. The soils were dried to equilibrium using a microwave oven as documented in Dobson, 1979.

For each data set, a mean moisture and standard deviation about the mean were calculated for each depth interval (0-1, 1-2, 2-5, 5-9 and 9-15 cm) which could then be ratioed as the coefficient of variation. These three statistics are summarized for the 0-1 cm layer of each field in Figure 3.5. The wide range of surface moisture observed during the experiment was due to repeated heavy rainfall incidents (3 in excess of 2 inches) which allowed surface soil moisture to vary from the wilting point at 15 bars of tension to saturation (in fields 2, 3 and 4). The large standard deviations around the mean moisture found predominantly in fields 2, 3 and 4 tended to occur shortly after precipitation events during the initial drying stages of the surface. Surface variance in soil moisture was heightened by the intersection of the water table with the soil surface in fields 2 and 4 which produced partial flooding within topographically low portions of the test fields. A comparison of the 0-1 cm moisture distributions with those at the 2-5 and 9-15 cm depths (Figures 3.5, 3.6 and 3.7, respectively) indicates that the large temporal variance in surface moisture approaches a field constant as depth increases. Also, the standard deviation of sampled soil moisture is observed to decrease with depth. An examination of these figures clearly indicates that soil moisture falls into three sample populations which become more distinct with increasing depth where field 1 (sandy loam) is driest, fields 2 and 3 (silty clay loams) are wet and field 4 (silty clay) is slightly but significantly wetter. This is to be

Figure 3.5 HISTOGRAMS OF 0-1 cm MEAN SOIL MOISTURE, STANDARD DEVIATION AND STANDARD DEVIATION TO MEAN RATIO

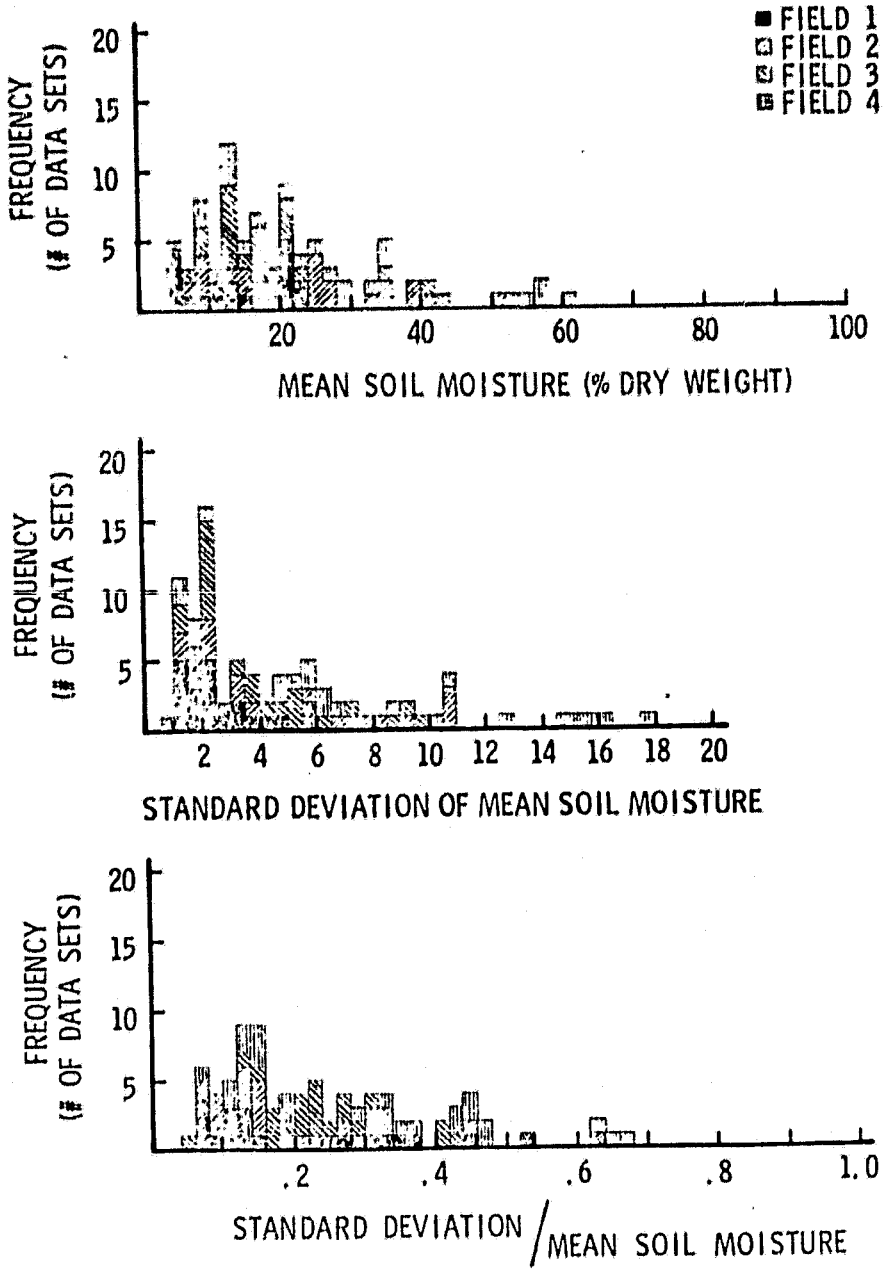

Figure 3.6 HISTOGRAMS OF 2-5cm MEAN SOIL MOISTURE, STANDARD DEVIATION AND STANDARD DEVIATION TO MEAN RATIO

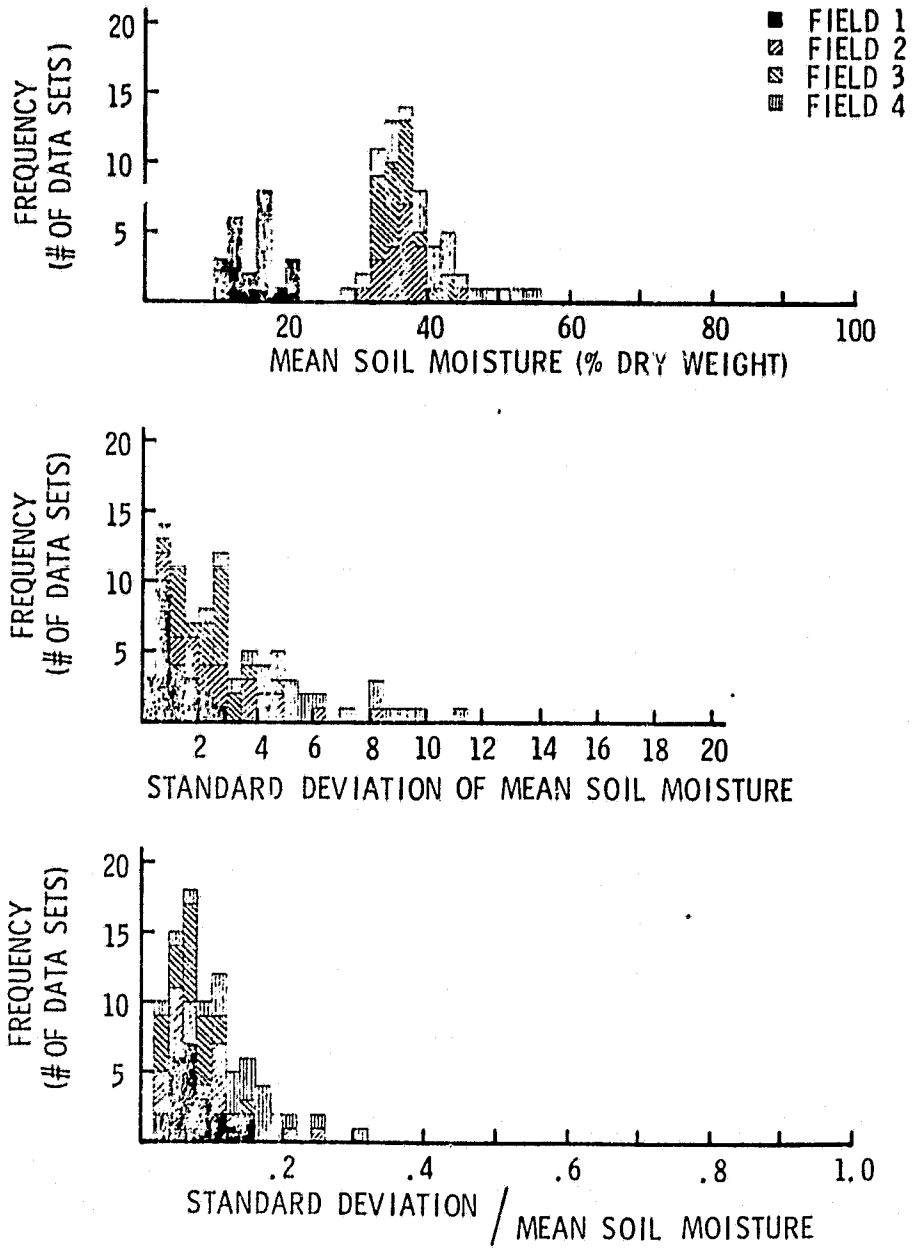

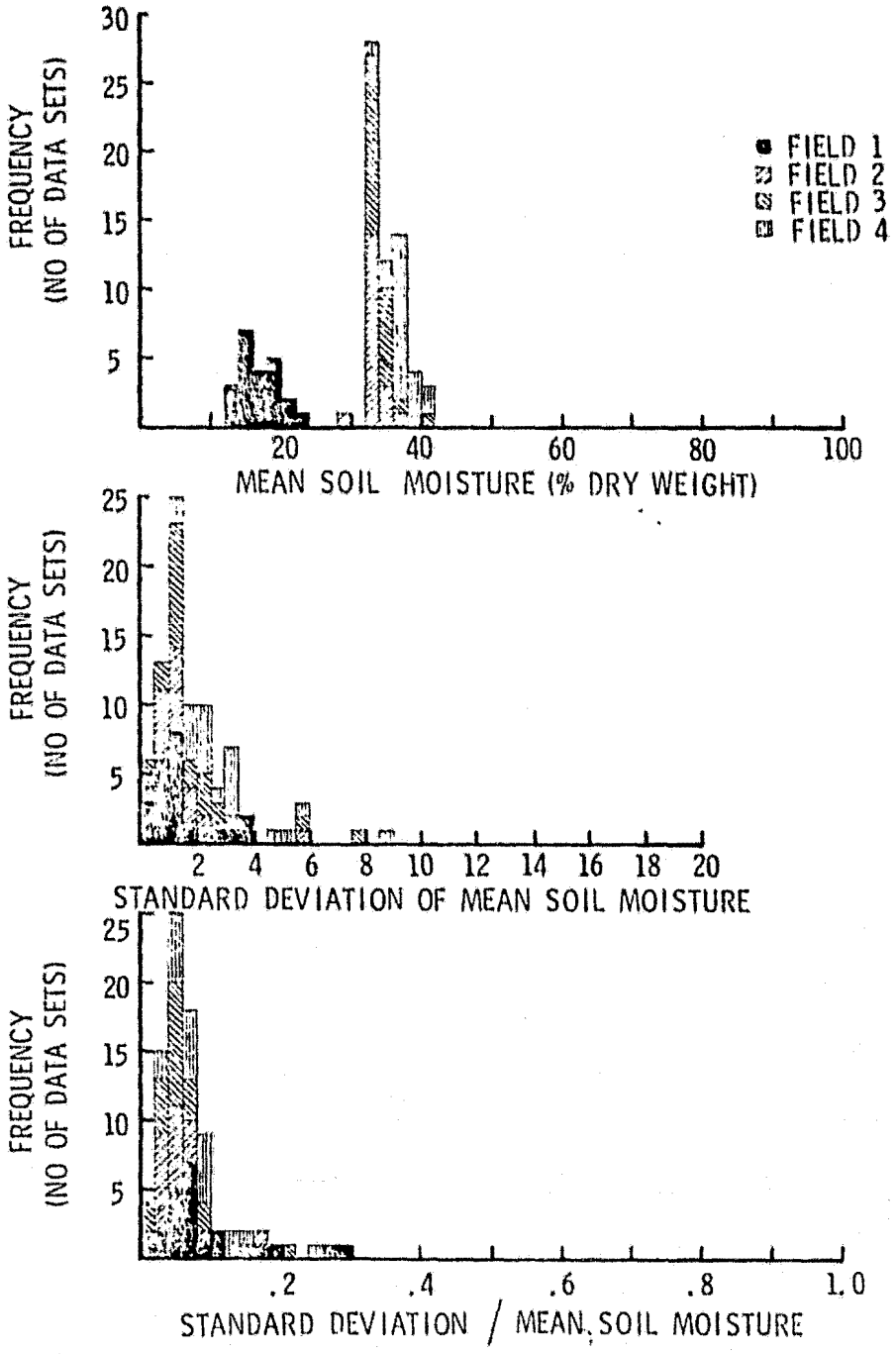

Figure 3.7 HISTOGRAMS OF 9-15cm MEAN SOIL MOISTURE, STANDARD AND DEVIATION AND STANDARD DEVIATION TO MEAN RATIO

expected and is a function of the drainage characteristics and textural composition of each field. Field 1 drained readily due to its height above a roadside drainage ditch and the high hydraulic conductivity of the sandy soil while fields 2, 3 and 4 had poor drainage and high clay contents which resulted in greater water retention.

The soil moisture histories of each field are given in Figures 3.8 to 3.11 to show graphically the change in the moisture profile of each field as a function of time and are annotated as to the presence of flooding.

3.3 Angular Response of Radar Backscatter

The radar backscattering coefficient σ^o was measured at three angles of incidence. σ^o is plotted as a function of incidence angle θ for a range of soil moistures at 1.6, 4.6 and 7.6 GHz for fields 1 to 4 in Figures 3.12 to 3.15 respectively. In general, the rate of decrease in σ^o as a function of θ indicates that all of the fields are relatively smooth within the 1-8 GHz frequency range and that all fields have similar roughness. The Rayleigh criterion, equation (2.21), establishes the values for a smooth surface given in Table 3.14 at 1.6, 4.6 and 7.6 GHz at 10° and 20° incidence angles. For fields with RMS heights less than these values the soil surface should appear electromagnetically smooth and exhibit a large drop in σ^o with increasing incidence angle θ, while the σ^o vs. θ curve should become increasingly flat for RMS heights greater than the criterion values in Table 3.14. The sensitivity of σ^o to θ for a given field and moisture condition tends to decrease as frequency increases especially for fields 1 and 3 which were slightly rougher than fields 2 and 4 in terms of RMS height; this is to be expected from the Rayleigh criterion for surface roughness.

Figures 3.12 to 3.15 indicate a clear dependence of σ^o on soil moisture within each field at all angles and frequencies. However, as soil moisture conditions approach and exceed saturation, there is a marked drop of σ^o to values comparable to those of moderately wet conditions (Figures 3.14 and 3.15) especially at 7.6 GHz. Saturation moisture Mg as defined by soil porosity is approximately 32, 44, 45 and 39% for the 0-1 cm layer of fields 1 to 4, respectively. This phenomenon can be explained as a roughness effect; at saturation the soil appears as a smooth surface

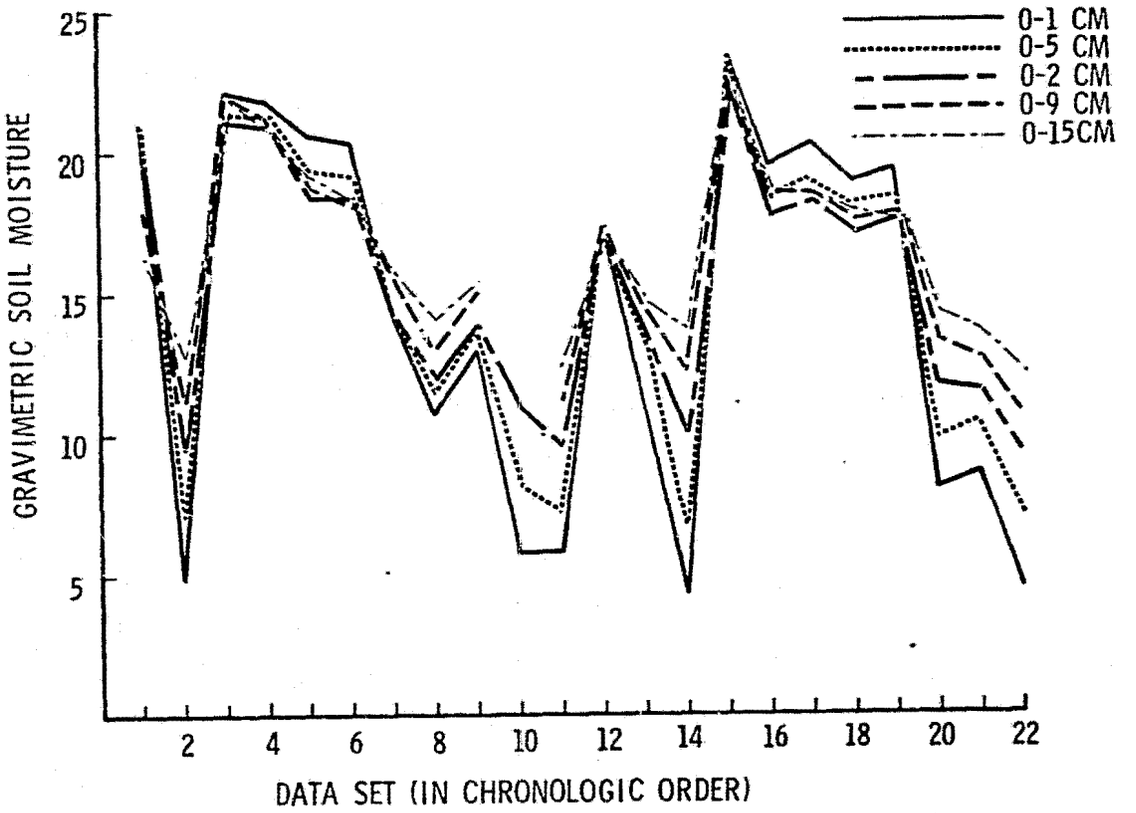

Figure 3.8 TEMPORAL SOIL MOISTURE FLUX, FIELD 1: Sandy loam.

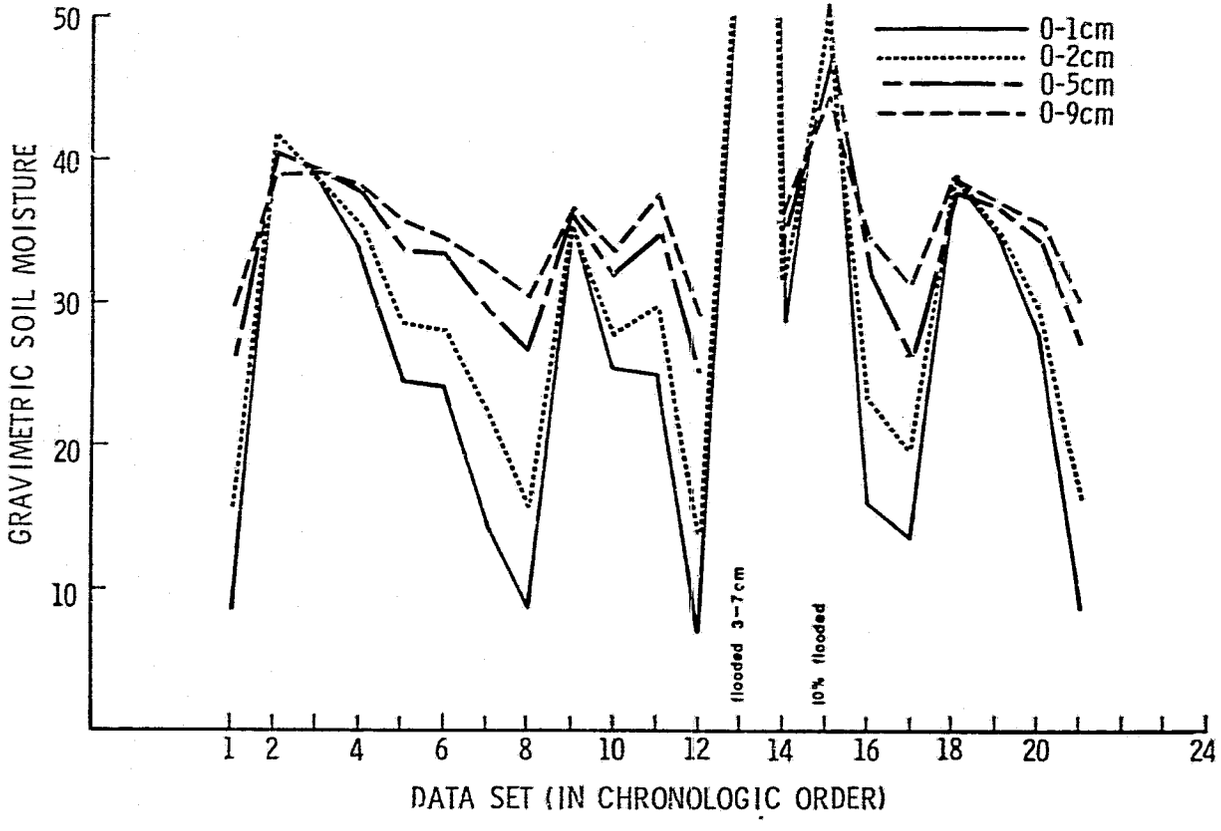

Figure 3.9 TEMPORAL SOIL MOISTURE FLUX, FIELD 2: Silty clay loam.

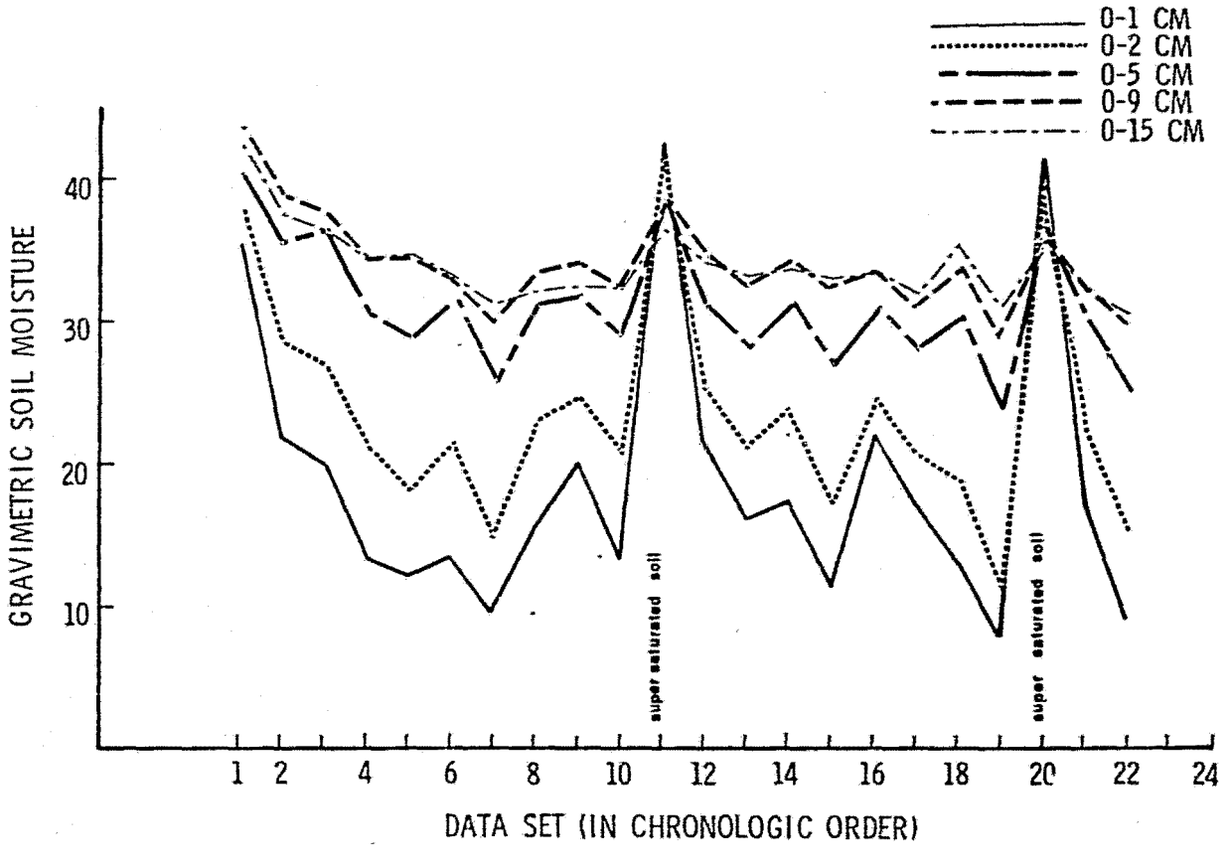

Figure 3.10 TEMPORAL SOIL MOISTURE FLUX, FIELD 3: Silty clay loam.

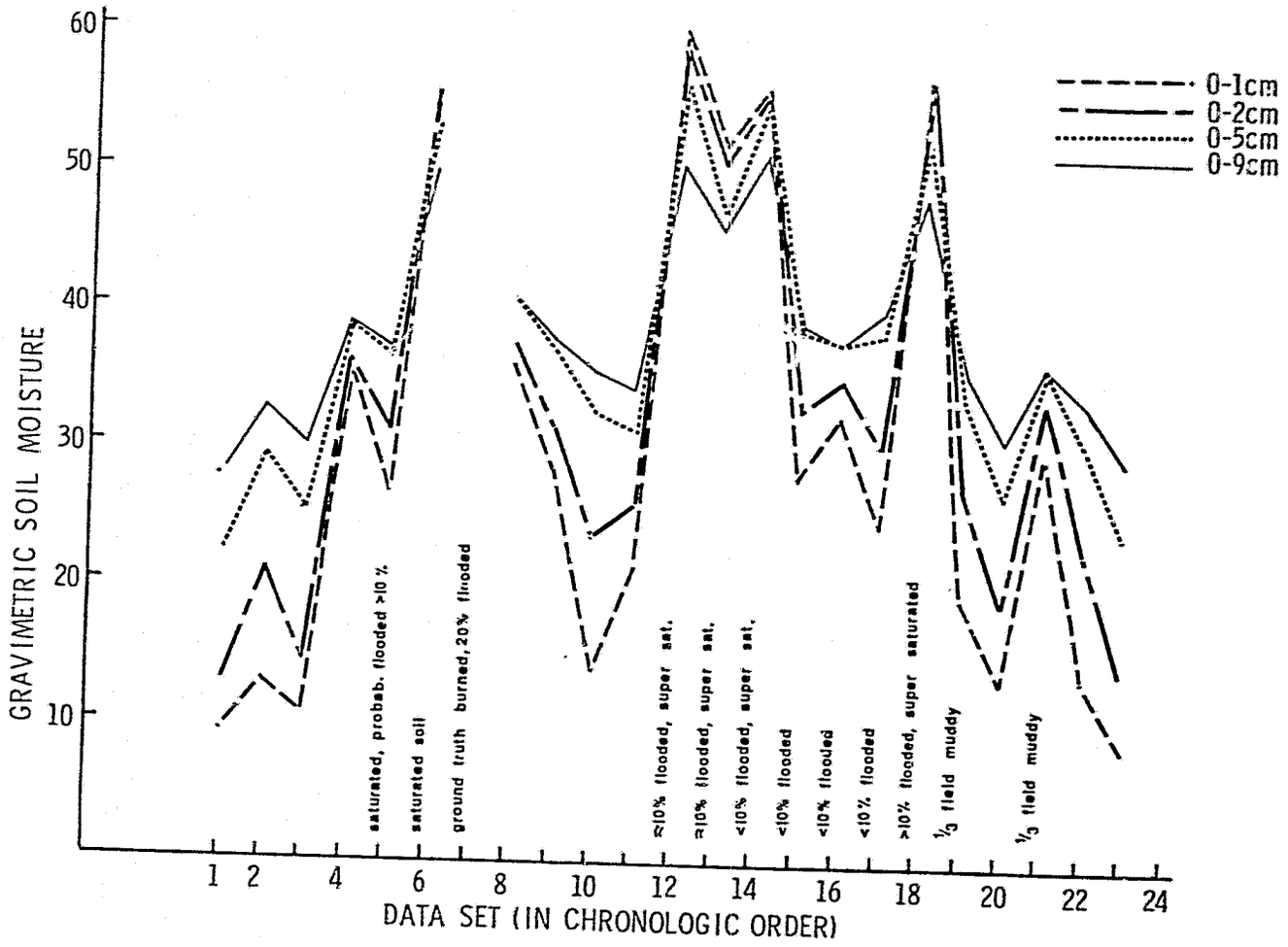

Figure 3.11 TEMPORAL SOIL MOISTURE FLUX, FIELD 4: Silty clay.

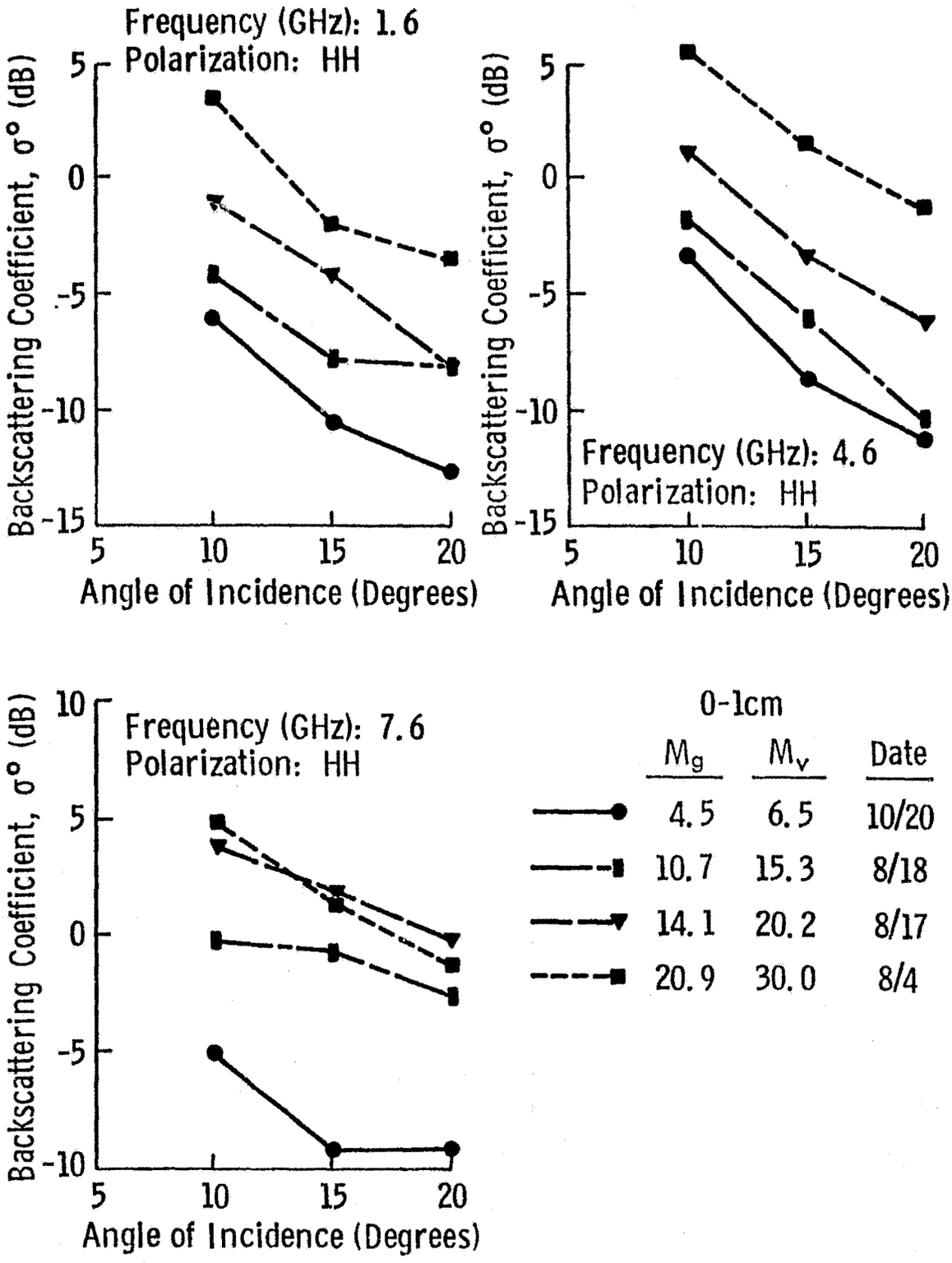

Figure 3.12. Angular response of σ° at 1.6, 4.6 and 7.6 GHz to a range of surface moisture conditions in Field 1, sandy loam.

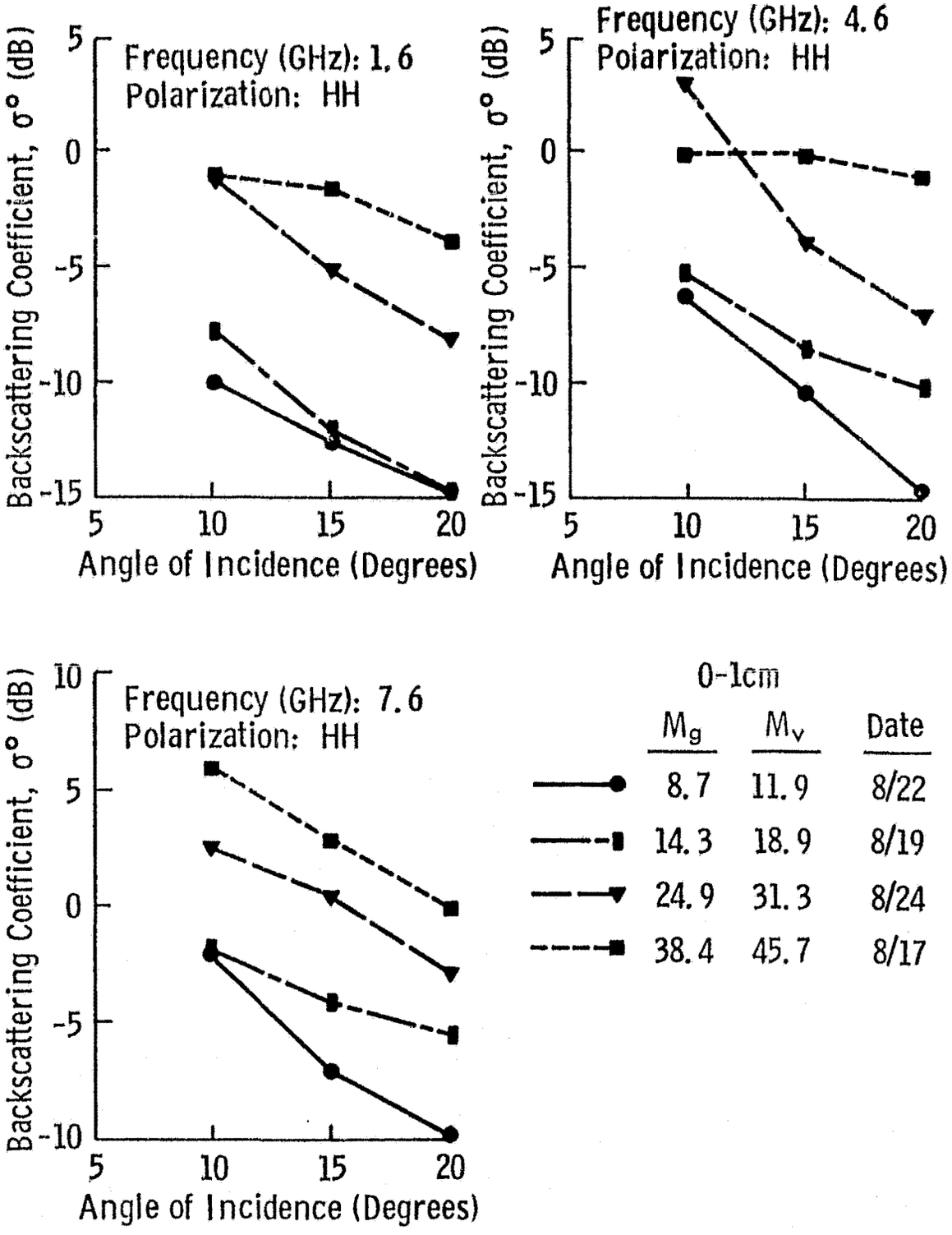

Figure 3.13. Angular response of σ° at 1.6, 4.6 and 7.6 GHz to a range of surface moisture conditions in Field 2, silty clay loam.

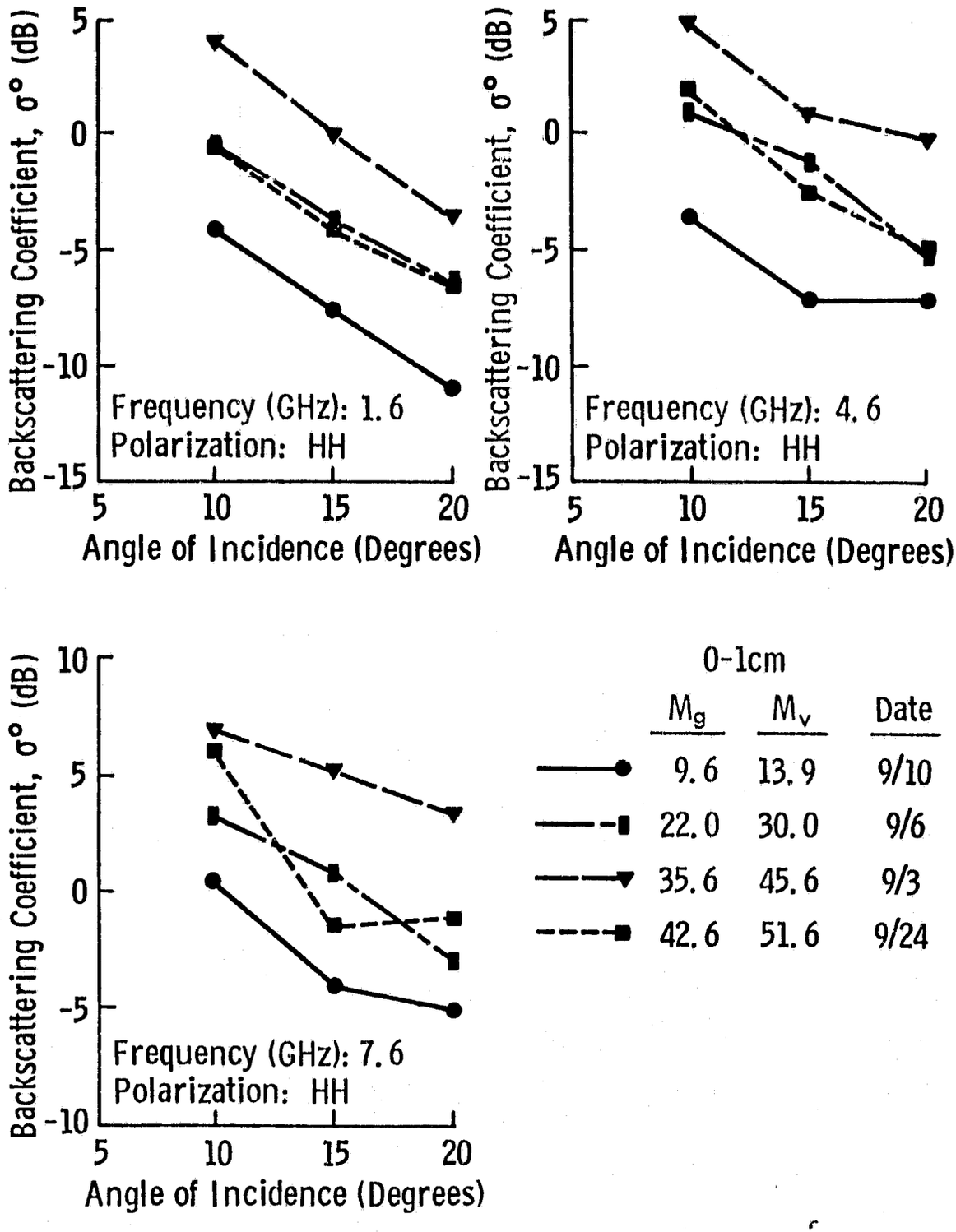

Figure 3.14. Angular response of σ° at 1.6, 4.6 and 7.6 GHz to a range of surface moisture conditions in Field 3, silty clay loam.

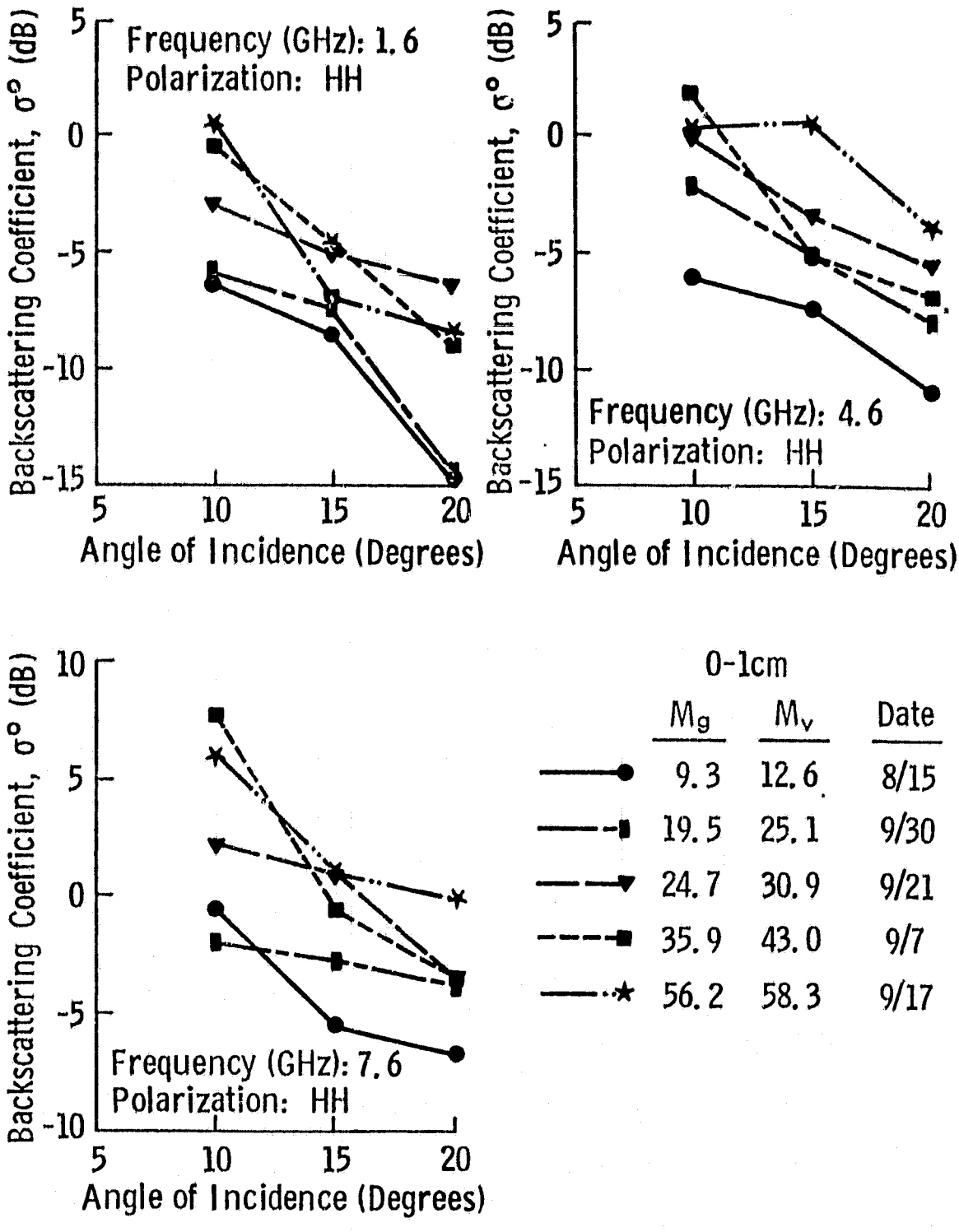

Figure 3.15. Angular response of σ° at 1.6, 4.6 and 7.6 GHz to a range of surface moisture conditions in Field 4, silty clay.

TABLE 3.14

The Rayleigh Criterion for Electromagnetic ally Smooth Surfaces. A smooth surface has variations relative to a reference plane $\leq$ to the values shown for 1.625, 4.625 and 7.625 GHz at 10° and 20°.

Frequency (GHz)	Criterion Values (cm) 10°	20°
1.625	2.35	2.46
4.625	0.825	0.865
7.625	0.495	0.519

and reflection is more specular, hence the backscattered portion of the signal falls more dramatically as θ increases. At nadir it is expected that σ^o of saturated soil would be higher than σ^o of unsaturated soil; unfortunately 0^o data was not acquired during the course of the experiment. Other polarization configurations display angular response characteristics similar to those shown for HH polarization.

3.4 Frequency Response of Radar Backscatter

Radar backscatter was measured at eight center frequencies between 1 and 8 GHz. The frequency responses of the like polarizations, HH and VV, were found to be almost identical while the response of the cross-polarized antenna configuration was difficult to characterize because a significant number of the measurements were below the noise floor of the system.

The HH polarized frequency response of σ^o is shown in Figures 3.16 to 3.19 for each field over a range of 0-1 cm moisture conditions. For soil moistures below saturation, σ^o is observed to increase monotonically as a function of frequency if small fluctuations on the order of +/- 1 dB due to signal fading are ignored. This behavior was expected based upon similar results from data sets acquired in 1974 and 1975 for non-vegetated fields of Miller clay and Eudora silt loam respectively using the MAS system. σ^o is observed to be proportional to soil moistures below saturation at all frequencies and incidence angles. However, soil moistures above saturation (Figures 3.18 and 3.19) produce a drop in σ^o relative to wet but unsaturated moisture conditions at all frequencies and angles. As previously stated, this is felt to be caused by more specular reflection from the saturated soil relative to the unsaturated state. Furthermore, when moisture conditions approach saturation, σ^o is observed to loose its monotonic dependence on frequency and tends to oscillate in excess of theoretical fading considerations. This non-monotonic behavior may be a resonance effect dependent upon frequency, incidence angle and the soil moisture profile as a function of depth. Additional experimentation is necessary to adequately account for this behavior in terms of moisture profile shape and moisture layering phenomena as they affect depth penetration and multiple reflections of the incident beam within the 1-8 GHz frequency region.

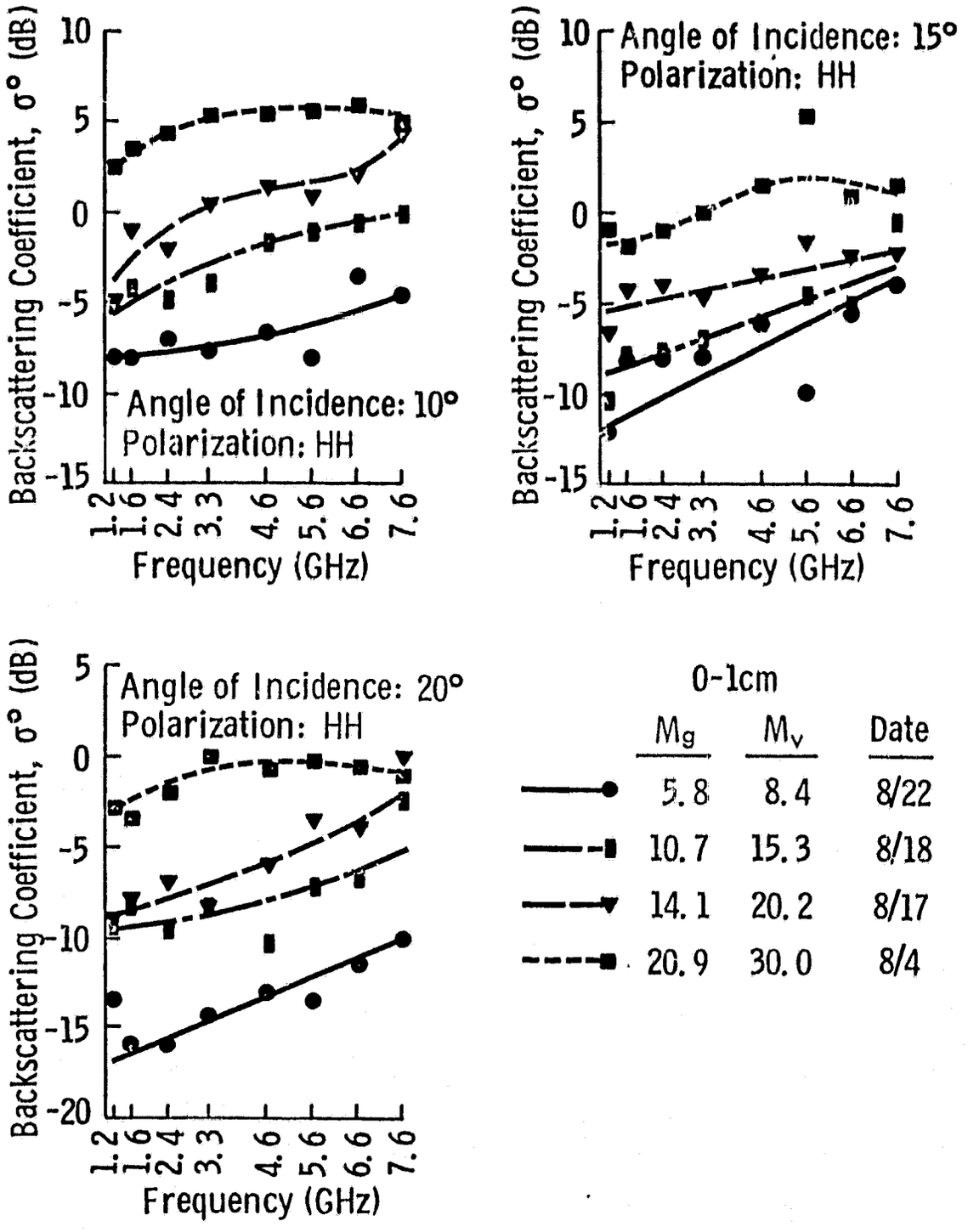

Figure 3.16. Frequency response of σ°, HH polarization at 10°, 15° and 20° for a range of surface moisture conditions in Field 1, sandy loam.

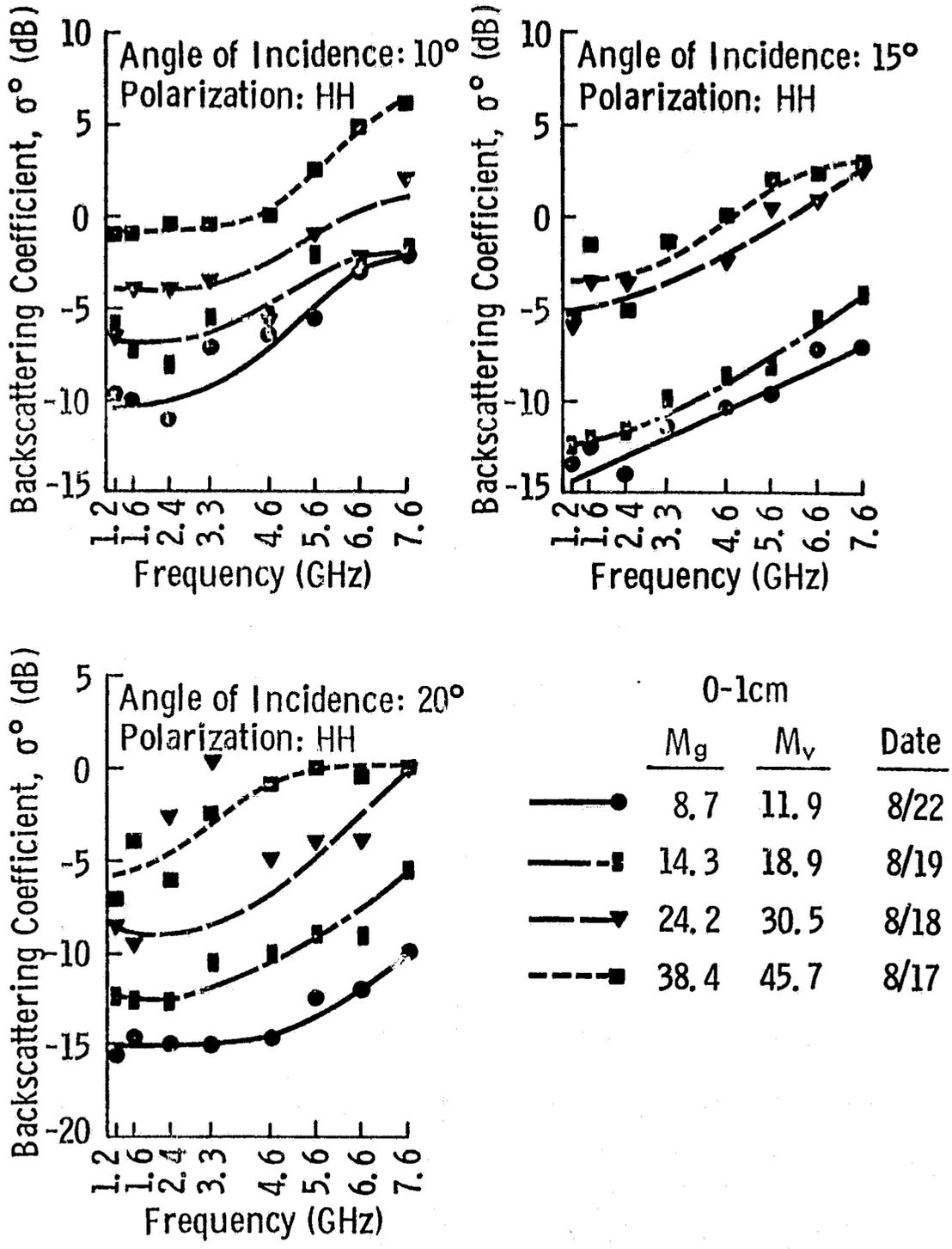

Figure 3.17. Frequency response of σ°, HH polarization at 10°, 15° and 20° for a range of surface moisture conditions in Field 2, silty clay loam.

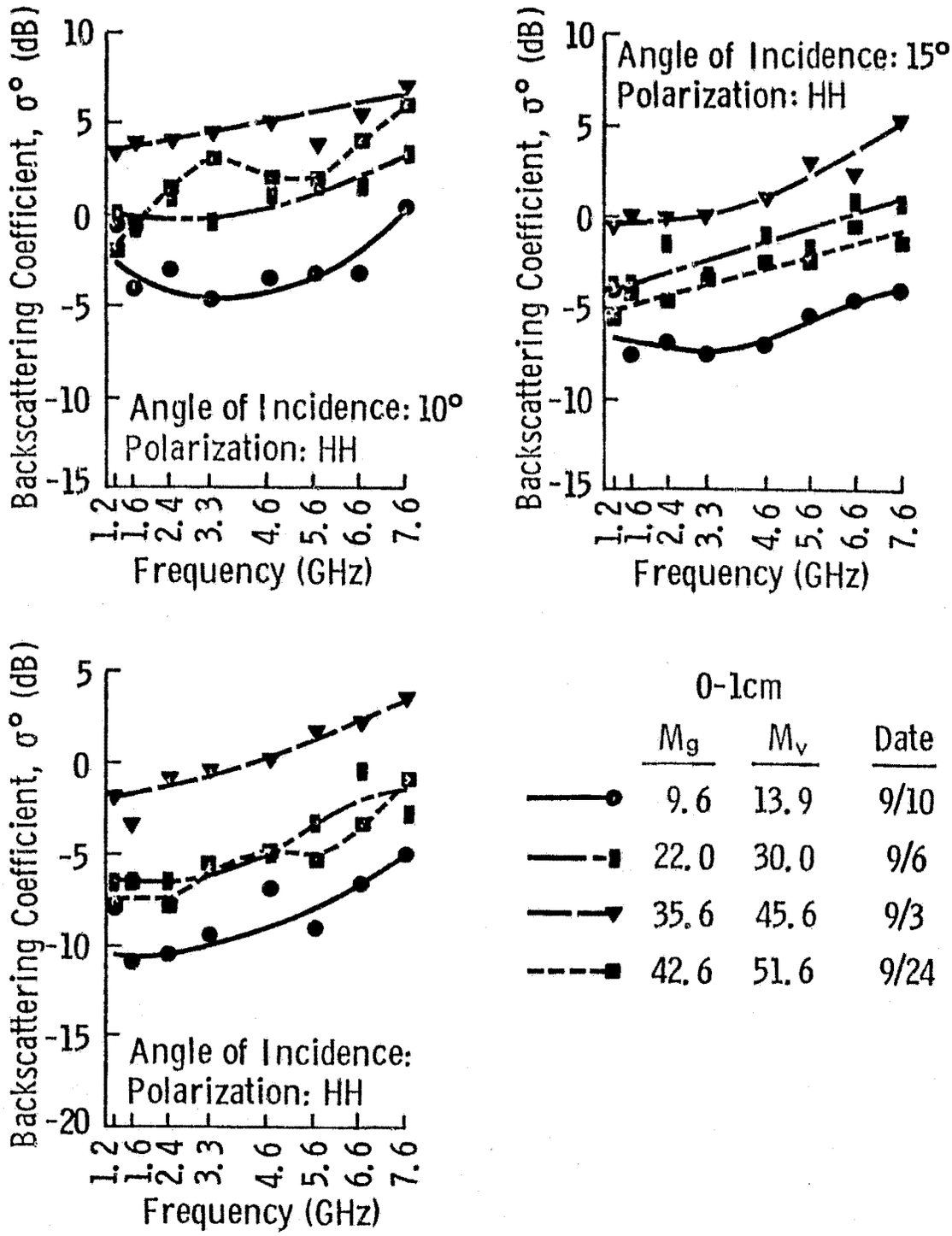

Figure 3.18. Frequency response of σ°, HH polarization at 10°, 15° and 20° for a range of surface moisture conditions in Field 3, silty clay loam.

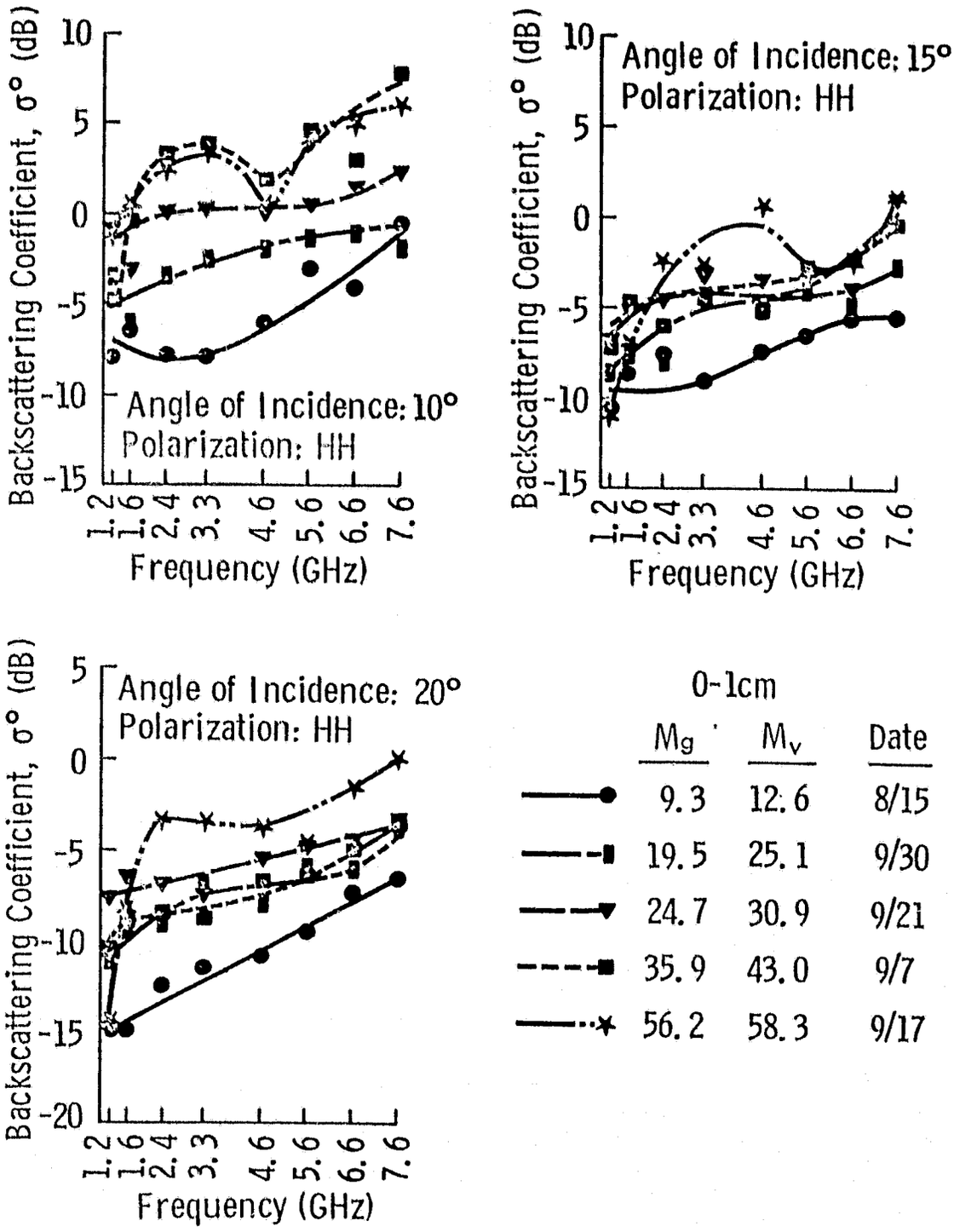

Figure 3.19. Frequency response of σ°, HH polarization at 10°, 15°, and 20° for a range of surface moisture conditions in Field 4, silty clay.

Also, field 2 tended to exhibit highly irregular frequency response at all intermediate moisture conditions although this is not readily apparent from examination of Figure 3.17. This was felt to be caused by variance in surface moisture, density and texture within the field and will be treated in Section 3.7.

3.5 Radar Backscatter Dependence on Gravimetric Soil Moisture

This section will consider the radar response to gravimetric soil moisture within each field separately; other soil moisture indicators such as volumetric moisture, normalized moisture and soil tension will be treated in the next chapter.

In the previous two sections a strong dependence of σ^o on soil moisture was observed at all frequencies and angles. The linear dependence of σ^o at 4.6 GHz, 10^o incidence angle and HH polarization on gravimetric moisture Mg is shown in Figure 3.20. The linear correlation coefficient is quite good for fields 1 and 4, .898 and .869, respectively, and also for field 3 at moistures below saturation, r = .844. Both fields 3 and 4 exhibit a leveling or a drop in σ^o as moisture approaches and exceeds saturation; as previously discussed, this is due to an increase in specular reflection at extremely high moisture conditions.

In contrast, field 2 exhibits poor sensor response to mean soil moisture with much scatter apparent in the data and a low resultant correlation coefficient of approximately 0.4. Because of the similarity between fields 2 and 3 in terms of soil texture, both are silty clay loams, sensor response was also expected to be similar. Poor sensor response to field 2 when compared to the other test fields is relatively independent of the sensor parameters (frequency and angle) and of the depth interval of soil considered. Table 3.15 presents the linear correlation between σ^o at 6 frequencies at 10° and 20° HH polarization and the 0-1, 0-2 and 0-5 cm mean gravimetric soil moisture of each field. Sensor response to mean moisture in Field 2 is clearly anomalous at all sensor combinations with correlation ranging between 0.3 and 0.5 whereas correlation coefficients of the other fields are typically on the order of 0.7 to 0.9. It should be noted that saturated conditions are included in the sample populations used to derive the correlation matrix given in

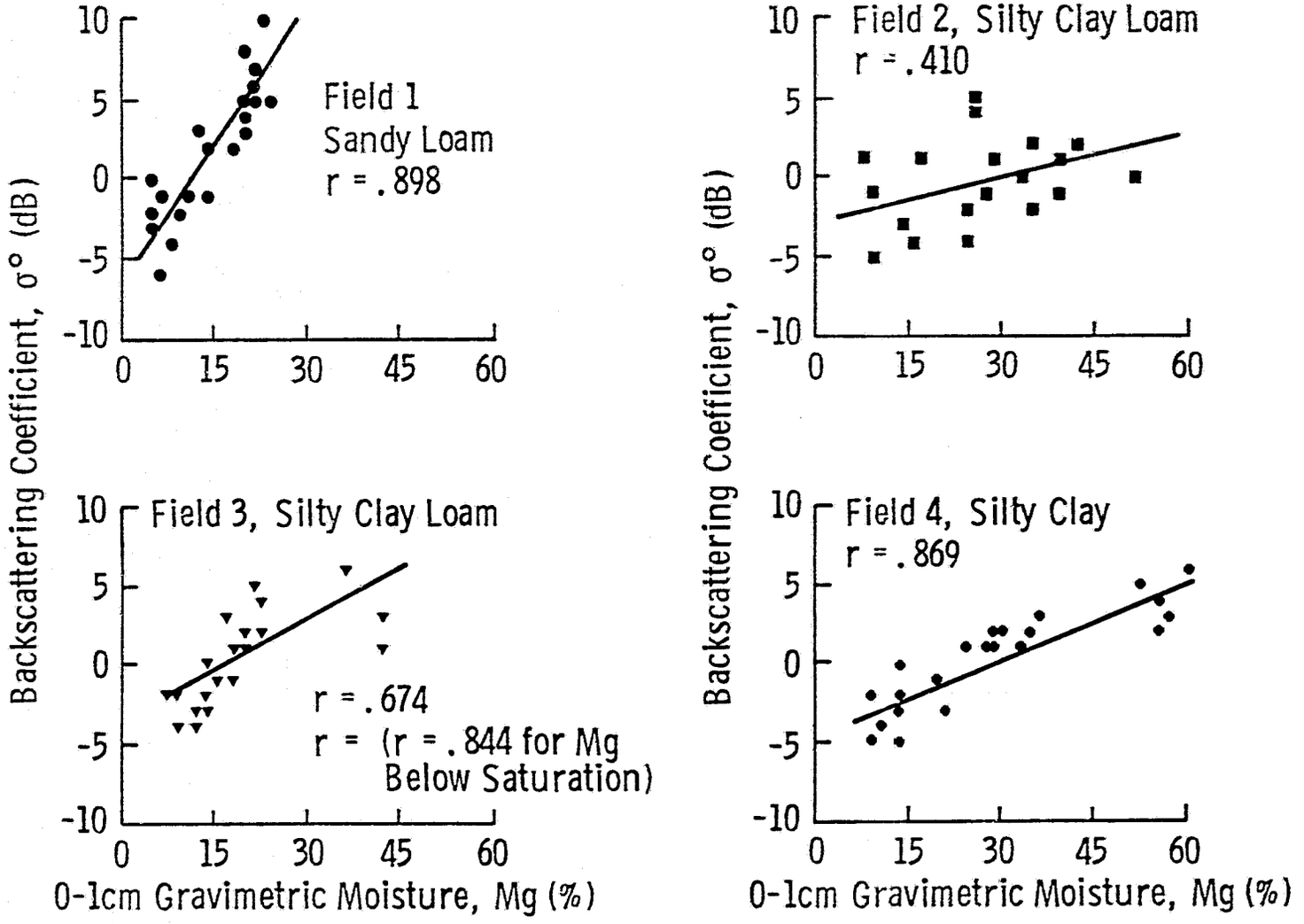

Figure 3.20. Backscattering coefficient at 4.6 GHz, 10°, HH polarization as a function of 0-1 cm gravimetric soil moisture.

TABLE 3.15

Correlation Matrix Between $\sigma^{\circ}_{f,\rho,\theta}$ and 0-1, 0-2 and 0-5 cm
Mean Gravimetric Soil Moisture for Each Field

Angle	Polarization	Frequency (GHz)	Linear Correlation Coefficient, R											
			0-1 cm Field				0-2 cm Field				0-5 cm Field			
			1	2	3	4	1	2	3	4	1	2	3	4
10	HH	2.385	.908	.548	.609	.805	.902	.547	.598	.808	.892	.521	.518	.838
		3.291	.894	.572	.685	.829	.892	.558	.672	.833	.894	.506	.592	.837
		4.625	.898	.411	.674	.876	.896	.390	.659	.871	.902	.370	.621	.854
		5.625	.881	.406	.551	.837	.877	.394	.534	.828	.873	.363	.528	.818
		6.625	.849	.430	.670	.881	.837	.418	.653	.879	.838	.419	.644	.878
		7.625	.836	.514	.742	.771	.825	.499	.732	.744	.828	.488	.720	.736
20	HH	2.385	.911	.541	.589	.744	.906	.532	.615	.746	.902	.523	.665	.738
		3.291	.780	.397	.539	.737	.786	.402	.606	.736	.778	.419	.721	.730
		4.625	.841	.556	.707	.740	.844	.546	.754	.741	.847	.545	.804	.718
		5.625	.813	.430	.549	.828	.805	.426	.595	.821	.797	.453	.700	.806
		6.625	.823	.465	.620	.743	.813	.444	.660	.722	.792	.451	.759	.728
		7.625	.709	.528	.684	.713	.699	.528	.722	.706	.704	.568	.815	.707

Table 3.15 and that the linear correlation of σ^o with M_g is slightly higher than shown for fields 3 and 4 when only nonsaturated moisture conditions are included in the analysis. Importantly, the exclusion of saturated data from field 2 does not significantly improve correlation coefficient.

3.5.1 Poor sensor response to target inhomogeneity in Field 2

The anomalously poor sensor response to mean moisture in field 2 was examined with respect to the following potential error sources:

1) failure of MAS system
2) spatial mismatch of σ^o and M_g sampling
3) temporal mismatch of radar and moisture sampling
4) inadequate quantification of mean moisture due to non-uniform field distributions of:
   a) soil moisture
   b) bulk density
   c) soil texture

Radar error was found to be inadequate to explain poor sensor response to moisture in field 2. External calibration of the MAS system with a Luneberg lens indicated no significant temporal drift of the system within the three month measurement period of the experiment (Dobson, 1979); and since all fields were examined throughout the entire period, all fields should be equally influenced by any calibration errors. Internal calibration of the MAS system was performed approximately twenty times within each data set by reference to a delay line. Inspection of delay line fluctuations indicated that the system was very stable within a data set; the delay line readings were typically found to vary by less than 1 dB.

Analysis of the radar data with respect to the mean of sampled soil moistures assumes that the same spatially defined target is sampled contemporaneously by both the radar and "ground truth" efforts. Furthermore, it must be assumed that measurement errors associated with the radar and moisture sampling are random and normally distributed and thus would have minimal effect upon the sample means. During a radar data set of typically two hours duration the antenna boom was swept in an azimuthal arc of up to 135° to cover the ground sampling grid shown in Figure 3.1. Since azimuth

position was not recorded with the data stream, it was not possible to identify data sets where the entire field was not scanned. Partial scanning of a field would result in a sampling bias between the radar and moisture samples due to a spatial mismatch which would be data set specific. In a similar fashion, a sample bias between radar and "ground truth" data could occur when the two sets of target samples were not contemporaneous thus resulting in a temporal mismatch.

Soil moisture is a time dependent variable. Moisture in the soil surface layer was observed to change by as much as 0.12 g/cm^3 in less than a 24-hour period during the 1975 Bare Soil Experiment. Temporal change in soil moisture can be particularly rapid when the soil surface is drying under the strong evaporative demands of solar irradiation and wind, especially when the soil is coarse textured or devoid of the moderating influence of a plant canopy. This temporal dependence of soil moisture poses a problem for the MAS system.

A typical MAS 1-8 GHz data set requires 2 to 3 hours to collect an adequate sample size at all sensor combinations, while acquisition of the corresponding "ground truth" may require only 1/2 to 1 hour. Thus, the radar data includes a moisture related variation of 2 to 3 hours while the corresponding "ground truth" only accounts for a maximum of 1 hour temporal moisture variation.

Three sets of procedures were incorporated in the 1977 data acquisition to help alleviate the uncertainty of correspondence between the soil moisture sampled by the radar and that sampled as "ground truth." First, the radar data acquisition time was reduced by limiting the number of incidence angles to three. Second, ground truth acquisition time was reduced such that soil moisture samples would reflect primarily spatial variations with minimal temporal variations. The use of additional manpower halved the acquisition time for ground truth; a normal ground truth data set did not include any sampling for bulk density, which can be a tedious and time-consuming process. And third, the temporal dependence of soil moisture was estimated by monitoring soil conductivity within the surface layers continuously through a data set. This was accomplished by using a set of conductivity probes buried in the soil.

Soil conductivity measurements were made at 15-minute intervals from three depth intervals at one location per field (Figure 3.21). The monitored depths were 0-1, 1-2 and 2-5 cm. The resistance probes were coated with an abrasion-resistant porous dental plaster, Duroc, to a thickness related to the depth interval at which the probes would be inserted. The probes were emplaced in a given field shortly after field preparation and remained in equilibrium with the soil, unless vandalized as in the case of the probes at field 2, until the termination of the experiment. Figure 3.21 shows the probe placement; probes were oriented either horizontally or vertically within the soil in order to average moisture over the appropriate depth interval.

Upon termination of the bare soil experiment, the conductivity probes were carefully removed from each field along with a block of the surrounding soil. The moisture dependence of the sensors was then calibrated in the lab. It should be noted that calibration curves are sensor and soil specific due to variance in the characteristics of the sensors themselves and also the variance between soil types in terms of hydraulic and salinity characteristics. Curtis and Trudgill (1974) offer an excellent review of the calibration technique.

A representative calibration curve is shown in Figure 3.22. Although the laboratory calibration procedure was admittedly crude, it was still possible to define hysteresis effects on the sensors by the establishment of wetting and drying curves. The calibration curves for Field 3 were used to predict soil moisture from the mean conductivity recorded during "ground truth" acquisition. These moisture estimates compare very well with the mean measured "ground truth" moistures obtained for each data set as seen in Figure 3.23. The conductivity probes indicate changes in gravimetric soil moisture of as much as 5% over three hour radar data sets at mid-day for drying soils.

An example of short-term moisture flux can be seen in Figure 3.24. Two consecutive radar data sets were taken on Field 3; during this time the measured "ground truth" indicates that mean soil moisture in the 0-1 cm layer is fairly constant as a function of time but has an increasing spatial variance (especially toward drier conditions) while the 2-5 cm layer mean is increasing with an increasing spatial variance. The soil conductivity

Figure 3.21 Placement of Conductivity Probes used to Measure Temporal Soil Moisture Response in the 1977 Bare Soil Experiment.

Plan View

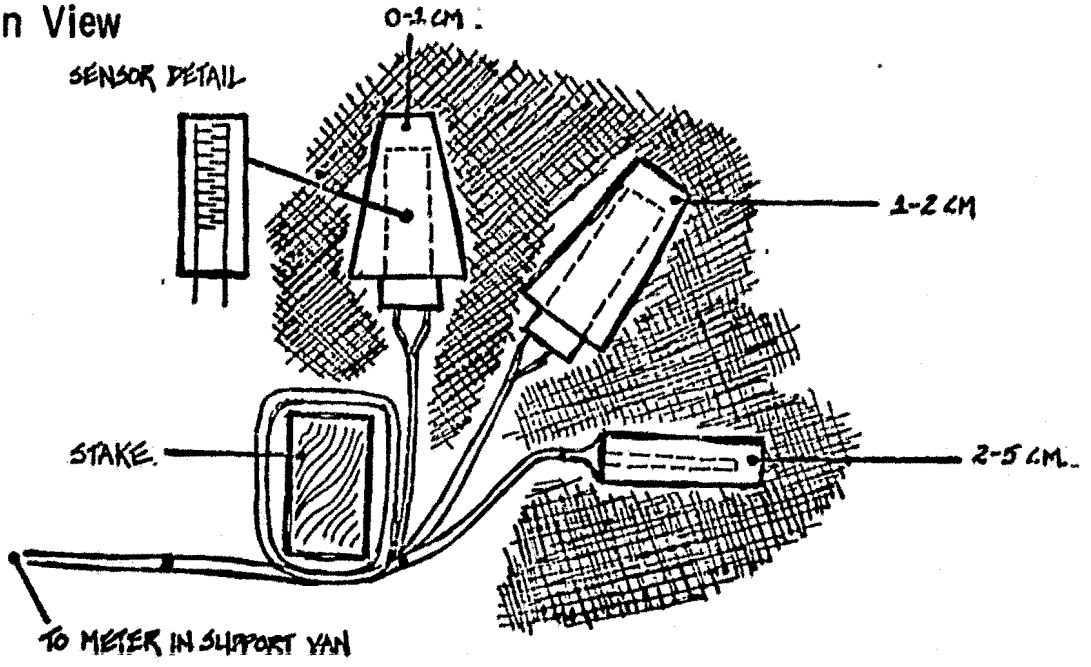

LOCATION-A

Cut-away Section

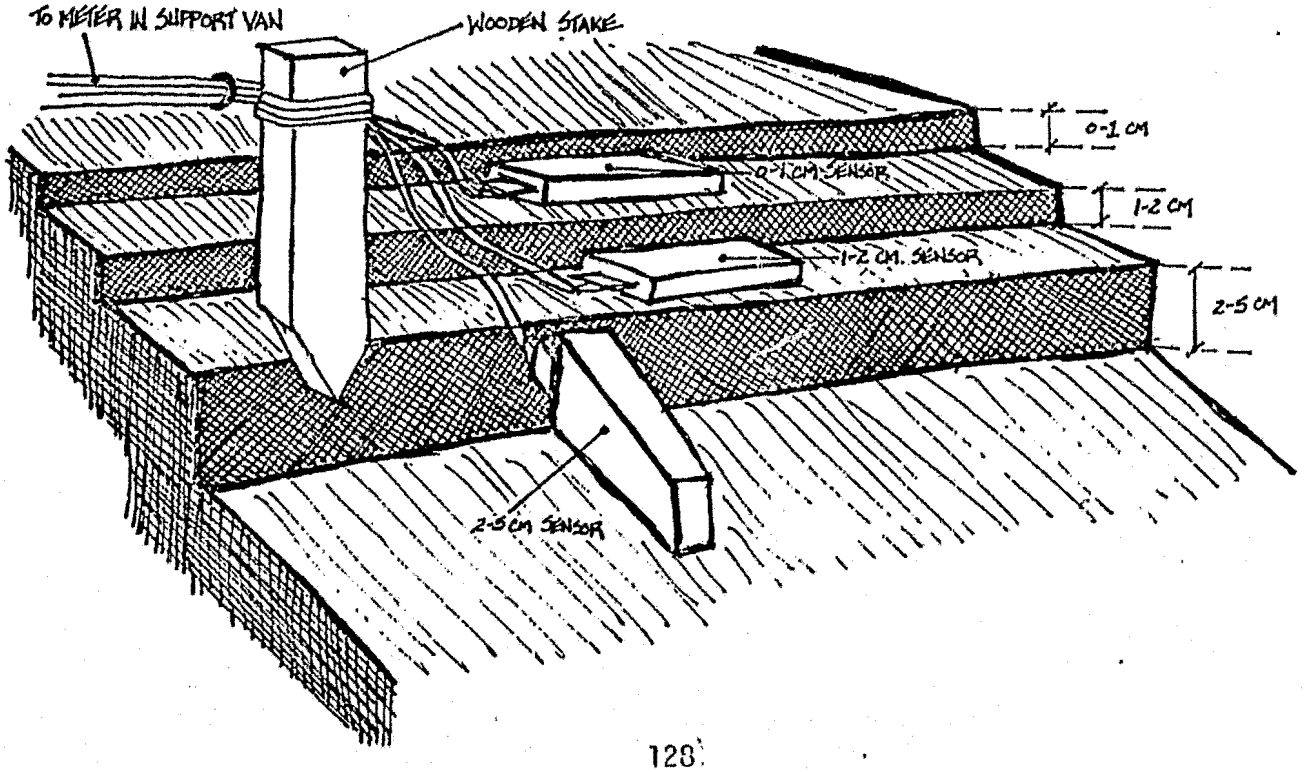

Figure 3.22 Soil Moisture Conductivity Probe Calibration Curve

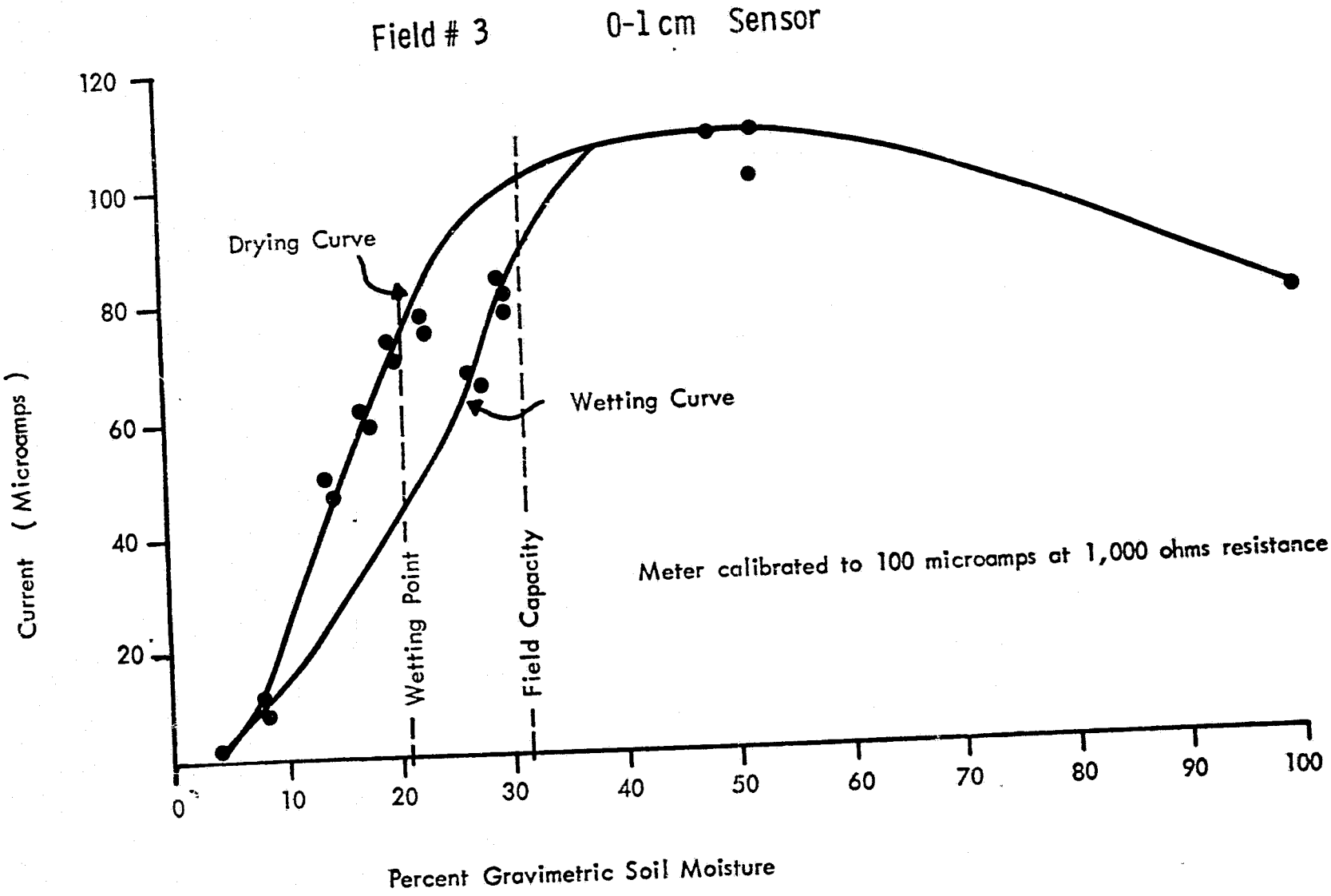

Figure 3.23 Conductivity Probe Estimate Accuracy in the 0-1 cm Layer
Field 3 - All Data Sets Included.

Drying or Wetting Phase is Determined by Rainfall History and the 0-1 cm Soil Moisture History.

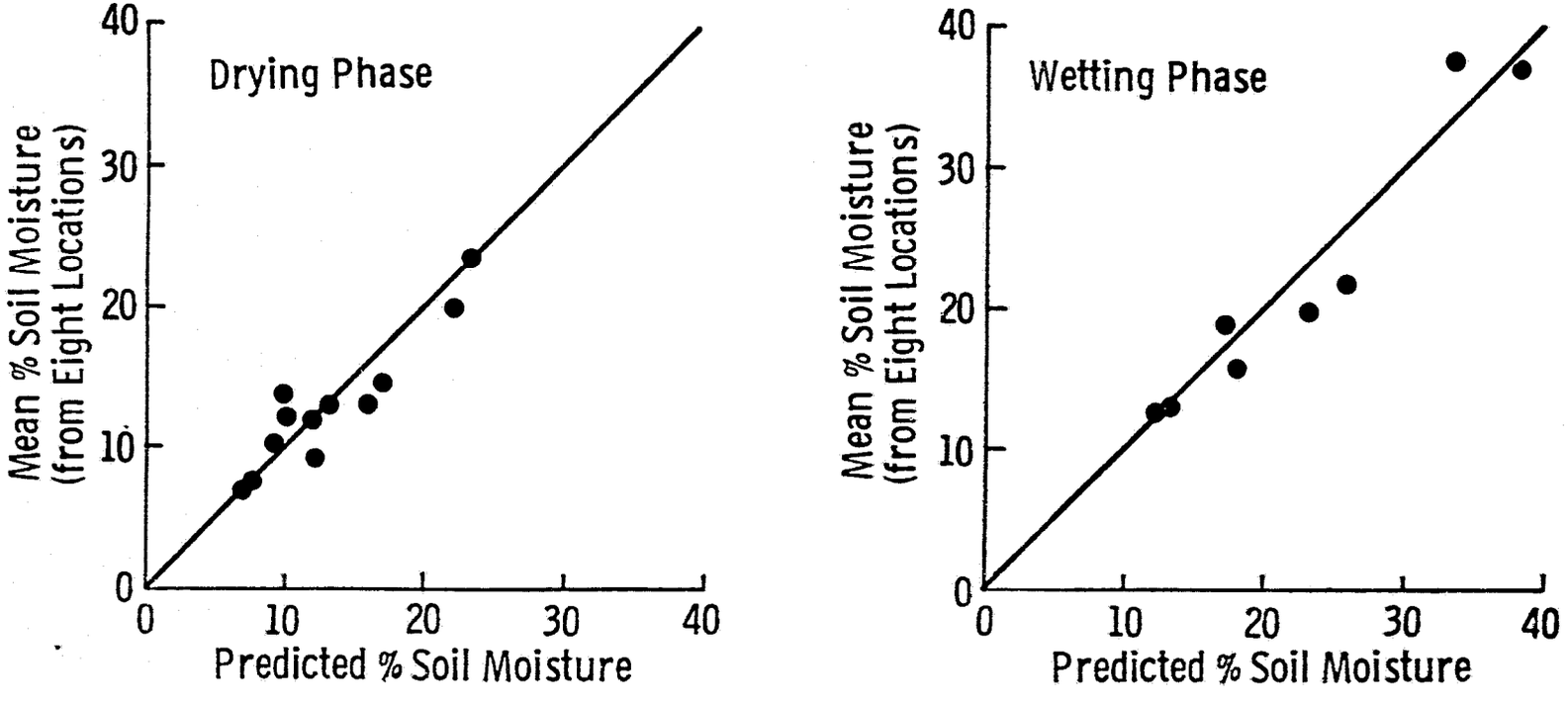

Figure 3.24 Predicted Soil Moisture in the 0-1 and 2-5cm Layers for Two Data Sets
Field # 3 9/27/77
Predicted Values Are Estimated from Calibration Curves

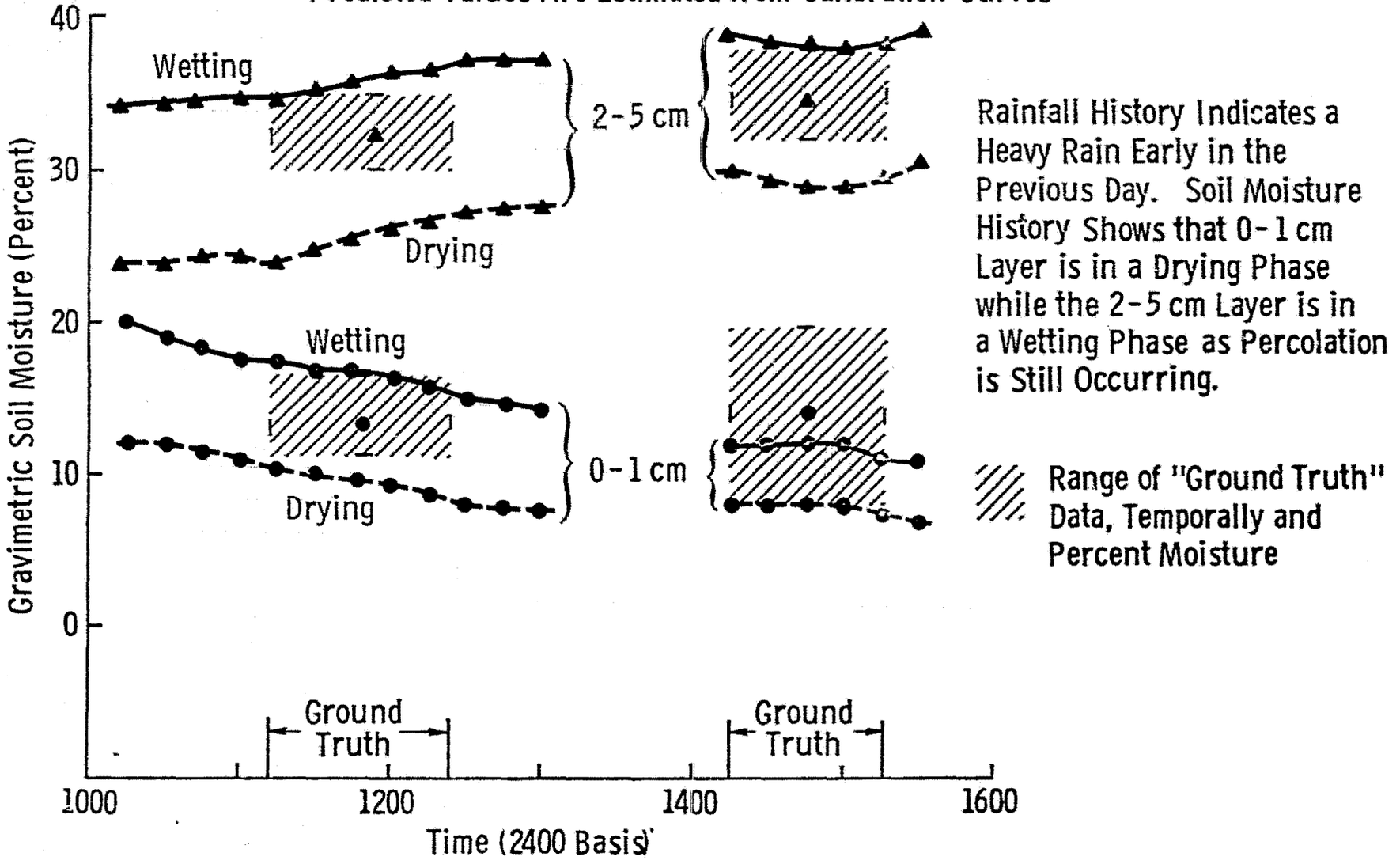

estimates of soil moisture, when plotted as a function of time, show that, at a given location, soil moisture is changing at a near constant rate. This change is not apparent from a comparison of the mean 0-1 cm "ground truth" moistures of the two data sets since the drying of the soil is masked by the spatial variance between the eight sampling locations.

Due to constraints on time and resources, the other sensors were not calibrated with respect to the soils in which they were emplaced. The initial results however, indicate that this may be a very valuable technique to augment other forms of soil moisture sampling. It is highly recommended that future experiments include equipment to continuously monitor soil conductivity or resistivity; especially in view of the fact that resistance is proportional to soil matric potential and can be calibrated to gravimetric soil moisture by tensiometric field measurements and the laboratory determined desorption characteristics of a given soil.

Since the conductivity sensors in field 2 were vandalized, it was not possible to compare its temporal variation in soil moisture within a data set with that of the other fields as estimated from the temporal change in soil conductivity. However, it is expected that this variance would be too small to account for all of the scatter observed in the radar response to field 2 (Figure 3.20).

A much more plausible explanation of the anomalous behavior of field 2 rests in the assumption that this field had a uniform distribution of moisture as sampled by both the radar and the ground sampling grid. If the true spatial distribution of target parameters such as texture, bulk density and moisture are not homogeneous but have large variance within the test field and complex spatial distributions, then the simple arithmetic mean moisture may be a very poor descriptor of the true mean moisture. The resulting bias imbedded in the mean would be compounded by any spatial mismatch between radar and "ground truth" for a given data set and also by any time transient conditions which could change the character of surface soil structure. During the course of the experiment, field 2 was subjected to repeated partial flooding with water standing approximately 6 cm deep over an irregular area of 30 to 50% of the test field. This produced a slaking of the soil surface in the flooded areas and resulted

in a puddled condition which increased soil density and altered the surface layer particle size distribution thus producing relatively impermeable surface crusts as a function of time.

The surface layer distributions of soil texture and mean bulk density are plotted for each field in Figures 3.25 and 3.26 respectively. The spatial variance of soil texture as determined from the eight sampling locations is observed to be small for fields 1, 3 and 4 with gentle gradients (Figure 3.25). In contrast, field 2 displays high variance and rather steep textural gradients which divide the fields into regions composed of approximately 9% sand and 35% clay separated by a region of 15% sand and 29% clay.

The mean bulk density distributions as plotted in Figure 3.26 for the 0-1 cm layer indicate that fields 1 and 3 are uniform compared to field 2 which shows a distinct progression toward higher mean density for the portion of the field most subject to flooding and puddling effects. Field 4 was not plotted because of the small sample size from which the mean could be determined.

Prior measurements have indicated that both density and texture have profound effect on radar response to soil moisture due to the influence of these characteristics on the complex dielectric constant of moist soils. The within field distributions of mean soil moisture as computed from all data sets (Figure 3.27) exhibit spatial patterns which are dominated by variance in surface elevation and drainage characteristics (Figures 3.28 to 3.31) and appear to be only weakly controlled by the spatial distributions of soil texture and soil bulk density.

Further analysis of the effects of soil texture on radar backscatter response to soil moisture requires that the data input into the analysis be from homogeneous test fields with strong sensor response to gravimetric moisture. The erratic nature of the radar response to moisture in field 2 is not consistent with prior experimental results and the data is therefore suspect. The observed non-uniformity of the surface layer of field 2 in terms of texture and bulk density combined with the compounding effects of sample bias due to spatial, and temporal mismatch between radar and "ground truth" is believed to be responsible for the observed scatter in Figure 3.20. In light of the foregoing and the fact that fields 2 and 3

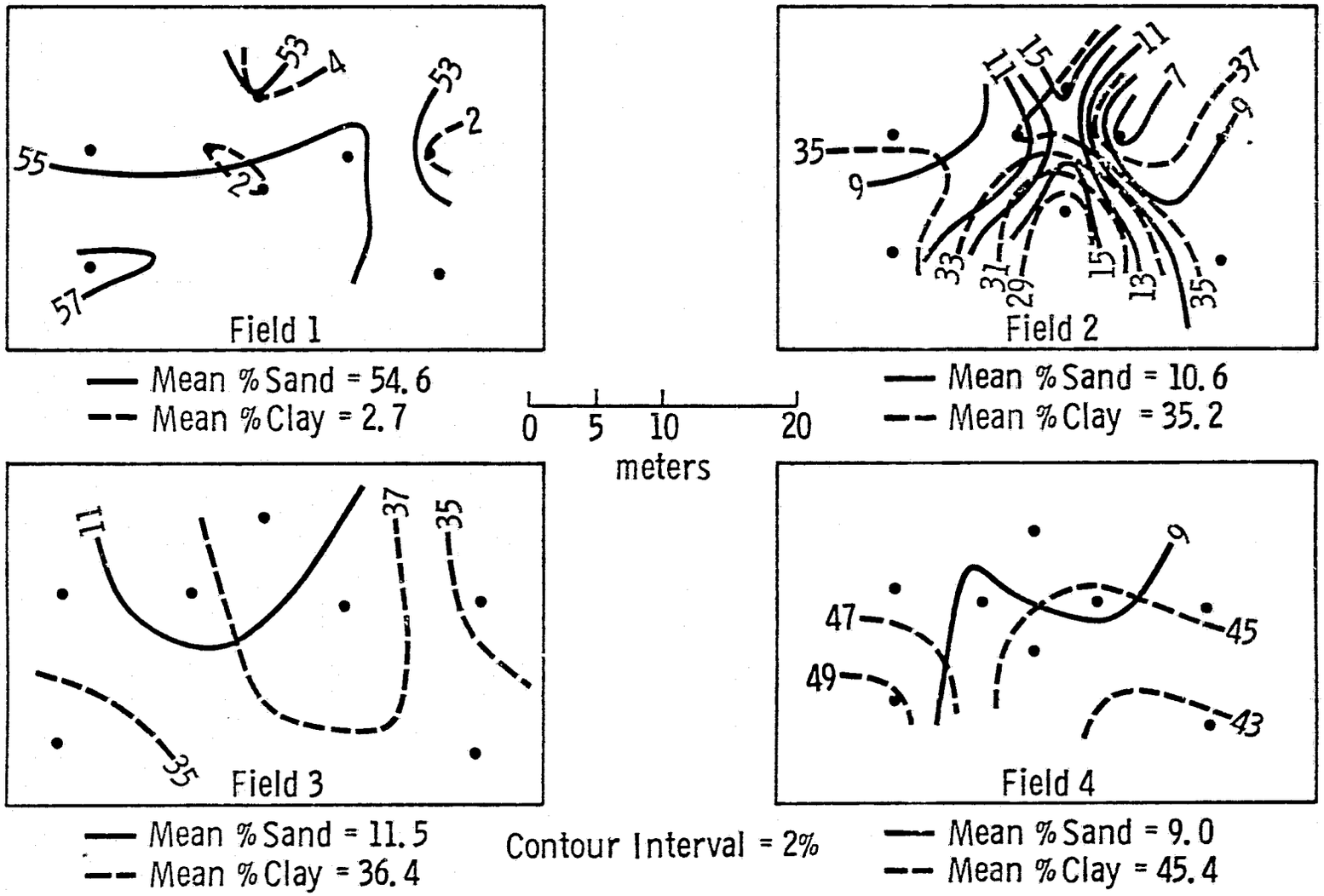

Figure 3.25. Contour plots of Mean Percent sand and clay.

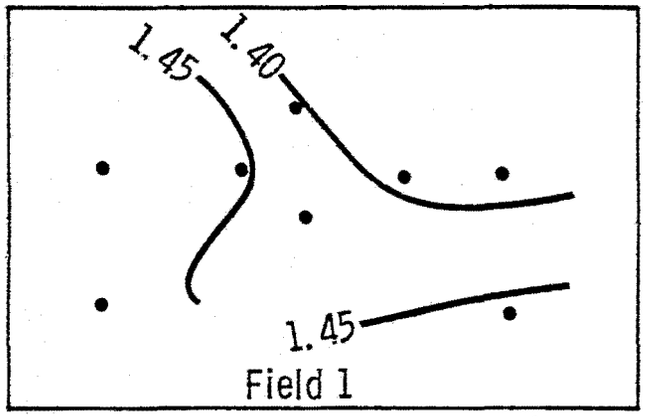

Mean 0-1cm Density = 1.43 g/cm^3

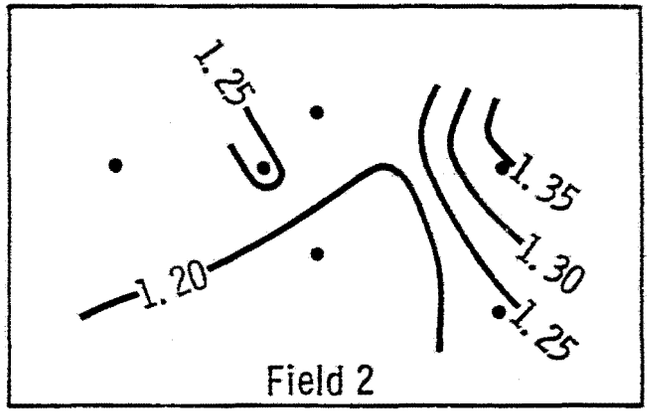

Mean 0-1cm Density = 1.22 g/cm^3

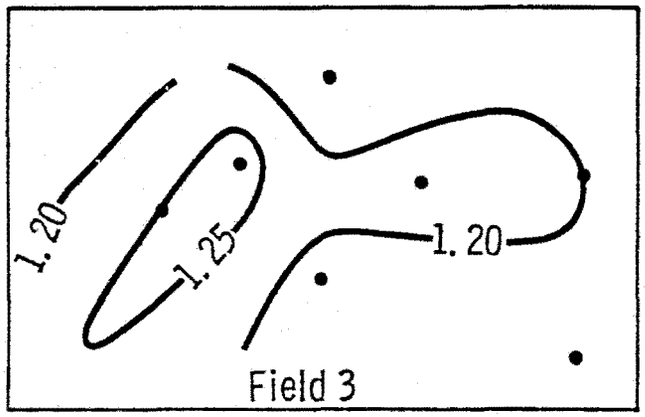

Mean 0-1cm Density = 1.20 g/cm^3

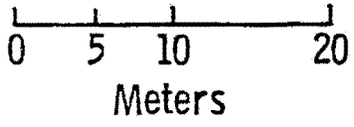

Contour Interval = .05 g/cm^3

• Sampling Locations

Figure 3.26. Contour plots of 0-1 cm Mean Bulk Density within Fields 1, 2 and 3.

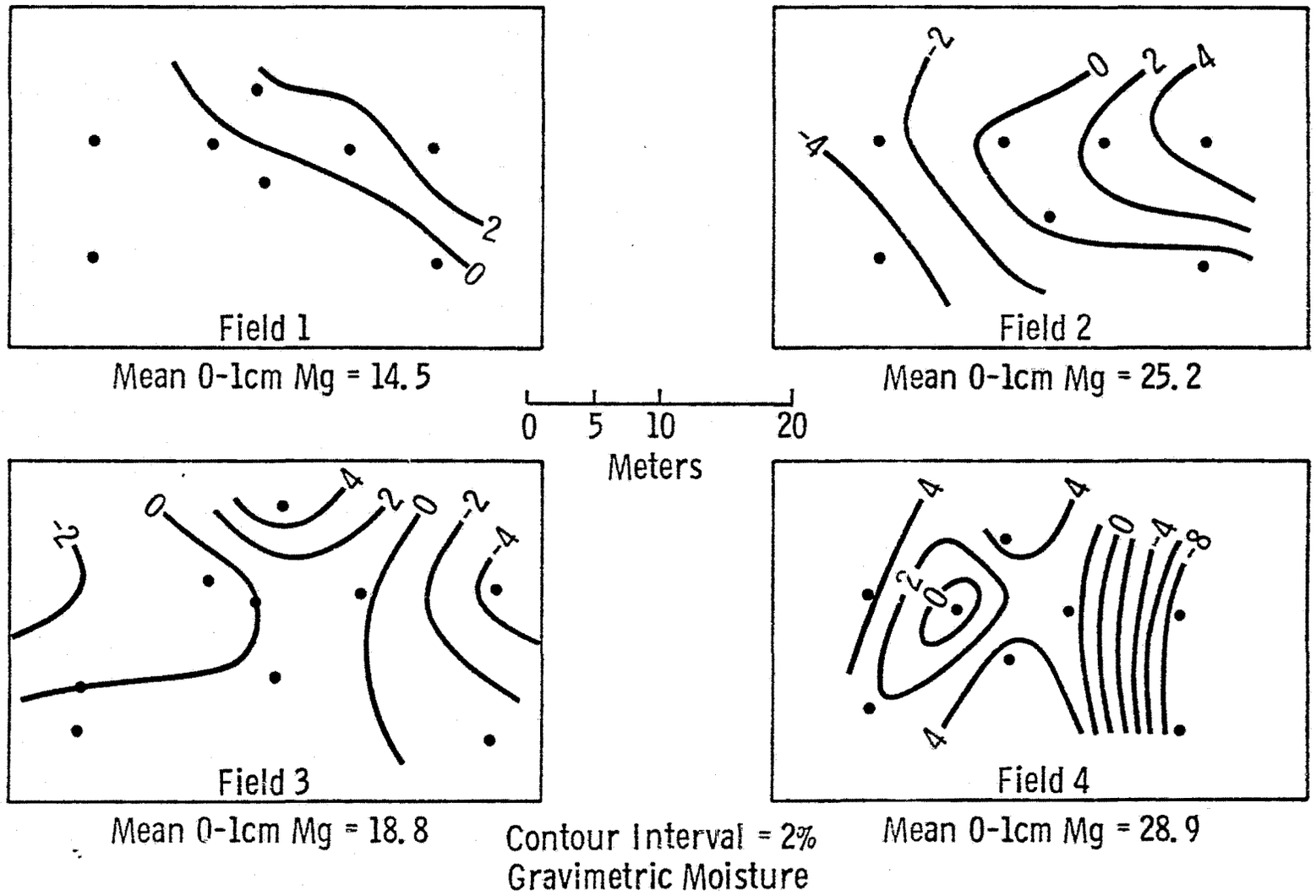

Figure 3.27. Contour plots of the variance in Mean 0-1 cm gravimetric moisture at each location.

Figure 3.28 Field I, sandy loam, surface elevation above an arbitrary datum plane.

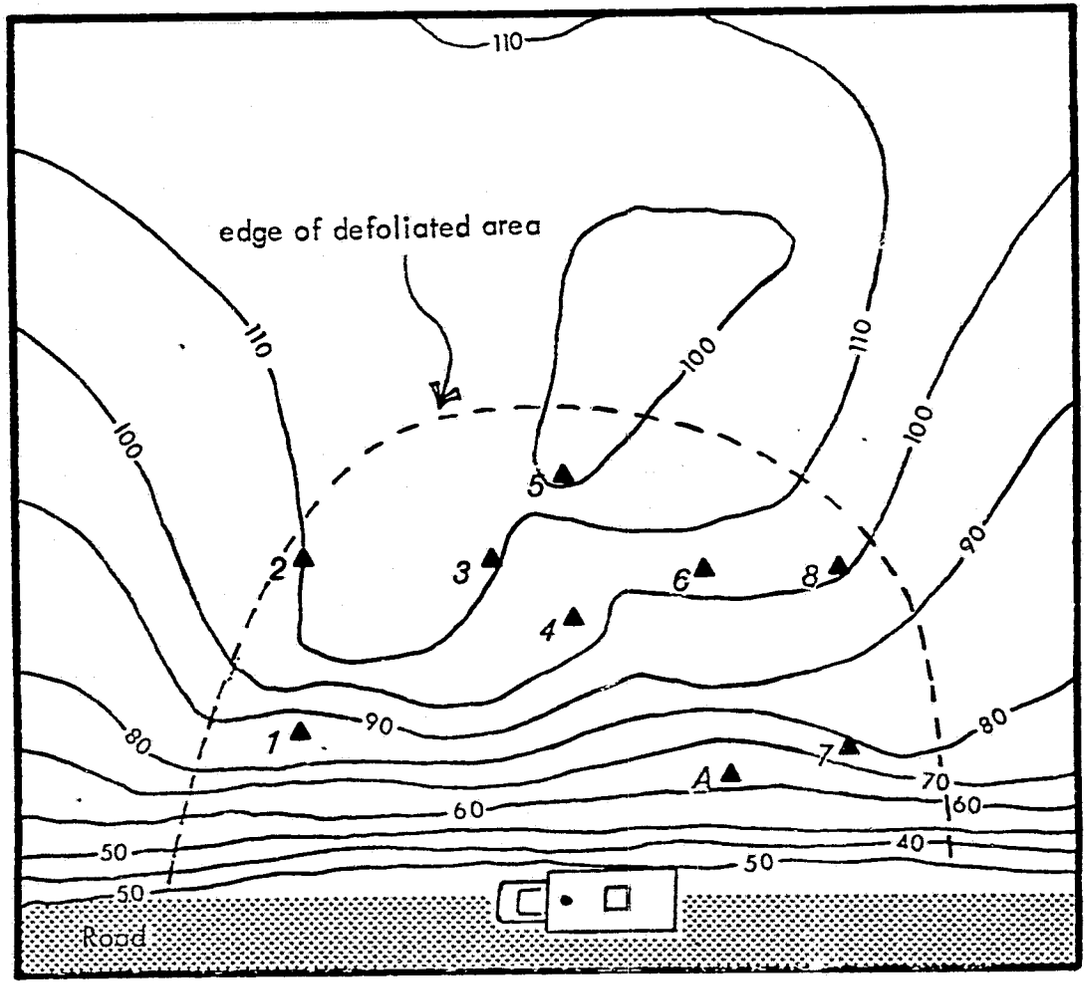

▲ sampling locations

Scale
0 5 10 20
meters

contour interval: 10 cm.

Figure 3.29 Field 2, silty clay loam, surface elevation above an arbitrary datum plane.

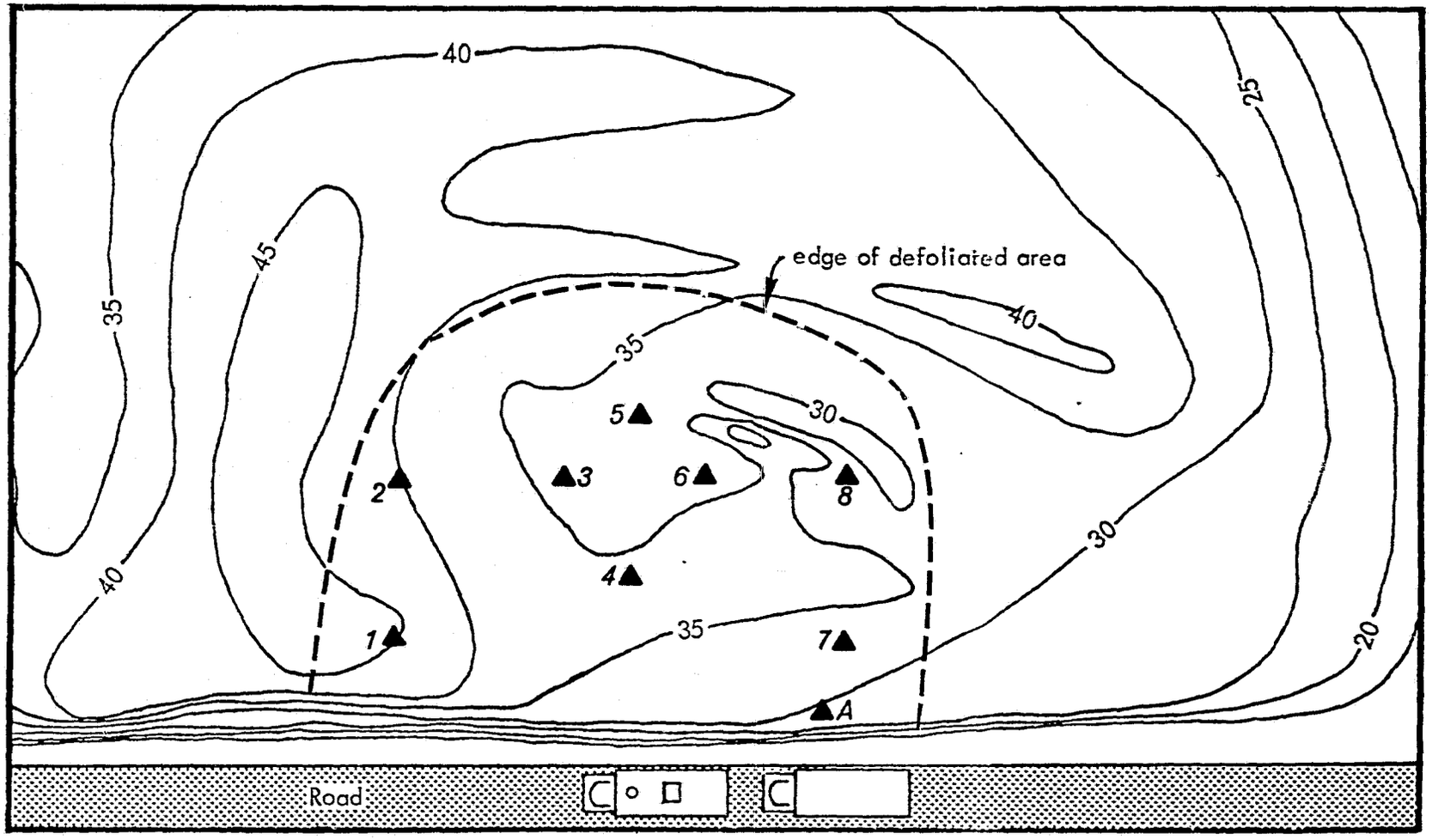

Figure 3.30 Field 3, silty clay loam, surface elevation above an arbitrary datum plane.

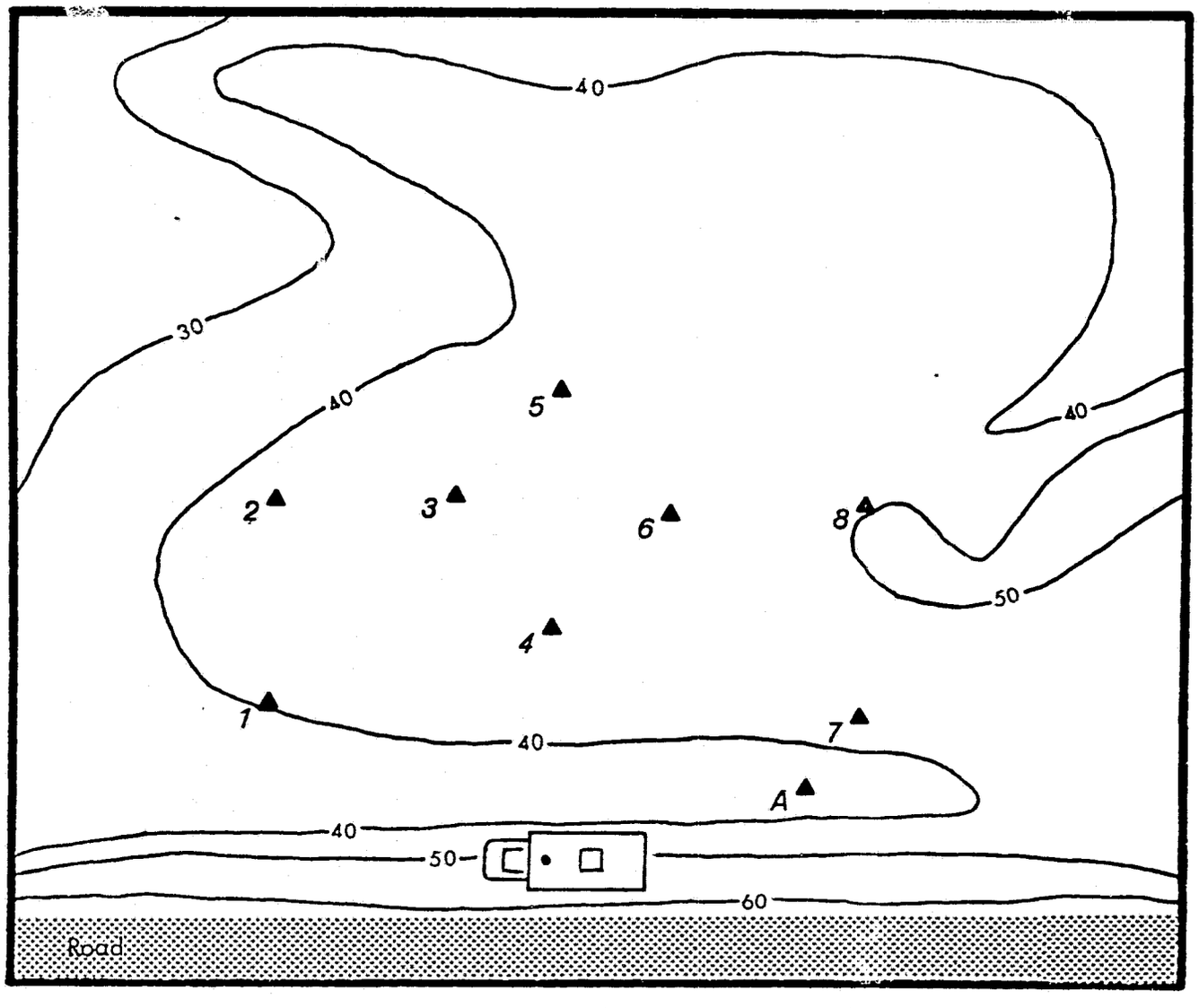

Figure 3.31 Field 4, silty clay, surface elevation above an arbitrary datum plane.

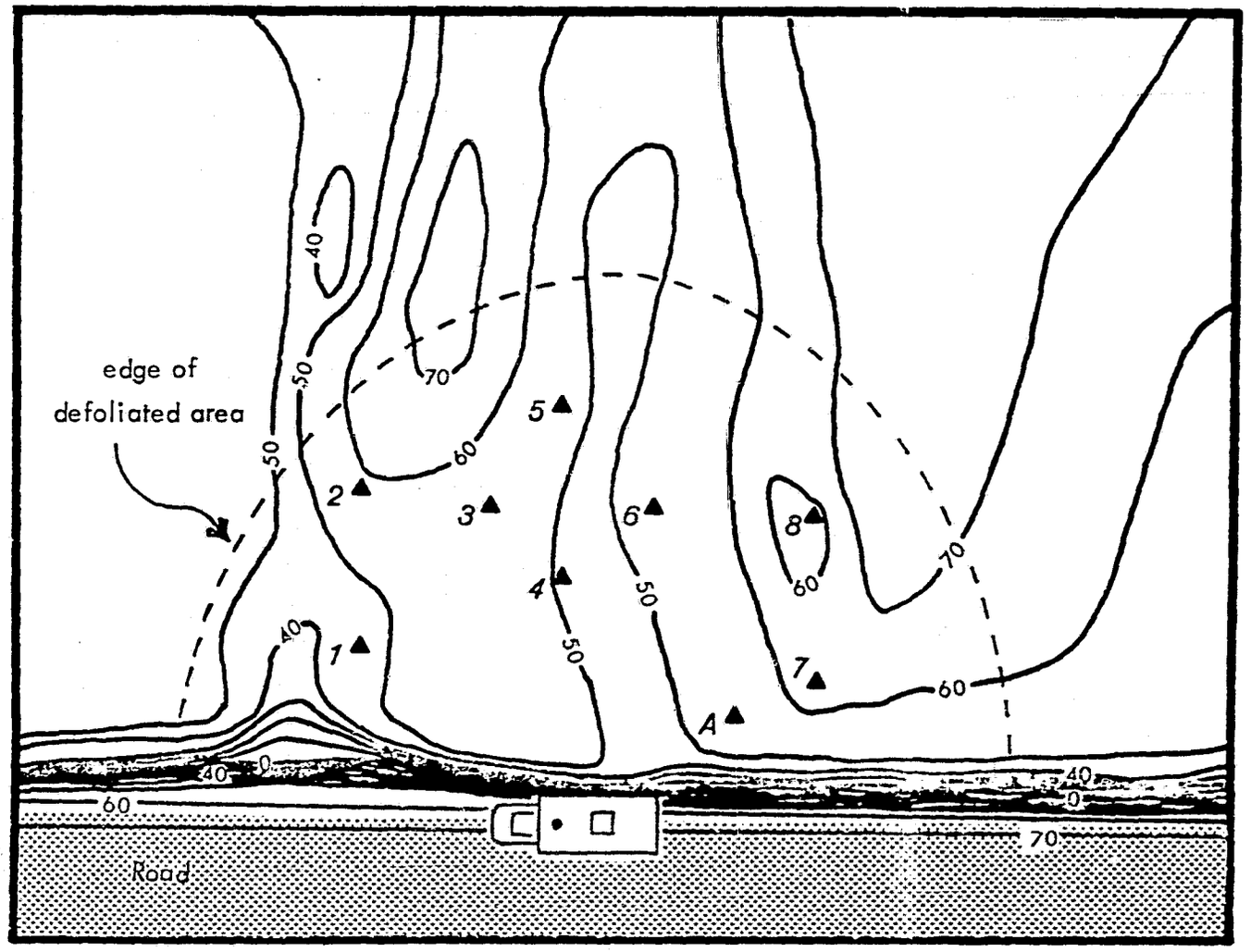

▲ sampling locations

Scale
0 5 10 20
meters

contour interval: 10 cm.

are both classified as silty clay loams, the data from field 2 is not required for analysis of soil textural effects.

4.0 SOIL MOISTURE INDICATOR ANALYSIS

Thus far, discussion of the data acquired during the 1977 Bare Soil Experiment has focussedon radar response to gravimetric soil moisture. The linear correlation results presented in Table 3.15 show strong correlation between radar backscattering coefficient and gravimetric soil moisture for homogeneous fields of sandy loam, silty clay loam and silty clay (fields 1, 3 and 4 respectively). However, prior experimental results as described in chapter 2 clearly point out the failure of a gravimetric moisture indicator to account for the microwave sensor response to a complex scene of mixed soil textures.

This chapter will discuss the 1977 Bare Soil Experiment results with the purpose of isolating those soil moisture indicators which are independent of soil texture in terms of sensor response. The combined textural data base of sandy loam, silty clay loam and silty clay fields will be used to establish the linear dependence of σ° on gravimetric moisture, volumetric moisture, moisture above some transition moisture, normalized moisture and soil tension.

In the experiments analyzed by Schmugge (1976a, b) and Batlivala and Ulaby (1977) and described in Chapter 2, normalized moisture was defined as a percent of estimated field capacity (equations 2.30 and 2.31). In order to avoid the uncertainty of estimating moisture at a given tension as some function of other typically measured soil parameters (Table 2.10) for the 1977 Bare Soil Experiment, the soil moisture versus tension desorption characteristic curve was measured directly, albeit at two points. Triplicate core samples of the 0-5, 5-9 and 9-15 cm layers of each field were submitted to the National Soil Survey Laboratory in Lincoln, Nebraska for desorption of soil water with pressure extractors. The mean resultant values are presented in Table 4.1 for soil tensions of 1/3 bar and 15 bars which are commonly used to describe the water retention of soil at field capacity and at the wilting point respectively. The 0-5 cm 1/3 bar gravimetric water content of the undisturbed core samples was found

TABLE 4.1

Soil Water Retention at 1/3 and 15 Bars Tension by Desorption, % Organic Carbon and Soil Bulk Density Determined by the National Soil Survey Laboratory, USDA Soil Conservation Service and Estimates of Water Retention at 31 Bars and Saturation.

Field	USDA Textural Classification	Depth	% Organic Carbon	Bulk Density (g/cm^3)		Gravimetric Water Content			
				1/3 bar	oven dry	1/3 bar	15 bar	air dry ≈31 bar	Saturation
1	sandy loam	0-5	.38	1.40	1.45	14.6	4.1	1.2	41.0
		5-9	.38	1.37	1.41	14.6	4.1	0.9	34.9
		9-15	.42	1.35	1.41	17.0	4.2	0.9	25.1
3	silty clay loam	0-5	1.84	1.31	1.55	30.1	18.8	3.6	54.1
		5-9	1.92	1.36	1.60	28.3	18.3	3.3	37.0
		9-15	2.01	1.39	1.62	25.9	19.0	3.3	31.9
4	silty clay	0-5	1.82	1.20	1.55	35.0	21.8	4.4	48.4
		5-9	1.74	1.24	1.65	34.8	23.1	4.1	36.2
		9-15	2.03	1.26	1.62	32.1	24.2	4.1	33.2

to vary from 14.6 for sandy loam to 35.0 for silty clay. Also found in Table 4.1 are values of the water retention of air dry soil which approximates the hygroscopic coefficient of soil at 31 bars tension and the observed gravimetric water retention of the soil when a field was saturated and partially flooded. Table 4.2 demonstrates that the laboratory values of Table 4.1 are closely approximated by estimation algorithms from Table 2.11; the error of the estimate is observed to increase with depth below the surface, and Schmugge's approximation is generally found to be the more accurate of the two at 1/3 bar and the Dobson-Ulaby approximation more accurate at 15 bars tension.

The measured values of moisture at 1/3 and 15 bars given in Table 4.1 were used to define log-linear estimates of tension for moistures from dry to field saturation. These functions are presented and shown graphically in Figures 4.1 to 4.3 for the 0-5, 5-9 and 9-15 cm depth intervals respectively.

A log-linear function was used to estimate soil tension instead of an exponential power function as proposed by Clapp and Hornberger (1978) because of 1) its simplicity, 2) a power function is not necessarily a good descriptor of the relationship between moisture and tension for soil textures finer than sandy loams, and 3) there would still persist error due to the hysteresis effect between adsorption and desorption curves which could not be accurately predicted (Mualem and Morel-Seytoux, 1978). In spite of its simplicity, the log-linear estimate still compares favorably with the desorption characteristic measured for various soils by Holtan (1968) and by Carlisle (1978). Figures 4.4 and 4.5 compare the log-linear estimate of tension for the 1977 Bare Soil Experiment sandy loam field with measured desorption curves of sands and sandy loams between .01 and 15 bars. Figures 4.6 and 4.7 compare the 1977 Bare Soil Experiment silty clay loam and silty clay fields to measured desorption curves between .1 and 15 bars. It should be noted that all soils plotted in Figures 4.4 to 4.7 are from the surface horizon of cultivated fields with bulk densities and textures similar to the 1977 Bare Soil Experiment fields.

Simple log-linear tension estimation algorithms, such as the ones shown in Figures 4.1 to 4.3, were used to compute estimates of soil tension from gravimetric moisture. A more complex model of the moisture-tension

TABLE 4.2

Comparison of Laboratory Determined Water Retention at 1/3 and 15 Bars Tension with Empirical Estimation Algorithms Derived by Schmugge (1976a) and Dobson and Ulaby

A = Schmugge's algorithms

1/3 bar Mg = 25.1 - .21 (% sand) + .22 (% clay)
15 bar Mg = 7.2 - .07 (% sand) + .24 (% clay)

B = Dobson and Ulaby algorithms

1/3 bar Mg = 35.29 + 3.74 (% organic carbon) - .30 (% sand) - .15 (% silt)
15 bar Mg = 4.8 + 2.47 (% organic carbon) + .24 (% clay)

Field	Depth	% by Weight			% Organic Carbon	Laboratory Values		A				B			
								Values		Estirate Error		Values		Estimate Error	
		Sand	Silt	Clay		1/3 bar	15 bar	1/3 bar	15 bar	1/3 bar	15 bar	1/3 bar	15 bar	1/3 bar	15 bar
1	0-5	55.7	42.0	2.3	0.36	14.6	4.1	13.9	3.9	-0.7	-0.2	13.6	6.2	-1.0	+2.1
	5-9	53.5	43.0	3.5	0.43	14.6	4.1	14.6	4.3	0	+0.2	14.4	6.7	-0.2	+2.6
	9-15	55.5	41.7	2.7	0.38	17.0	4.2	14.0	4.0	-3.0	-0.2	13.8	6.4	-3.2	+2.2
3	0-5	12.3	52.4	35.2	2.26	30.1	18.8	30.3	14.8	+0.2	-4.0	32.2	18.8	+2.1	0
	5-9	11.1	52.7	36.1	2.24	28.3	18.3	30.7	15.1	+2.4	-3.2	32.4	19.0	+4.1	+0.7
	9-15	11.1	51.8	37.1	2.26	25.9	19.0	30.9	15.3	+5.0	-3.7	32.6	19.3	+6.7	+0.3
4	0-5	9.7	46.4	43.9	2.38	35.0	21.8	32.7	17.0	-2.3	-4.8	34.2	21.2	-0.8	-0.6
	5-9	9.7	42.3	47.9	2.12	34.8	23.1	33.6	18.0	-1.2	-5.1	34.0	21.5	-0.3	-1.6
	9-15	8.1	45.9	46.0	2.05	32.1	24.2	33.5	17.7	+1.4	-6.5	33.7	20.9	+1.6	-3.3
									Mean	0.2	-3.1			0.9	0.3

Figure 4.1

1977 BARE SOIL 0-5cm WATER RETENTION CHARACTERISTICS

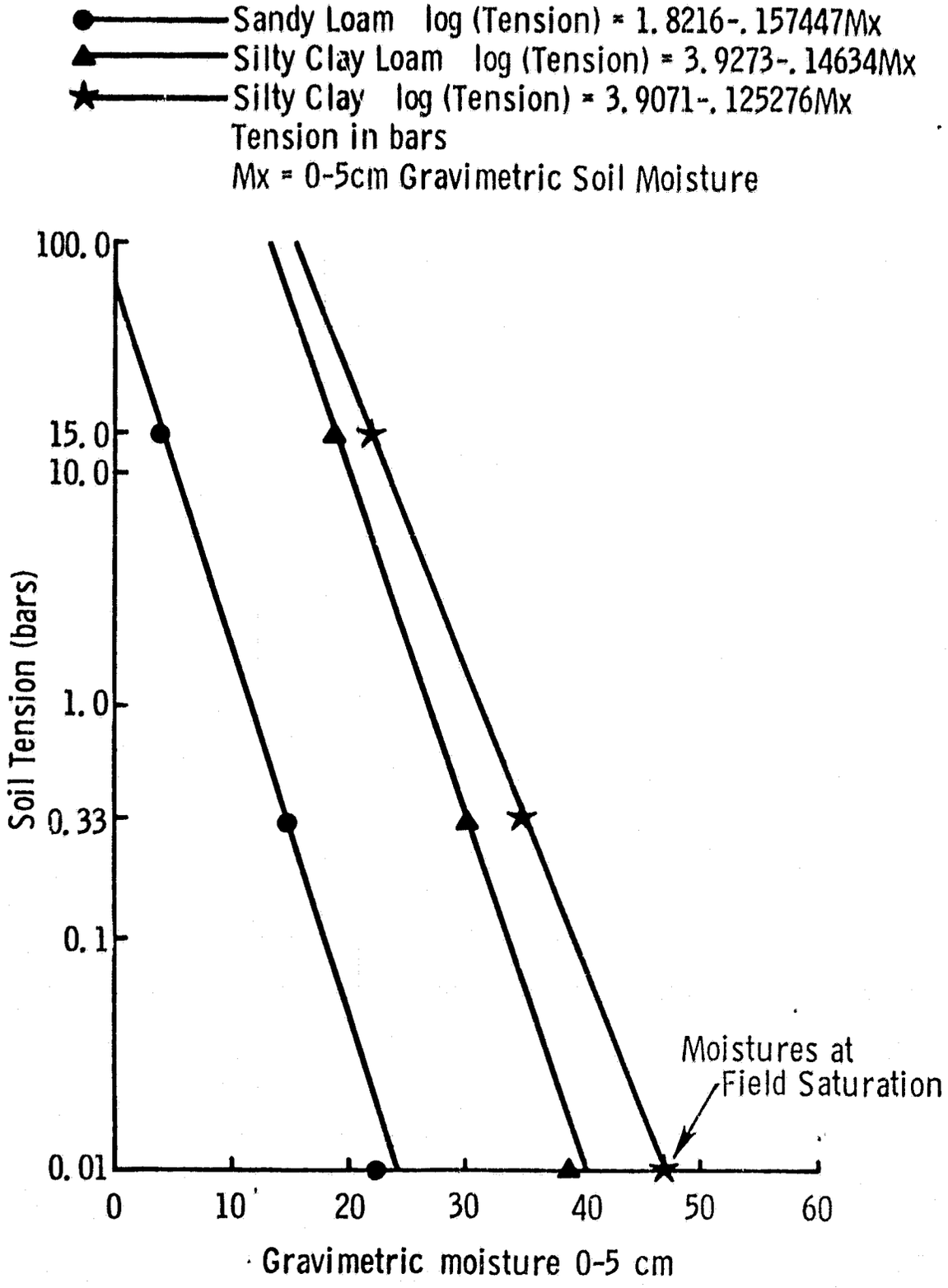

Figure 4.2

1977 BARE SOIL 5-9cm WATER RETENTION CHARACTERISTICS

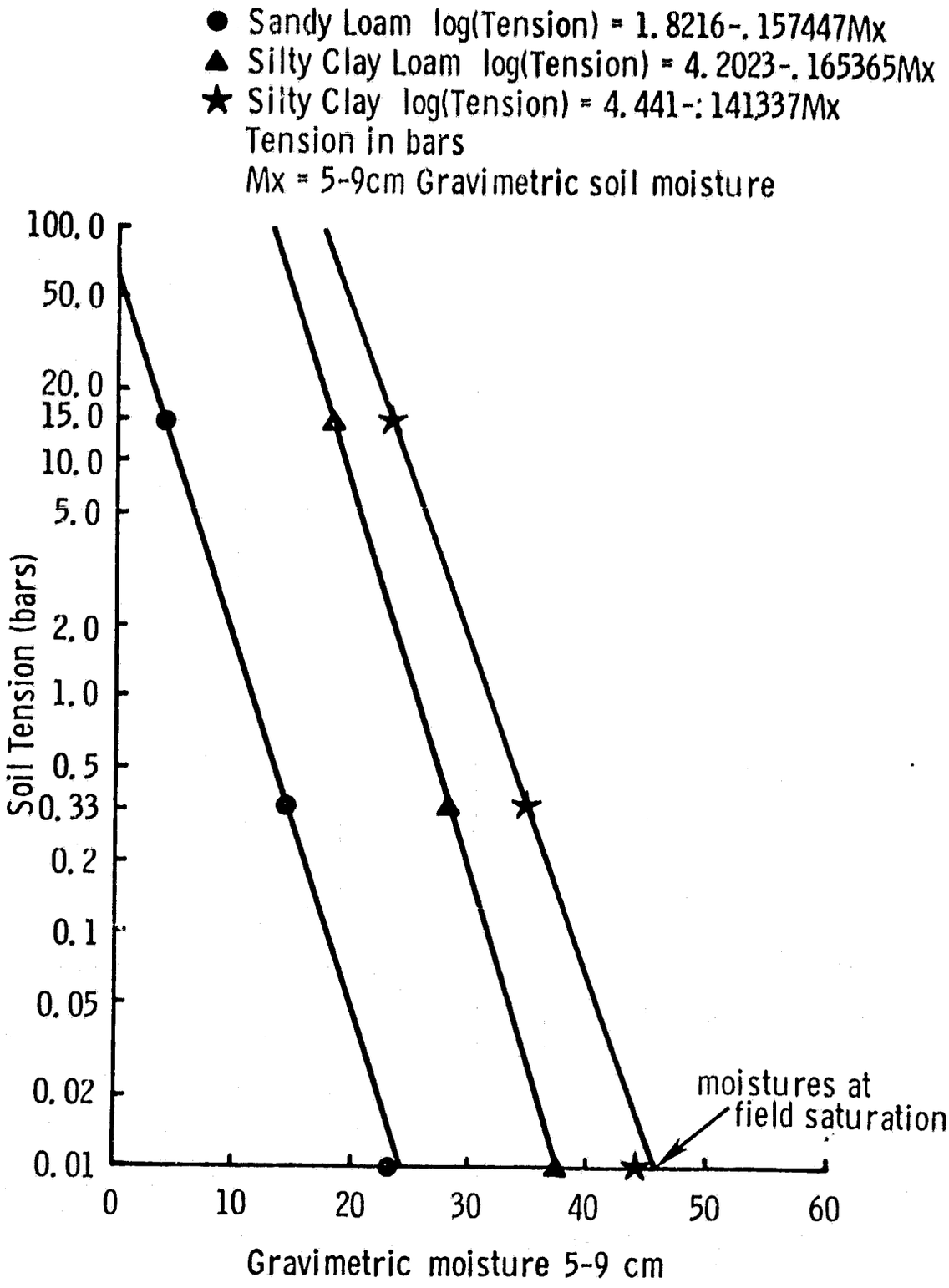

Figure 4.3

1977 BARE SOIL 9-15cm WATER RETENTION CHARACTERISTICS

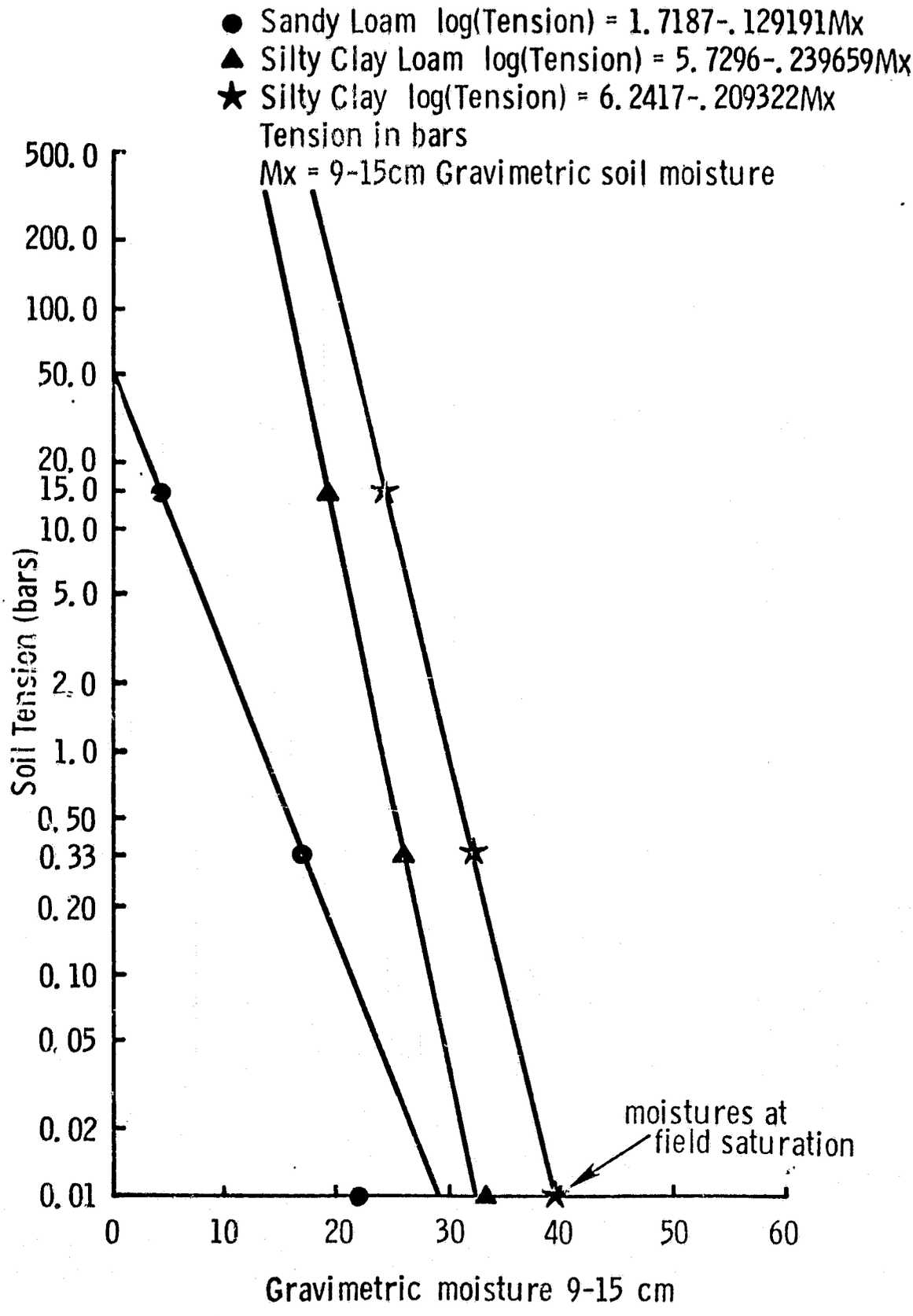

Figure 4.4

WATER RETENTION OF SANDS AND LOAMY SANDS

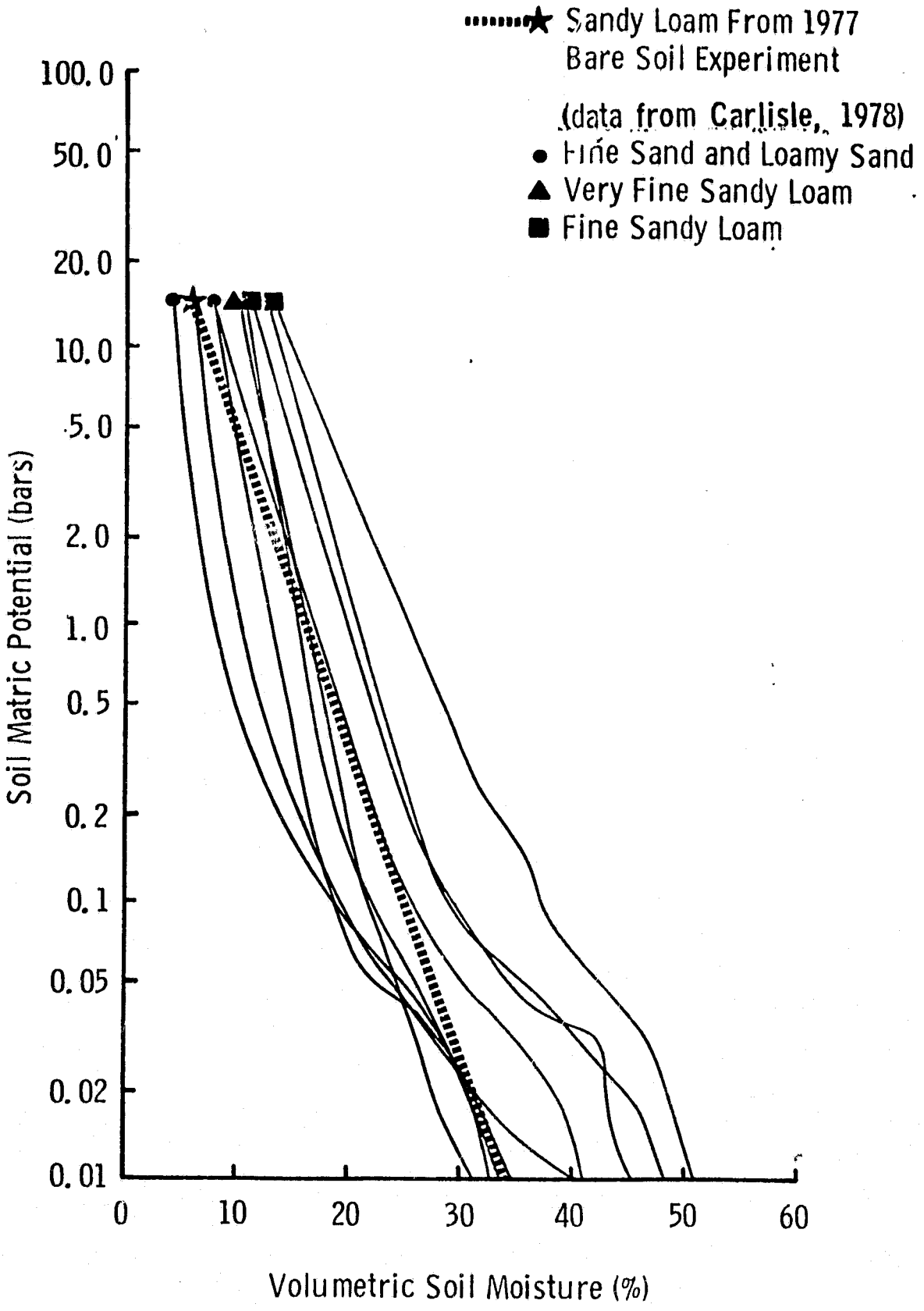

Figure 4.5

WATER RETENTION OF SANDY LOAM AND FINE SANDY LOAM
(data from Holtan, 1968).

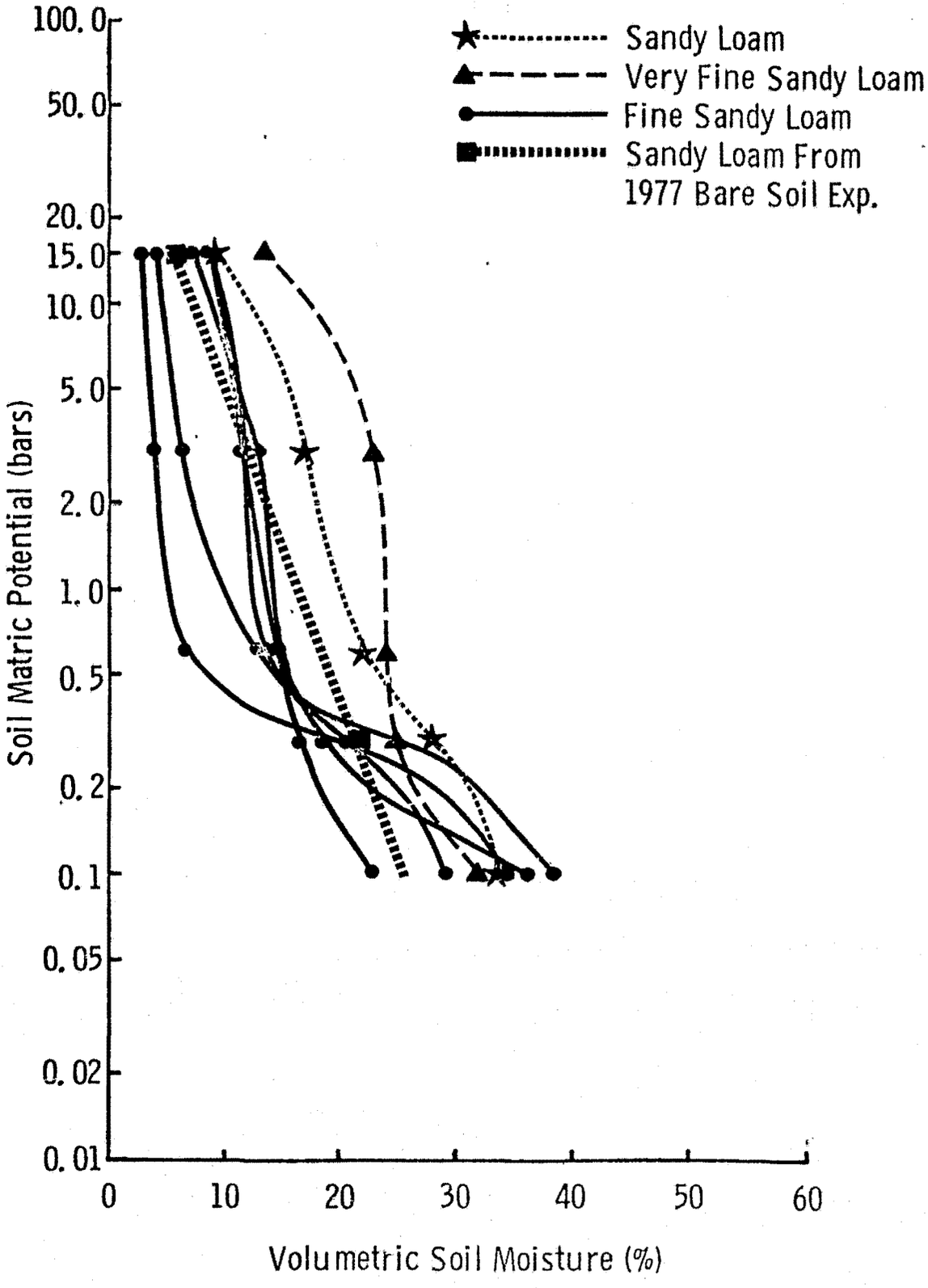

Figure 4.6 WATER RETENTION OF SILTY CLAY LOAM

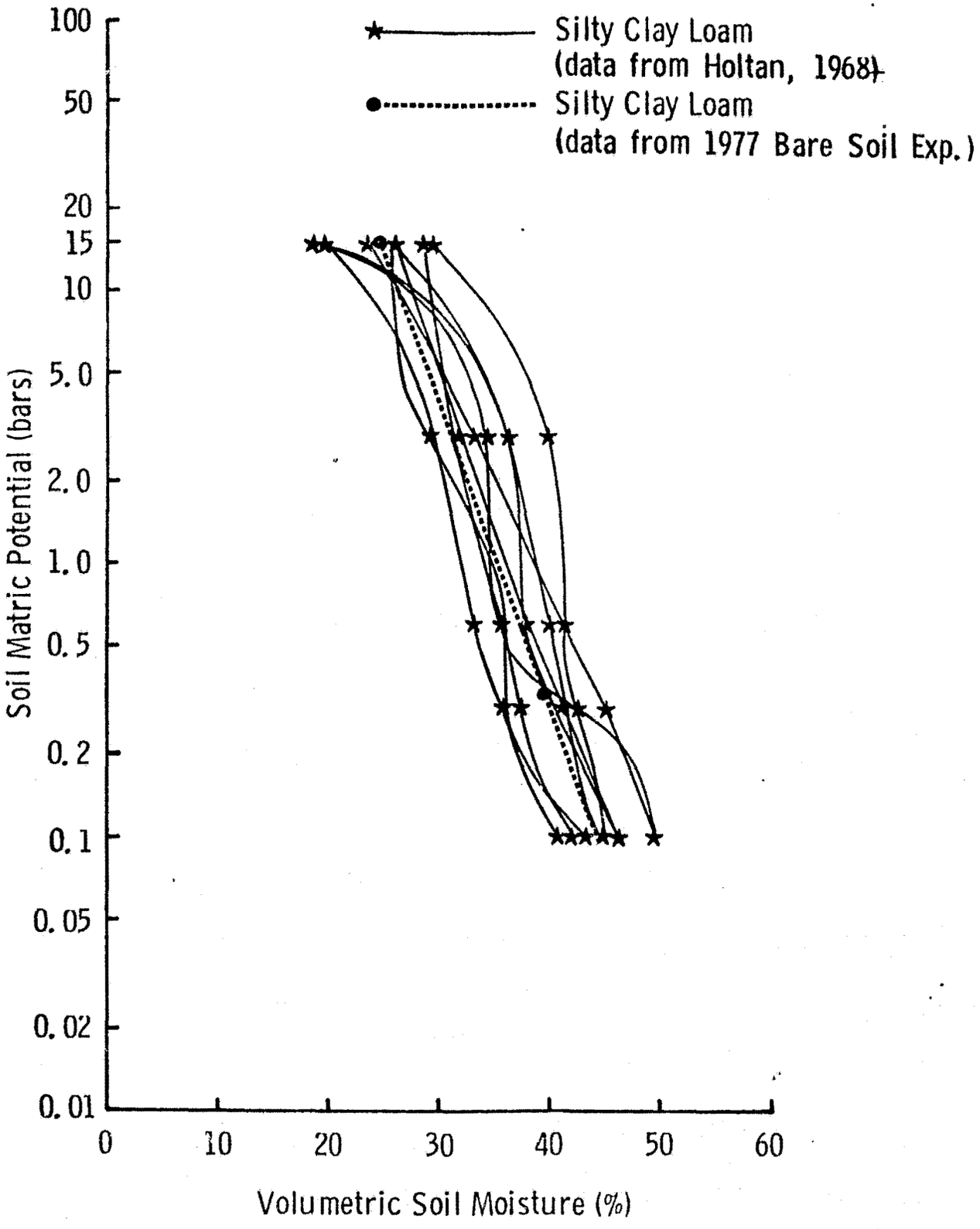

Figure 4.7 WATER RETENTION OF SILTY CLAY AND CLAY

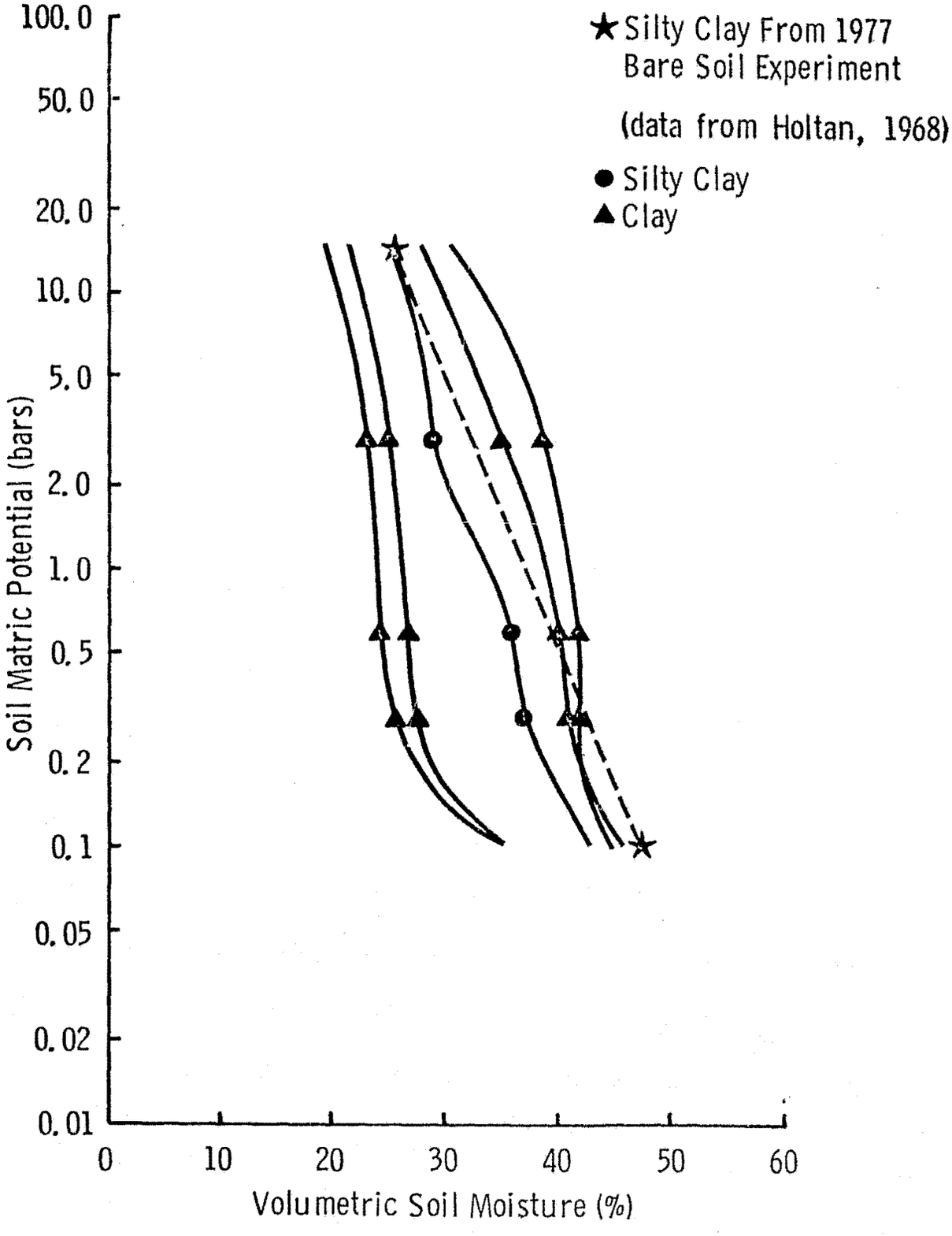

characteristic assumes that all gravimetric moisture is desorbed at 10,000 bars tension and inputs estimates of the water retention at 31 bars and saturation (0 bars) into the algorithm.

For purposes of comparison, the prime soil moisture sensor configuration of 4 GHz, 10° incidence angle and HH polarization determined by Batlivala and Ulaby (1977) is used throughout most of the following analysis.

4.1 Gravimetric and Volumetric Soil Moisture

The 1977 Bare Soil Experiment radar response to gravimetric and volumetric moistures is shown in Figures 4.8 and 4.9 for fields of sandy loam, silty clay loam and silty clay. The least squares linear fits of σ^o with respect to moisture are shown for each soil texture with line lengths representing the range of measured moisture values. Individually, the pearson's product moment correlation coefficient between σ^o and moisture is quite high, ranging from ≈.7 to .9 at all depth intervals (Table 3.15) and irrespective of soil moisture indicator. This emphasizes that for a given soil texture, regardless of the depth interval considered less than 0-15 cm, radar backscatter at 4.6 GHz, 10° and HH polarization is highly dependent upon soil moisture. The strength of the dependence of σ^o on the soil moisture of a specific soil texture, as measured by correlation coefficient, compares favorably to the results obtained from the 1974 and 1975 bare soil experiments (Batlivala and Ulaby, 1977). However, it is obvious from Figures 4.8 and 4.9 that the sensitivity of σ^o to gravimetric and volumetric soil moisture is highly dependent upon soil texture. Sensitivity is observed to be greatest for the coarse textured sandy loam and least for the fine textured silty clay field; these are precisely the findings of Schmugge (1976a, b) and Batlivala and Ulaby (1977). When the three soil types are equally represented, the combined regression fits (Figures 4.8 and 4.9) have a low slope and poorly predict the observed variance between soil textures. The poor correspondence of the combined texture algorithm to the texture specific algorithms indicates that the correlation of σ^o with either gravimetric or volumetric moisture will be low for ground scenes of varied soil texture and will degrade rapidly with increasing depth interval.

Figure 4.8

Linear regression fits of radar response to gravimetric soil moisture in the 0-1, 0-2, 0-5 and 0-9 cm Layers. σ^{o} at 4.625 GHz, 10^{o}, HH. 1977 Bare Soil Experiment Data for fields of sandy loam, silty clay loam and silty clay.

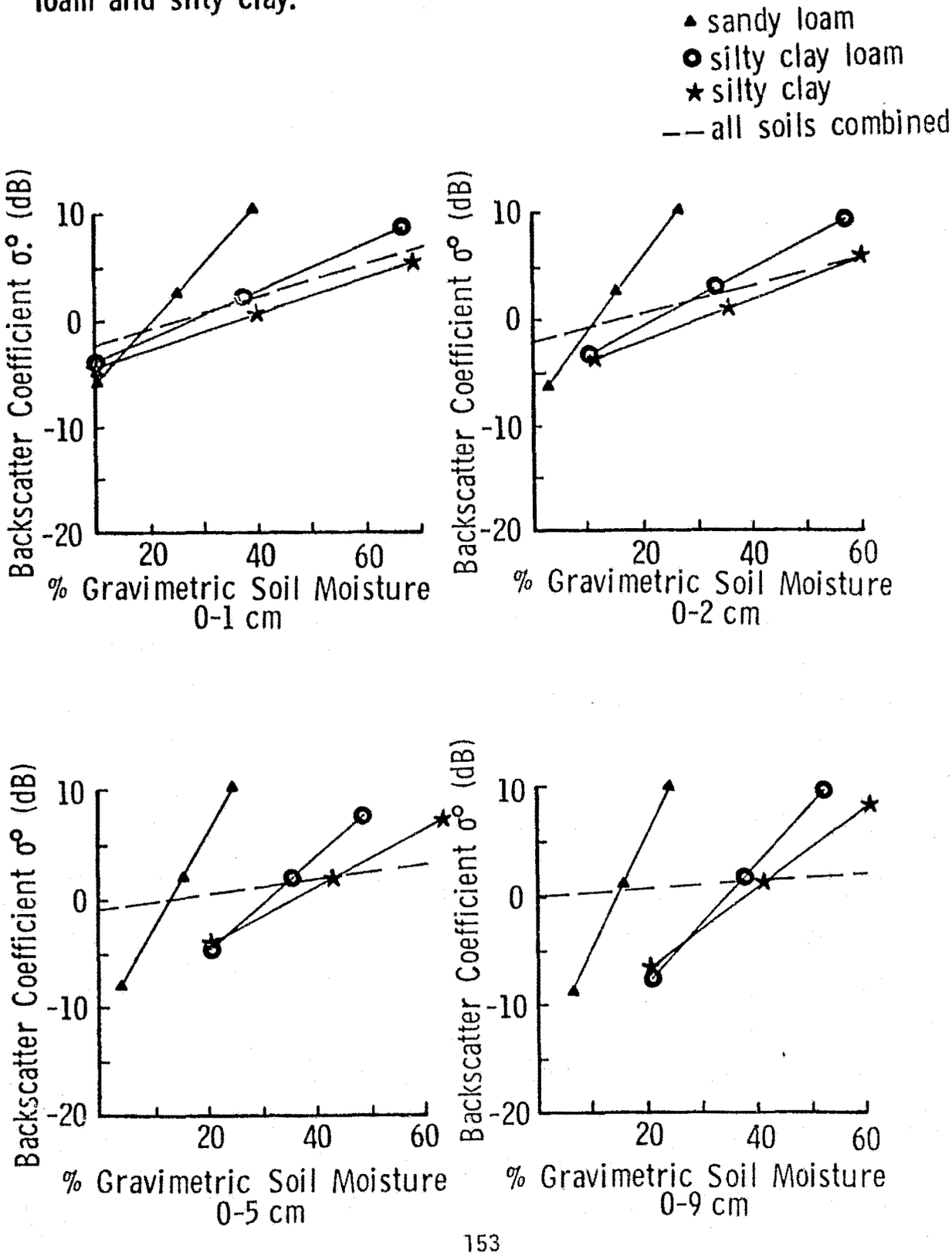

Figure 4.9

Linear regression fits of radar response to volumetric soil moisture in the 0-1, 0-2, 0-5 and 0-9 cm Layers. σ^0 at 4.625 GHz, 10^0, HH. 1977 Bare Soil Experiment Data for fields of sandy loam, silty clay loam and silty clay.

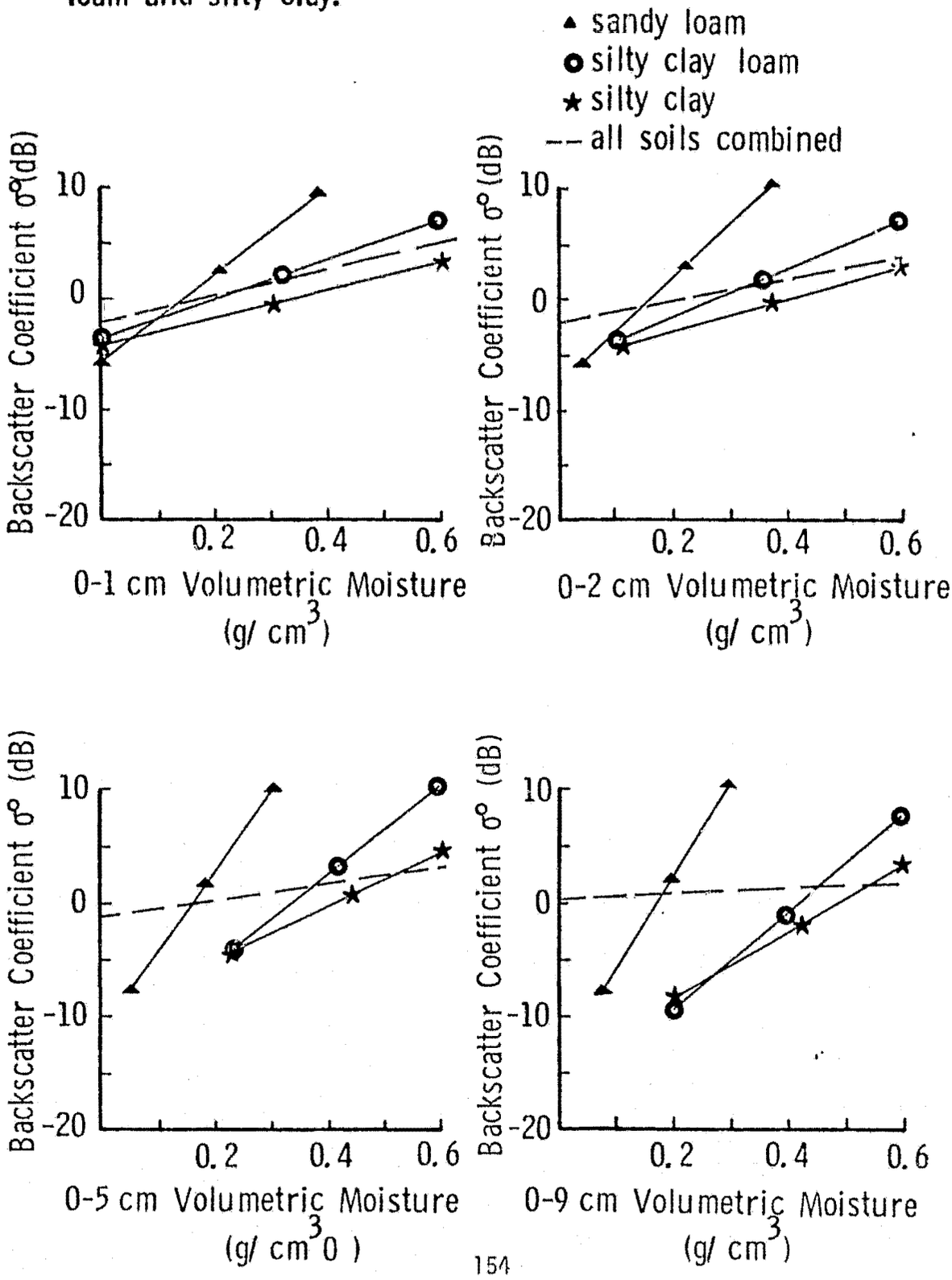

4.2 Normalized Soil Moisture

In equation 2.29, normalized moisture M_n was defined as a percent of the 1/3 bar moisture. However, the normalized moisture concept can be broadened to examine the effects of the tension at which moisture is normalized.

$$M_n = 100 \times Mg/M_T \qquad (4.1)$$

where: M_n = normalized moisture, %
M_T = Mg at tension, T

Using the values from Tables 4.1 and 4.2 and the algorithms given in Figures 4.1 to 4.3, M_T can be varied as a function of T. At each M_T the linear dependence of σ^o on M_n can be established and the resulting normalized moisture algorithms can be compared to those incorporating gravimetric, volumetric and Schmugge's percent of field capacity moisture indicators.

The 1977 Bare Soil Experiment radar response to soil moisture expressed as a percent of the 1/3 bar moisture, which approximates field capacity for fine-textured soils, is shown in Figure 4.10 for the 0-1, 0-2, 0-5 and 0-9 cm depth intervals. Upon inspection, it is immediately evident that dependence of sensitivity on soil texture is greatly reduced when compared to gravimetric or volumetric moisture indicators. The remaining apparent dependence of sensitivity on soil texture was found to be statistically insignificant with the standard error of regression coefficients typically exceeding the difference between the sensitivities of various soil textures. Not surprisingly, the correlation between σ^o and % 1/3 bar moisture for the combined data base of all textures considered simultaneously is very high, in excess of 0.8 for the 0-1 cm layer, and degrades only slightly with increasing depth.

A direct comparison of linear algorithms using gravimetric and 1/3 bar normalized moisture indicators is shown graphically in Figures 4.11 to 4.13 for the 0-1, 0-2 and 0-5 cm depths respectively. As expected, the combined algorithms incorporating normalized moisture exhibit a dramatic improvement in correlation coefficient. Line lengths of the regression fits indicate the range of measured moisture values. In the gravimetric moisture plots (Figures 4.11a to 4.13a) the levels of σ^o for the 50, 100 and 150% of 1/3 bar moistures are nearly constant for all soil textures.

Figure 4.10

Linear regression fits of radar response to % of 1/3 Bar Moisture in the 0-1, 0-2, 0-5 and 0-9 cm Layers. σ^0 at 4.625 GHz, 10^0, HH. Data from 1977 Bare Soil Experiment for fields of sandy loam, silty clay loam and silty clay.

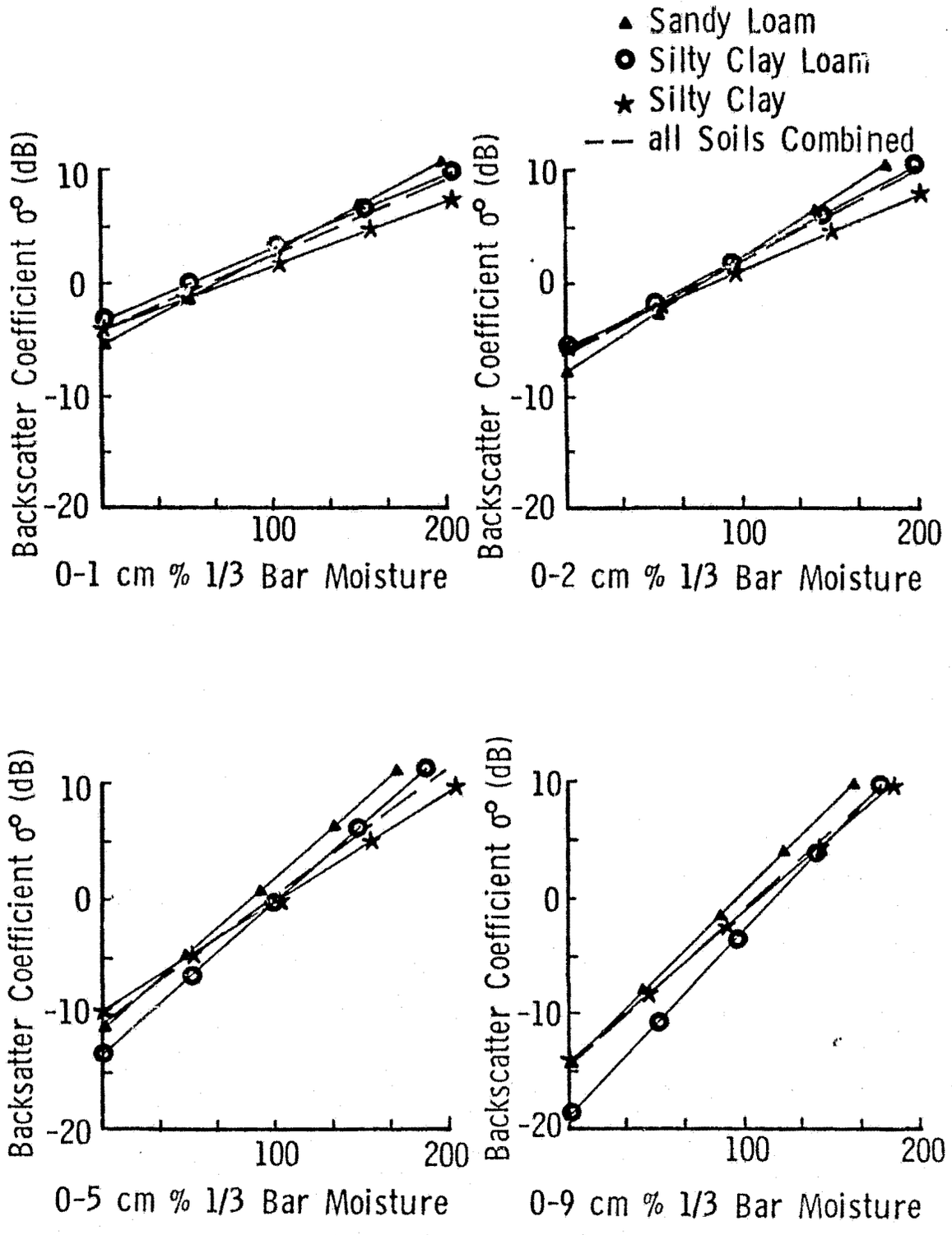

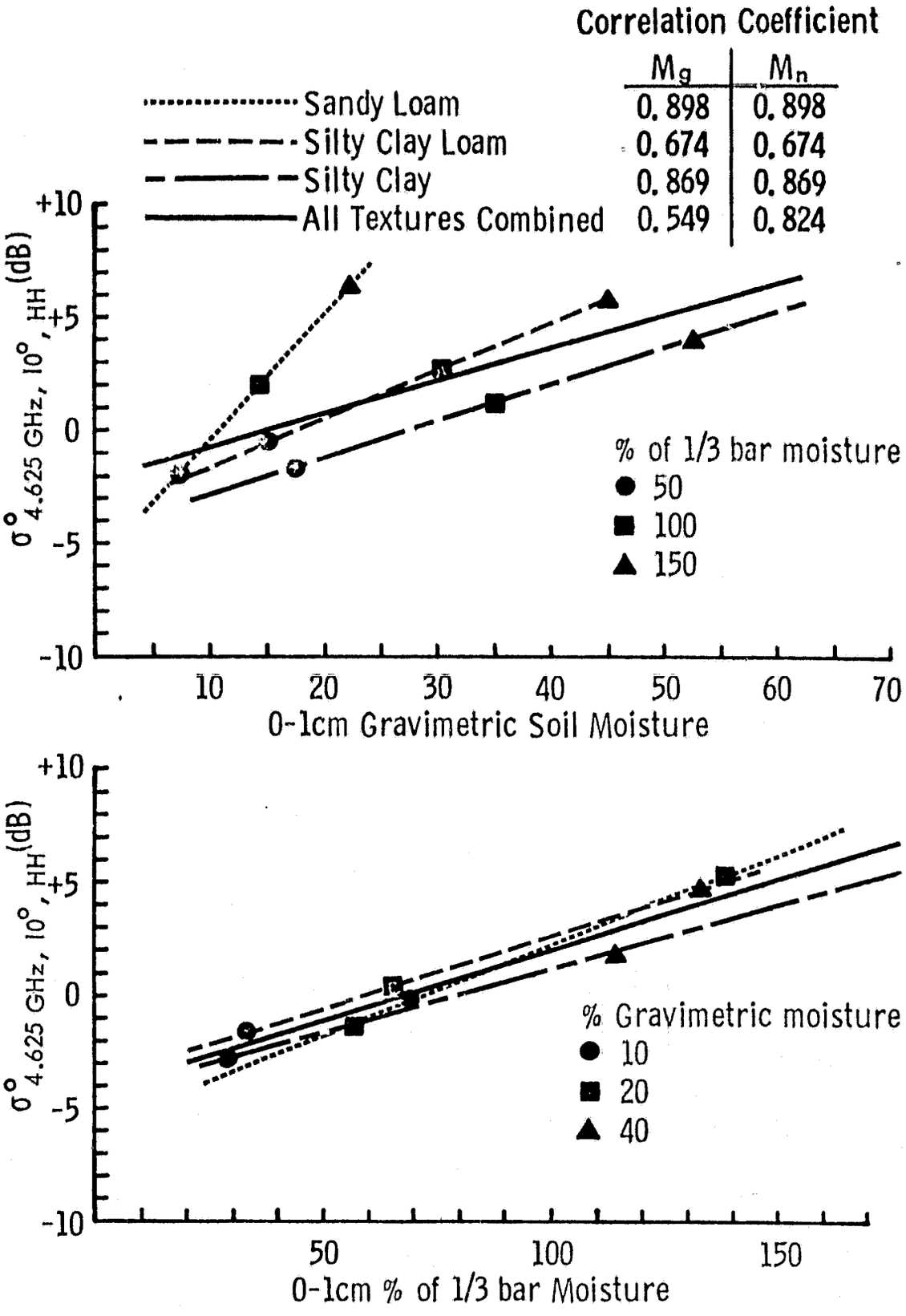

Figure 4.11. Comparison of 0-1 cm moisture algorithms for individual and combined soil textures at 4.6 GHz, 10°, HH polarization. a) gravimetric soil moisture and b) moisture normalized at 1/3 bar.

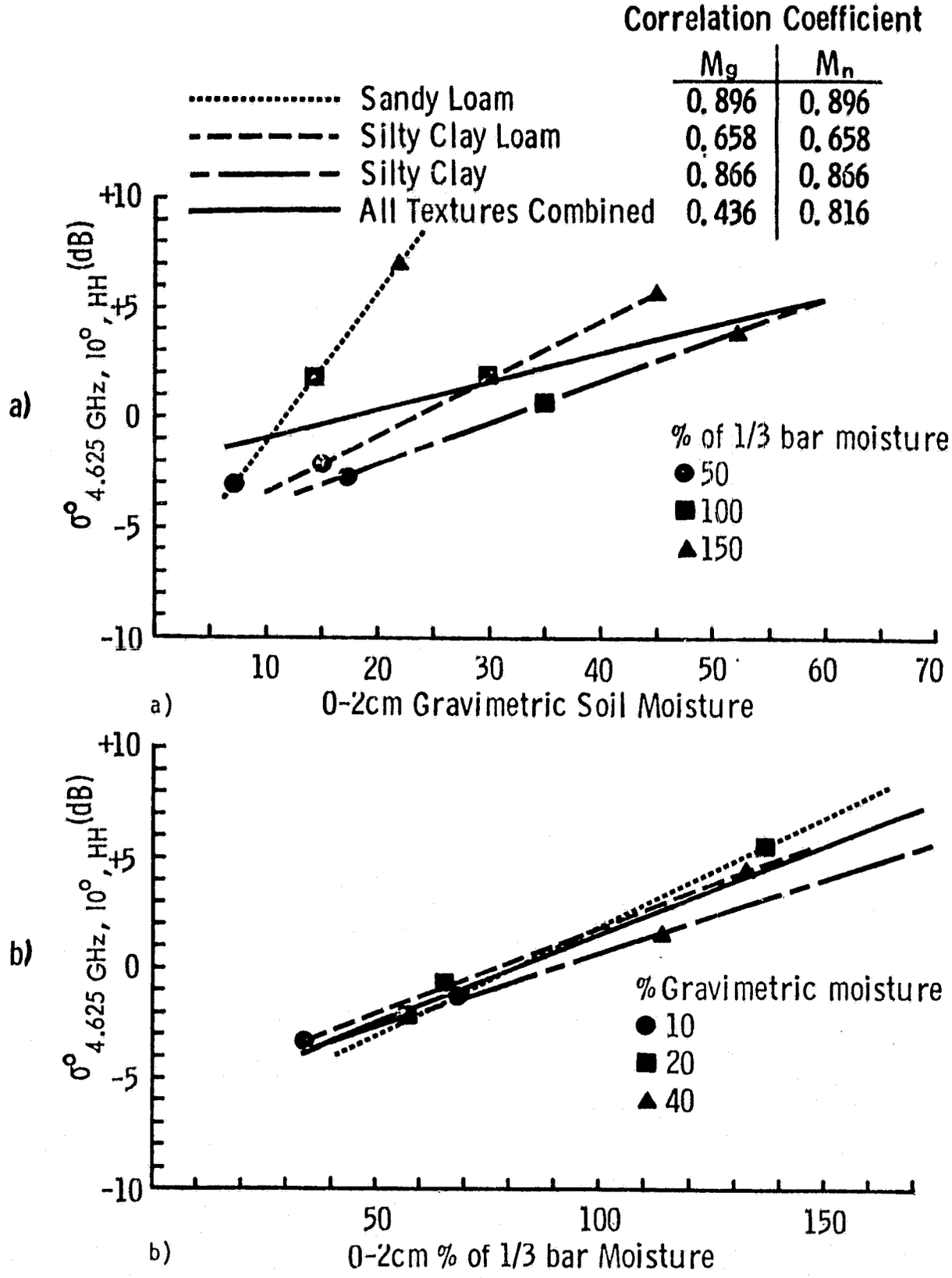

Figure 4.12. Comparison of 0-2 cm moisture algorithms for individual and combined soil textures at 4.6 GHz, 10° HH polarization. a) gravimetric soil moisture and b) moisture normalized at 1/3 bar.

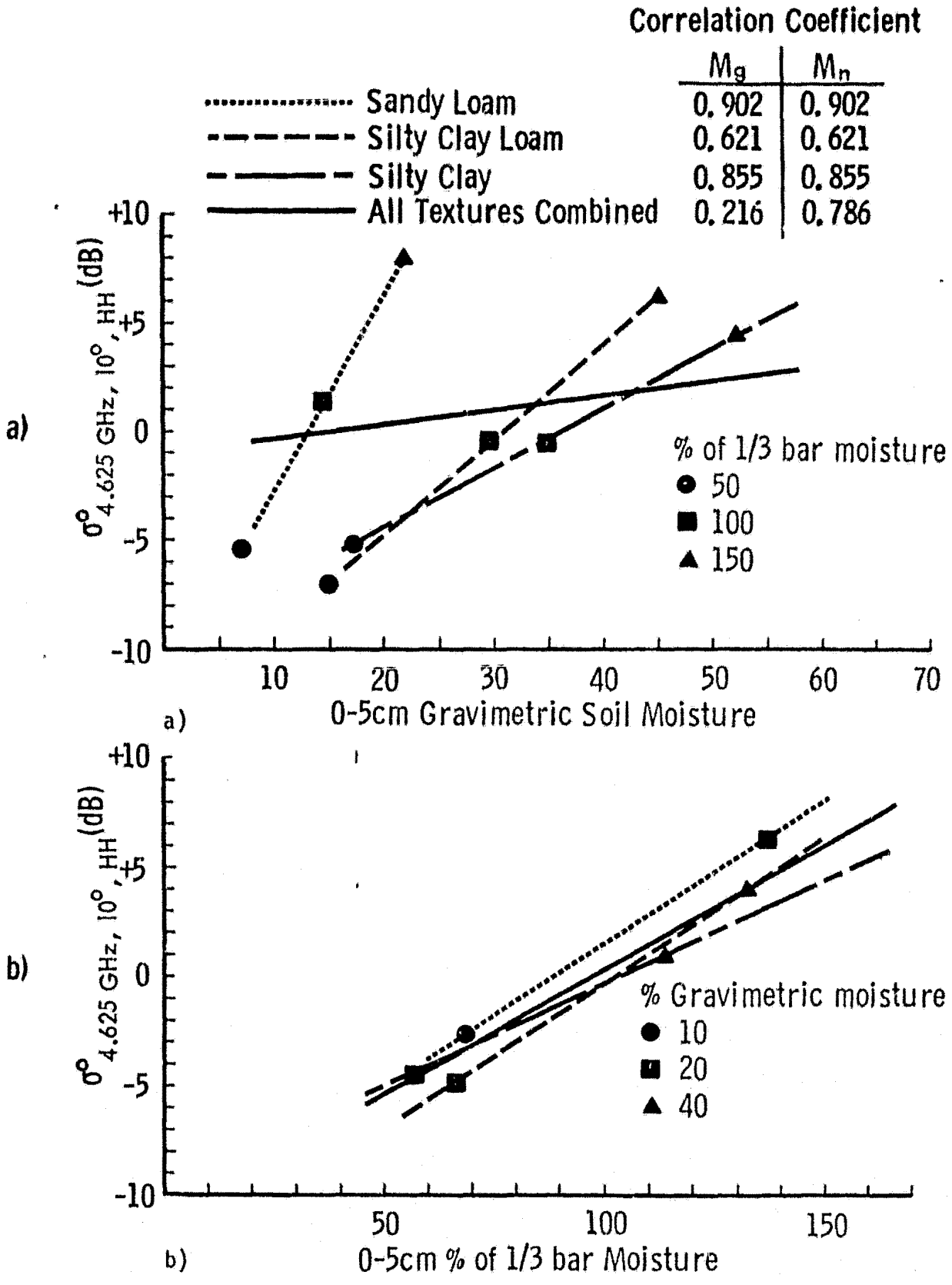

Figure 4.13. Comparison of 0-5 cm moisture algorithms for individual and combined soil textures at 4.6 GHz, 10°, HH polarization. a) gravimetric soil moisture and b) moisture normalized at 1/3 bar.

For all three soil textures considered simultaneously and given equal weighting, the relationship between correlation coefficient and soil depth interval is shown in Figure 4.14 for moisture expressed gravimetrically, volumetrically, normalized to 1/3 bar moisture, normalized to 1 bar moisture and percent of field capacity as estimated by the hueristic relationship between texture and 1/3 bar moisture given by equations (2.30) and (2.31). The correlation with σ^o of both simple moisture indicators decreases rapidly with depth in spite of the fact that volumetric moisture shows some improvement over gravimetric moisture within the 0-2 cm interval. In sharp contrast, all of the normalized moisture indicators have correlation coefficients in excess of 0.8 for the 0-1 cm interval and correlations exhibit only mild decay as a function of increasing depth interval.

The effect of normalizing moisture at the 1/3 bar tension on the 0-N cm moisture sample distributions explain the improved correlation coefficient. Histograms of the radar response to the soil for each soil texture are shown in Figure 4.15 at 4.6 and 7.6 GHz at all angles of incidence measured during the experiment. When the σ^o values of all textures are considered as one sample population, σ^o assumes a normal distribution at both frequencies and at all angles. The backscattering coefficient was also found to be normally distributed for the entire experiment at all other sensor combinations of frequency, polarization and angle. Histograms of the mean soil moisture sample populations for the 0-1, 0-5 and 0-15 depth intervals are shown in Figure 4.16. As soil depth interval increases gravimetric soil moisture assumes a multimodal distribution with the sampled mean moistures from each texture defining a statistically distinct sampling population, while for moisture expressed as a percent of 1/3 bar moisture the total sampling distribution becomes increasingly normal about a mean of approximately 95% for the 0-15 cm layer. Comparing Figures 4.15 and 4.16, the σ^o distributions clearly display a high correspondence to the distribution of normalized moisture even on a field by field basis.

It can be concluded from the foregoing that simple descriptors of soil water such as gravimetric and volumetric soil moisture, while adequate for single texture targets, are insufficient to describe the moisture perceived by radar for more complex and realistic targets. When soil

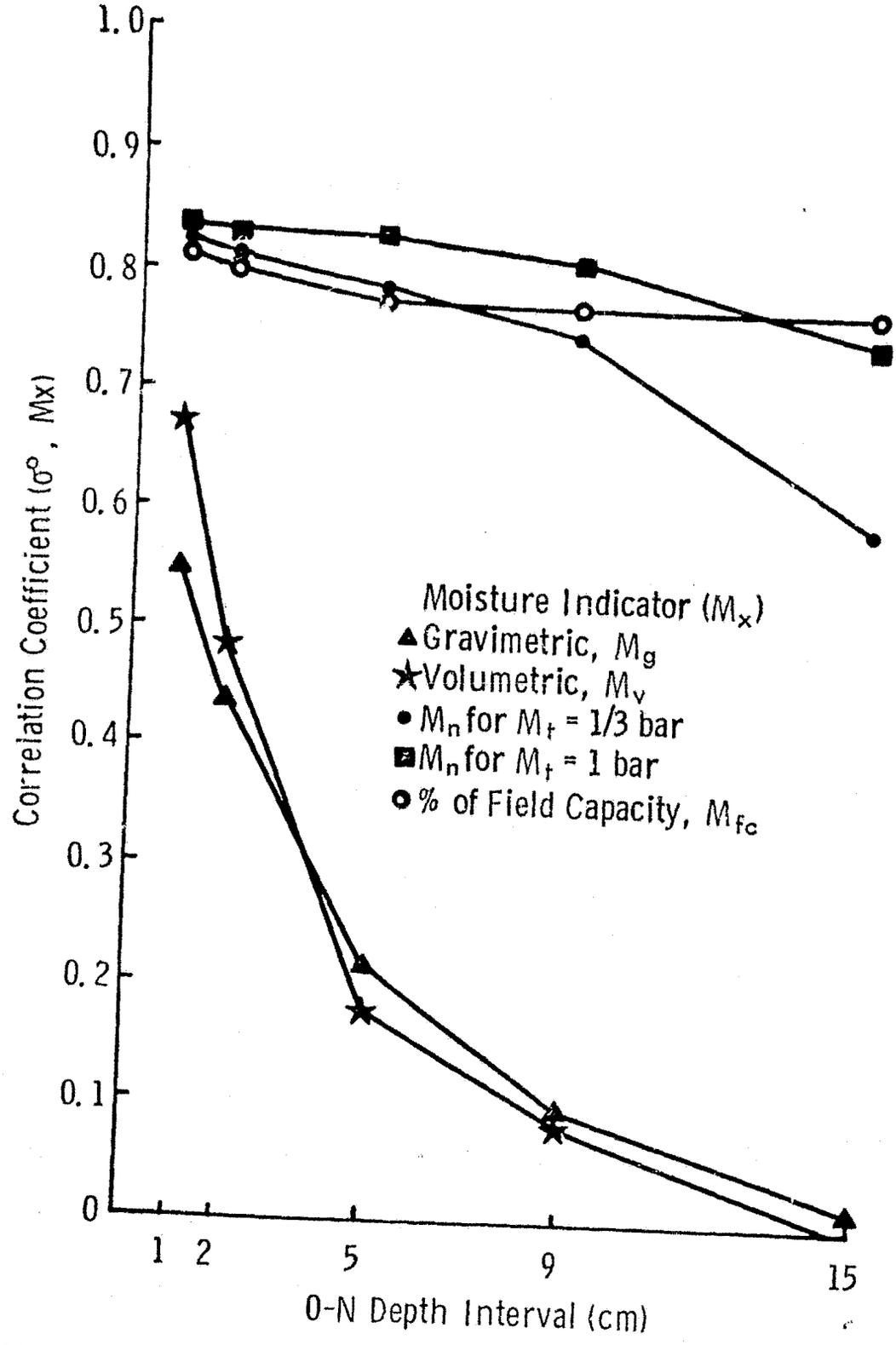

Figure 4.14. Correlation Coefficient as a Function of Depth Interval for σ° at 4.625 GHz, 10°, HH and Mx. Data from 1977 Bare Soil Experiment Fields of Sandy Loam, Silty Clay Loam and Silty Clay.

Figure 4.15 Histograms of Radar Backscattering Coefficient from Fields of Sandy Loam, Silty Clay Loam and Silty Clay at 4.625 and 7.625 GHz, HH polarization, 10^0, 15^0 and 20^0 incidence angles.

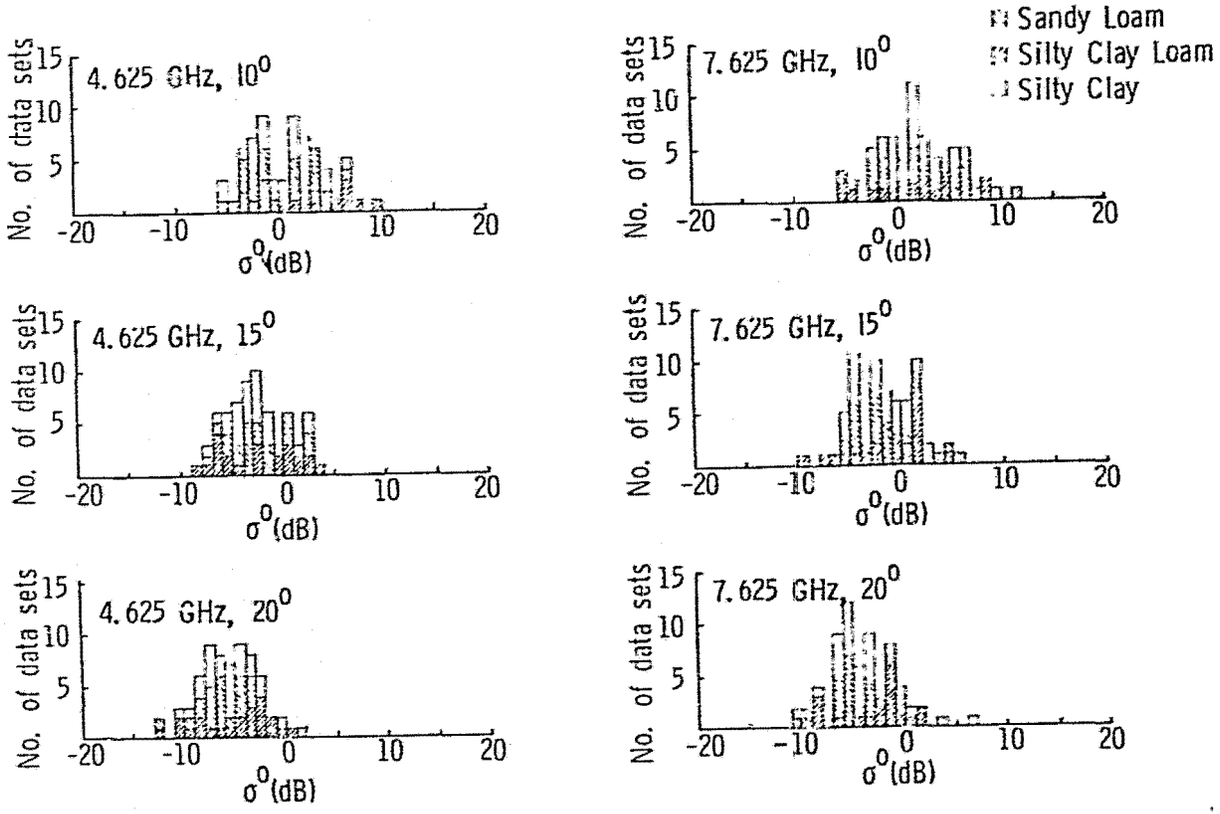

Figure 4.16 Histograms of 0-1, 0-5 and 0-15 cm Layer Gravimetric Moisture and Percent of 1/3 bar Moisture for fields of Sandy Loam, Silty Clay Loam and Silty Clay.

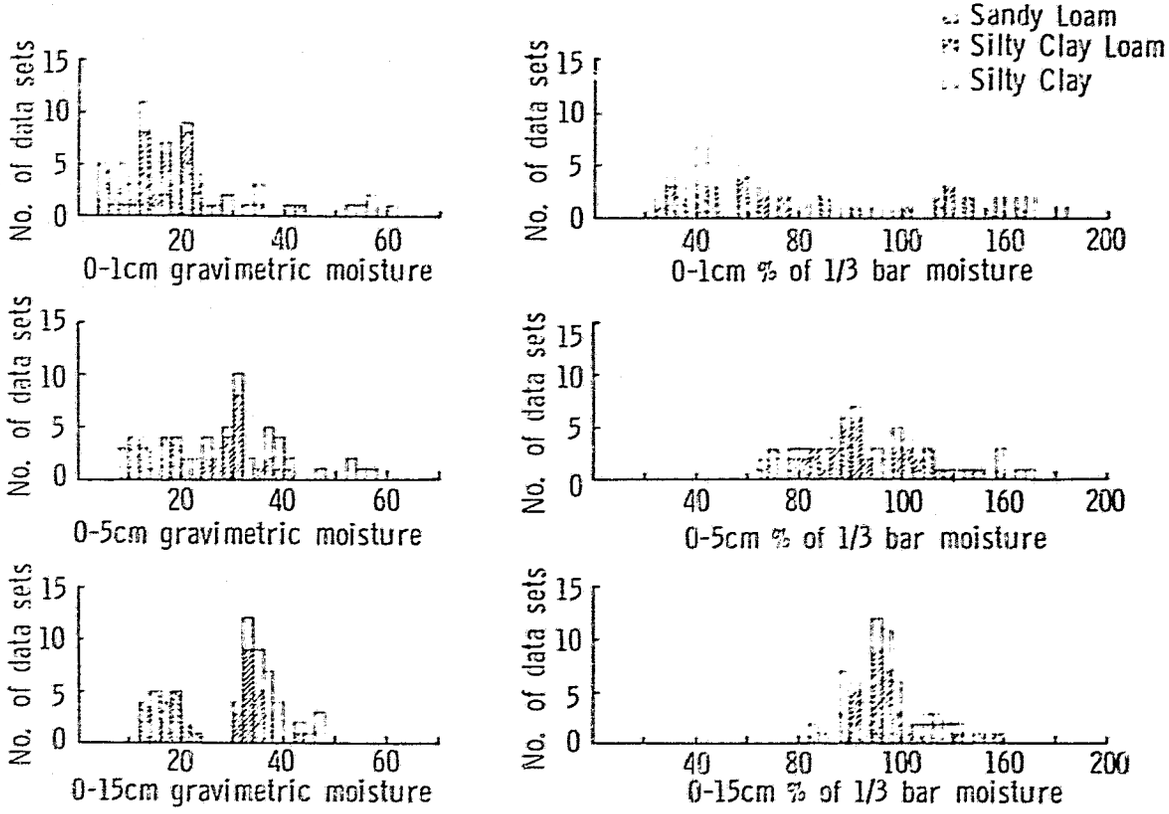

moisture is normalized by the percent of field capacity concept, the observed soil moisture distribution becomes less dependent upon textural effects. Since the distributions of σ° in Figure 4.15 are observed to be relatively independent of soil texture, the concept of soil moisture expressed as a percent of field capacity appears to be a good first approximation of the quantity of soil water to which radar is responsive. Furthermore, the normalized moisture indicators are superior to either gravimetric or volumetric moisture at all measured frequencies for ground scenes of mixed soil texture (Figure 4.17).

M_T in equation 4.1 was calculated for each soil texture at a range of tensions between 0.04 and 31 bars using the simple log-linear functions from Figures 4.1 to 4.3. At each normalizing tension the following linear regression model was fit to each soil texture separately and to the combined data base:

$$\sigma^\circ \text{ (dB)} = a + b\, M_n \qquad (4.2)$$

The correlation coefficient of the combined texture algorithm as a function of the normalizing tension T is presented in Figure 4.18 for the 0-1, 0-2 and 0-5 cm depth intervals. It is evident that the optimal normalizing tensions, with respect to linear correlation coefficient, lie in the region between $\approx$0.3 and 2 bars of tension. Outside of this range the correlation coefficient is observed to decline, especially with increasing soil depth interval. It should be noted that the results presented in Figure 4.18 are based upon the full range of moisture conditions present during the experiment and includes data from fields which were 10 to 20% covered with standing water.

While Figure 4.18 shows correlation coefficient to maximize at approximately 1 bar normalizing tension for all depth intervals (also Figure 4.14), the statistical significance of the apparent improvement in correlation coefficient at large depth intervals is not obvious. The predominance of high surface soil moistures prevalent throughout the experiment suggests that there should be only small contributions to σ° from moisture at soil depths greater than 2 cm below the surface. It is argued that the high correlations for depth intervals greater than 0-2 cm are the result of the high correlation between 0-N cm soil layers (Table 4.3).

Figure 4.17. Correlation coefficient as a function of frequency for various 0-5 cm soil moisture indicators at 10° incidence angle and HH polarization. Soil moisture is expressed as gravimetric, volumetric, % of 1/3 bar moisture, % of Schmugge's estimate of 1/3 bar moisture and % of 1 bar moisture.

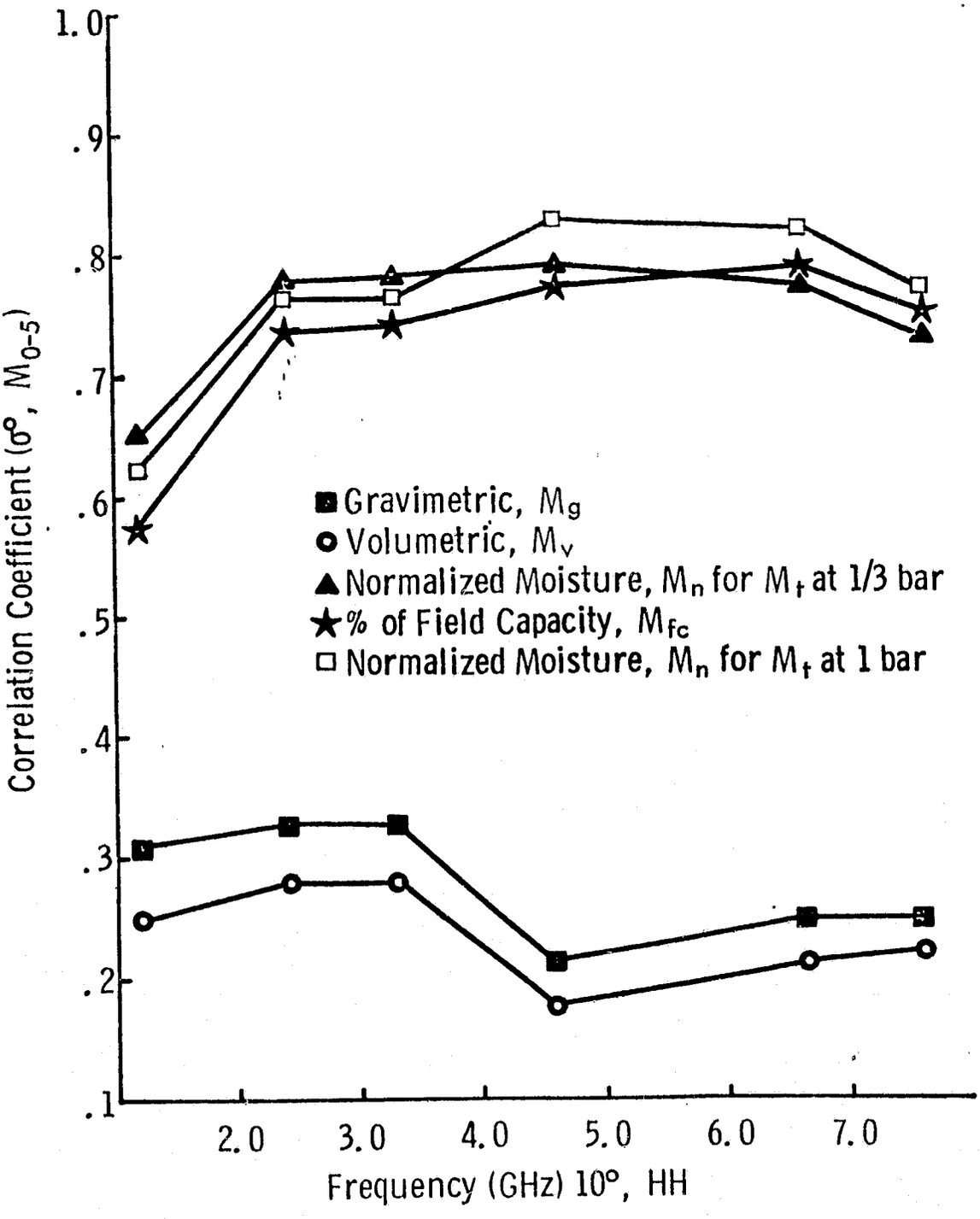

Figure 4.18 Correlation Coefficient as a Function of Normalizing Tension. σ° at 4.625 GHz, 10°, HH polarization Soil Moisture in the 0-1, 0-2, 0-5 cm Layers of sandy loam, silty clay loam and silty clay.

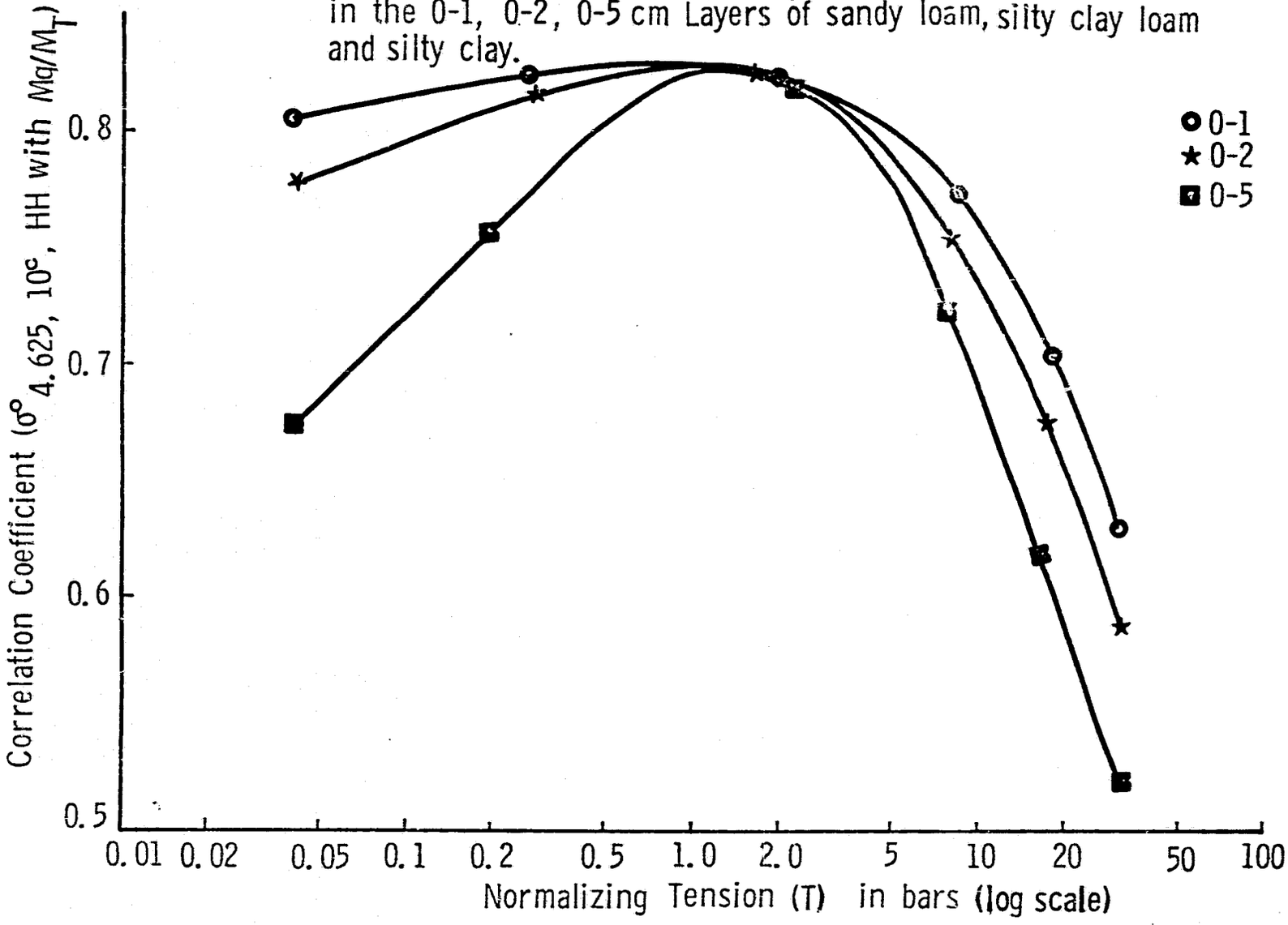

TABLE 4.3

Correlation Matrix of Soil Moisture Expressed as a Percent of 1/3 Bar Gravimetric Moisture for 0-N cm Depth Intervals, 1977 Bare Soil Experiment.

Depth (cm)	0-1	0-2	0-5	0-9	0-15
0-1	1.0				
0-2	.9893	1.0			
0-5	.9215	.9589	1.0		
0-9	.8732	.9113	.9758	1.0	
0-15	.8517	.8767	.9315	.9762	1.0

Algorithm constants and linear correlation coefficients from equation (4.2) are plotted as a function of normalizing tension M_T in Figure 4.19 for radar response at 4.6 GHz to the 0-1 cm moisture of all soil textures combined. The sensitivity of σ^o to M_n of the combined texture algorithm (Figure 4.19) is compared to the sensitivities computed for each independent soil texture in Figure 4.20 as a function of normalizing tension. The under prediction of sensitivity by the combined algorithm at tensions in excess of 1.5 bars is largely responsible for the decline in correlation coefficient when moisture is normalized at tensions greater than 1 bar (Figures 4.18 and 4.19). The exclusion of flooded and saturated soil data sets from the combined texture algorithm is observed to improve correlation coefficient by approximately 0.05 at all normalizing tensions (Figure 4.21).

The empirical results obtained from the 1977 Bare Soil Experiment clearly demonstrate the superiority of normalized moisture over gravimetric and volumetric moisture as texture independent indicators of the soil water observed by radar between 1 and 8 GHz. However, the value of normalized moisture to a user community is inhibited by its poor interpretability over most of the range of normalizing tensions. Normalized moisture is perhaps most meaningful at the 1/3 bar tension where it approximates field capacity. When interpreted as a percent of field capacity, 0% is completely dry, 50% approximates the wilting point of agronomic plant species, 100% approximates field capacity of the soil and 150% is observed to correspond to complete soil saturation in the field.

4.3 Transition Moisture Concept

A transition moisture W_T was defined in Chapter 2 which separates the behavior of the dielectric constant of soil into two moisture response regions. The volume of soil water adsorbed to the soil particle surfaces which is structurally and dielectrically similar to ice is believed to be separated from bulk water by the transition moisture (Wang and Schmugge, 1978). The tightly adsorbed water below the transition moisture should be several monomolecular layers thick depending upon the strength of the electric double layers. The transition moisture has been observed to vary with soil texture (Wang and Schmugge, 1978), and is found to be

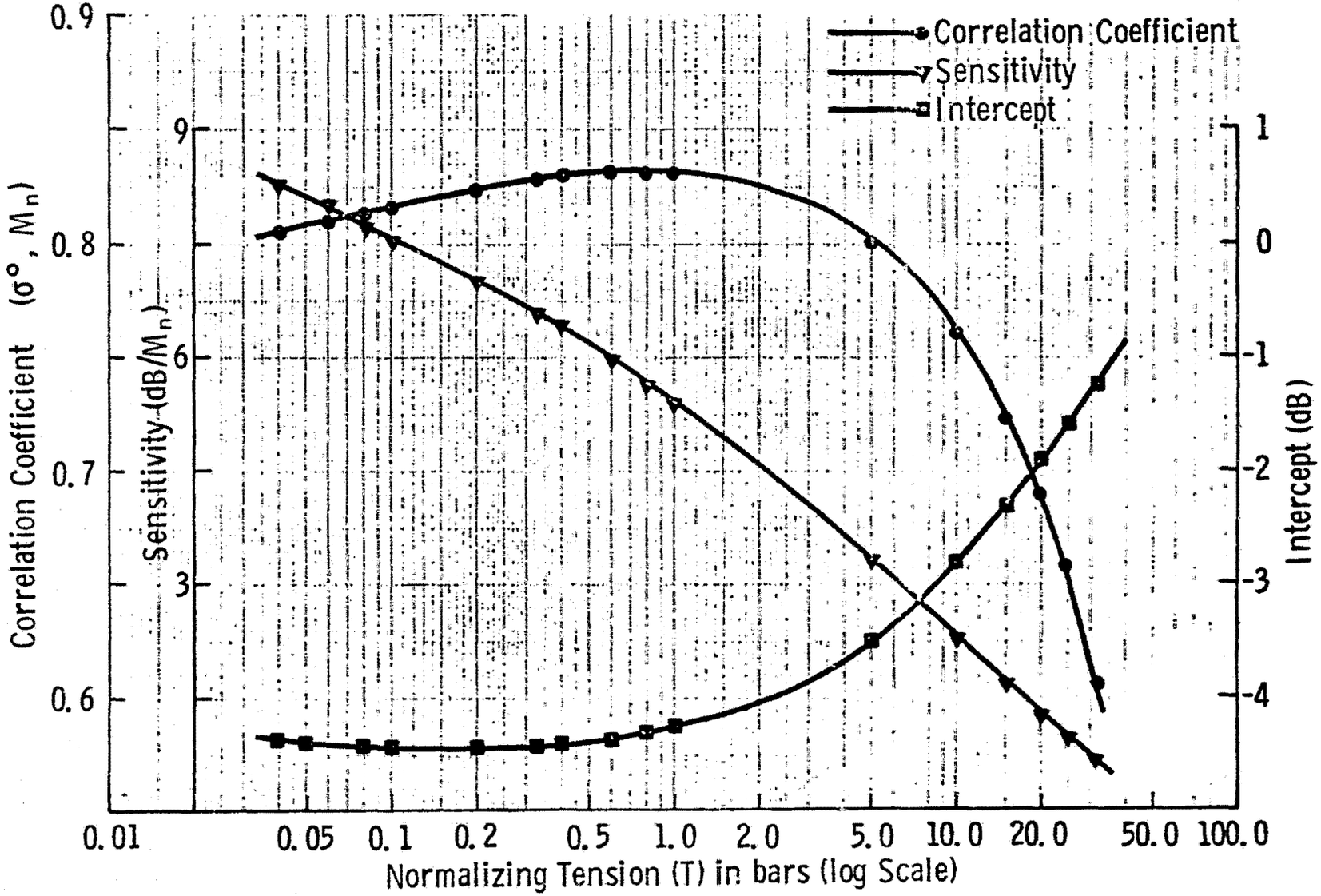

Figure 4.19. Correlation coefficient, sensitivity and intercept as a function of normalizing tension for the combined data algorithm: $\sigma^\circ = a + bM_n$ for 0-1 cm moisture at 4.625 GHz, 10°, HH polarization.

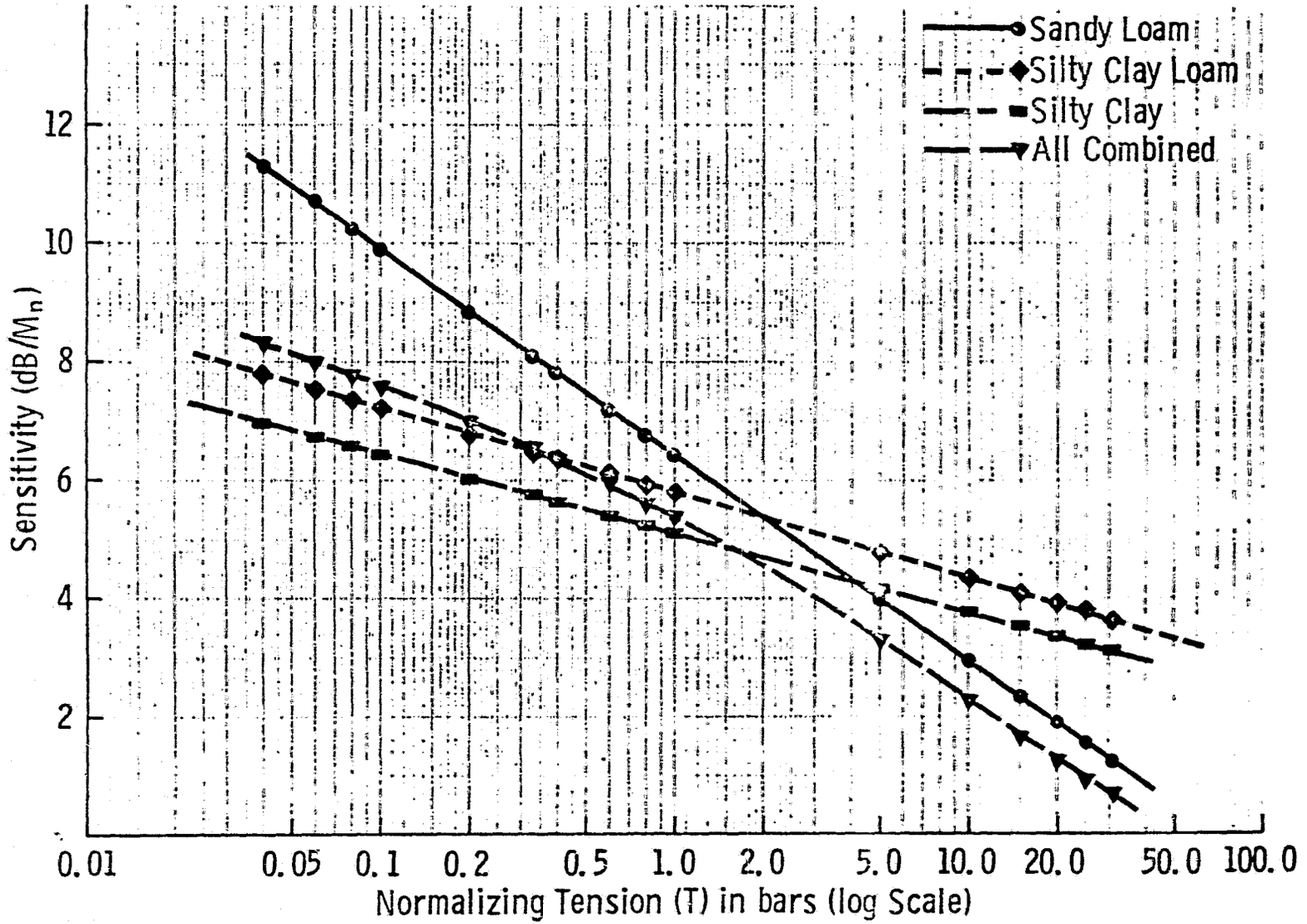

Figure 4.20. 0-1 cm algorithm sensitivity as a function of normalizing tension for individual soil textures and all textures combined at 4.6 GHz, 10°, HH polarization.

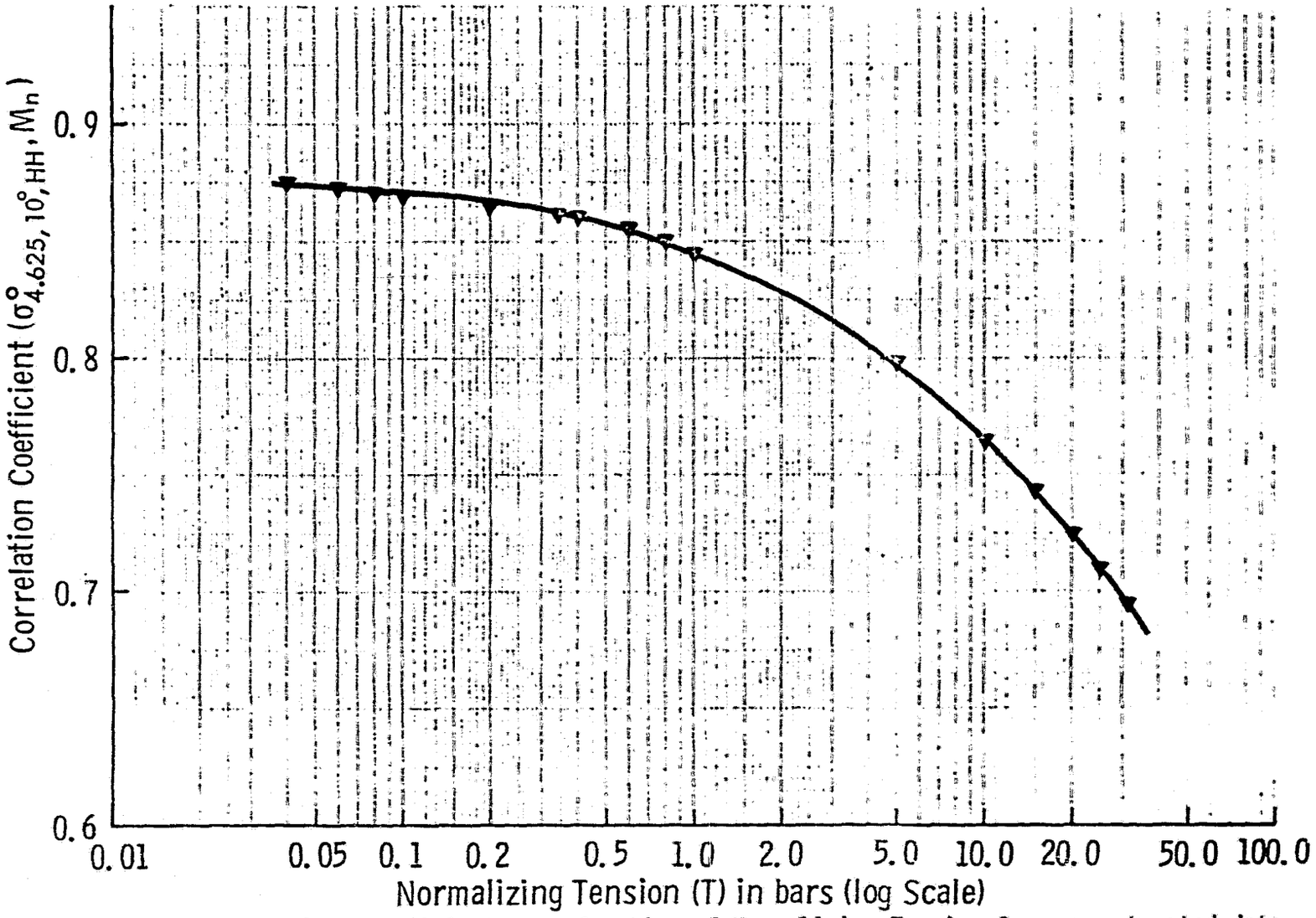

Figure 4.21. Correlation coefficient as a function of Normalizing Tension for non-saturated data from Fields 1, 3 and 4.

smaller for sandy soils than for clayey soils as predicted by the double layer model and considerations of specific surface.

The transition moisture concept was evaluated as a descriptor of the radar response to soil moisture by assuming that the bulk water in excess of the transition moisture is dielectrically equivalent regardless of soil texture. The validity of this assumption should depend largely upon the salinities of the bulk soil solutions which the model tacitly assumes to be equivalent. In addition, all measured M_v during the bare soil experiment is assumed to be in excess of the transition moisture W_T. Thus, the postulated model of radar response to M_v can be presented graphically as a series of parallel lines, one for each soil texture, offset from each other by their respective transition moistures and is described by the following equation for M_v in excess of W_T:

$$\sigma^o = \alpha M_v + \beta_1 F_1 + \beta_2 F_2 + \beta_3 F_3 + \beta_4 F_4 \qquad (4.3)$$

where: α = sensitivity

β = intercept of ordinate axis

F = dichotomous soil texture variable which can assume a value of 1 or 0

1 = field 1, sandy loam

2 = field 2, silty clay loam

3 = field 3, silty clay loam

4 = field 4, silty clay

Multiple linear regression fits of the above model were computed for M_v as corrected for soil shrink-swell effects as described in Appendix A at 2.4, 4.6 and 7.6 GHz, HH polarization and incidence angles of 10° and 20°. The multiple correlation coefficients R are between 0.7 and 0.8, even when erratic field 2 is included in the analysis (Table 4.4). R is observed to increase only slightly when field 2 is excluded from analysis. These correlations are comparable to those obtained from algorithms using normalized soil moisture indicators.

The regression fits of equation 4.3, at 4.6 GHz, HH polarization are shown in Figures 4.22 and 4.23 for 10° and 20° incidence angles respectively

TABLE 4.4

Multiple Correlation Coefficients of Radar Response
to Volumetric Moisture in Excess of the Transition Moisture

Test Fields Included	Polarization	Frequency (GHz)	Incidence Angle	Soil Depth Interval (cm) 0-1	0-2	0-5	0-9
All	HH	2.4	10	.745	.722	.752	.702
			20	.732	.721	.754	.740
		4.6	10	.735	.714	.748	.709
			20	.704	.676	.710	.671
		7.6	10	.703	.675	.717	.678
			20	.679	.647	.689	.658
1, 3, 4	HH	2.4	10	.774			
			20	.734			
		4.6	10	.795			
			20	.744			
		7.6	10	.746			
			20	.703			

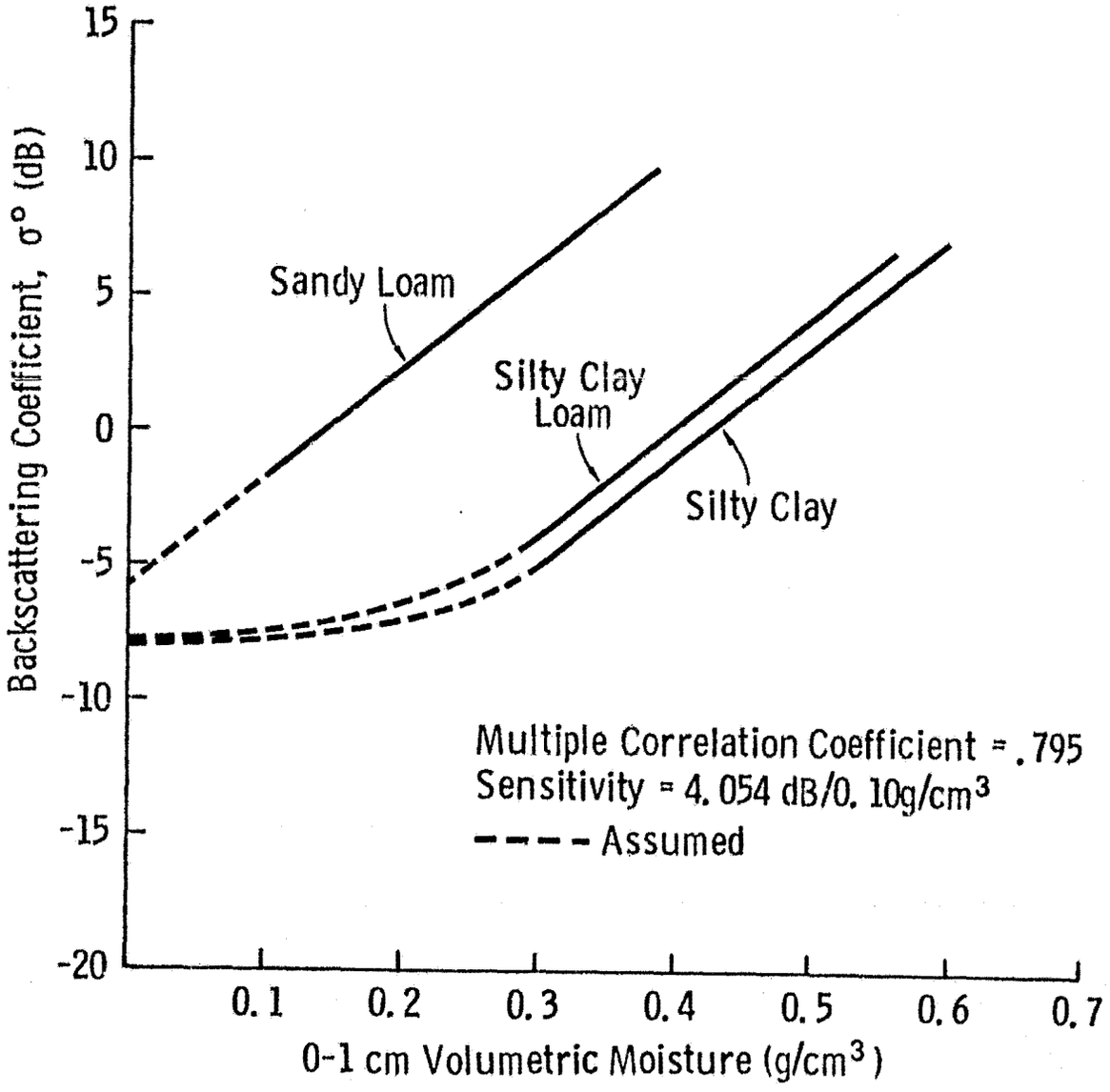

Figure 4.22. Multiple linear regression fit of 0-1 cm volumetric soil moisture in excess of the transition moisture with radar backscatter at 4.6 GHz, HH polarization and 10° incidence angle.

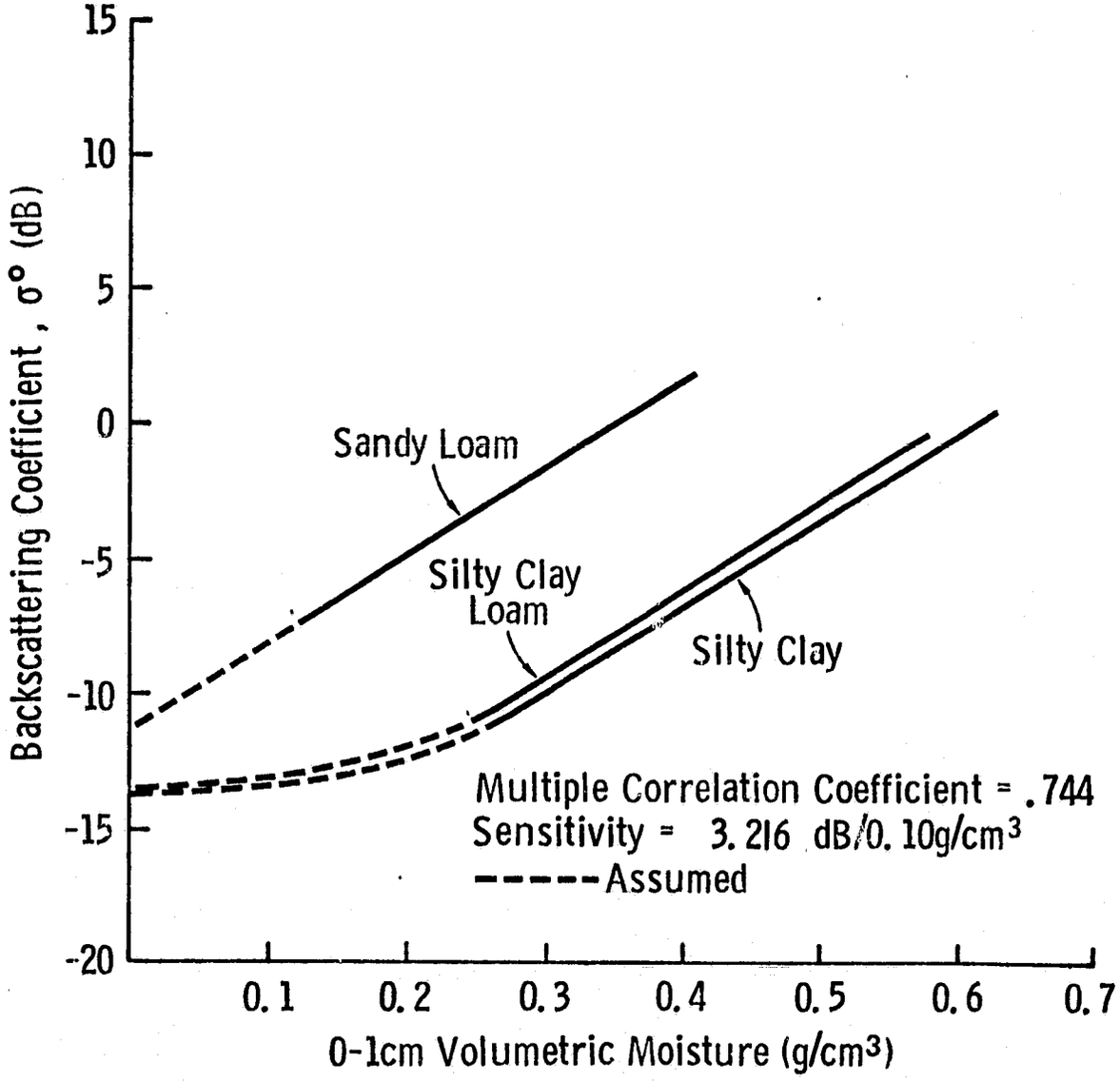

Figure 4.23. Multiple linear regression fit of 0-1 cm volumetric soil moisture in excess of the transition moisture with radar backscatter at 4.6 GHz, HH polarization and 20° incidence angle.

C-3

as a function of 0-1 cm volumetric moisture. The assumptions made in postulating the above model make impossible an exact determination of the transition moistures for each soil texture. However, the offsets of the regression fits along the abscissa indicate the relative differences between the transition moistures of each soil texture. These offsets, in terms of M_v, are calculated by inverting equation (4.3) and solving for M_v of each soil texture at a constant value of σ^o. According to the model, the relative differences between these values of M_v should be equivalent to the differences between W_T for each soil texture. By this method, W_T of silty clay loam and silty clay is calculated to be from 0.18 to 0.28 g/cm^3 greater than W_T of sandy loam depending upon sensor f, p and θ.

Values of transition moisture can be converted to an estimate of the number of monomolecular water layers enveloping the soil solids given the specific surface and bulk density of the soil. Specific surface was not directly measured for the soils examined during the 1977 Bare Soil Experiment, but can be estimated from knowledge of the particle size distribution (Figures 3.2 and 3.3) and the clay mineralogy of the field soils. The volumetric moisture in one monolayer is approximated by:

$$M_L = S \times D_W \times \rho_b \times 10^{-4} \qquad (4.4)$$

where: M_L = volumetric moisture of soil having one monomolecular water layer, g/cm^3

S = specific surface of soil, m^2/g

ρ_b = soil bulk density, g/cm^3

D_W = diameter of a water molecule ≈2.76A^o

Specific surface is estimated as the sum of mean specific surface values of the soil textural separates of sand, silt and clay given in Table 3.6. The specific surface of the sand and silt size fractions are shown by Figure 2.4 to be ≈0.01 and 0.1 m^2/g respectively. The clay fraction of soils in the test site area commonly consist of approximately 50% montmorillonite and 30% illite (Dickey, 1979). The remaining 20% of the clay sized fraction is presumed to consist of non-clay minerals with a specific surface of approximately 10.0 m^2/g. Net specific surface

is calculated using values of the specific surface of various clay minerals from Table 2.8 by:

$$S = S_{sand}(\%sand) + S_{silt}(\%silt) + S_{clay}(\%clay) \qquad (4.5)$$

and

$$S_{clay} = 0.5\ S_M + 0.3\ S_I + 0.2\ S_o. \qquad (4.6)$$

where: S_M = specific surface of montmorillonite ≈700 m^2/g

S_I = specific surface of illite ≈100 m^2/g

S_o = specific surface of non-clay minerals ≈10 m^2/g

Solving equation (4.5) for S using S_{clay} = 382 m^2/g from equation (4.6) yields the specific surface estimates presented in Table 4.5 for each soil texture (ignoring the specific surface of the organic soil fraction). Using the mean soil bulk densities in the 0-1 cm layer the volumetric moisture of one monomolecular water layer M_L is computed from equation (4.4) to be 0.004, 0.048 to 0.046 and 0.063 g/cm^3 for sandy loam, silty clay loam and silty clay respectively (Table 4.5). The above values are very similar to the measured air-dry water contents of the soil (Table 4.1). Thus, the estimated values of M_L are closely related to the hygroscopic coefficient at 31 bars of tension. If the offsets in volumetric moisture from the linear regression fits of σ^o to M_v (Figures 4.22 and 4.23) are interpreted as the transition moistures W_T, then the ratio W_T/M_L yields a tightly adsorbed water layer on the order of 4 to 6 molecules thick which exhibits dielectric properties dissimilar to that of the bulk soil solution. This estimate compares favorably to the ≈8-9 molecular layers of water estimated to be below the transition moisture from dielectric measurements (Wang and Schmugge, 1978). Furthermore, the computation of estimated W_T from the 15 bar water retention of the soils examined during the 1977 Bare Soil Experiment by equation (2.13) yields values almost identical to those obtained from comparison of the multiple linear regression fits in Figures 4.22 and 4.23.

4.4 Soil Tension

The data acquired during the 1977 Bare Soil Experiment was used to test the hypothesis that radar response is linearly dependent upon soil

TABLE 4.5

Estimates of Specific Surface and the Volumetric Moisture of One Monomolecular Water Layer for Each Field Examined During the 1977 Bare Soil Experiment.

Field	ρ_b g/cm^3	Percent			Specific Surface, m^2/g				M_L g/cm^3
		Sand	Silt	Clay	Sand	Silt	Clay	Total	
1	1.43	55.0	42.2	2.8	.0055	.0422	10.696	10.7435	.0042
2	1.22	9.1	53.9	37.0	.00091	.0539	141.34	141.39481	.0476
3	1.20	11.5	52.2	36.2	.00115	.0522	138.284	138.33735	.0458
4	1.30	9.0	45.1	45.8	.0009	.0451	174.956	175.002	.0628

tension. Since soil tension was not directly measured in the field duirng the acquisition of radar data, values of soil tension were estimated from the desorption characteristics of each field given in Table 4.1 and shown in Figures 4.1 to 4.3. The assumption that laboratory defined desorption characteristics adequately define the actual soil tension of structurally dynamic field soils is particularly poor for soils of high clay content such as silty clay loam and silty clay which commonly exhibit large hysteresis effects. Thus, the presented results can be considered as a "worst case" approximation which should show dramatic improvement if field tension values were available to account for the hysteretic dependence of tension on some function of moisture history.

Using the simple log-linear estimates of soil tension from Figures 4.1 to 4.3, σ^o at 4.6 GHz, 10° and HH polarization is plotted as a function of the logarithm of the 0-2 cm layer tension in Figure 4.24. The observed scatter in Figure 4.24 is felt to be primarily caused by hysteresis in the true moisture-tension characteristics of the fields which is not accounted for in the tension estimates used herein and caused by signal fading. While the 0-2 cm linear correlation coefficient r for the above sensor combination is -0.82 for data sets without partial flooding conditions as noted in Figures 3.8 to 3.11, the inclusion of all such data in the analysis only decreases r to -0.80.

A more complex model of the estimated moisture-tension desorption characteristic is shown in Figure 4.25 for the 0-5 cm layer. The model assumes the following:

1) all water is desorbed at pressures of 10,000 bars (Brady, 1976);

2) air dry soil moistures from Table 4.1 are equal to the hygroscopic coefficient at 31 bars (Lahav and Bresler, 1973);

3) 15 and 1/3 bar moistures are those determined by the National Soil Survey Laboratory in Lincoln, Nebraska;

4) saturation occurs at the values of Mg given in Appendix A as determined by the porosity of each soil, and

5) tension is not allowed to fall below that at saturation which is defined at 0.001 bars for the very porous sandy loam and at 0.1 bars for silty clay loam and silty clay which are fine textured and have small pore diameters. This is necessary because the logarithm of zero, where saturation truly occurs, is infinite.

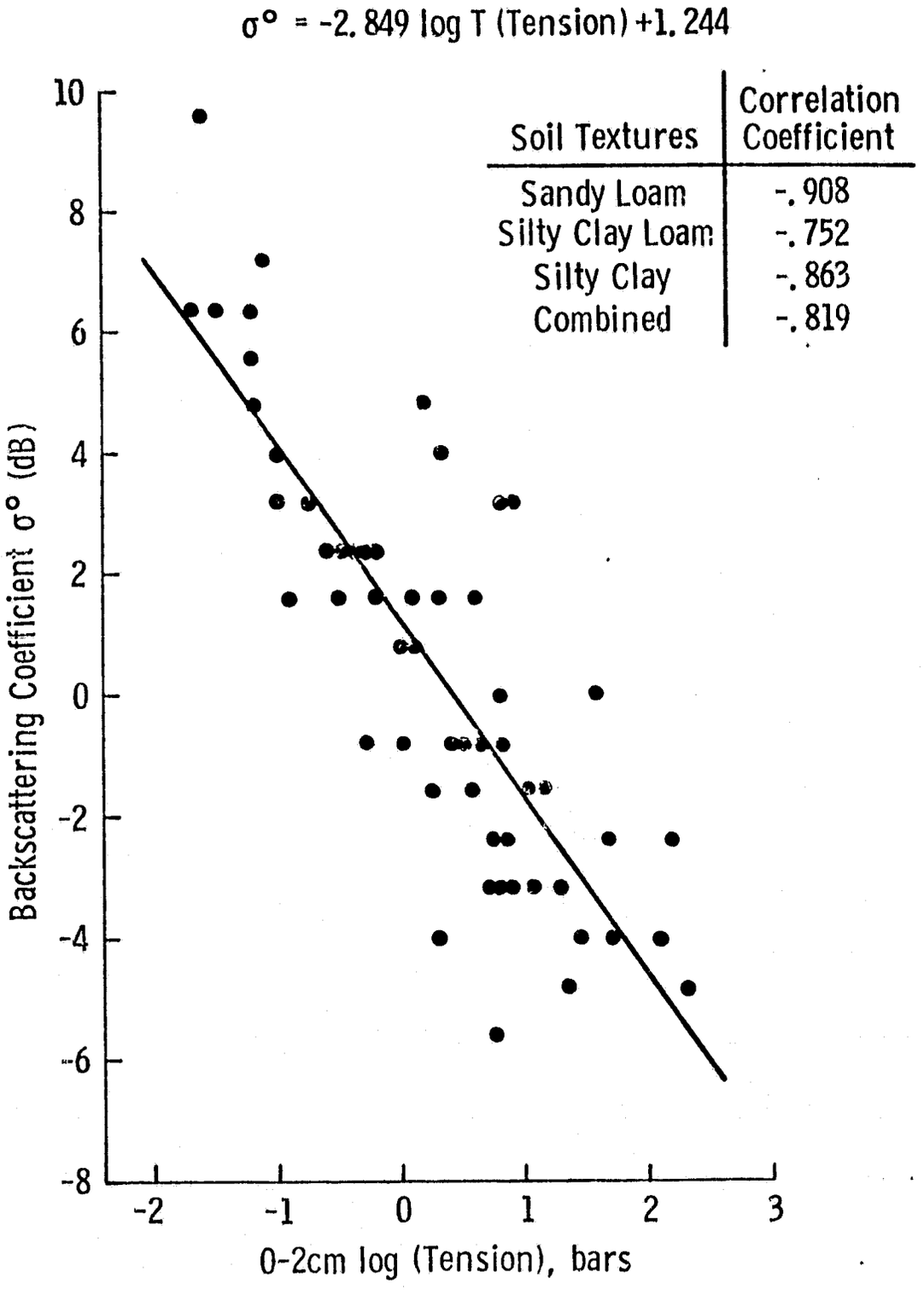

Figure 4.24. Radar response at 4.6 GHz, 10° and HH polarization to 0-2 cm estimated soil tension as defined by a simple log-linear model of the moisture tension characteristic.

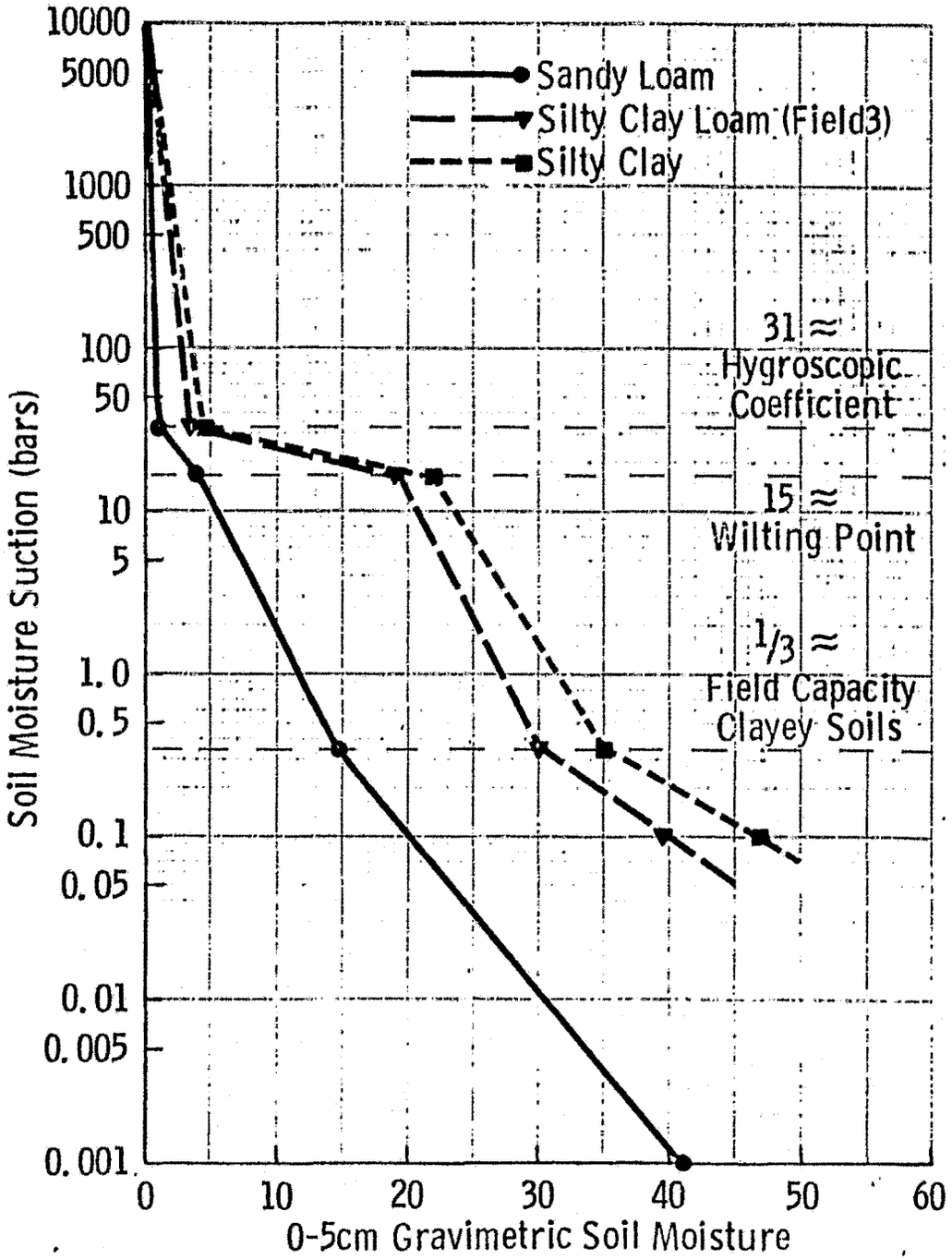

Figure 4.25. Desorption characteristic of 0-5 cm layer of sandy loam, silty clay loam and silty clay using estimates of water retention at the hygroscopic coefficient and at saturation.

Linear regression fits of the radar data to the negative logarithms of tension as estimated using the above assumptions produce correlation coefficients comparable to those obtained using normalized moisture indicators. Figure 4.26 shows r to be approximately 0.8 and constant as a function of depth at 4.6 GHz, 10° and HH polarization. Correlation coefficients at other sensor combinations are also similar to those for the normalized moisture indicators.

5.0 CONCLUSIONS AND RECOMMENDATIONS

Analysis of the 1977 Bare Soil Experiment substantiates an effect of soil texture on the behavior of soil water at microwave frequencies as noted by other investigators in Chapter 2. It has been shown that for realistic mixed texture ground scenes the simple soil moisture descriptors of total gravimetric or volumetric moisture fail to account for the inter-field variance observed by radar. Conversely, all moisture indicators which incorporate the concept of water potential have been shown to correlate highly with radar backscatter independent of soil texture.

5.1 Evaluation and Interpretation of Soil Moisture Indicators

The electric double layer model and considerations of the energy potential of soil water predict that as distance increases from soil particle surfaces there is an exponential decay of forces restricting the mobility of water and the capacity of water to oscillate at microwave frequencies.

Evidence to date suggests substantial changes in the structure of water as a function of distance from hydrophilic soil particle surfaces. The density of water adsorbed to Na-montmorillonite is known to be far greater than that of pure water up to distances of approximately 10 A^{o} (Figure 5.1) and its density is less than that of pure water, similar to ice, even at gravimetric moistures of 20-30%. Although the transient structure of pure liquid water is only poorly understood, it is safe to assume that the high density of an absorbed water layer approximately 3 to 4 molecular layers thick indicates a densely packed and highly ordered molecular structure.

The tension of soil water is also known to decrease exponentially with distance from soil particle surfaces. Soil tension has proven

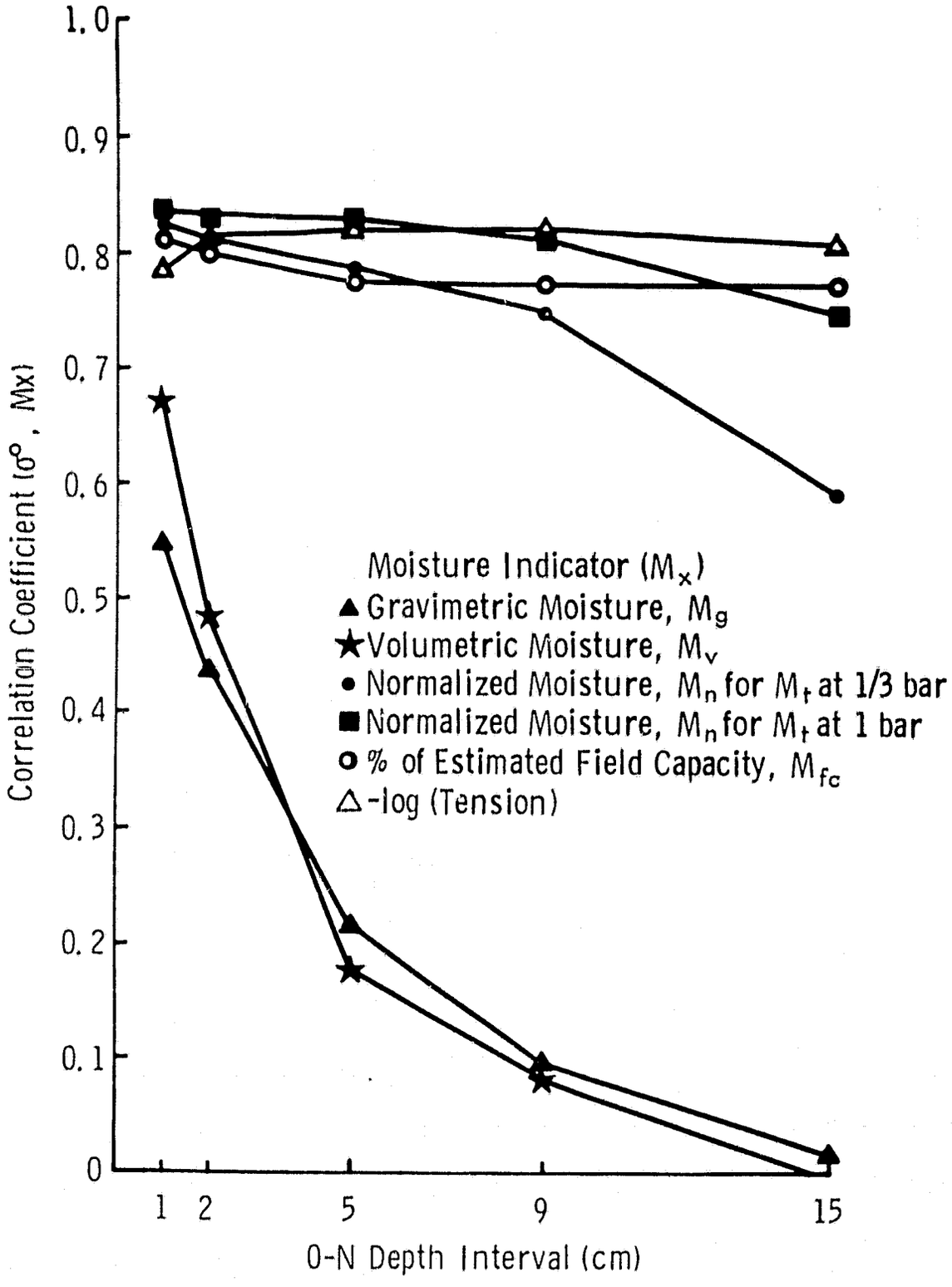

Figure 4.26. Correlation coefficient as a function of depth interval for ·° at 4.625 GHz, 10°, HH with various moisture indicators Mx for combined data from fields of sandy loam, silty clay loam and silty clay.

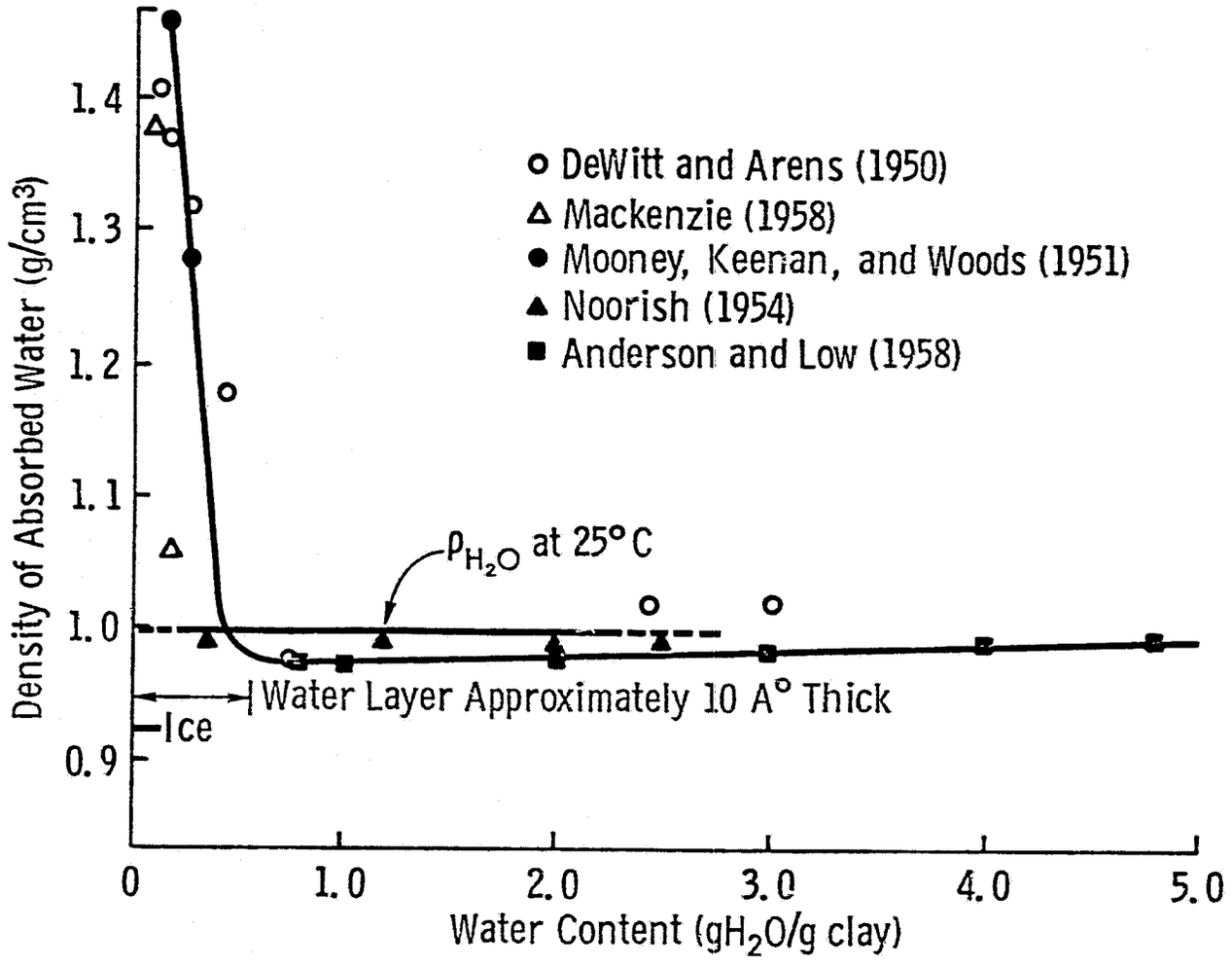

Figure 5.1. Density of adsorbed water on Na-montmorillonite (from Mitchell, 1976).

itself to be highly interpretable and can be related to a host of soil-water-plant relationships. Specific tension values have long been used in the literature to define critical points in the hydrodynamic behavior and agronomic influence of soil water (Figure 5.2).

The volume of soil water held at a given total water potential is soil specific and is determined by the specific surface of a soil, the surface charge density, the concentration and type of soil solutes and the bulk structure and pore size distribution within the soil relative to a water table. Since surface charge density is known to be within the same order of magnitude for most soil mineral components, differences between soils in the volume of water held at high tensions as thin films enveloping soil particles is primarily determined by the specific surface of the soil. For most soils evidence indicates that the thicknesses of these water films, which include adsorbed and solvate water, are relatively independent of soil texture when measured in molecular layers of water (Figure 5.3). The volume of additional water which can be retained by soils at low tensions is primarily limited by the pore size distribution of the soil.

Proceeding from the above and considering the soil water potential and dielectric constant responsive to an equivalent assemblage of forces existent within the soil medium, the following explanations can be offered for the failure of total gravimetric or volumetric moisture to account for the observed radar backscatter from diverse soil textures:

1. Neither measure accounts for particle surface effects on adsorbed films of soil water which vary between soil textures and mineralogical compositions as a function of specific surface.
2. Solute effects on the behavior of adsorbed and solvate water are disregarded by measures of gravimetric and volumetric water content.
3. Variance between soils in the amount of water held at low tensions, which should be dielectrically equivalent to bulk water, are ignored by gravimetric moisture but are considered by volumetric moisture because of the relationship between bulk density and porosity. Thus, volumetric moisture adequately explains the structural differences between various soils which control soil water retention at low tensions.

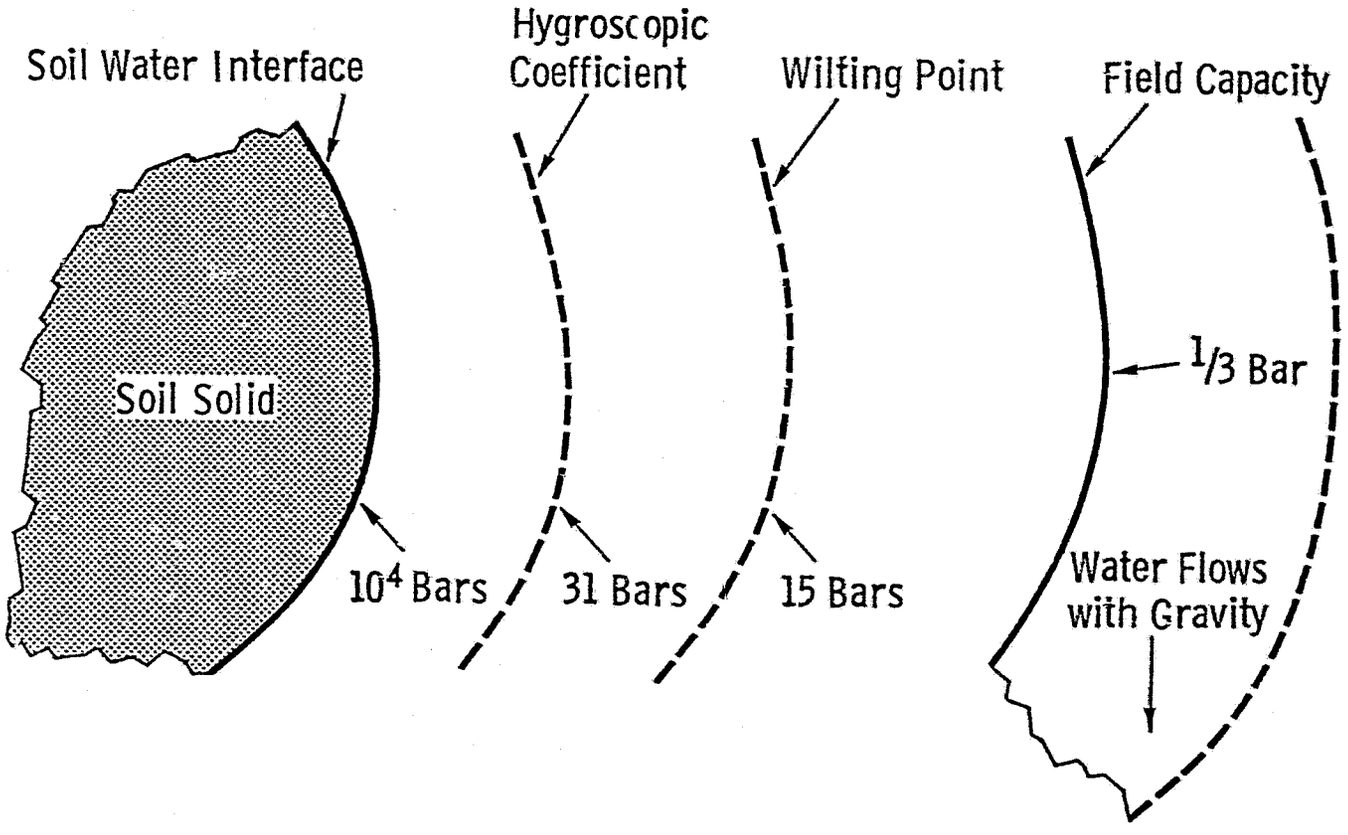

Figure 5.2. Sketch of a typical soil-water system. The wilting point and field capacity are defined at the tensions of 15 bars and 1/3 bar respectively (from Wang and Schmugge, 1978).

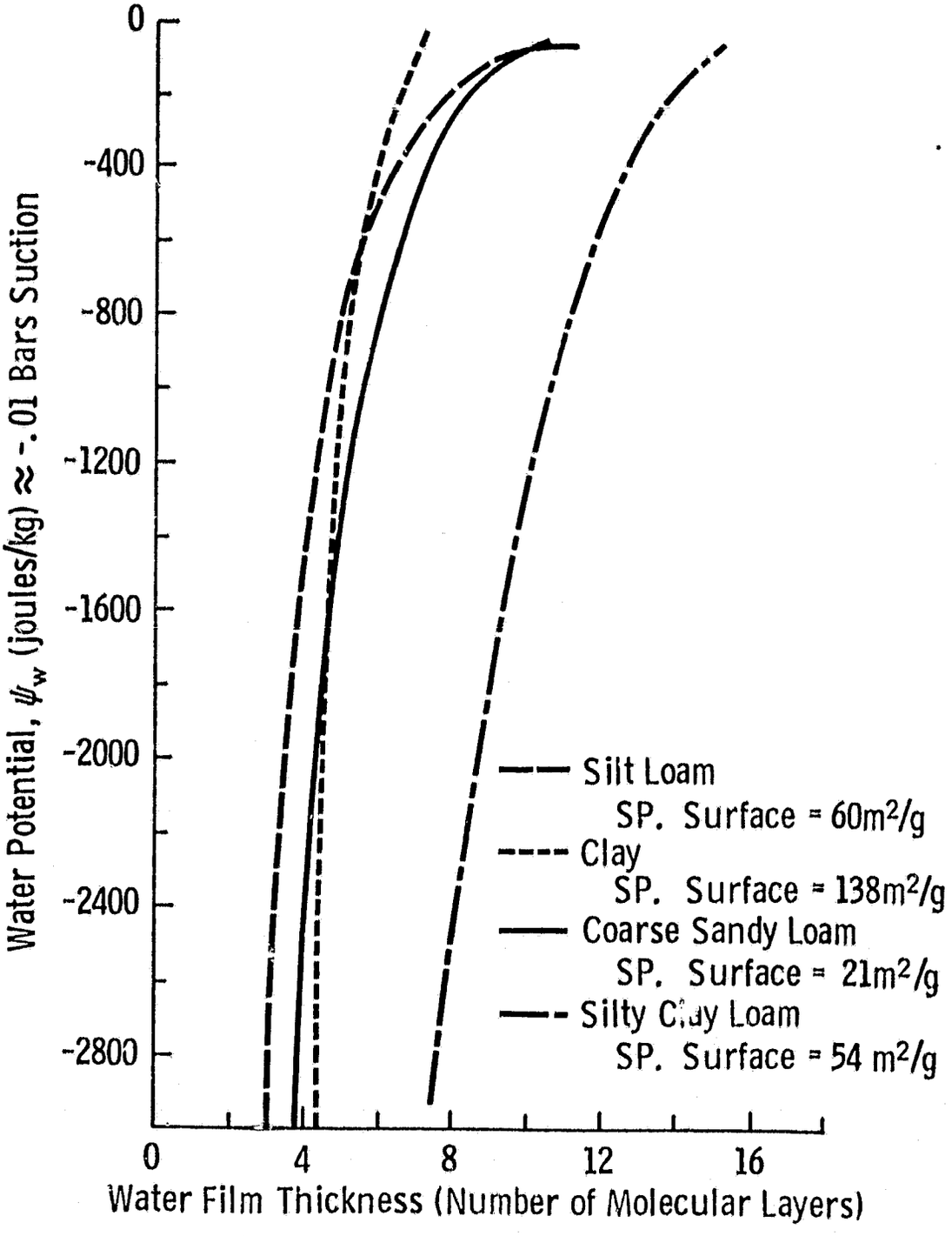

Figure 5.3. Water potential as a function of the film thickness as measured by the weight of water retained divided by the weight of water needed to cover the soil with one molecular layer of water. The curves for clay, silt loam, and coarse sandy loam are brought close together. The silty clay loam is still quite different (from Taylor and Ashcroft, 1972).

Although solute concentration is known to affect the behavior of soil water even at high moisture values, up to $M_v \geq 0.5$ for pure montmorillonite, it may be adequate in geographic regions of nearly constant soil salinity to use algorithms that predict the volumetric moisture in excess of a transition moisture. The moisture in excess of the transition moisture model as proposed by Wang and Schmugge (1978) is supported by the data from the 1977 Bare Soil Experiment. The transition moisture model was found to produce correlation coefficients from 0.7 to 0.8 for frequencies between 2.4 and 7.6 GHz at 10^{o} and 20^{o} incidence angles.

The evidence to date suggests that the empirically derived transition moistures correspond to a water layer 4 to 9 molecules thick and soil matric potentials between 15 and 31 bars. Thus far, there is insufficient evidence from either soil physics or microwave studies of soil water to establish whether the transition moisture is defined by a sharp boundary differentiating two distinct phases of water each possessing unique structures and electromagnetic behavior or is defined at an arbitrary value within a transition zone. Studies of water density (Figure 5.1) suggest a sharp transition while electric double layer theory and studies of fluid mobility adjacent to soil particle surfaces (Kemper, 1960; Kemper, et al., 1964; McBride, 1977) suggest a transition region.

If further research demonstrates the transition moisture to be defined by the soil water retention at a unique tension such as 15 bars, then algorithms based upon this model will produce highly interpretable information to the soil moisture user community.

Normalized moisture was found to be highly correlated to radar backscatter independent of soil texture. Using data from the 1977 Bare Soil Experiment, linear correlation coefficients exceeded 0.8 when soil moisture was indexed to water retention at soil tensions between 0.3 and 2.0 bars. While empirically determined algorithms using normalized moisture offer strong correlations, they may be heuristic in that the indexing procedure is not supported by a theoretical foundation. The estimating power of normalized moisture algorithms seems to reside in an inherent value of linking the quantity of soil water to soil tension T. Normalized moisture algorithms should be treated as

approximations of a more exact solution where for a given sensor configuration and surface roughness:

$$\sigma^{o} \approx \int f(M_v, T) \qquad (5.1)$$

In spite of the observed predicting power of normalized moisture algorithms, they suffer from poor interpretability by the potential user community of soil moisture information. It will be difficult to define the physical properties of normalized moisture indices. For example, when moisture is normalized at a tension of 1/3 bar, the resultant index is only a crude approximation of the following:

0% ≈ dryness
50% ≈ the wilting point
100% ≈ field capacity
150% ≈ saturation

On the other hand, soil tension has long been used as the preferred descriptor of the soil-water system; its use has been inhibited by the difficulty of measuring soil tension under field conditions over a large range of values. Direct reading devices such as tensiometers are only accurate for wet conditions ranging from saturation to matric potentials of ≈0.85 bars, while non-direct devices such as soil resistivity blocks operate effectively only at higher tensions and must be calibrated for each specific soil sampled. Analysis of the 1977 Bare Soil Experiment shows a strong log-linear dependence of radar backscatter on estimated soil tension which is independent of soil texture.

As a descriptor of remotely sensed soil moisture, soil tension seems to account for observed variance associated with the affinity of water for soil particle surfaces below the postulated transition moisture and account for variance due to soil structural control of porosity and the volumetric moisture content in excess of the transition moisture. The use of soil tension may also account for solute effects on the dielectric behavior of soil water; however, this has not been experimentally verified since only soil matric potential was measured during the 1977 Bare Soil Experiment and not the total water potential (which would include the osmotic potential).

Furthermore, if the dielectric properties of moist soils can be treated solely as a function of soil tension, it can be argued that hysteresis in the moisture-tension characteristic will produce variance in radar backscatter which cannot be explained by either gravimetric or volumetric moisture even for a specific soil texture. Since the estimated matric potentials used in the analysis of the 1977 Bare Soil Experiment are based solely upon laboratory desorption and not on in situ field measurements of tension (which would reflect hysteretic dependence, as seen in Figure 5.4), it is possible that hysteretic effects could explain much of the remaining scatter observed by radar in Figure 4.24. Until field measurements of tension are made in conjunction with microwave sensor observation of soils, the impact of hysteresis on sensor response cannot be fairly evaluated.

However, if there is a hysteretic effect, then it should display itself most prominently in soils with high clay content. It is well documented that sandy soils exhibit very small hysteresis compared to clayey soils. In addition, soils that have a high percentage of expanding clay such as montmorillonite are particularly susceptible to hysteretic effects since episodes of soil shrinking and swelling act to modify the pore size distribution as a function of time.

The above is supported by radar backscatter measurements from the 1977 Bare Soil Experiment. Gravimetric soil moisture in field 1, a sandy loam, was found to be highly correlated with radar backscatter (in excess of 0.9) over the entire 3-month observation period; this is to be expected for a sandy soil with little hysteresis. Fields 2 and 3, silty clay loams, and field 4, silty clay, contained a high percentage of montmorillonite. In Table 3.15 the linear correlation coefficients between radar backscatter and gravimetric moisture typically ranged between 0.7 and 0.9 for fields 3 and 4 and between 0.4 and 0.6 for field 2; these comparatively lower correlations for high clay content soils are to be expected if there is a hysteretic dependence of the radar response to gravimetric moisture. The exceptionally low correlations for field 2 may be explained by the repeated flooding and dessication of the field which exacerbated changes in clay platelet orientation and porosity as a function of time which are typical of poorly drained

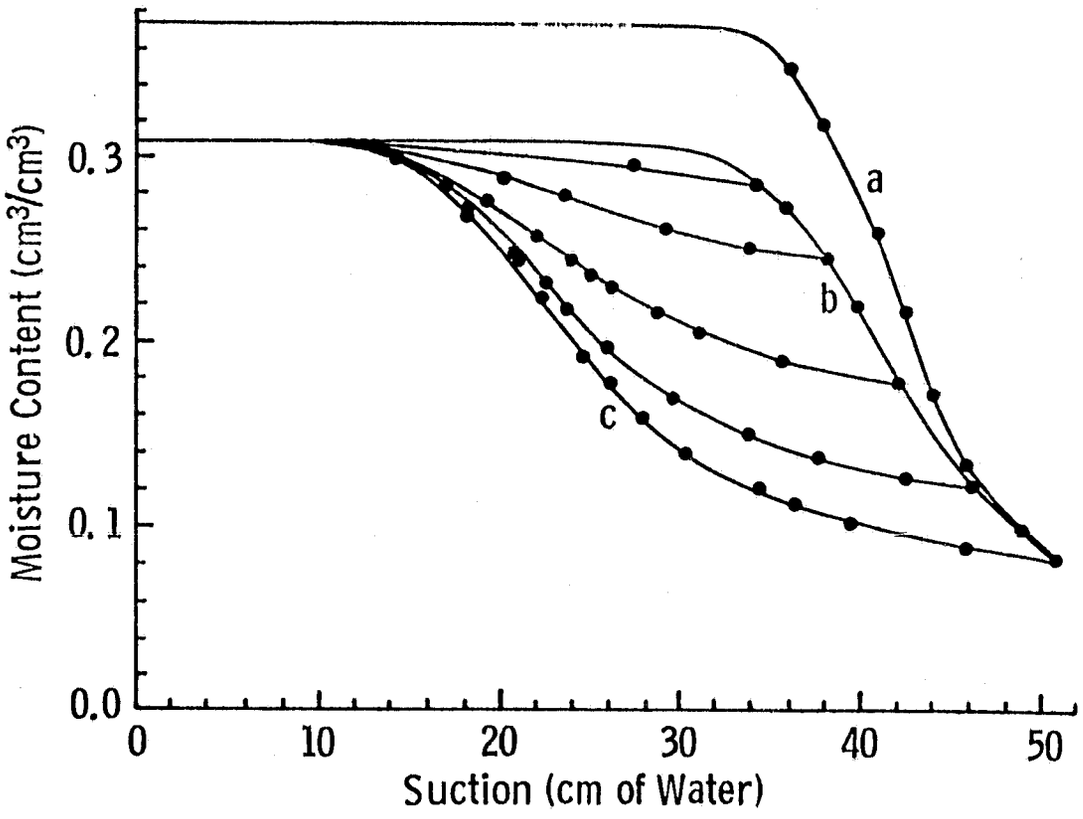

Figure 5.4. Hysteresis Scanning Curves. The experimental saturation boundary curve (a); the ultimate drying boundary curve (b): the wetting boundary curve (c); and a set of primary wetting curves (from Poulovassilis, 1973).

montmorillonitic soils. It is also significant to note that the radar backscatter response to field 2 was characterized by a pronounced time dependence explainable only in terms of soil surface layer structural changes and hysteresis.

The foregoing discussion is relevant in that if there is a hysteretic effect on the radar response to gravimetric and volumetric soil moisture, then moisture estimation algorithms incorporating these soil moisture descriptors could be expected to exhibit poor performance even if the soil textures of a complex ground scene were mapped in detail and their locations and spatial extents were differentially treated in microwave sensor processing. Potential estimation error due to hysteresis is irrelevant for algorithms utilizing soil tension as the pertinent soil moisture quantifier.

The major advantage of algorithms incorporating soil tension is that they express soil moisture with reference to the properties of soil. Total water potential accounts for the effects of soil particle surfaces, solute effects present in saline and alkaline soils of dry regions or the acid soil of bogs and highly fertilized agricultural soils, the effects of soil structure and hysteretic effects. Agriculturalists are interested in the effects of soil water on plants which respond to the energy status of water. Numerous studies of water uptake by plants have utilized matric potential as the relevant texture independent descriptor for the production of maximum yields of agronomically important crops (Table 5.1). Besides establishing the amount of soil water available to plants (Figure 5.5), soil tension determines (Table 5.2):

1. the amount of water that can be accepted by the soil before percolation starts,
2. the aeration available to plants,
3. saturation of the soil,
4. the water available for drainage and run off,
5. the vapor pressure of soil water if salinity is negligible (Figure 5.6),
6. the freezing point of soil water (Figure 5.7),

TABLE 5.1

Matric potentials at which water should be applied for maximum yields of various crops grown in deep, well-drained soil that is fertilized and otherwise manages for maximum production. Where two values are given, the higher value is used when evaporative demand is high and the lower value when it is low; intermediate values are used when the atmospheric demand for evapotranspiration is intermediate. (These values are subject to revision as additional experimental data become available). (From Taylor and Ashcroft, 1972).

Crop	*Matric potential (joules/kg)*	*Equivalent matric suction (centibars)*	*Reference*
Vegetative crops			
Alfalfa	-150	150	S. A. Taylor[a]
Beans (snap and lima)	-75 to -200	75 to 200	Vittum et al. (1963)
Cabbage	-60 to -70	60 to 70	Vittum et al. (1963), and Pew (1958)[b]
Canning peas	-30 to -50	30 to 50	S. A. Taylor[a]
Celery	-20 to -30	20 to 30	A. W. Marsh,[a] and Marsh (1961)
Grass	-30 to -100	30 to 100	Vissar (1959)
Lettuce	-40 to -60	40 to 60	A. W. Marsh,[a] Vissar (1959), and Pew (1958)[b]
Tobacco	-30 to -80	30 to 80	Jones et al. (1960)[c]
Sugar cane			
Tensiometer	-15 to -50	15 to 50	Waterhouse et al. (1954)[d]
Blocks	-100 to -200	100 to 200	Robinson (1963)
Sweet corn	-50 to -100	50 to 100	S. A. Taylor,[a] and Vittum et al (1963)
Turfgrass	-24 to -36	24 to 36	Morgan (1964)
Root crops			
Onions			
Early growth	-45 to -55	45 to 55	Pew (1958)[b]
Bulbing time	-55 to -65	55 to 65	Pew (1958)[b]
Sugar beets	-40 to -60	40 to 60	S. A. Taylor[a]
Potatoes	-30 to -50	30 to 50	S. A. Taylor,[a] Vittum et al. (1963), and Pew (1958)[b]
Carrots	-55 to -65	55 to 65	Pew (1958)[b]
Broccoli			
Early	-45 to -55	45 to 55	Pew (1958)[b]
After budding	-60 to -70	60 to 70	Pew (1958)[b]
Cauliflower	-60 to -70	60 to 70	Pew (1958)[b]
Fruit crops			
Lemons	-40	40	A. W. Marsh[a]
Oranges	-20 to -100	20 to 100	Stolzy et al. (1963)
Deciduous fruit	-50 to -80	50 to 80	A. W. Marsh,[a] and Vissar (1959)
Avocadoes	-50	50	Richards et al. (1962)
Grapes			
Early season	-40 to -50	40 to 50	A. W Marsh[a]
During maturity	< -100	> 100	A. W. Marsh[a]
Strawberries	-20 to -30	20 to 30	A. W. Marsh,[a] and Marsh (1961)
Cantaloupe	-35 to -40	35 to 40	Marsh (1961), and Pew (1958)[b]

Crop	*Matric potential (joules/kg)*	*Equivalent matric suction (centibars)*	*Reference*
Tomatoes	−80 to −150	80 to 150	Vittam et al. (1958),[c] and Vittam et al. (1963)
Bananas	−30 to −150	30 to 150	Schmeuli (1953)[f]
Grain crops			
Corn			
Vegetative period	−50	50	S. A. Taylor[d]
During ripening	−800 to −1200	800 to 1200	S. A. Taylor[d]
Small grains			
Vegetative period	−40 to −50	40 to 50	S. A. Taylor[d]
During ripening	−800 to −1200	800 to 1200	S. A. Taylor[d]
Seed crops			
Alfalfa			
Prior to bloom	−200	200	Taylor et al. (1959)
During bloom	−400 to −800	400 to 800	Taylor et al. (1959)
During ripening	−800 to −1500	800 to 1500	Taylor et al. (1959)
Carrots			
During seed year at 60 cm depth	−400 to −600	400 to 600	Hawthorn (1951)[g]
Onions			
During seed year at 7 cm depth	−400 to −600	400 to 600	Hawthorn (1951)[g]
at 15 cm depth	−150	150	Hawthorn (1951)[g]
Lettuce			
During productive phase	−300	300	Hawthorn et al. (1956)[g]
Coffee	Requires short periods of low potential to break bud dormancy, followed by high water potential		Alvin (1960)

[a]Unpublished research

[b]See also Marsh (1961) which includes a revision of Pew's work

[c]Based on converting 50 percent available water to matric potential equivalent using Figure 14.16.

[d]Tensiometers were located at 18 inches, which is below the zone of maximum root concentration.

[e]Based on converting 50 percent available water to matric potential equivalent for loam to clay loam using Figure 14.16.

[f]Based on converting 67 percent available water to matric potential equivalent for clay soils using Figure 14.16.

[g]Resistance values of plaster moisture blocks were converted to matric potential from calibration of similar plaster units.

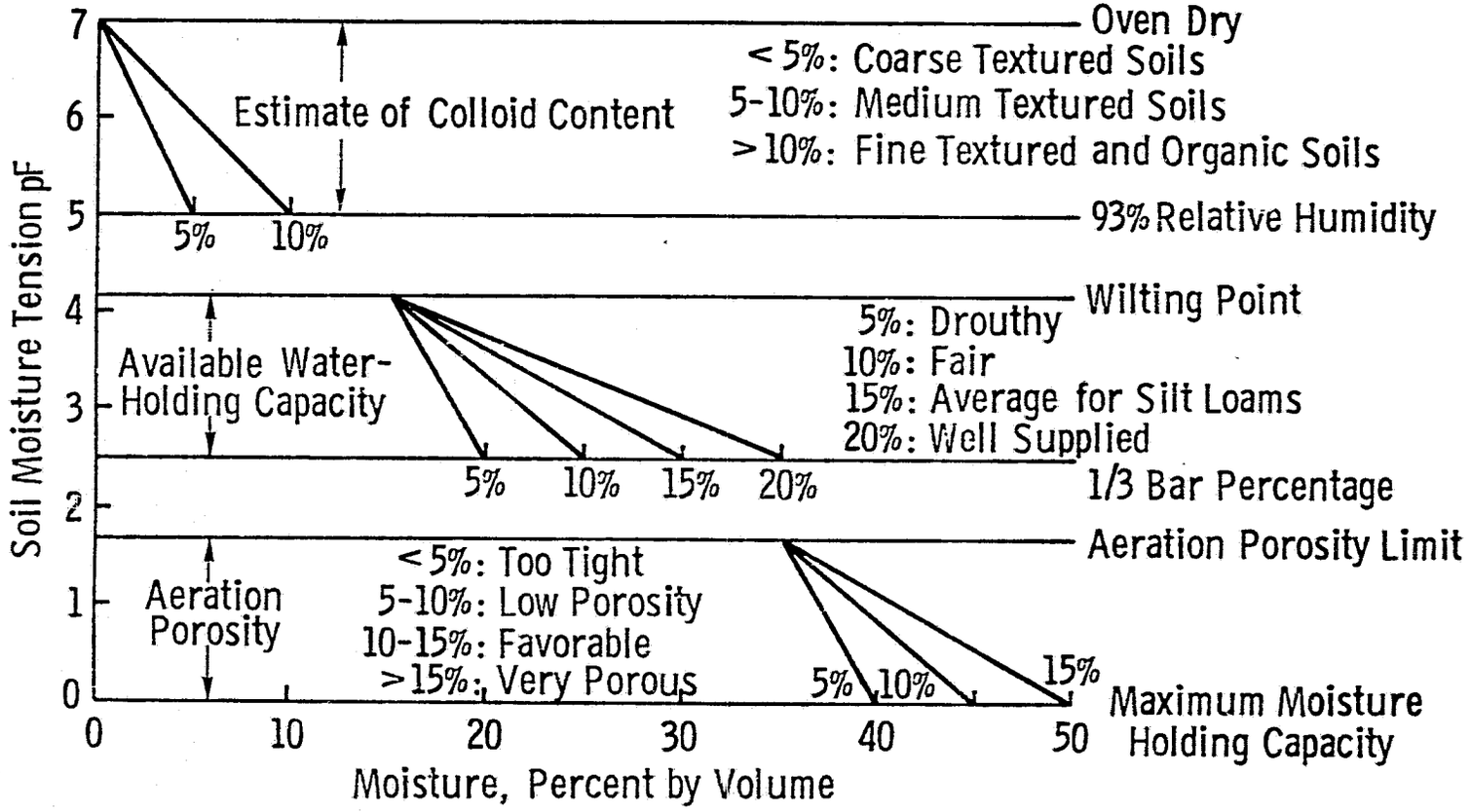

Figure 5.5. Guide for the interpretation of soil moisture retention data (from Kohnke, 1968).

TABLE 5.2

Soil-Moisture Tension Relationships
(from Kohnke, 1968).

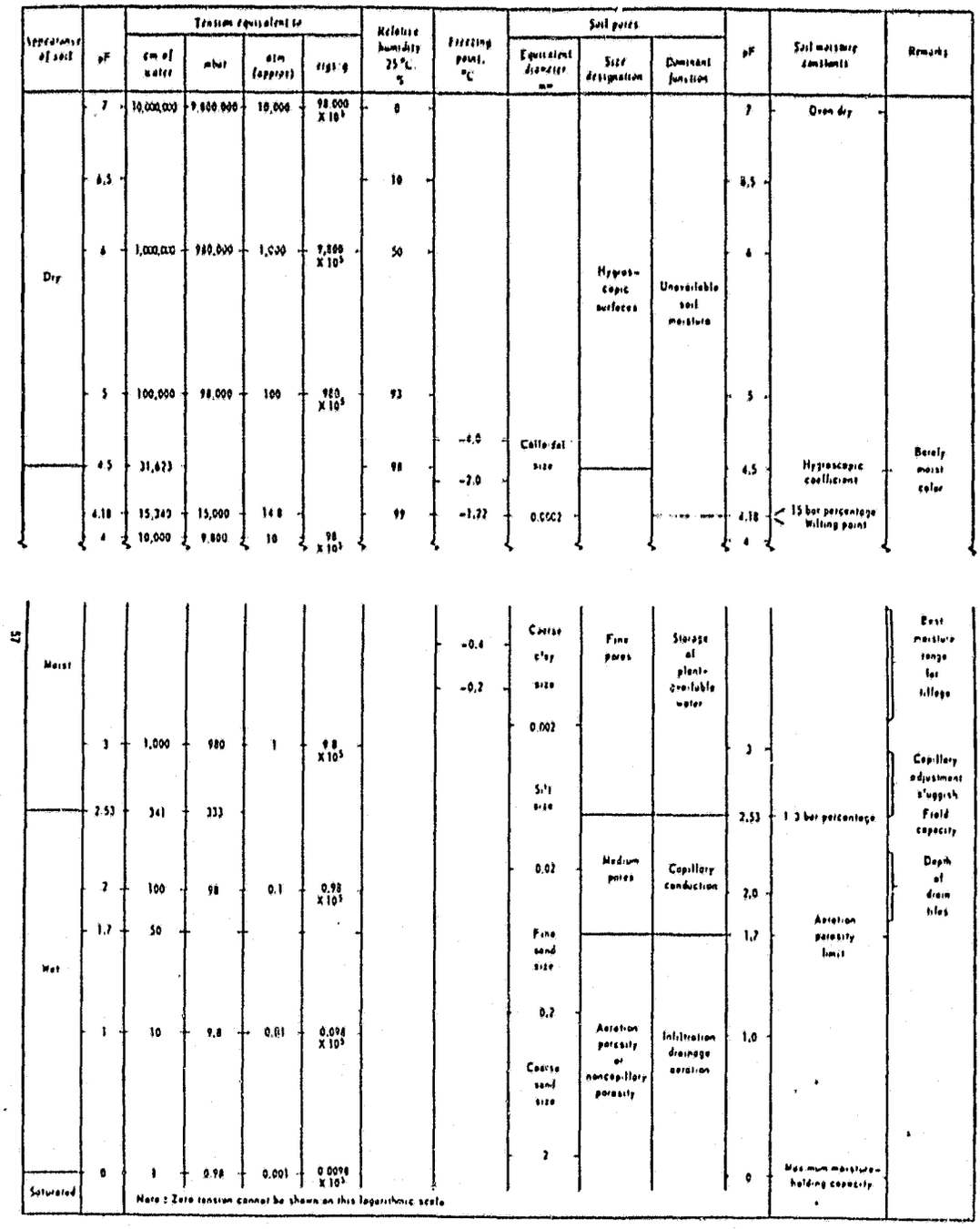

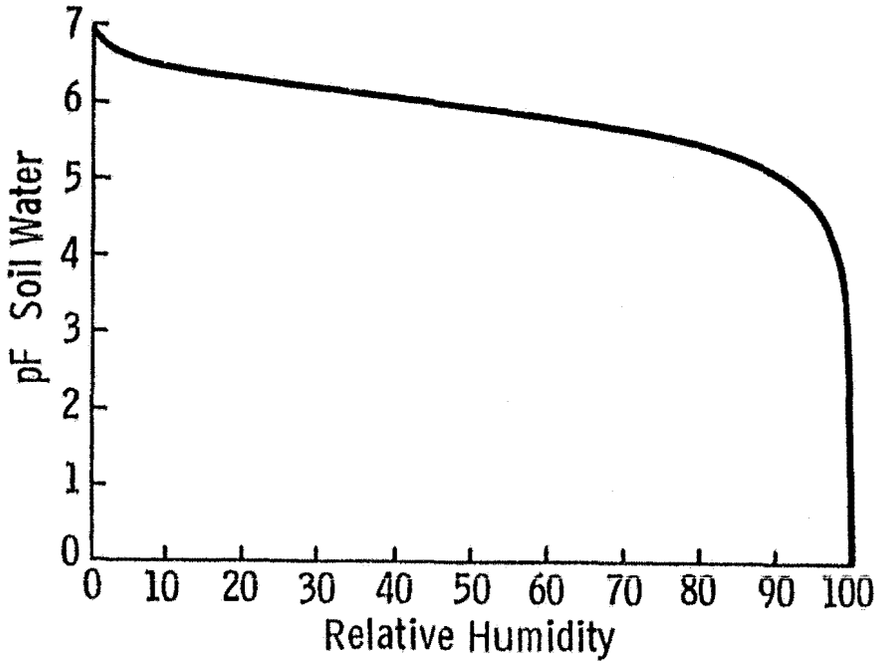

Figure 5.6. Relation between relative humidity and pF (from Kohnke, 1968).

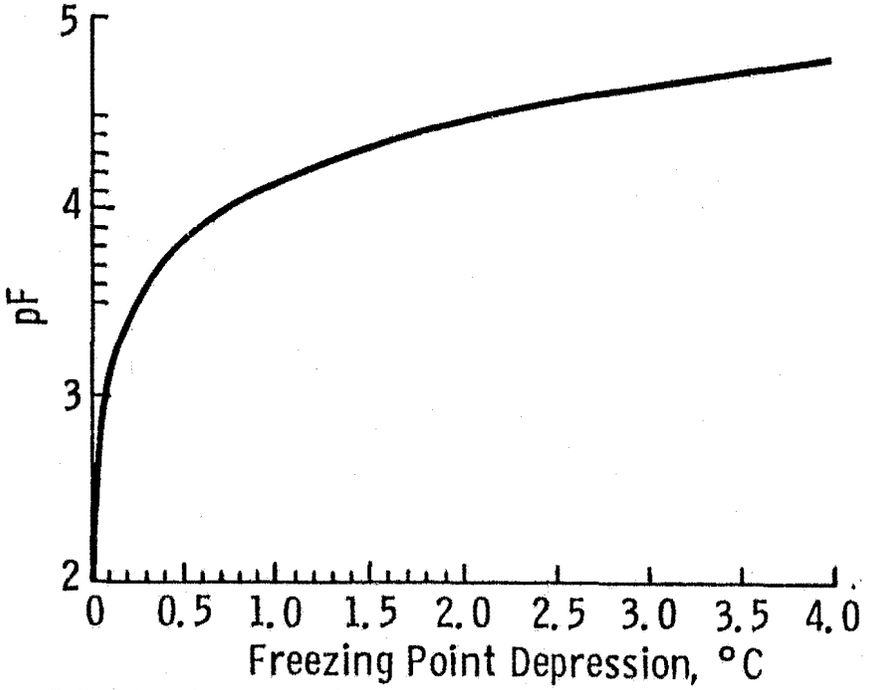

Figure 5.7. Relation between the freezing point of water and pF (from Kohnke, 1968).

7. the hydraulic conductivity of the soil,
8. the evapotranspiration rate during periods of high atmospheric demand (Figure 5.8), and
9. when a soil is in the optimum moisture range for tillage with agricultural implements.

5.2 Recommendations

In light of the results of the 1977 Bare Soil Experiment the following recommendations are offered for further investigations:

1. There exists a need for experimental verification of the relationship between the complex dielectric constant of moist soils and soil water potential. Such an experiment should strive to establish the dependence of the dielectric constant on soil tension, gravimetric and volumetric moisture for a wide variety of soil textures and clay mineralogies and seek a definition of the transition moisture in terms of a specific tension or range of tensions. The value of soil water potential in describing the dielectric behavior of saline soils should be investigated at low microwave frequencies.
2. Radar experiments should be conducted for a wide range of soil textures where soil tension is measured in the field contemporaneously with radar data acquisition. This could be accomplished using a network of tensiometers to measure tension up to ≈0.85 bars and resistivity or conductivity probes to be calibrated to soil tensions at drier moistures. Such an experiment would serve to verify the stated conclusions of the 1977 Bare Soil Experiment and investigate the existence of hysteretic effects on the radar backscattering response to soil moisture. The investigation of hysteresis effects is not suited to the past format of limited time window airborne sensor experiments but should be pursued via long term experiments using ground based microwave sensor systems.

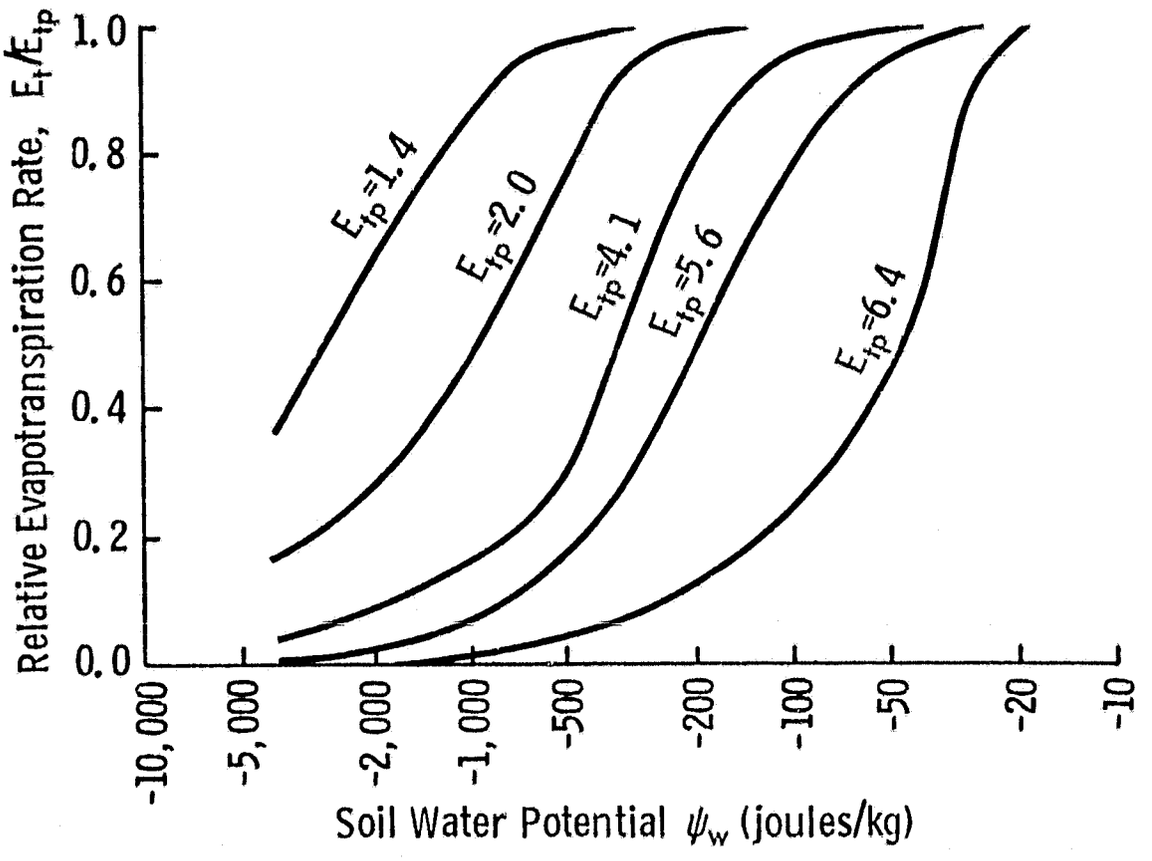

Figure 5.8. Relative evapotranspiration rate as a function of soil water potential for different potential evapotranspiration conditions. The E_{tp} values for the curve are expressed in millimeters of water evapotranspired in a 24-hour period (from Taylor and Ashcroft, 1972).

REFERENCES

Allison, L. E., "Organic Carbon," Methods of Soil Analysis Part II: Chemical and Microbiological Properties, C. A. Black, ed., Agronomy No. 9, American Society of Agronomy, Inc., Madison, Wisconsin, 1965.

Anderson, D. M. and P. F. Low, 1958, "The density of water adsorbed by lithium, sodium and potassium bentonite," Soil Sci. Soc. Amer. Proc., 22:99-103.

Armstrong, B. L., 1978, "Derivation of initial soil moisture accounting parameters from soil properties for the National Weather Service River Forecast System." NOAA Technical Memorandum NWS Hydro. 37, National Weather Service, Office of Hydrology, Silver Springs, Maryland.

Baier, W. and G. W. Roberton, "A new versatile soil moisture budget," Canadian Journal of Plant Science, 46:299-315, 1966.

Baier, W. and G. W. Roberton, "The performance of soil moisture estimates as compared with the direct use of climatological data for estimating crop yeilds," Agricultural Meteorology, 5:17-31, 1968.

Batlivala, P. P. and J. Cihlar, "Joint Soil Moisture Experiment (TEXAS): Documentation of Radar Backscatter and Ground Truth Data," RSL Technical Report 264-1, University of Kansas Center for Research, Inc., Lawrence, Kansas, April, 1975.

Batlivala, P. P. and F. T. Ulaby, 1977, "Feasibility of Monitoring Soil Moisture using Active Microwave Remote Sensing," RSL Technical Report 264-12, University of Kansas Center for Research, Inc., Lawrence, Kansas, January 1977.

Batlivala, P. P. and C. Dobson, "Soil Moisture Experiment (KANSAS): Documentation of Radar Backscatter and Ground Truth Data," RSL Technical Report 264-7, University of Kansas Center for Research, Inc., Lawrence, Kansas, March, 1976.

Baver, L. D., W. H. Gardner and W. R. Gardner, 1977, Soil Physics, John Wiley & Sons, New York, N.Y.

Berndt, R. D. and K. J. Coughlan, 1977, "The Nature of Changes in Bulk Density with Water Content in a Cracking Clay," Aust. J. Soil Res., 15(1):27-37.

Birchak, J. R., C. G. Gardner, J. E. Hipp and J. M. Victor, 1974, "High Dielectric Constant Microwave Probes for Sensing Soil Moisture," Proceedings of the IEEE, 62(1):93-98.

Birkeland, P. W., 1974.. Pedology, Weathering and Geomorphological Research, Oxford University Press, New York.

Black, C.A., ed., 1965. Methods of Soil Analysis Part I: Physical and Mineralogical Properties Including Statistics of Measurement and Sampling. Number 9 in the series Agronomy. American Society of Agronomy, Inc., Madison, Wisconsin.

Black, C. A., D. D. Evans, J. L. White, L. E. Ensminger and F. E. Clark, 1965. Methods of Soil Analysis, Part 2: Chemical and Microbiological Properties. Agronomy No. 9, American Society of Agronomy, Madison, Wisonsin.

Bolt, G. H. and M. G. M. Bruggenwert, ed., 1976. Soil Chemistry: A. Basic Elements. Elsevier Scientific Publishing Co., New York.

Böttcher, C. J. F., Theory of Electric Polarization, Elsevier, Amsterdam, 1952.

Brady, N. C., 1974. The Nature and Properties of Soils, 8th ed., MacMillan Publishing Co., Inc., New York.

Brown, W. F., "Dielectrics," in Encyclopedia of Physics, 17, Berlin: Springer, 1956.

Bruggeman, D. A. G., "Bereshnung Verschiedener Physikallischer Konstanten von Heterogenen Substanzen," Ann Phys. (Leipzig), 24:636-664, 1935.

Brunfeldt, D., F. T. Ulaby and H. Stiles, "System Description and Hardware Specification of MAS 1-8," RSL Technical Report 264-17, University of Kansas Center for Research, Inc., Lawrence, Kansas, April, 1979.

Bryson, R. A. and T. J. Murray, 1977, Climates of Hunger. The University of Wisconsin Press, Madison, Wisconsin.

Bush, T. F. and F. T. Ulaby, "On the Feasibility of Monitoring Croplands with Radar," Proceedings Tenth International Symposium on Remote Sensing of Environment, University of Michigan, Ann Arbor, October, 1975.

Bush, T. F. and F. T. Ulaby, "Cropland Inventories Using an Orbital Imaging Radar," RSL Technical Report 330-4, University of Kansas Center for Research, Inc., Lawrence, Kansas, January, 1976.

Bush, T. F. and F. T. Ulaby, "Radar Return from a Continuous Vegetation Canopy," IEEE Transactions on Antennas and Propagation, AP-24(3):269-276, May, 1976.

Bush, T. F. and F. T. Ulaby, "An Evaluation of Radar as a Crop Classifier," Remote Sensing of Environment, 7:15-36, 1978.

Campbell, M. J. and J. Ulrichs, 1969, "Electrical Properties of Rocks and Their Significance for Lunar Radar Observations," Journal of Geophysical Research, 74:5867-5881.

Carlisle, V. W., R. E. Caldwell, F. Sodek, III, L. C. Hammond, F. G. Calhoun, M. A. Granger, and H. L. Breland, 1978. Characterization Data for Selected Florida Soils. Soil Science Research Report Number 78-1, University of Florida, Institute of Food and Agricultural Sciences and USDA Soil Conservation Service.

Central Intelligence Agency Office of Political Research, 1976, "Potential implications of trends in world population, food production and climate," Library of Congress, Washington, D.C.

Chapman, D. L., 1913, "A contribution to the theory of electrocapillarity," Philosophical Magazine, 25(6):475-481.

Childs, E. C., 1969. An Introduction to the Physical Basis of Soil Water Phenomena, John Wiley & Sons, New York.

Cihlar, J. and F. T. Ulaby, "Dielectric Properties of Soils as a Function of Moisture Content," RSL Technical Report 177-47, University of Kansas Center for Research, Inc., Lawrence, Kansas, November, 1974.

Cihlar, J. and F. T. Ulaby, "Microwave Remote Sensing of Soil Water Content," RSL Technical Report 264-6, University of Kansas Center for Reserach, Inc., Lawrence, Kansas, August, 1975.

Clapp, R. B. and G. M. Hornberger, 1978, "Empirical equations for some soil hydraulic properties," Water Resources Research, 14(4):601-604.

Curtis, L. F. and S. Trudgill, 1974, "The Measurement of Soil Moisture," British Geomorphological Research Group, Technical Bulletin No. 13, Geo. Abstracts Ltd., University of East Angli, Norwich, England.

Dane, J. H., C. King, J. C. Holtzman, and R. K. Moore, 1974, "Moisture Dependence of Radar Backscatter from Irrigated and Non-Irrigated Fields at 400 MGz and 13.3 GHz," IEEE Transactions on Geoscience Electronics, GE-12(L):19-22.

Dickey, H., 1979, personal communication.

Dobson, M. C., "1977 Bare Soil Moisture Experiment Data Documentation," RSL Technical Report 264-26, University of Kansas Center for Research, Inc., Lawrence, Kansas, May, 1979.

Eagleman, J. and F. T. Ulaby, (August, 1974). Remote Sensing of Soil Moisture by Skylab Radiometer and Scatterometer Sensors. Advances in the Astronomical Sciences, v. 31, the American Astronomical Society, Tarzana, California.

Eagleman, J. R., "Detection of Soil Moisture and Snow Characteristics from Skylab, Final Report" 239-23, University of Kansas Center for Research, Inc., Lawrence, Kansas, October, 1975.

Edgerton, A. T., R. M. Mandl. G. A. Poe, J. E. Jenkins, F. Soltis and S. Sakomoto, "Passive Microwave Measurements of Snow, Soils, and Snow-Ice-Water Systems," Technical Report No. 4, Aerojet General Corporation, El Monte, California, 1968.

Edgerton, A. T., F. Ruskey, D. Williams, A. Stogryn, G. Poe, D. Meeks and O. Russell, "Microwave Emission Characteristics of Natural Materials and the Environment," Final Technical Report 9016R-8, Aerojet General Corporation, El Monte, California, 1971.

El-Swaify, S. A. and D. W. Henderson, "Water retention by osmotic swelling of certain colloidal clays with varying ionic concentrations," Journ. Soil Sci., 18:223-232, 1967.

Erickson, J. D., "Satellite-Aided Global Crop Monitoring," Proceedings Microwave Remote Sensing Symposium, Houston, Texas, December, 1977. NASA Johnson Space Center and Texas A&M University Remote Sensing Center.

Fox, W. E., 1964, "A Study of Bulk Density and Water in a Swelling Soil," Soil Science, 98(5):307-316.

Geiger, F. E. and D. Willimas, 1972, "Dielectric Constants of Soils at Microwave Frequencies," Goddard Space Flight Center, Greenbelt, Maryland, 30 pp.

Gieseking, J. E., ed., 1975. Soil Components, Vol. 2, Inorganic Components, Springer-Verlag, New York.

Gouy, G., 1910, "Sur la constitution de la charge electrique a la surface d'un electrolyte," Anniue Physique (Paris), Serie 4, 9:457-468.

Grim, R. E., 1962. Applied Clay Mineralogy. McGraw-Hill Book Co., Inc., New York.

Grim, R. E., 1968, Clay Mineralogy, McGraw-Hill Book Co., New York.

Hadas, A., D. Swartzendruber, P. E. Rijtema, M. Fuchs and B. Yaron, eds., 1973, Physical Aspects of Soil Water and Salts in Ecosystems, Springer-Verlag, New York.

Hammond, A. L., "Crop forecasting from space: Toward a global food watch," Science, 188:434, 1975.

Hendricks, S. B. and M. E. Jefferson, "Crystal Structure of Vermiculites and Mixed Vermiculite-Chlorites," Am. Mineralogist, 23:851-863, 1938.

Hildredth, W. W., 1978, "Soil Moisture Modeling Review," Lockheed Technical Memorandum LEC-11857, Houston, Texas.

Hipp, J. E., 1974, "Soil Electromagnetic Parameters as a Function of Frequency, Soil Density, and Soil Moisture," Proceedings of the IEEE, 62(1):98-103.

Hoekstra, P. and A. Delaney, 1974, "Dielectric Properties of Soils at UHF and Microwave Frequencies," Journal of Geophysical Research, 79(1):1699-1708.

Holtan, H. N., C. B. England, G. P. Lawless and G. A. Schumaker, 1968. Moisture-Tension Data for Selected Soils on Experimental Watersheds. RS 41-144, Agricultural Research Service, United States Department of Agriculture.

Idso, S. B., R. D. Jackson, R. J. Reginato, B. A. Kimball and F. S. Nakayama, 1975a, "The Dependence of Bare Soil Albedo on Soil Water Content," J. Appl. Meteorology, 14:109-113.

Idso, S. B., T. J. Schmugge, R. D. Jackson and R. Reginato, 1975b, The Utility of Surface Temperature Measurements for the Remote Sensing of Soil Water Status," J. Geophys. Res., 80:3044-3049.

Idso, S. B., R. D. Jackson and R. J. Reginato, 1975c, "Detection of Soil Moisture by Remote Surveillance," American Scientist, 63:549-557.

Idso, S. B., R. D. Jackson and R. J. Reginato, 1976, "Compensating for Environmental Variability in the Thermal Inertia Approach to Remote Sensing of Soil Moisture," Journal of Applied Meteorology, 15:811-817, August.

Jamison, V. C. and G. A. Thompson, 1967, "Layer Thickness Changes in a Clay-Rich Soil in Relation to Soil Water Content Changes," Soil Science Soc. Amer. Proc., 31(4):441-444.

Kavanau, J. L., Water and Solute Water Interactions. Holden-Day, Inc., San Francisco, 1964.

Kemper, W. D., 1960, "Water and Ion Movement in Thin Films as Influenced by the Electrostatic Charge and Diffuse Layer of Cations Associated with Clay Mineral Surfaces," Soil Sci. Soc. Amer. Proc., 24(1):10-16.

Kemper, W. D., D. E. L. Maasland and L. K. Porter, 1964, "Mobility of water adjacent to mineral surfaces," Soil Sci. Soc. Amer. Proc., 28:164-172.

Kezdi, Arpad, Handbook of Soil Physics, Vol. 1, Elsevier Scientific Publishing Company, New York, 1974.

Khardly, M. M. Z. and W. Jackson, "Properties of Artificial Dielectrics Comprising Arrays of Conducting Elements," Proc. Inst. Elec. Eng., 100:199-212, 1953.

Kohnke, Helmut, 1968. Soil Physics, McGraw-Hill, New York.

Lahav, N. and E. Bresler, 1973, "Exchangeable Cation-Structural Parameter Relationships in Montmorillonite," Clays and Clay Minerals, 21:249-255.

Lane, J. A. and J. A. Saxton, 1952, "Dielectric dispersion in pure polar liquids at very high radio frequenices. III. The effect of electrolytes in solution," Proc. Royal Soc. London, 214:531-545.

Lawrence, G. P., 1977, "Measurement of Pore Sizes in Fine-Textured Soils: A Review of Existing Techniques," 28(4):527-540.

Lawson, D. W., The application of Remote Sensing to Water Resources Planning, Watershed Modelling and Real-Time Flood Forecasting, 1976-1977.

Leschanskii, Yu. I., G. N. Lebedeva and V. D. Schumilin, 1971, "Electrical Parameters of Sandy and Loamy Soils in the Range of Centimeter, Decimeter and Meter Wavelengths," Izvestiya Vysschich Uchebnich Zavedenii, Radiofizika, 14(4):562-569.

Lord Rayleigh, "On the Influences of Obstacles Arranged in Rectangular Order on the Properties of a Medium," Phil. Mag., 34:481-502, 1892.

Low, P. F., 1961, "Physical chemistry of clay-water interaction," Adv. in Agron., 13:269-327.

Lundien, J. R., 1966, "Terrain Analysis by Electromagnetic Means, Technical Report No. 3-693, Report 2, U.S. Army Engineer Waterways Experiment Station, Vicksburg, Mississippi, 55 pp.

Lundien, J. R., 1971, "Terrain Analysis by Electromagnetic Means, Technical Report No. 3-693, Report 5, U. S. Army Engineer Waterways Experiment Station, Vicksburg, Mississippi, 33 pp.

Marshall, C. E., 1964. The Physical Chemistry and Mineralogy of Soils. Vol. I: Soil Materials. John Wiley & Sons, N.Y.

McBride, M. B., 1977, "Adsorbed molecules on solvated layer silicates: surface mobility and orientation from ESR studies," Clays and Clay Minerals, Vol. 25, pp. 6-13.

Miller, A. and J. C. Thompson. 1970. Elements of Meteorology. Charles E. Merrill Publishing Co., Columbus, Ohio.

Mitchell, J. K., 1976. Fundamentals of Soil Behavior. John Wiley & Sons, New York, N.Y.

Moore, C. A. and J. K. Mitchell, 1974, "Electromagnetic forces and soil strength," Geotechnique, Vol. 24, No. 4, pp. 627-640.

Mualem, Y. and H. J. Morel-Seytoux, 1978, "Analysis of a capillary hysteresis model based on a one-variable distribution function," Water Resources Res., Vol. 14, No. 4, pp. 605-610.

Nielson, D. R., R. D. Jackson, J. W. Cary, D. D. Evans, eds., 1972. Soil Water. American Society of Agronomy, Soil Sci. Soc. Amer., Madison, Wisconsin.

Nerpin, S. V. and A. F. Chudnovskii, Physics of the Soil, Israel Program for Scientific Translations, Jerusalem, 1970, p. 317.

Newton, R. W. and W. R. McClellan, III, "Permittivity Measurements of Soils at L-Band," Technical Report RSC-58, Remote Sensing Center, Texas A&M University, College Station, Texas, June, 1975.

Newton, Richard Wayne, (January) 1977. "Microwave Remote Sensing and Its Application to Soil Moisture Detection," Technical Report RSC-81, Texas A&M University Remote Sensing Center, College Station, Texas. (Dissertation).

Parker, J. C., D. F. Amos, and D. L. Kaster, 1977, "An Evaluation of Several Methods of Estimating Soil Volume Change," Soil Science Soc. Amer. Journal, 41(6):1059-1064.

Peake, W. H., "Interaction of Electromagnetic Waves with Some Natural Surfaces," IRE Transactions on Antennas and Propagation, December, 1959.

Peake, W. H., et al., "The Mutual Interpretation of Active and Passive Microwave Sensor Outputs," Proceedings Fourth Symposium on Remote Sensing of Environment, University of Michigan, Ann Arbor, Michigan, pp. 771-777, 1966.

Pearce, C. A. R., "The Permittivity of Two-Phase Mixtures," Brit. J. Appl. Phys., 6:358-361, October, 1955.

Poulovassilis, A., 1969, "The effect of hysteresis of pore-water on the hydraulic conductivity," Jour. of Soil Sci., 20(1):52-56.

Poulovassilis, A., 1974, "The Uniqueness of the Moisture Characteristic," Jour. of Soil Sci., 25(1):27-33.

Rango, A., 1978, Remote Sensing Soil Moisture Research Working Session, NASA Goddard Space Flight Center, Dec. 14-15, 1978.

Ravina, I. and D. Zaslavsky, 1972, "The water pressure in the electrical double layer," Israel Journal of Chemistry, 10:707-714.

Ravina, I. and P. F. Low, 1972, "Relation between swelling, water properties and b-dimension in montmorillonite-water systems," Clays and Clay Minerals, 20:109-123.

Reed, C. S., 1977, "The utility of microwave remote sensing techniques for soil moisture profile determination," University of Arkansas, Department of Electrical Engineering, Fayetteville, Arkansas.

Rhode, A. A., 1969, "Theory of Soil Moisture, Vol. 1: Moisture Properties of Soils and Movement of Soil Moisture," Translated from Russian. Israel Program for Scientific Translations. Jerusalem.

Salomonson, V. V., R. Armbaruch, A. Rango and J. P. Ormsby, "Remote Sensing Requirements as Suggested by Watershed Model Sensitivity Analyses," Proc. 10th International Symposium on Remote Sensing of Environment, October 6-10, 1975, Ann Arbor, Michigan.

Schmugge, T., B. J. Blanchard, W. J. Burke, J. F. Paris and J. R. Wang, 1976a, "Results of Soil Moisture Flights During April, 1974," NASA Technical Note D-8199, Washington, D.C.

Schmugge, T., T. Wilheit, W. Webster, Jr. and P. Gloersen, 1976b, "Remote Sensing of Soil Moisture with Microwave Radiometers, II," NASA Technical Note TN-D-8321, GSFC, Greenbelt, Maryland.

Schmugge, T., 1978, "Remote Sensing of Surface Soil Moisture," Journal of Applied Meteorology, 17(10):1549-1557.

Schmugge, T., B. Blanchard, A. Anderson and J. Wang, "Soil Moisture Sensing with Aircraft Observations of the Diurnal Range of Surface Temperature," Water Resources Bulletin, 14(1):169-178, February, 1978.

Schneider, S. H. and L. E. Mesirow, 1976. The Genesis Strategy, Plenum, New York.

Shainberg, I. and W. D. Kemper, 1966, "Hydration status of adsorbed cations," Soil Sci. Soc. Amer. Proc., 30:707-713.

Shainberg, I. and W. D. Kemper, 1966. Electrostatic forces between clays and cations as calculated and inferred from electrical conductivity. Proc. 14th Natl. Conf. on Clays and Clay Minerals, Berkeley, California, pp. 117-132.

Smith, P. E. L., 1976, Food Production and Its Consequences, Cummings Publishing Co., Inc., Menlo Park, California.

Soil Survey Staff, 1951. Soil Survey Manual, USDA Agriculture Handbook No. 18. U.S. Government Printing Office, Washington, D.C.

Stern, O., 1924, "Zur Theorie der Electrolytischen Doppelschriht," Zietschrift Electrochem, 30:508-516.

Stiles, W. H., D. Brunfeldt and F. T. Ulaby, "Performance Analysis of the MAS (Microwave Active Spectrometer) Systems: Calibration, Precision and Accuracy," RSL Technical Report 360-4, University of Kansas Center for Research, Inc., Lawrence, Kansas, February, 1979.

Taylor, S. A., 1958, "The activity of water in soils," Soil Sci., 86:83-90.

Taylor, S. A. and G. L. Ashcroft, 1972, Physical Edaphology: The Physics of Irrigated and Non-irrigated Soils, W. H. Freeman and Co., San Francisco.

Townsend, W. N., 1973. An Introduction to the Scientific Study of the Soil. St. Martin's Press, New York.

Ulaby, F. T. and R. K. Moore, 1973, "Radar Sensing of Soil Moisture," Proceedings 1973 International IEEE-GAP and USNC/URSI Meeting, Boulder, Colorado, August, pp. 362-365.

Ulaby, F. T., (March, 1974), "Radar Measurement of Soil Moisture Content," IEEE Transactions on Antennas and Propagation, AP-22(2): 257-265.

Ulaby, F. T., J. Cihlar and R. K. Moore, 1974, "Active Microwave Measurement of Soil Water Content," Remote Sensing of Environment, 3:185-203.

Ulaby, F. T., L. F. Dellwig and T. Schmugge, 1975, "Satellite Observations of the Utah Great Salt Lake Desert," Radio Science, 10(11):947-963.

Ulaby, F. T. and P. P. Batlivala, 1976, "Optimum Radar Parameters for Mapping Soil Moisture," IEEE Transactions on Geoscience Electronics, GE-14(2):81-93.

Ulaby, F. T., 1977, "Microwave Remote Sensing of Hydrologic Parameters," Proceedings Eleventh International Symposium on Remote Sensing of Environment, University of Michigan, Ann Arbor, April 25-29.

Ulaby, F. T., M. C. Dobson, and G. A. Bradley, 1977, "If you want to Remotely Sense Soil Moisture, Use a C-band Radar," Proceedings Microwave Remote Sensing Symposium, Houston, Texas, Dec., 1977.

Ulaby, F. T., P. P. Batlivala and M. C. Dobson, 1978, "Microwave Backscatter Dependence on Surface Roughness, Soil Moisture and Soil Texture, Part I: Bare Soil," IEEE Transactions on Geoscience Electronics, GE-16(4):286-295.

Ulaby, F. T. and J. E. Bare, "Look Direction Modulation Function of the Radar Backscattering Coefficient of Agricultural Fields," RSL Technical Report 360-3, University of Kansas Center for Research, Inc., Lawrence, Kansas, October, 1978.

Ulaby, F. T., G. A. Bradley and M. C. Dobson, 1979, "Microwave Backscatter Dependence on Surface Roughness, Soil Moisture and Soil Texture, Part II: Vegetation-Covered Soil," IEEE Transactions on Geoscience Electronics, April.

Ulaby, F. T., G. Bradley and C. Dobson, "Potential Application of Satellite Radar to Monitor Soil Moisture, AWRA Fifth Annual Willaim T. Pecora Symposium, Sioux Falls, SD, June 11-15, 1979.

van Olphen, H., 1963. An Introduction to Clay Colloid Chemistry. John Wiley & Sons, New York.

Wagner, K. W., Arch. Elektrochem, 3:100, 1914.

Wang, J., T. Schmugge, and D. Williams, "Dielectric Constants of Soils at Microwave Frequencies-II," NASA Technical Paper 1238, Goddard Space Flight Center, Greenbelt, Maryland, May 1978.

Wang, J. R. and T. J. Schmugge, (October) 1978, "An Empirical Model for the Complex Dielectric Permittivity of Soils as a Function of Water Content," NASA Technical Memorandum 79659, Goddard Space Flight Center, Greenbelt, Maryland.

Weiner, O., "Leipziger Berichte," 62:256, 1910.

Wiebe, M. L., "Laboratory Measurement of the Complex Dielectric Constant of Soils," RSC Technical Report 23, Remote Sensing Center, Texas A&M University, College Station, Texas, October, 1971.

Wobschall, D., 1977. "A Theory of the Complex Dielectric Permittivity of Soil Containing Water: The Semidisperse Model." IEEE Transactions on Geoscience Electronics, GE-15(1).

Appendix A: Physical Model to Account for Soil Shrink-Swell Characteristics

The total pore space of the soil defines that fraction of the soil volume not occupied by soil particles.

$$T = 100 \times (1 - \rho_b/\rho_p) \qquad (A.1)$$

where: T = percent pore space

ρ_b = soil bulk density, g/cm^3

ρ_p = particle density 2.65 g/cm^3.

When the soil is saturated with water, the pore space is completely filled. Thus,

$$M_{sat} = T \qquad (A.2)$$

where: M_{sat} = the percent volumetric soil moisture at saturation.

Assuming particle density equal to 2.65 g/cm^3, the mean bulk density values measured during the 1977 Bare Soil Experiment are used to compute the values of M_{sat} presented in Table A.1. M_{sat} is the total possible volumetric soil moisture that soil layers can attain unless the soil is permitted to swell in volume. Due to the prevalence of heavy rains before and during the experimental period, many of the measured soil moisture values were found to exceed Mg_{sat} as given in Table A.1 indicating that soil bulk density was dependent upon moisture content.

Montmorillonite is the predominant clay mineral within the test site and is widely known for its capacity to swell. Test plots of silty clay loam and silty clay all exhibited extensive cracking of the soil surface as dessication caused soil shrinkage. Although the bulk density of these soils was measured in the field over a relatively narrow range of moistures near field capacity, density was found to be linearly dependent upon gravimetric soil moisture with a correlation of up to -0.74.

Because of the dependence of density on moisture within fields of silty clay loam and silty clay, the calculation of volumetric soil moisture values from the mean measured soil bulk density was judged to be unacceptable. In spite of measured linear correlations of -0.6 to -0.7, the limited range and sample size of the measurements yielded a low significance to empirical moisture-density algorithms. In order to estimate volumetric soil moisture as a function of soil density, field and laboratory measurements of density were inserted into a simple

TABLE A.1

Total Porosity and Gravimetric Moisture at Soil Saturation as Computed From Mean Bulk Density and Assuming Particle Density Equals 2.65 g/cm^3.

$$T = 100(1-\rho_b/\rho_p)$$

$$Mg_{sat} = T/\rho_b$$

Depth	FIELD 1			2			3			4		
(cm)	ρ_b	T	Mg_{sat}	ρ_b	T	Mg_{sat}	ρ_b	T	Mg_{sat}	ρ_b	T	Mg_{sat}
0-1	1.434	45.9	32.0	1.225	53.8	43.9	1.205	54.5	45.2	1.305	50.7	38.9
1-2	1.402	47.1	33.6	1.212	54.3	44.8	1.268	52.1	41.1	1.372	48.2	35.1
2-5	1.187	55.2	46.5	0.863	67.4	78.1	1.009	61.9	61.4	1.066	59.8	56.1
5-9	1.377	48.0	34.9	1.273	52.0	40.8	1.339	49.5	36.9	1.353	48.9	36.2
9-15	1.592	39.9	25.1	1.464	44.7	30.6	1.437	45.8	31.8	1.410	46.8	33.2

physical model proposed by Fox (1964). Also of interest are the data and models presented in Berndt and Coughlan (1977), Jamison and Thompson (1967), Lawrence (1977) and Parker, Amos and Kaster (1977).

The model treats soil volume change as a three dimensional process at moistures below field capacity to account for the presence of crack systems and as a uni-dimensional process at moistures above field capacity where soil cracks are closed and further expansion can only occur in the vertical dimension. The following assumptions are made:

1) Volume change is normal and three dimensional from oven dryness until all of the vertical interstices of the soil are just filled with water and no further horizontal expansion is possible. The swelling is similar to that observed by Berndt and Coughlan (1977) for semi and unconfined soil cores.
2) Soil volume changes uni-dimensionally in the vertical dimension at soil moistures greater than those required to reduce the percent volume of entrapped air to 3%. This swelling is similar to that observed by Berndt and Coughlan (1977) for confined soil cores.
3) The model is tied to values of soil moisture, bulk density and air capacity determined for undisturbed core samples from each field at a soil tension of 1/3 bar.
4) The volume of entrapped air cannot be reduced below 3%.

The three-dimensional model is given by:

$$\rho_{bx} = \rho_s/(\rho_s/A + M_x\rho_s + E_1)^{1/3} \qquad (A.3)$$

and the uni-dimensional model by:

$$\rho_{bx} = \rho_s/(\rho_s/A + M_x\rho_s + E_2) \qquad (A.4)$$

which reduces to:

$$\rho_{bx} = 1/(1/A + M_x + E_2/\rho_s) \qquad (A.5)$$

where: A = absolute density of soil = 2.65 g/cm^3
ρ_{bx} = bulk density of soil at moisture M_x, g/cm^3
ρ_s = bulk density at which all vertical interstices in the soil are assumed filled with water. This is assumed to occur at 1/3 bar tension.

M_x = gravimetric moisture, g/g
E_1 = air capacity at 1/3 bar tension, cm^3/cm^3
E_2 = air capacity at saturation = 0.03 cm^3/cm^3

Figures A.1 to A.3 show bulk density as a function of gravimetric soil moisture for fields 2 to 4 respectively as computed from equations (A.3 and A.4). The three-dimensional model predicts density will decrease gradually with increasing moisture. When air capacity decreases to 3% all vertical interstices of the soil are assumed to have been filled with water and further swelling must occur uni-dimensionally. The figures show the uni-dimensional volume change to be quite dramatic because each additional gram of water swells the soil by 1 cm^3. Figure A.4 compares the volumetric moistures predicted by the model with those calculated for each field using a moisture constant mean bulk density. At low gravimetric moistures, M_v from the model tends to be slightly greater than that computed from mean bulk density. At moistures approaching and in excess of saturation, the model predicts M_v much lower than that computed from mean bulk density.

Figures A.5 to A.8 show the volume percent of air, water and soil as a function of gravimetric moisture for fields 1 to 4 respectively. Field 1, a sandy loam, is assumed to have a constant bulk density as a function of moisture, this is firmly supported by the field bulk density measurements and the fact that this soil exhibited no surface cracking when the surface layer was dry. Fields 2 to 4 are each plotted using values derived from the physical soil shrink-swell model.

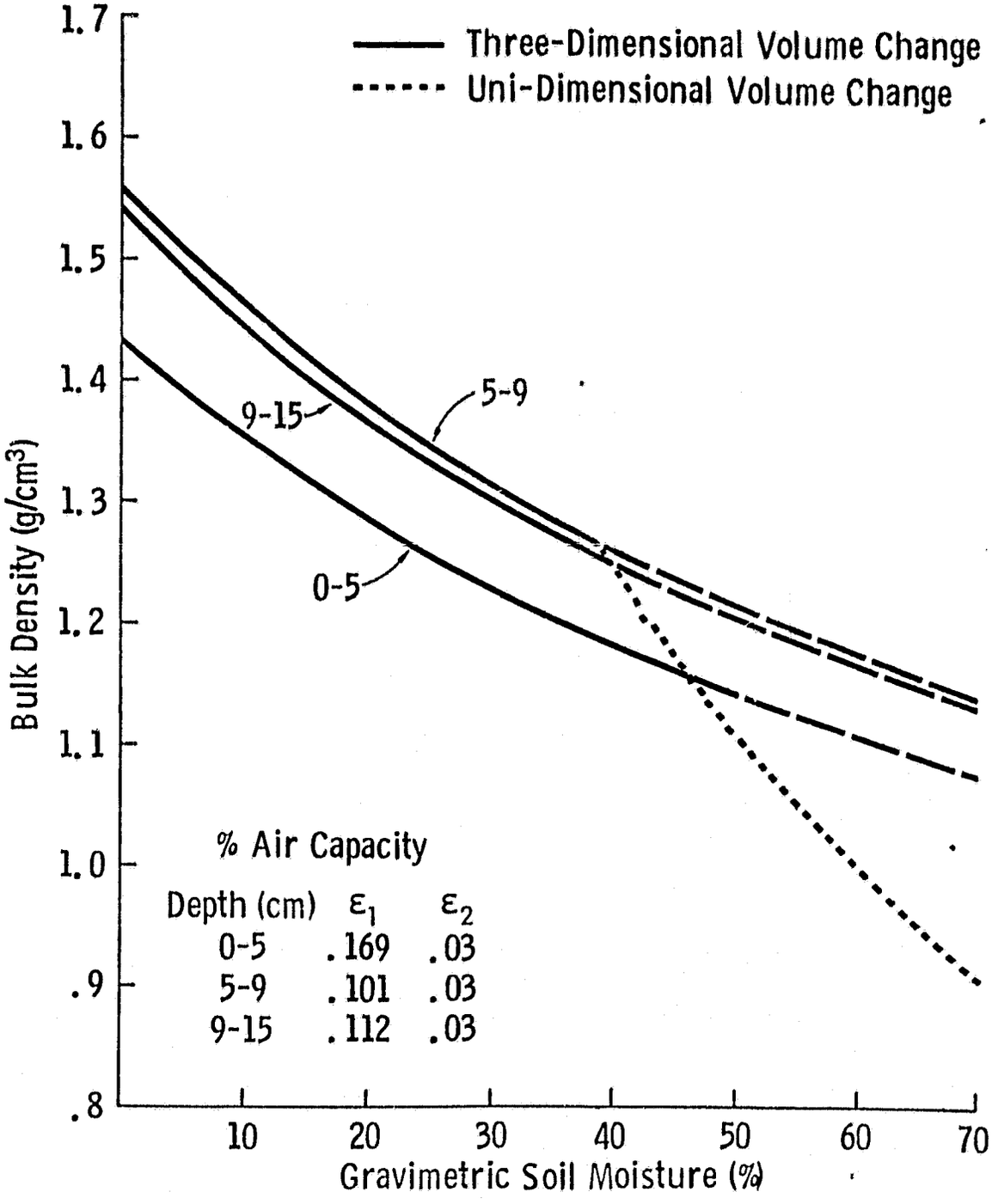

Figure A.1. Bulk density as a function of gravimetric soil moisture for Field 2, silty clay loam, as predicted by the physical model.

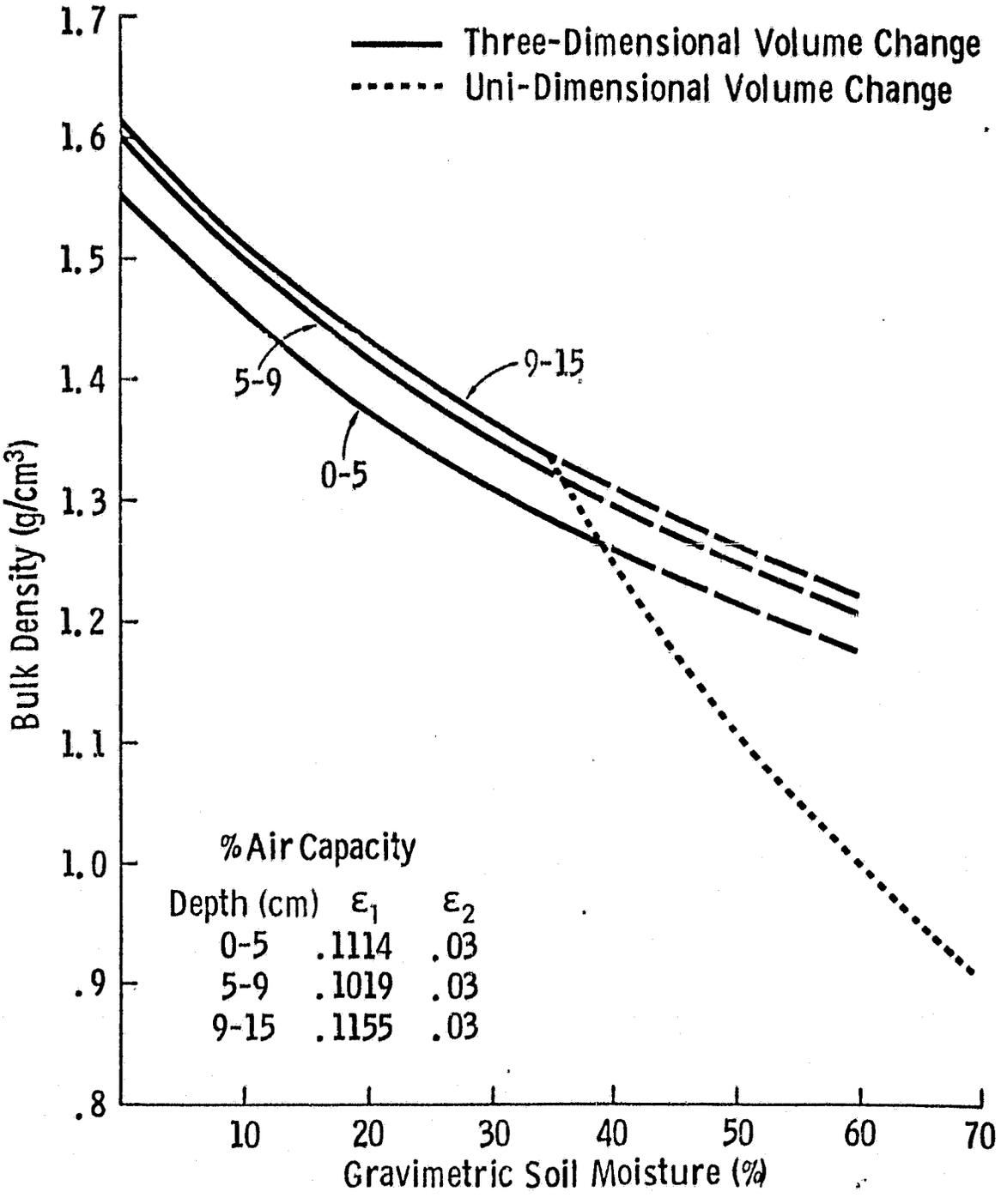

Figure A.2. Bulk density as a function of gravimetric soil moisture for Field 3, silty clay loam, as predicted by the physical model.

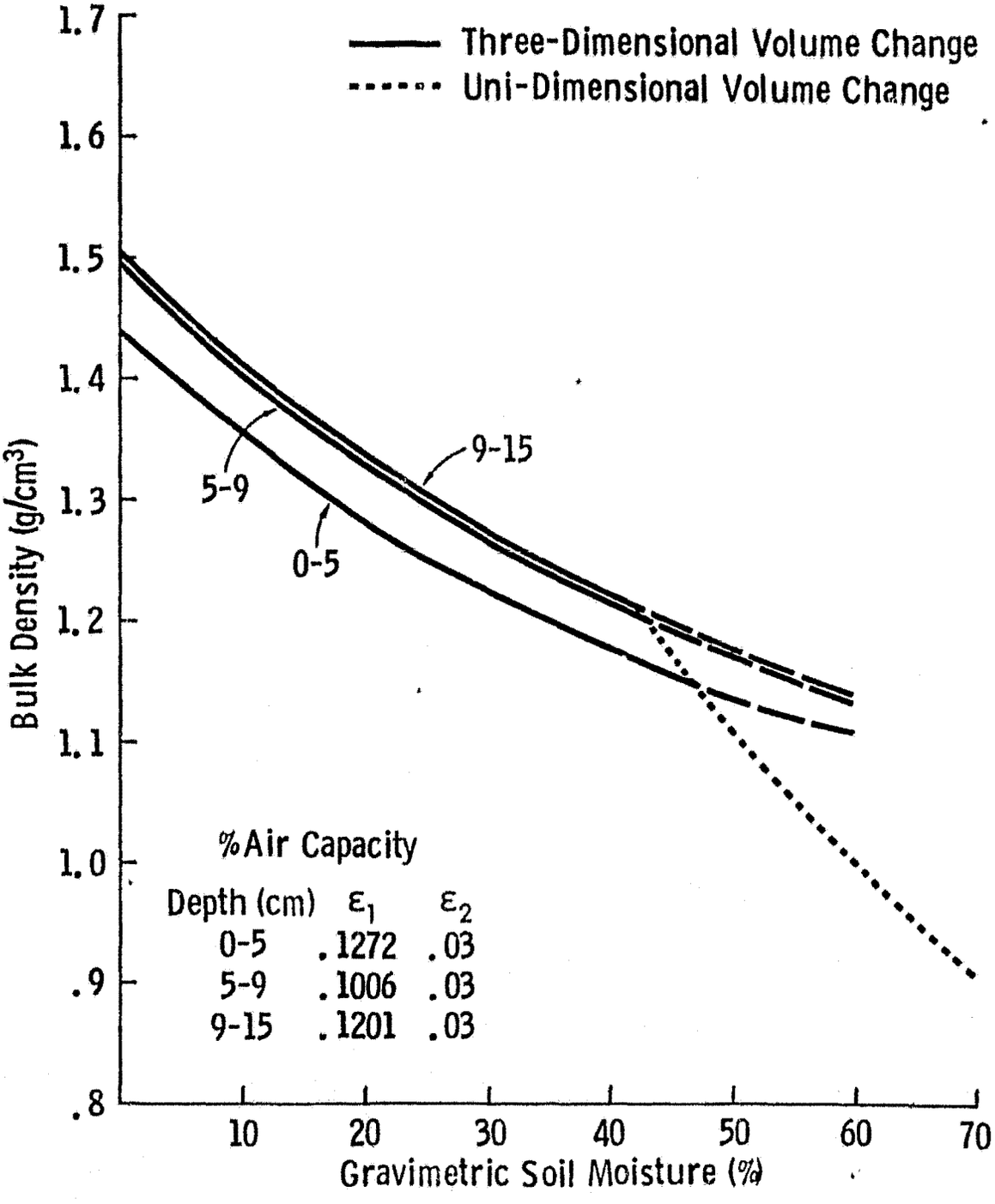

Figure A.3. Bulk density as a function of gravimetric soil moisture for Field 4, silty clay, as predicted by the physical model.

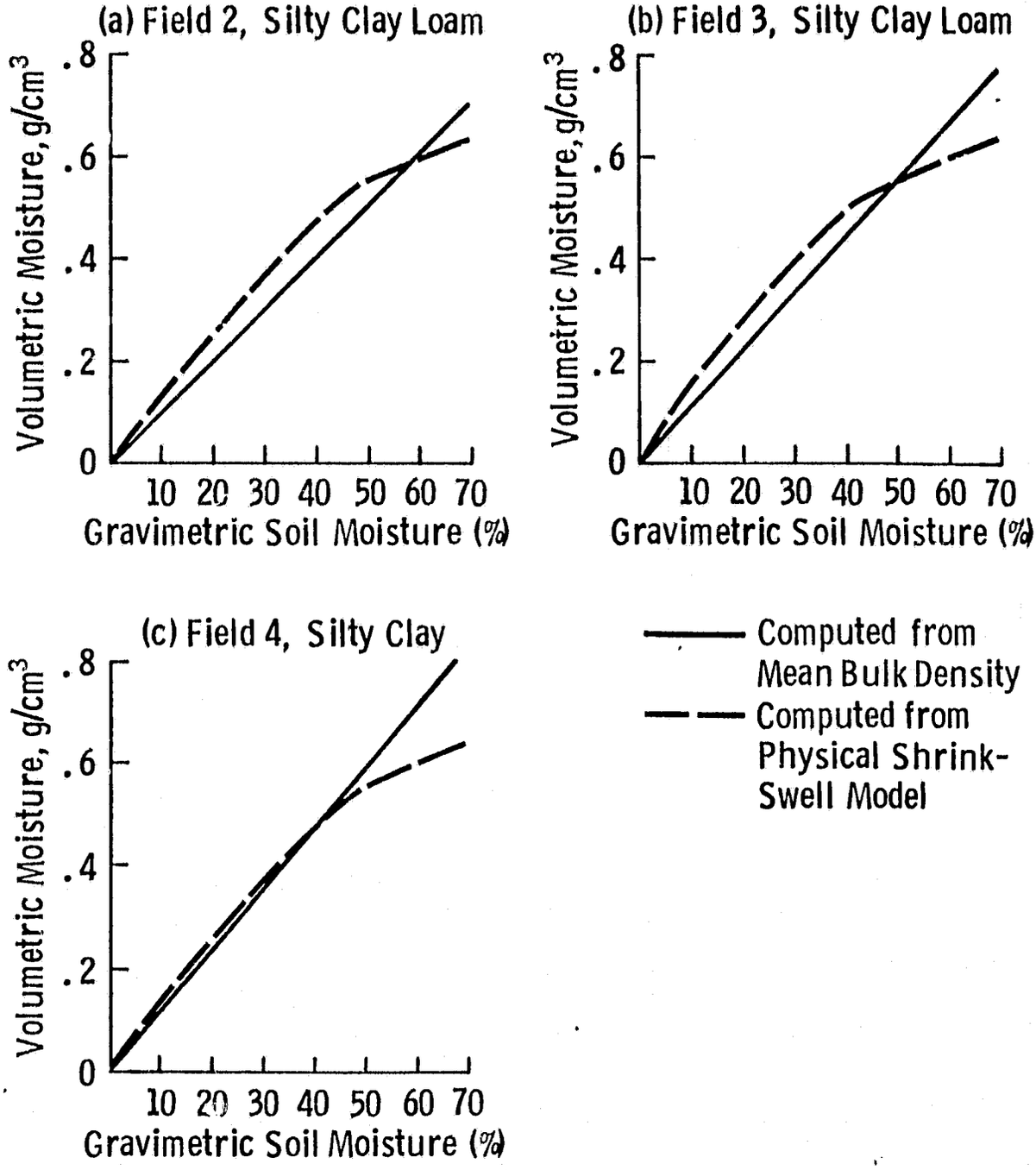

Figure A.4. 0-5 cm volumetric soil moisture as a function of gravimetric soil moisture, comparison of results from the physical model to account for shrink/swell effects and results using a constant mean bulk density. (a) Field 2, (b) Field 3 and (c) Field 4.

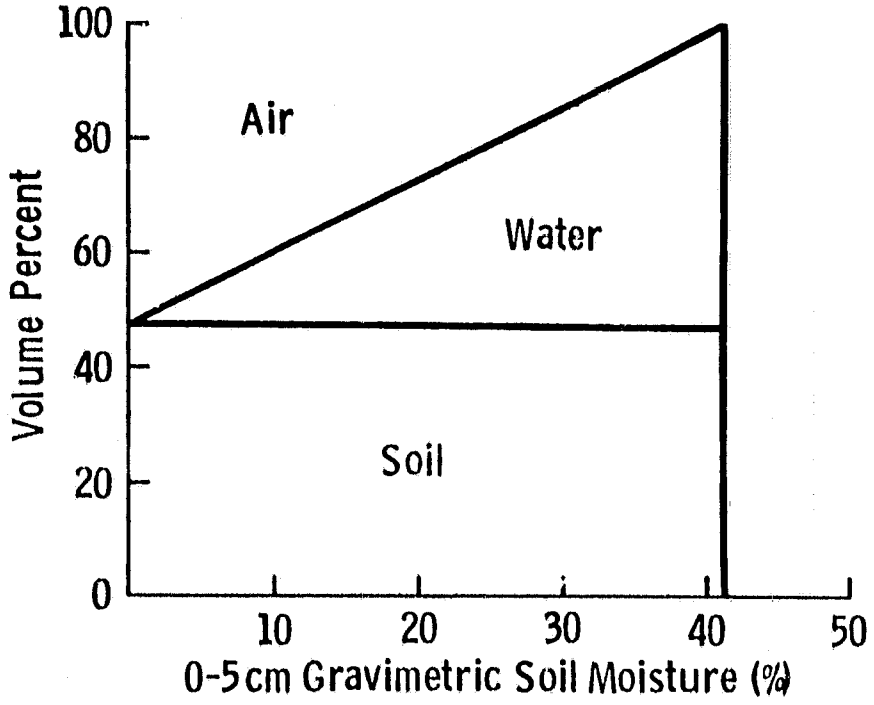

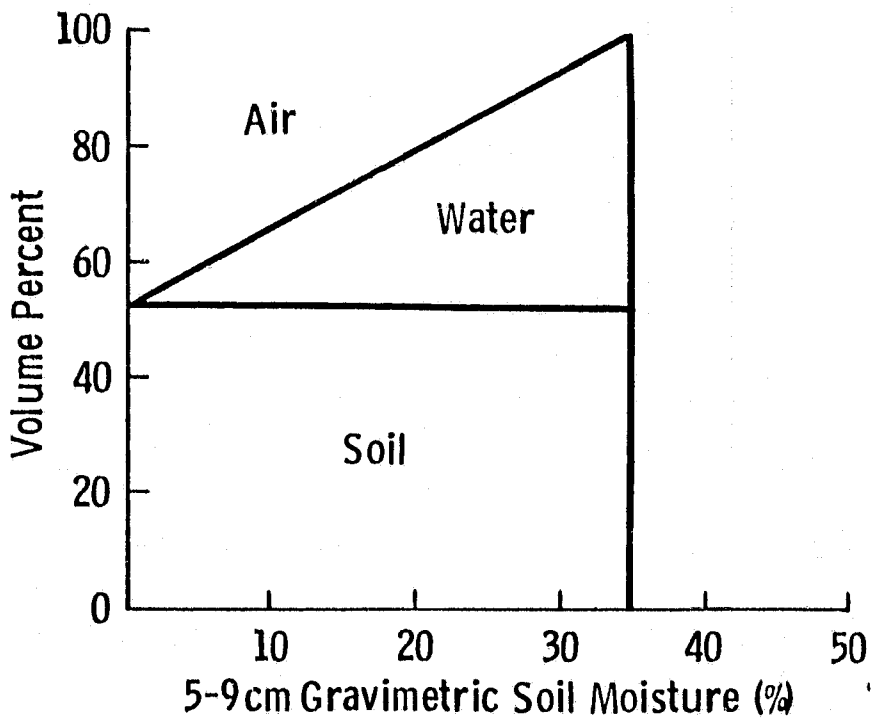

Figure A.5. Volume percent of air, water and soil as a function of gravimetric soil moisture for the 0-5 and 5-9 cm layers of Field 1, sandy loam. Values are computed with the assumption that mean measured bulk density is constant as a function of moisture content.

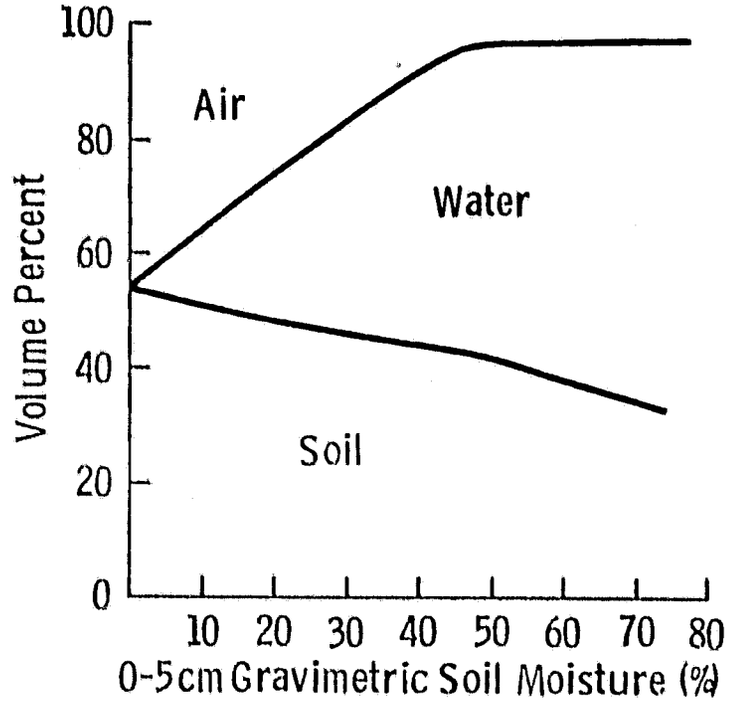

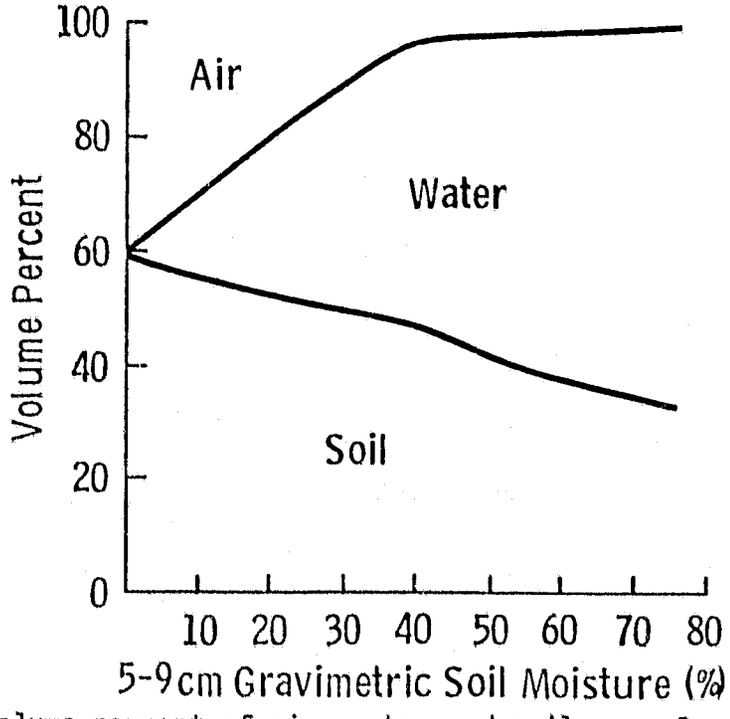

Figure A.6. Volume percent of air, water and soil as a function of gravimetric soil moisture for the 0-5 and 5-9 cm layers of Field 2, silty clay loam. Values are computed from the physical volume change model to account for soil shrink and swell as a function of moisture content.

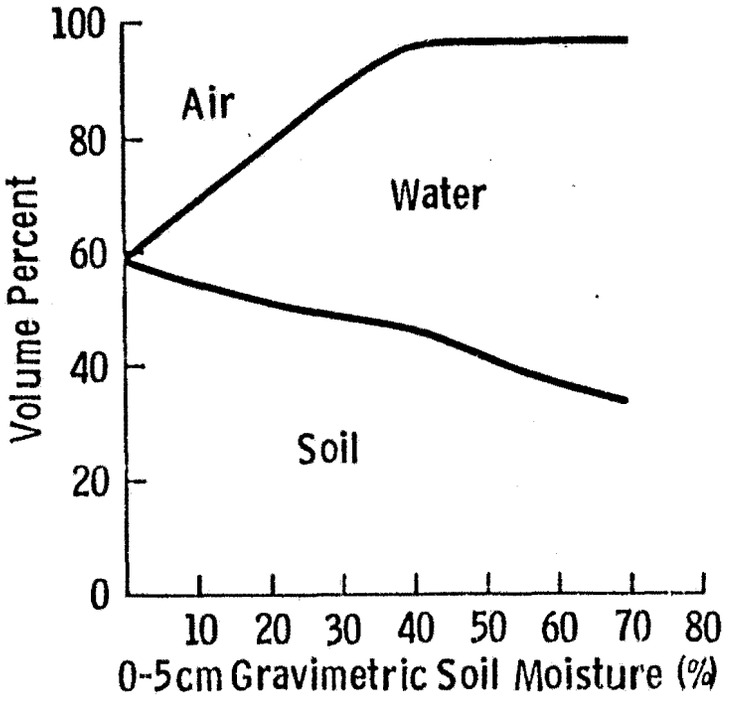

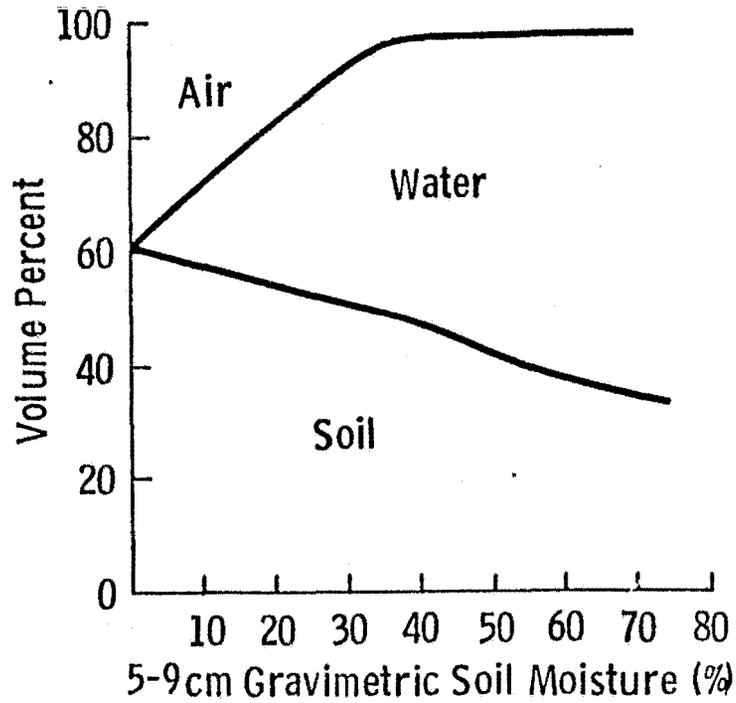

Figure A.7. Volume percent of air, water and soil as a function of gravimetric soil moisture for the 0-5 and 5-9 cm layers of Field 3, silty clay loam. Values are computed from the physical volume change model to account for soil shrink and swell as a function of moisture content.

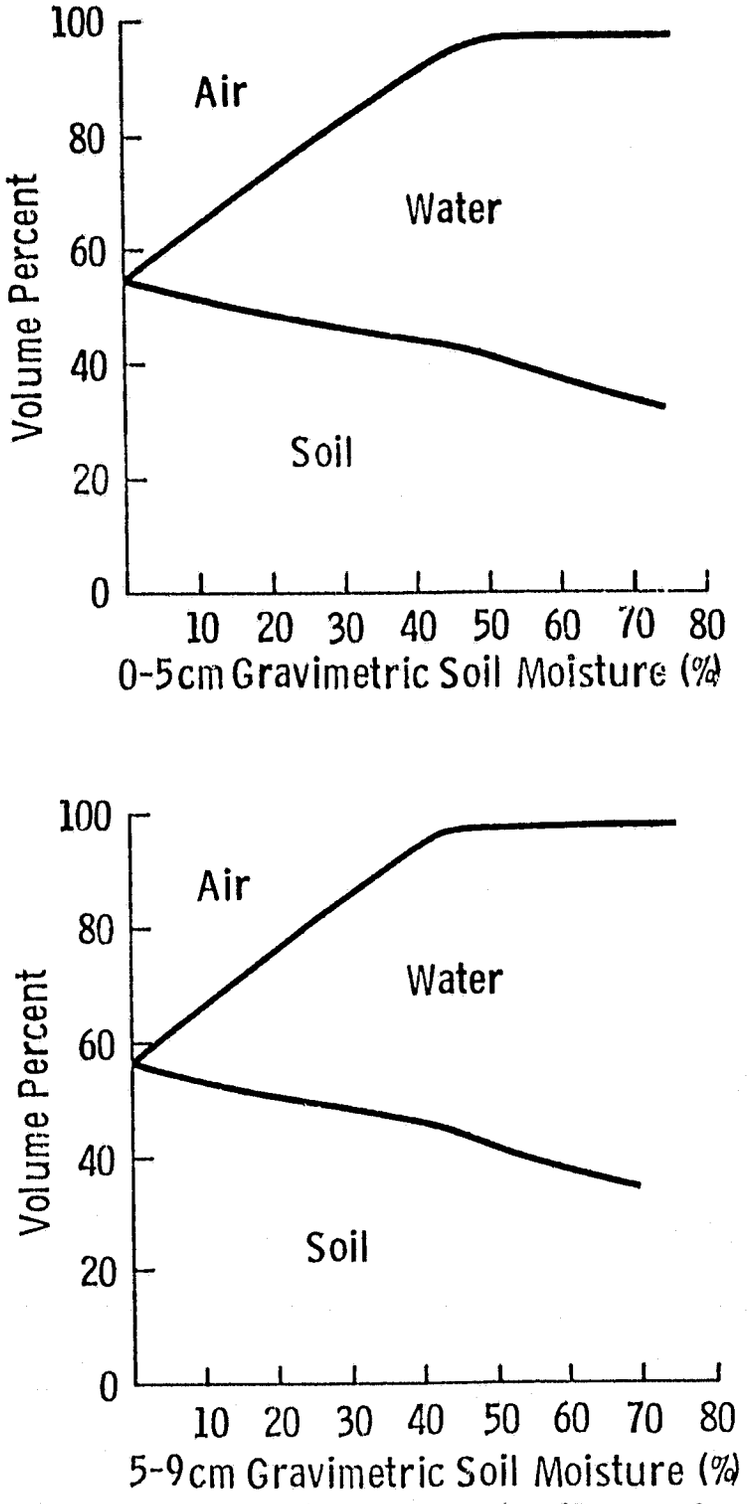

Figure A.8. Volume percent of air, water and soil as a function of gravimetric soil moisture for the 0-5 and 5-9 cm layers of Field 4, silty clay. Values are computed from the physical volume change model to account for soil shrink and swell as a function of moisture content.

NASA-JSC